ICID•CIID
INTERNATIONAL COMMISSION ON IRRIGATION AND DRAINAGE

INCID
INDIAN NATIONAL COMMITTEE ON IRRIGATION AND DRAINAGE

25TH ICID INTERNATIONAL CONGRESS ON IRRIGATION AND DRAINAGE

1-8 NOVEMBER 2023, VISAKHAPATNAM (VIZAG), ANDHRA PRADESH, INDIA

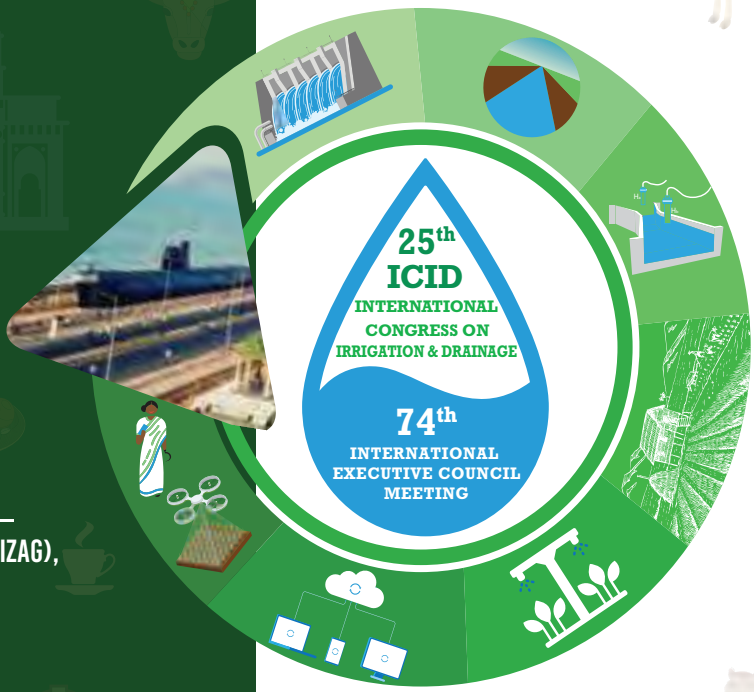

PROCEEDINGS

International Workshop on Innovated Agricultural Water Management under Climate Change

TACKLING WATER SCARCITY IN AGRICULTURE

LUTTER CONTRE LA PENURIE D'EAU DANS L'AGRICULTURE

INTERNATIONAL COMMISSION ON IRRIGATION AND DRAINAGE
COMMISSION INTERNATIONALE DES IRRIGATIONS ET DU DRAINAGE

ICID•CIID

The International Commission on Irrigation and Drainage (ICID), established in 1950 is the leading scientific, technical and not-for-profit Non-Governmental Organization (NGO). The Commission through its network of professionals spread across more than a hundred countries, has facilitated sharing of experiences and transfer of water management technology for over six decades. ICID supports capacity development, stimulates research and innovation and strives to promote policies and programs to enhance sustainable development of irrigated agriculture through a comprehensive water management framework.

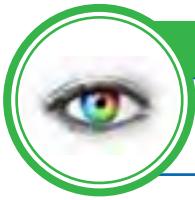

VISION

Water secure World, free of poverty and hunger achieved through sustainable rural development.

MISSION

To work together towards sustainable agriculture water management through inter-disciplinary approaches to economically viable, socially acceptable and environmentally sound irrigation, drainage and flood management.

Organizational Goals to realise the ICID Vision 2030

- **A** Enable Higher Crop Productivity with Less Water and Energy
- **B** Be a Catalyst for a Change in Policies and Practices
- **C** Facilitate Exchange of Information, Knowledge and Technology
- **D** Enable Cross-Disciplinary and Inter-Sectoral Engagement
- **E** Encourage Research and Support Development of Tools to Extend Innovation into Field
- **F** Facilitate Capacity Development

For more information on ICID Vision 2030, please access document on 'A Road Map to ICID Vision 2030' available on ICID website - http://www.icid.org/icid_vision2030.pdf

Proceedings of the

International Workshop on

Innovated Agricultural Water Management under Climate Change

Presented at:

25th ICID Congress and 74th IEC Meeting,

1-8 November 2023

Visakhapatnam (Vizag), Andhra Pradesh State, India

This Workshop is organized with the support of the International Commission for Irrigation and Drainage's (ICID) Working Group on **"Innovated Agricultural Water Management under Climate Change."** It is held in conjunction with ICID's 25th ICID Congress and the 74th International Executive Council (IEC) Meetings, from 01-08 November 2023 in Vishakhapatnam (Vizag), Andhra Pradesh State, India.

ISBN: 978-89610-40-1

CONTENTS

Preface

The "Innovative Agricultural Water Management under Climate Change" workshop emphasizes cutting-edge techniques and strategies to navigate climate-induced challenges in agriculture. As climate change disrupts the water cycle and intensifies droughts, the availability of water for agriculture is at risk. Addressing this with innovative management is the key to ensuring food security and sustainable farming. Combining the power of technology with insightful strategies allows for a proactive approach to agricultural water challenges. This convergence ensures not only the strategic sourcing of irrigation but also maximizes efficiency in water consumption for farming. Such efficiency paves the way for sustainable water resources, underpinning food security.

The compilation of 15 papers presented here offers an eclectic mix of research that sheds light on the challenges and solutions associated with agricultural water management in the face of changing climatic patterns. From the in-depth optimization model for agricultural water resource management under climate change put forth by Hu et al. in WS-CLIMATE-01, to sustain and adapt agricultural water management in Asian Deltas, an integrated water management platform combined with GIS-based and machine learning technology presented by Nagano et al. in WS-CLIMATE-12, these papers cover a spectrum of geographic specificities, technical innovations, and strategic insights. The importance of localized strategies is exemplified by the review in WS-CLIMATE-03 on East Java's water management adaptations. A leap into technological innovations is seen in WS-CLIMATE-06 by Lin and Ho, emphasizing non-invasive technology in irrigation. Similarly, the embrace of modern technology and data analytics resurfaces in WS-CLIMATE-10 and WS-CLIMATE-13, underscoring the benefits of data-driven approaches in water management. The need to adapt to the exigencies of climate change is further underscored by papers such as Takigawa's exploration of Japan's climate adaptation measures in agricultural infrastructure in WS-CLIMATE-02 and Meegastenna's deep dive into the impacts of climate change on tank cascade systems in Sri Lanka in WS-CLIMATE-05. Additionally, it's noteworthy that several papers delve into the intersections of various phenomena impacted by climate change. For instance, the final paper, WS-CLIMATE-15, doesn't solely focus on agricultural water management, but broadens the lens to explore urban heat island phenomena and thunderstorm patterns in Taipei, reflecting the interconnectedness of these issues.

In summary, this compilation not only highlights the multifaceted nature of challenges posed by climate change to agricultural water management but also offers a range of innovative, adaptive solutions, spanning technological advancements, policy measures, and community-driven interventions. As global stakeholders grapple with the repercussions of climate change, this body of work serves as a timely, invaluable resource in shaping resilient, sustainable strategies for the future.

Prof. Ray-Shyan Wu
Chairman, Working Group on Innovated Agricultural Water Management under Climate Change (WG-CLIMATE)

SPECTRUM NETWORK FLOW OPTIMIZATION OF AGRICULTURAL WATER RESOURCES MANAGEMENT UNDER CLIMATE CHANGE

Ming-Che Hu,[1] Wei-Yin Chen, Chao-Ting Lee

Abstract

Under climate change, extreme hydrological events have a serious impact on the water supply of the agricultural water resource system. This study will provide systematic analysis methods and tools to evaluate the agricultural water resource dispatching capability and the purpose of the study is to evaluate how agricultural water resource management affects water supply stability and drought resistance.

The research uses the network programming model to simulate and analyze the agricultural water supply and demand. Rainfall, river flow, groundwater, water storage, crop production, and agricultural water demand of water resources system are functions of time, so the allocation of agricultural water resources is time-dependent. It is a dynamic management problem over time and agricultural water resource management strategy is a function of time. Then this study conducts a Fourier spectrum analysis of hydrological and agricultural water demand time series data. To analyze the dynamic network programming of agricultural water management, the study incorporates network optimization with Fourier spectrum analysis for agricultural water resource systems. Fourier analysis is one of the most common spectrum analysis methods. Fourier analysis transforms a time function into a summation of serial orthogonal functions (sine functions and cosine functions with different frequencies). Through this procedure, the function is then shifted from the time domain onto the frequency domain. Functions are time functions of rainfall, river flow, groundwater, water storage, crop production, and agricultural water demand of the water resources system. Coefficients of Fourier analysis are determined based on the orthogonality of sine and cosine functions. To incorporate network optimization with Fourier spectrum analysis, agricultural water supply and demand are time functions in the model. Those time function are transformed using Fourier analysis. Confronting the increasingly worsening climate change, people should take immediate steps to be prepared for extreme weather events. The proposed framework has practical significance for guiding the implementation of agricultural water resources management and the provision of a scientific basis for making decisions. In addition, while concentrating on the current situation is crucial, taking a long-term approach is also indispensable, which stimulates the nuclear concept of this proposal.

1. Introduction

In 2020, for the first time in 56 years, no typhoons made landfall in Taiwan during the wet season. From the month of June 2020 to May 2021, Taiwan experienced severe water shortages, and many areas' irrigation water was cut off. The estimated production loss of the drought (Sep.~Oct., 2020) is 5.7 million NTD by the Council of Agriculture. The incident indicates a changing precipitation patters and highlights water stress as a growing environmental risk.

The investment in infrastructure will determine the resilience of economies to water stress. Executive Yuan has announced the flexible deployment of water as one of the major strategies to secure Taiwan's water supply in 2018. Since then, several water pipeline projects have been completed or are currently in the planning/construction stage. For example, a water pipeline in Hsinchu, near the country's largest science park, was completed in 2020, which supports the area with water from Shimen Reservoir located in northern Taoyuan. A pipeline connecting the Tseng-Wen Reservoir and the Nanhua Reservoir is expected to be completed in 2024, which was chosen as the subject of the case study in this study.

[1] Department of Bioenvironmental Systems Engineering, National Taiwan University, Taiwan

Year	Farmland area in Taiwan affected by irrigation curbs (hectares)
2002	14,778
2003	27,646
2004	65,385
2006	30,828
2010	22,366
2015	43,659
2020	95,000

Table 1. Annual records of the total area of farmland affected by irrigation water curbs in Taiwan. The statistics are provided by the Council of Agriculture.

2. Methodology

The problem of optimizing a water resource system's investment decision of establishing conjunctive use of different resources and the operation decisions of allocating the available resources across space and time is formulated as a two-stage stochastic optimization model to account for the uncertainties in future reservoir inflow. The first stage concerns all investment decisions, including the location and capacity of the connecting pipes, which can only be adaptive to the forecast of the distribution/statistics of the stochastic variables. The second stage concerns operation decisions of the water resource system, which has been converted to a network flow model. The operation decisions include reservoir release and the allocation of water among users, which are adaptive to the realization of the stochastic variables.

This study proposes a model that optimizes the continuous flow functions regulated by the controlled outflow at individual nodes of the water resource network, especially at the reservoir nodes since their large storage capacity allows the largest flexibility to adjust its outflow, instead of directly optimizing the discretized quantities of flow in each time intervals.

In the first part of the study, 15 years of monthly reservoir inflow data is first analyzed by Fourier analysis and a continuous function characterizing the specific river regime is reconstructed by inverse Fourier transform of the dominant frequencies. The reconstructed river flow function is then cut into 15 segments of length 12, representing 15 scenarios each with equal probability of occurrence of 1/15. Then, the reconstructed flow functions are incorporated into the two-stage stochastic optimization model as the stochastic variable. Finally, the network-flow problem is solved and the optimal long-term investment decision and scenario-specific monthly sets of water allocation decisions are obtained.

Weather data, river discharge data, and reservoir inflow data are all seasonal time series, besides the most obvious annual periodicities, there may also exist other periodicities driven by large-scale climate oscillations or local factors such as terrain. Thus, such variables can be seen as periodic functions that can be transformed from the time domain to the frequency domain by the Fourier Transform. In the frequency domain, we can detect seasonality of the data. The frequencies with large amplitudes are called the dominant frequencies, and by extracting the dominant frequencies of the data, we reconstruct the inflow function that characterizes the conditions of different watersheds. It is noted that this study makes the assumption that the dominant frequencies characterizes the important periodicities, however, the study would benefit from a detailed analysis with insights from atmospheric science and hydrology to select the important frequencies.

The available data do not record the river discharge as a continuous function over time, instead the information is measured at equally-spaced intervals of time. Thus, Discrete Fourier Transform (DFT) is implemented by the Fast Fourier Transform (FFT) algorithm.

Let $x_n, n = 0, 1, \dots, N-1$, denote N values of river discharge sampled at equally-spaced times. The formula of Discrete Fourier Transform can be written as:

$$X_k = \sum_{n=0}^{N-1} x_n \cdot e^{-\frac{i2\pi}{N}kn}, \text{ for } 0 \le k \le N-1$$

X_k is a complex number which holds the information of amplitude and phase of a sinusoidal wave with frequency k/N cycles per unit time. This comes from Euler's formula:

$$e^{i2\pi kn/N} = cos(2\pi kn/N) + isin(2\pi kn/N)$$

The phase amplitude and phase of $X_k = a + bi$ can be calculated by:

$$magnitude = A = |a + bi| = \sqrt{a^2 + b^2}$$

$$phase = \phi = \arctan b/a$$

The two-stage stochastic optimization problems are also called recourse problems because the second stage decisions are can be interpreted as corrective actions to the first stage decisions made before the uncertainties are revealed. The corrective decisions are made by solving a second stage decision problem to minimize the second stage costs Q_1, which is a function of the first stage decision x_0, the second stage decision x_1, and the realization of the random parameters ξ:

$$minimize\{Q_1(x_0, x_1, \xi) : x_1 \in \mathbb{X}_1(x_0, \xi)\}$$

The total cost function is the sum of the first stage cost Q_0 and the second stage cost. The complete two-stage problem is formulated as:

$$min\{Q_0(x_0) + min\{\mathcal{R}[Q_1(x_0, x_1, \xi)] : x_1 \in \mathbb{X}_1(x_0, \xi)\} : x_0 \in \mathbb{X}_0\}$$

$\mathcal{R}$ is a risk functional. The simplest risk functional is the expectation and the represented objective function will be risk neutral and linear.

Risk-aversion describes the preference of certainty over uncertainty. Certain outcomes with lower expected value in payoff may be preferred over uncertain outcomes with a higher payoff. The goal of investment decision is not only to lower the overall cost of water deficit, but also prevent high-loss outcomes. Thus, the objective function should reflect the risk aversion of the decision maker and the second stage decision problem is solved as a quadratic term in the objective function, with higher cost at higher deficits.

To simulate water supply and demand, the water resource system is first converted to a network flow model. A network consists nodes connected by arcs. A flow can occur between two nodes via an arc. In this study, the nodes of the network are reservoir intake locations, reservoirs, water treatment plants, and users with water demand, while the arcs represent the possible routes over which water can be transported with assigned cost per unit of water transported and capacity limits. The reservoir intake locations are considered source nodes and the sectors with water demand are considered sink nodes.

The constraints on a network flow model is described as follows:

- For each source node: the net outflow must be (less than or) equal to the available supply, which is given as parameters from river discharge data.
- For each reservoir node: the net outflow must be equal to the net change in storage quantity.

  There is also an associated constraint on the upper and lower limits of storage quantity.
- For each water treatment plant node: the net outflow must be zero, and the total outflow has an upper limit constraint equivalent to the capacity of the treatment plant.
- For each arc: the amount of flow transported must be lower than the capacity of the pipe.

The optimization model is formulated in the Python language using Pyomo, an open-source software package. The model created is an abstract model, which is defined without data. An instance of the abstract model is created by inputting the data file and only then can it be solved. The separation of the model and the data means that the model can be easily expanded or applied to other networks by altering the input data file. Pyomo supports multiple solvers. This study uses COIN-OR IPOPT (Interior Point Optimizer) for its ability to solve nonlinear programming problems.

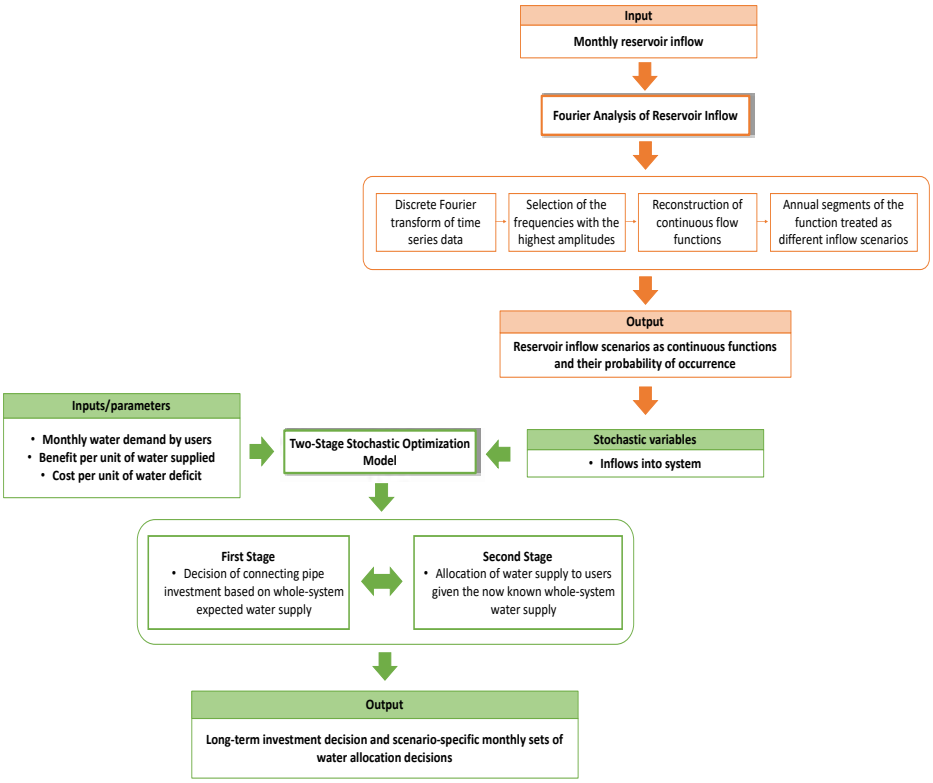

Fig. 1. Schematic diagram of the research framework in this study.

3. Results and Discussions

The data are recorded at four flow stations in located in southern Taiwan: Yufon Bridge, Chukou, Yutain, and Liling Bridge. Information about the average flow rates and the names of its watershed are recorded. Their relative location to each other and the reservoirs are mapped.Discrete Fourier Transform (DFT) of the monthly average flow data of three stations is computed with the Fast Fourier Transform (FFT) algorithm. The amplitude of the result is plotted as follows. The x-axis represents the period (months/cycle) and the y-axis represents the amplitude (CMS) of the flow data at period x. The most distinctive annual river flow pattern is indicated by the existence of peaks of amplitude values at 12 months/cycle periods among all three stations. The other periodicities are less distinctive.

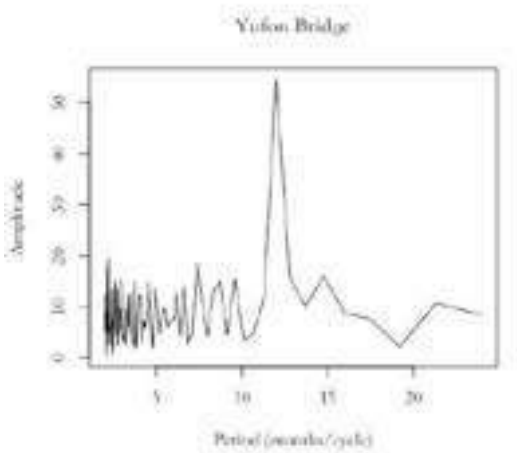

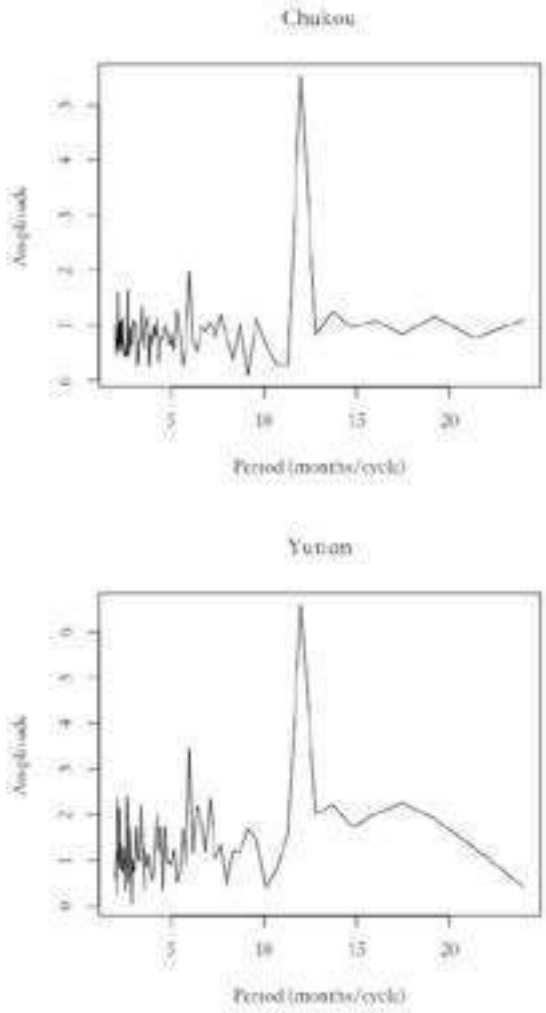

Fig. 2. Periodograms of the four flow stations. (Yufon Bridge, Chukou, Yutian, Liling Bridge)

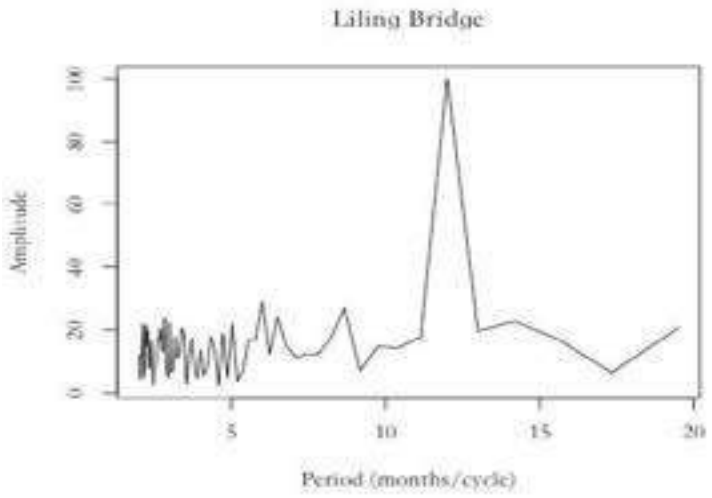

The river flow functions (16 years) of each station are reconstructed by summing ten terms of the Fourier Series with the largest amplitudes.

Table 2. The dominant frequencies of the Discrete Fourier Transformed river flow data and their corresponding amplitude and phase

Yufon Bridge Station			Liling Bridge Station		
period	amplitude	phase	period	amplitude	phase
Inf	123.636198	0	Inf	186.913269	0
12	54.4817846	2.86216187	12	99.993696	2.8257747
2.232558	19.3193983	1.78955818	26	31.993478	-1.4111265
7.384615	18.6099179	-1.1790065	52	31.661909	-0.1150458
2.133333	17.8476025	1.49599177	31.2	29.826223	-2.4498837
64	16.7677098	-2.6011962	6	28.909575	-0.6565643
14.769231	15.9977971	-0.4227583	8.666667	26.999052	0.34693643
12.8	15.7008433	-2.8997266	156	25.716892	-0.9489612
3	15.6865834	2.53585659	22.285714	25.516939	-1.686561
9.6	15.5167969	2.34908465	6.5	24.257936	-0.4756073
Yutian Station			Chukou Station		
period	amplitude	phase	period	amplitude	phase
Inf	8.7961458	0	Inf	8.7961458	0
12	5.5256593	2.92326273	12	5.5256593	2.92326273
6	1.9778986	-0.53429	6	1.9778986	-0.53429
2.666667	1.6430862	2.54122253	2.666667	1.6430862	2.54122253
2.181818	1.6116524	-1.1830159	2.181818	1.6116524	-1.1830159
3.428571	1.3428834	-0.2141283	3.428571	1.3428834	-0.2141283
5.333333	1.2657548	-1.6094175	5.333333	1.2657548	-1.6094175
32	1.2614371	-1.5601505	32	1.2614371	-1.5601505
96	1.2442202	-0.8721625	96	1.2442202	-0.8721625
13.714286	1.2416858	-2.1947029	13.714286	1.2416858	-2.1947029

The flow function of Yufon Bridge Station is visualized in the following.

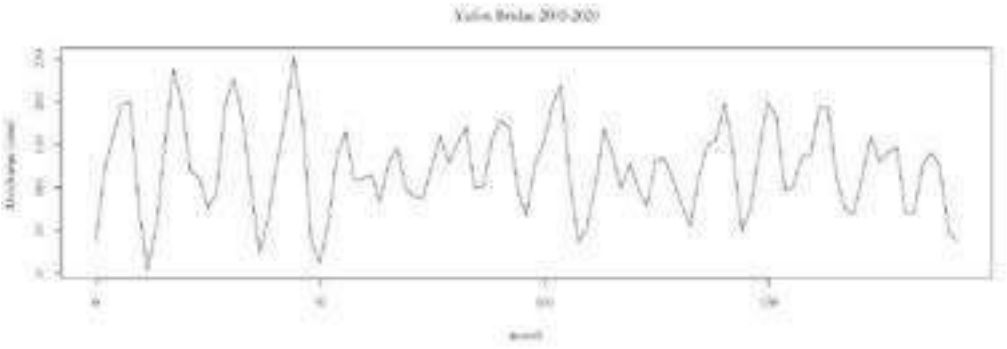

Fig. 3. The reconstructed river flow function of Yufon Bridge Station from the ten most dominant frequencies.

The inflow scenarios are extracted by truncating the function into segments. This can be done by multiplying the river flow function by a rectangular window function. For each station, 16 scenarios are extracted, each assumed equal probability of 1/16. 4 randomly selected inflow scenarios of Yufon Bridge are plotted for illustration purpose in Fig. X.

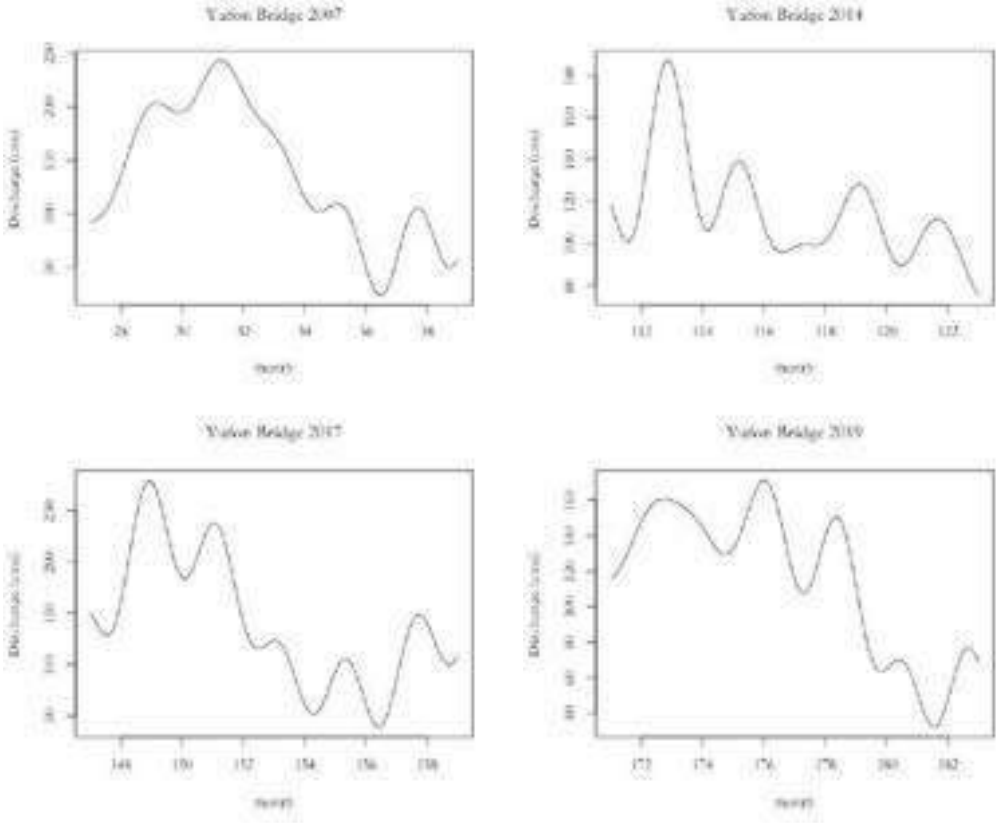

Fig.4. Four scenarios of different inflow functions of Yufon Bridge station.

A simple hypothetical system with six nodes is set up to investigate the effectiveness of constructing connecting pipes between two reservoirs in separate systems. The diagram of the network is shown in the following Figure.

Node 1 and 2 are source nodes, node 3 and 4 are storage nodes which represent the two reservoirs, and node 5 and 6 are sink nodes. The investment problem is to consider a project to build connecting pipes between the two reservoirs so that the supply from the sources with different periodic characteristics can be deployed with more flexibility. The goal is to solve for the optimal capacity of the connecting pipes.

The constraints include the upper limit on the flow across each arc (i.e. the capacity of the existing pipes), the upper limit on the storage of each storage node, and mass balance across each node.

Although the system is hypothetical, the reconstructed flow functions of Yufon Bridge Station and Liling Bridge Station are used as the outflow of the source nodes 1 and 2. It is noted that the average flow rate of Liling Bridge Station is larger than Yufon Bridge Station's by about 40%. To keep the analysis simple, the other parameters are assigned symmetrically. Specifically, the capacity of the two storage nodes, the demand of the two sink nodes, the cost of construction of the two connecting pipes are assigned the same value in both systems. In total, 4352 variables are defined, 6510 constraints are set up, and the optimal solution was found.

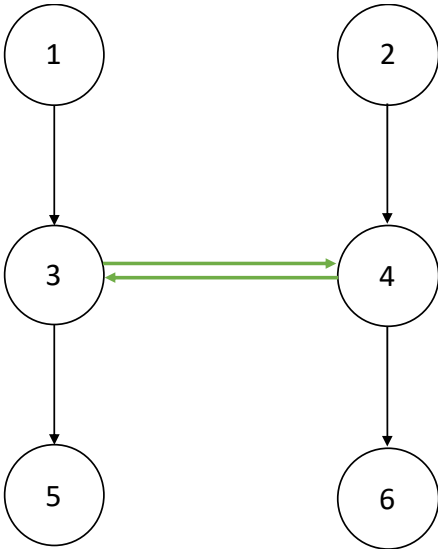

Fig. 5. Diagram of the hypothetical network.

3.1.1.1. Sensitivity Analysis:

Sensitivity analyses are conducted by altering the values of parameters and re-solving iteratively. Only one type of parameter is altered at a time, and all other parameters are fixed to the default parameters defined in the base model of the analysis. Default Parameters: Demands = 100 (units), Investment costs = 50 ($/unit of capacity), and Storage capacities = 50 (units). Cost of construction determines the cost-effectiveness of the infrastructure project. Sensitivity analysis helps quantify how much the cost has to be lowered in order for the project to be cost-effective.

From the result of the analysis, it is concluded that the capacity limit of the storage nodes can be a key determinant of whether the coordination of the resources between two areas will be required to stabilize the water supply. If the reservoir storage was large enough, the storage itself can allocate the supply across time, which lowers the requirement for cross-regional coordination. Since reservoir capacity decreases over time due to sedimentation, investment decisions regarding connecting pipes should also consider the future change in systems' reservoir capacity.

From the perspective of evaluating the need for new dam infrastructures, it should be noted that the coordination of water between systems can reduce the systems' reliance on reservoirs.

Demand also determines whether cross-regional water coordination will be needed. However, from the sensitivity result, it can be seen that in the analyzed case, when facing rising demands, the connecting pipe only offers the function of a one-way deployment from the area with more sufficient supply to the area with more deficiency in supply instead of regulating the periodicities of the sources.

Table 3. Model solution with different demand parameter value.

Demand	Optimal capacity	
	Arc(3 to 4)	Arc(4 to 3)
10	0	0
20	1.33	0
30	4.98	0
40	4.98	0

Table 4. Model solution with different storage capacity parameter value.

Storage capacity	Optimal capacity	
	Arc(3 to 4)	Arc(4 to 3)
110	0	0
100	0.53	0
90	1.64	0
80	2.76	0
60	3.87	0
50	4.98	0
40	6.09	0.55
30	8.33	1.59
20	11.66	2.83
10	14.99	4.25
0	20.00	6.75

4. Conclusions

The model built and used in this study provides insight into the value of water resource infrastructure projects in ensuring the stability of the water supply given the risks that arise from uncertainties about future water supply. The proposed method finds the underlying periodicities of the river flows then optimizes the problem with functions containing the periodic information instead of with discrete raw data. This is done by evaluating the periodic characteristics of different rivers first by Discrete Fourier Transform and reconstructs continuous functions as scenarios of the possible future inflow to reservoirs. The form that the model is written allows users to apply the tool to other networks for analysis by entering the specifications of their water system into a data file without altering the model itself. The basic analysis on hypothetical system demonstrated the following relations when the networks connected only differ in the periodic characteristics of the source flow and are similar in connectivity, and demand. When the reservoir capacity is limited, the contribution of the connecting pipe to regulate the periodicities of supply plays a significant role in decreasing the risk of water deficit. The importance of regulating the periodicities become secondary when the reservoir capacities are sufficient, however, the connecting pipes still serve the purpose of deploying the supply from area with less deficit to the area with more deficit when facing rising demands.

References

Adeyemo, J., O. Olofintoye. 2014. Optimized fourier approximation models for estimating monthly streamflow in the Vanderkloof Dam, South Africa. In EVOLVE-A Bridge between Probability, Set Oriented Numerics, and Evolutionary Computation V (pp. 293-306). Springer, Cham.

Tao Bai, Ming Zhang, Xia Liu, Qiang Huang. 2019. Multi-Objective Optimization of Transferable Water for Cascade Reservoirs in the Upper Yellow River. Journal of Marine Science and Technology: Vol. 27: Iss. 5, Article 2.

Po Chun Chen, Yuan Heng Wang, Gene Jiing Yun You. 2016. Comparison of Methods for Non-Stationary Hydrologic Frequency Analysis: Case Study using Annual Maximum Daily Precipitation in Taiwan. Journal of Hydrology, 545, 197-211.

Chin Tsai Hsiao, Liang Chen Chang, Jui Pin Tsai. 2017. Features of spatiotemporal groundwater head variation using independent component analysis. Journal of Hydrology, 547, 623-637.

IPCC, 2014: Synthesis Report. Contribution of Working Groups I, II and III to the Fifth Assessment Report of the Intergovernmental Panel on Climate Change [Core Writing Team, R.K. Pachauri and L.A. Meyer (eds.)]. IPCC, Geneva, Switzerland, 151 pp.

Kreyszig, E. 2011. Advanced Engineering Mathematics, Tenth Ed, Wiley, London.

Momtahen, S., and A. B. Dariane. 2007. Direct search approaches using genetic algorithms for optimization of water reservoir operating policies. Journal of water resources planning and management, 133(3), 202-209.

Venkata Ramana, R., B. Krishna, S. R. Kumar, N. G. Pandey. 2013. Monthly rainfall prediction using wavelet neural network analysis. Water resources management, 27(10), 3697-3711.

Wen Ping Tsai, Fi John Chang, Li Chiu Chang, Edwin E. Herricks. 2015. AI techniques for optimizing multi-objective reservoir operation upon human and riverine ecosystem demands. Journal of Hydrology, 530, 634-644.

Wei, Z., A. Pagani, G. Fu, I. Guymer, W. Chen, J. McCann , W. Guo. 2019. Optimal sampling of water distribution network dynamics using graph fourier transform. IEEE Transactions on Network Science and Engineering, 7(3), 1570-1582.

J. Pablo Ortiz-Partida, T. K., Tatiana Ermolieva, Yuri Ermoliev, Belize Lane, Samuel Sandoval-Solis, Yoshihide Wada. (2019). A Two-Stage Stochastic Optimization for Robust Operation of Multipurpose Reservoirs. Water Resources Management.

Saremi, A., Pashaki, M. H. K., Sedghi, H., Rouzbahani, A., & Saremi, A. (2011). Simulation of river flow using Fourier series models. Paper presented at the International Conference on Environmental and Computer Science.

Sleziak, P., Hlavcova, K., & Szolgay, J. (2015). Advantages of a time series analysis using wavelet transform as compared with a fourier analysis. Slovak Journal of Civil Engineering, 23(2), 30.

Stephen Polasky, S. R. C., Carl Folke, Bonnie Keeler. (2011). Decision-making under great uncertainty: environmental management in an era of global change. Trends in Ecology & Evolution, 26(8), 398-404. doi:https://doi.org/10.1016/j.tree.2011.04.007

Tilmant, A., & Kelman, R. (2007). A stochastic approach to analyze trade-offs and risks associated with large-scale water resources systems. Water Resources Research, 43(6). doi:https://doi.org/10.1029/2006WR005094

APPLICATION OF CLIMATE CHANGE PROJECTIONS IN DRAINAGE PROJECT PLANNING FOR AGRICULTURAL INFRASTRUCTURE IN JAPAN

Takigawa Takuya[1], Watanabe Yasuhiro[2], Tsuruda Shinya[2], Yuasa Kazuhiro[2], Hotta Naoyuki[2], Washino Kenji[2]

1. Background

As the impact of climate change has become a bigger problem in recent years, damage to farmlands and agricultural facilities caused by heavy rainfall have become more severe and frequent in Japan. For this reason, the Ministry of Agriculture, Forestry and Fisheries of Japan (MAFF) is currently promoting inundation prevention measures in rural areas such as the installation of pump stations. Additionally, the utilization of flood control functions of agricultural dams and rainwater storage functions of paddy fields are being promoted by MAFF.

To design pump stations and other facilities, MAFF also sets standards for the size of drainage facilities by calculating an approximately 10-30 year return period based on observed precipitation in the past. However, there is a risk that inundation damage in rural areas will become more severe because the frequency of extreme weather events such as heavy rainfall is expected to increase due to climate change. MAFF is urged to develop new design standards in consideration of projected future precipitation, keeping in mind that MAFF needs to avoid building unnecessarily large-scale facilities.

Therefore, more accurate and reasonable projection methods for precipitation are needed.

Based on recent advancements and discussions of climate change projections through the Coupled Model Intercomparison Projects (CMIPs) and the Intergovernmental Panel on Climate Change (IPCC), Japanese universities and research institutes are developing datasets for future precipitation projections, especially for assessing weather extremes in small areas.

In light of the above, we conducted a case study to design drainage facilities using the latest climate change outlook.

2. Climate Change Projection Methods in Japan

Climate change projection relies on simulations of global atmospheric and land surface properties with three-dimensional grid networks (general circulation models, GCMs). GCMs simulate atmospheric properties (wind direction, pressure, and water vapor content) at each grid point with basic equations of atmospheric motion.

The high-resolution GCMs are recently developed and often used to assess the impact of climate change on regional extreme weather events. However, the high-resolution GCMs are computationally intensive and require a longer time for simulations. To keep the consistency of regional assessment with the global phenomena, the initial stage of GCM simulation generally covers the entire globe, and then the nested simulations with finer resolution regional climate models (RCMs) are used to downscale the projected datasets.

The initial simulations usually employ the atmosphere-ocean coupled GCMs (AOGCMs) to reflect the long-term trend of sea surface temperatures on atmospheric circulations. The spatial resolutions are approximately 100-300 km. Then, the atmospheric models are nested within the results of AOGCMs to simulate the atmospheric circulation alone with the grid of 20-60 km. Lastly, the finer resolution RCMs are used to evaluate the regional climate at 2-5 km resolutions.

[1] Water Resources Division, Rural Infrastructure Department, Rural Development Bureau, Ministry of Agriculture, Forestry and Fisheries
[2] Design Division, Rural Infrastructure Department, Rural Development Bureau, Ministry of Agriculture, Forestry and Fisheries

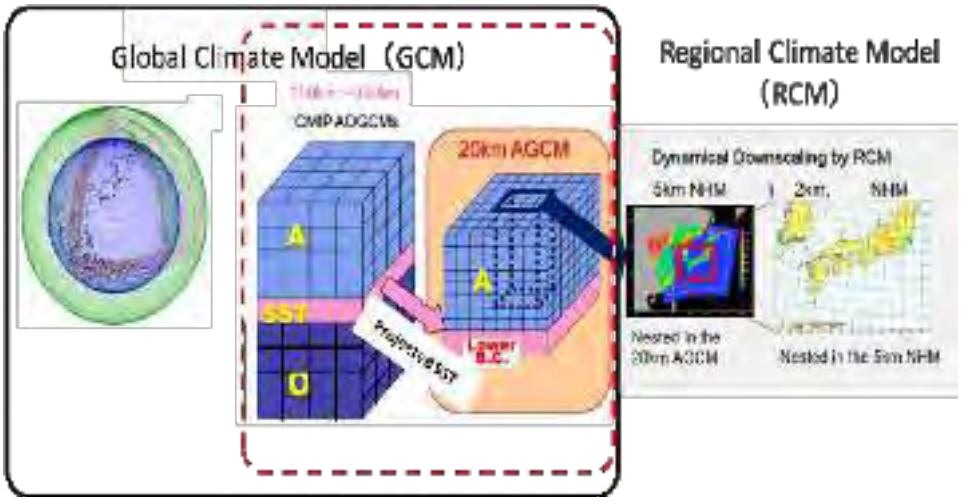

Fig. 1 Relationship of Climate Change Projection Models
(Japan Meteorological Agency, 2022, p213)
(Ministry of Education, Culture, Sports, Science and Technology, 2017, p5)

In Japan, the Meteorological Research Institute (MRI) compiled high-resolution climate change projections over Japan with the Atmospheric Global Climate Model (MRI-AGCM) and the Nonhydrostatic Regional Climate Model (NHRCM). Typical examples of Japanese high-resolution climate scenarios include d4PDF/d2PDF (database for policy decision-making for future climate change) and WRF02 (weather and research forecast).

The d4PDF/d2PDF consists of large ensembles of climate scenarios to assess the uncertainties including extreme weather events. It contains the results of simulations using high-resolution global (60 km spatial resolution) and regional (20 km) atmospheric models affected by the long-term projections in sea surface temperatures with an increase by 4 degrees Celsius/2 degrees Celsius. The datasets are further downscaled with MRI-AGCM and NHRCM to the spatial resolution of 5 km. Another typical dataset, WRF02, is based on the continuous (1950-2099) simulations of the MRIAGCM3.2S (spatial resolution: 20 km) under the RCP (Representative Concentration Pathway) 8.5 scenario (the highest emission scenario), downscaled using a WRF model to 2 km resolution. WRF is a regional climate model, mainly developed by the National Center for Atmospheric Research (NCAR).

3. Planning an Inundation Prevention Project in Consideration of Climate Change

Thanks to the development of climate change projection methods in Japan, MAFF started to examine climate adaptation measures for agricultural infrastructure design in 2020. We selected the Shironego district in Niigata Prefecture as a model area to plan an inundation prevention project and applied climate change projection methods.

(1) Selection of a Model Area

The Shironego district (Fig. 2) in the Niigata Prefecture is located in a lowland plain. The main crop is rice, but they also produce soybeans, vegetables, and fruits, of which yields decrease significantly when the area is flooded.

In this area, large-scale pump stations and drainage channels (Fig. 2) have been installed. Frequent inundation damage, however, is a recent concern in this area, which is caused by heavy precipitation under changing climate.

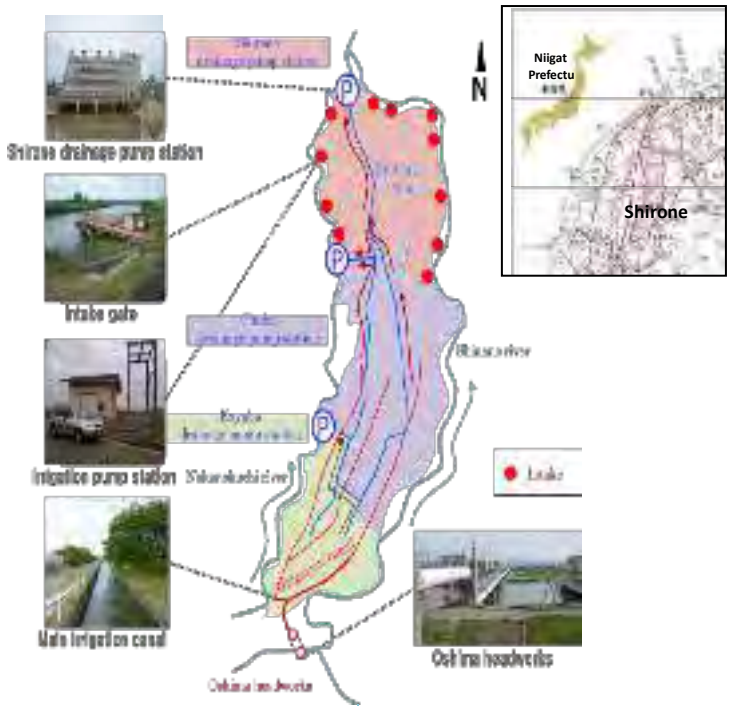

Fig.2: Irrigation and Drainage Facilities Map
(Shironego District in Niigata Prefecture)

(2) Application of Datasets in the Model Area

A large number of datasets for climate projections have been created because there are multiple scenarios for climate change. Downscaling the datasets in grids of 2 km, 5 km, 20 km, etc. is also conducted by some research institutes. We compared several datasets under different conditions to determine which datasets were appropriate to be used when planning an inundation prevention project in this area.

Because the cycle of national land improvement projects in Japan is approximately 40 years, we assumed that the drainage facilities installed around the 2020s would work until the 2060s. Thus, we selected datasets of d2PDF (assumed around 2040 under RCP 8.5 with 5 km resolution) and WRF02 (continuous simulations from 2020 to 2059 under RCP 8.5 with 2 km resolution) (Figure 3).

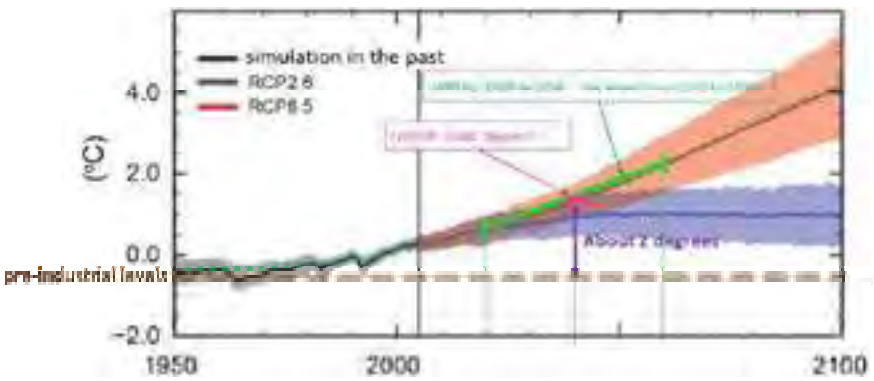

Fig.3: Calculation Period of d2PDF and
WRF02 (IPCC, 2013, p21)

To assess the reliabilities and bias of the simulated precipitation datasets, we compared the historical simulations of d2PDF and WRF02 with the observed precipitation (1980 to 2010). We calculated 1-to-3-day cumulative precipitation in the 30-year return period from (1) the observed precipitation in the past, (2) the simulated precipitation in the past, and (3) the simulated precipitation in the future. Then, we calculated (5) 1-to-3-day cumulative 30-year precipitation based on future projections by multiplying (1) the observed precipitation in the past by (4) the rate of change between (2) and (3).

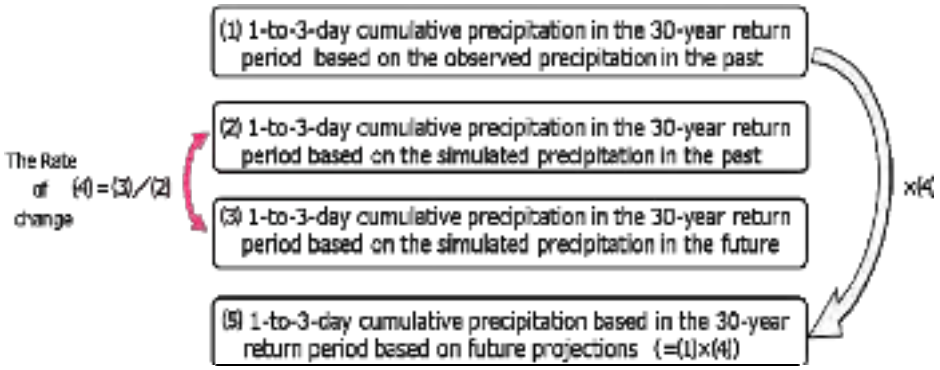

Fig.4: Procedure to Calculate 1-to-3-day cumulative precipitation in the 30-year return period based on future projections

Since the rate of change ((4) = (3) / (2)) was 1.12-1.19 in d2PDF and 1.03-1.30 in WRF02, we set the rate of change at 1.2, and (1) the observed precipitation in the past (1980 to 2010) in this area was multiplied by 1.2 to calculate (5).

Table 1 shows the result of the calculation in comparison with 30-year precipitation from 1940 to 1986, which was determined as the return period of precipitation in the previous inundation prevention project in this area.

Table 1: 3-day Cumulative Precipitation in the 30-year Return Period in the Shironego District

a. 3-day cumulative precipitation in the 30-year return period based on observed precipitation from 1980 to 2010	223.5mm
b. 3-day cumulative precipitation in the 30-year return period based on future projections (a * 1.2)	268.2mm
c. 3-day cumulative precipitation in the 30-year return period based on observed precipitation from 1940 to 1986	268.3mm

As a result, it is conceivable that the size of the facility can be reduced if the conventional designing method (a method to calculate a return period based on observed precipitation) is applied because the precipitation in the Shironego district seems to be decreasing from the period of 1940-1986 to 19802010 (a/c = 0.83). However, it is suggested that if the design method is based on future projections, it is appropriate to make the size of the facility equivalent to that of the previous project. Therefore, it is concluded that MAFF can determine the optimal size of facilities for future inundation prevention projects by applying the cumulative precipitation in the 30-year return period based on future projections, and then estimate the project cost, taking account of cost-effectiveness, a return period of the previous project, etc. through consultation and coordination with facility managers and relevant entities.

4. Future Necessary Works

We organized an approach to designing drainage facilities using projections of future precipitation in addition to observed precipitation in the past. MAFF plans to revise its design standards for

agricultural infrastructure after testing this method in other districts.

In this study, we primarily used d2PDF because of the general cycle of national land improvement projects, but it is expected that other new datasets will be developed in the future. Government agencies using these datasets need to beware that information is continuously updated.

This study is based on the outcomes of MAFF's "Study Group on Climate Change Measures for Rural Development". We thank the members of this study group for their guidance and cooperation.

This study also utilized the dynamical downscaling data, which are produced from d4PDF using the Earth Simulator, by the Social Implementation Program on Climate Change Adaptation Technology (SI-CAT) sponsored by the Ministry of Education, Culture, Sports, Science and Technology (MEXT).

References

- Japan Meteorological Agency, 2022, The Outline of The Numerical Weather Prediction 2021 , pp.35-38

https://www.jma.go.jp/jma/kishou/books/nwpkaisetu/R3/No54_all.pdf

- Ministry of Education, Culture, Sports, Science and Technology, 2017, Program for Risk Information on Climate Change: SOUSEI, p.5

https://www.jamstec.go.jp/sousei/jp/product/images/170303_sousei_seika_UP.pdf

- SI-CAT Guidebook Editorial Committee, 2020, SI-CAT Social-Implementation GuideBook, pp.106-107
- Ministry of Education, Culture, Sports, Science and Technology (MEXT) and Japan Meteorological Agency (JMA),2020, Climate change in Japan Report on Assessment of Observed/Projected Climate Change Relating to the Atmosphere, Land and Oceans December 2020, p.213

https://www.data.jma.go.jp/cpdinfo/ccj/2020/pdf/cc2020_shousai.pdf

- IPCC, 2013: Summary for Policymakers. In: Climate Change 2013: The Physical Science Basis. Contribution of Working Group I to the Fifth Assessment Report of the Intergovernmental Panel on Climate Change [Stocker, T.F., D. Qin, G.-K. Plattner, M. Tignor, S.K. Allen, J. Boschung, A. Nauels, Y. Xia, V. Bex and P.M. Midgley (eds.)]. Cambridge University Press, Cambridge, United Kingdom and New York, NY, USA., p.21

  https://www.ipcc.ch/site/assets/uploads/2018/02/WG1AR5_SPM_FINAL.pdf

A REVIEW: CLIMATE CHANGE AND AGRICULTURE WATER MANAGEMENT ADAPTATION STRATEGIES IN EAST JAVA, INDONESIA

Lina Indawati[1,2], Ray-Shyan Wu[2*], Riyan Benny Sukmara[1,3]

ABSTRACT

Climate change is a global issue. This has had an impact on many sectors. The agricultural sector is one of the sectors affected by climate change. Indonesia is an agricultural country. Indonesia has two annual seasons, namely the dry season and the rainy season. The existence of climate change causes changes in the precipitation cycle. The cycle of precipitation causes the duration of the annual season in Indonesia to be erratic. These conditions can disrupt the availability of water for agriculture, the availability of water exceeds the rainy season, causing flooding and reduced water availability in the dry season. The annual season is very influential on food security in Indonesia, especially rice agricultural production. There is a need for a water management strategy for agricultural sector in the face of climate change. To identify the right strategy in agricultural water management, it is necessary to analyze long term data related to precipitation in Indonesia and a critical review related to irrigation system in the agricultural sector. Based on long-term data from precipitation analysis and critical review shows that climate change has less influence on the increasing of temperature. However, it highly influence on shifting season which cause unpredictable planting season and time. Moreover, an adaptation strategy for agriculture water management in East Java, Indonesia is to provide facilities which store water sources to preserve water needs for planting season in dry season.

Keywords: Adaptation, Climate Changes, Temperature, Rainfall,

1. Introduction

Global temperatures are estimated to rise by approximately1.4-5.8 ℃ between 1990 and 2100 (IPCC, 2001) The global temperatures tend to approach 1 ℃ untill 2050. Then, they vary adequately, ranging from 2° C to 4° C by 2100 (Nelson et al., 2010). The increasing of global temperatures significantly raised heat waves (22%) and cold waves (20%), declined rainfall (19%), raised drought conditions (17%), declined Kalbaishakhi/tornadoes (14%), and floods (8%) (Abdullah-Al-Faisal et al., 2021). Rising temperature may increase evapo-transpiration, reduce surface and underground water and may lead to drought and water scarcity in the long run, which may cause grave reduction in crop yields due to lack of water for crops (IPCC, 2018) (Asare-Nuamah & Botchway, 2019). The increasing of global temperature caused by excessive greenhouse gases concentration from human activities leads climate change (Guo et al., 2021). Climate change due to global warming becomes a global issue. Climate change caused extreme weather, unpredictable and fluctuating rainfall. Climate change can lead to food security in Indonesia due to the effects of climate change such as causing water shortages, reducing soil moisture, reducing soil fertility, increasing sea level which causes flooding of rice and shrimp ponds, increasing evaporation and rainfall (Saptutyningsih et al., 2020). Climate change greatly affects on the water availability of the agricultural sector in the dry season and causes flooding problems

[1] Department of Civil Engineering, National Central University, Chung-Li, Taiwan
[2] Department of Civil Engineering, Faculty of Engineering, Universitas Sebelas Maret, 57126, Surakarta, Indonesia
[3] Department of Civil Engineering, Institut TeknologiKalimantan, Balikpapan, 76127, Indonesia
***Corresponding Author:** Lina Indawati, Email: linainda@staff.uns.ac.id

in the rainy season. Rainfall intensity in Indonesia is around 50-500mm/year (BMKG, 2022). Rainfall intensity in most of Indonesia area increase 5% until 25% with increasing temperature around 1. ℃ until over 1.3 ℃ in 2020-2049. Moreover, Indonesia's agriculture consists entirely of 34.58 million hectares of land available for wet land for rice production around 7.38 million ha which is highly dependent on water availability and the rest agriculture land available for other food crops which is low to medium dependent on water availability (Agricultural Research and Development Agency, 2015) The reduced availability of water in the dry season and flooding in the rainy season cause crop failures so that it can disrupt food security in Indonesia.. Indonesia's rice production decreased by around 25% due to climate change in 2014 (Fadhliani, 2016).

Therefore, the aim of this study is to mitigate the impacts of climate change on agriculture water resources of Indonesia which focus on two approaches of adaptation and strategy invention, simultaneously. This study reviews recent advances in understanding and reducing the impact of climate change on agricultural water resources by finding the best adaptation, strategies and policies invention presented in the form of a literature study. The obtained result may also be adapted outside Indonesia, especially in the island countries with similar season and rain intensity characteristics which the agricultural sector is important concern.

2. Methodology

2.1. Study area

This study was carried out in several regions in East Java Province, Indonesia, as shown in Figure 1 (Red colored area). There are 5 regions were chosen, such as Surabaya City, Lamongan Regency, Bojonegoro Regency, Ngawi Regency, and Banyuwangi Regency. We selected these regions because East Java is the largest agricultural region in Indonesia (IndonesiaBaik, 2022). According to data from Badan Pusat Statistik (BPS-Statistics Indonesia), the total crop (gabah kering) production of East Java Province in 2022 will be approximately 9.52 million tons, or approximately 17.4 percent of the national total (BPS, 2022).

Figure 1. Study Locations

According to the Indonesia Statistics Agency, East Java is occupied the first rank to be the largest Rice production in Indonesia followed by Central Java in the second and West Java in the third (BPS, 2023). Total rice produced by East Java approximately 5,593,330 tons in 2023 with the highest production region is Lamongan Regency with approximately 513,766.76 tons (see Figure 2).

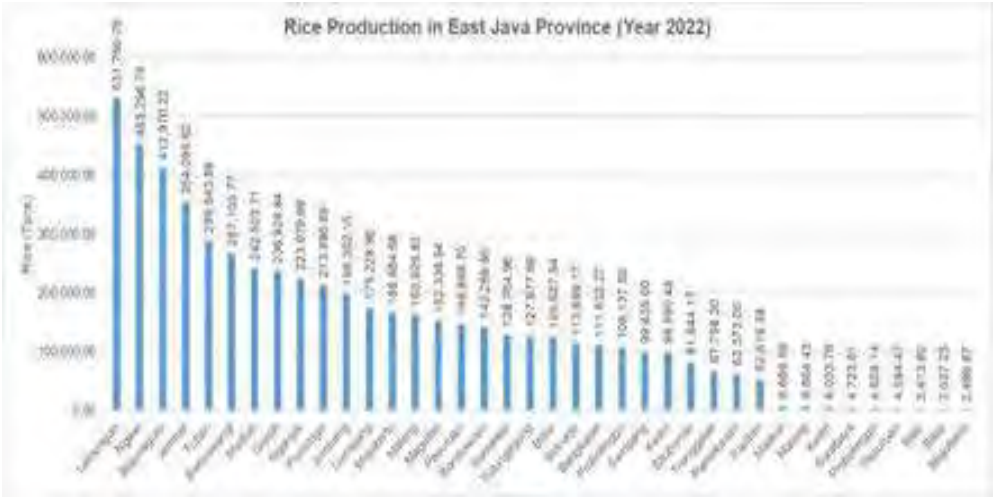

Source: (BPS Jawa Timur, 2022)

Figure 2. Rice Production of East Java Province

2.1.1. Surabaya City

Surabaya, the capital of East Java province and the second-largest city in Indonesia, is located at latitude -7^{O}14'57.01'' S and longitude 112^{O}45'2.9'' E, covering an approximate area of 32,636 square kilometers. Located in the east coast of Java Island and near the Madura strait, most of Surabaya's terrain comprises low-laying areas, constituting about 80.72 percents of the total area. The remaining area is characterized by the low-hilly regions, ranging from 25 to 50 meters above sea level which scattered in the western and southern parts of Surabaya.

Surabaya is categorized as the topical monsoon climate with two distinct seasons, rainy season (November to April) and dry season (May to October). During rainy season, Surabaya experiences heavy rainfall and increased humidity, the monsoon wind bring moisture from the northwest and lead to frequent rain showers and thunderstorms and often can be a trigger of flood events. In other hand, during dry season, Surabaya has lower humidity and decreasing rainfall intensity. However, due to the location of Surabaya near the coastal area, the climate is influenced by the coast and still can lead to the occurrence of occasional rain showers during the dry season.

The average temperature for the city was 28.7^{O}C, and it receives between 36% and 89% sunshine. The peak rainfall occurs during February, with an average monthly rainfall of approximately 155 mm and the mean of relative humidity of 75.2% (Wibawa et al., 2023).

2.1.2. Lamongan Regency

Lamongan Regency is located on Northern coastal area of Java Island. Astronomically, Lamongan is located at latitude 6^{O}51'64'' to 7^{O}23'06'' S and longitude 112^{O}33'45'' to 112^{O}34'45'' E, with a total area of 1759.85 square kilometers, or approximately 3.78% of the total area of East Java Province. Lamongan Regency geographical boundaries include the Java Sea to the north, Gresik Regency to the east, Jombang and Mojokerto Regencies to the south, and Bojonegoro Regency to the west. Due to its location which in coastal location, Lamongan Regency has 47 mile of coastline (Rudianto et al., 2022).

Topography of Lamongan Regency is dominated by three main altitude ranges. Approximately 50.17 percent of the region consist of lowland areas with altitude 0 to 25 msl (mean sea level). Areas with altitude ranging from 25 to 100 msl make up 45.68 percent of the region, while

remaining portion is occupied by areas above 100 msl. According to the data from Statistic Agency of Lamongan regency, Lamongan is divided by three types characteristic zones (see Figure 3), namely Zone 1 is a lowland area with moderate fertile soil which located in the center-south of the region. Zone 2 is a karst area with moderate soil fertility. Zone 3 is the flood prone area which located in the center-north of the region and close to the Bengawan Solo River (BPS Lamongan, 2021). The land cover composition in Lamongan regency is dominated by forest/garden with total coverage is 32.63 percents of the total region area and the Paddy field covers about 16.882 percents (Hariyanto et al., 2019).

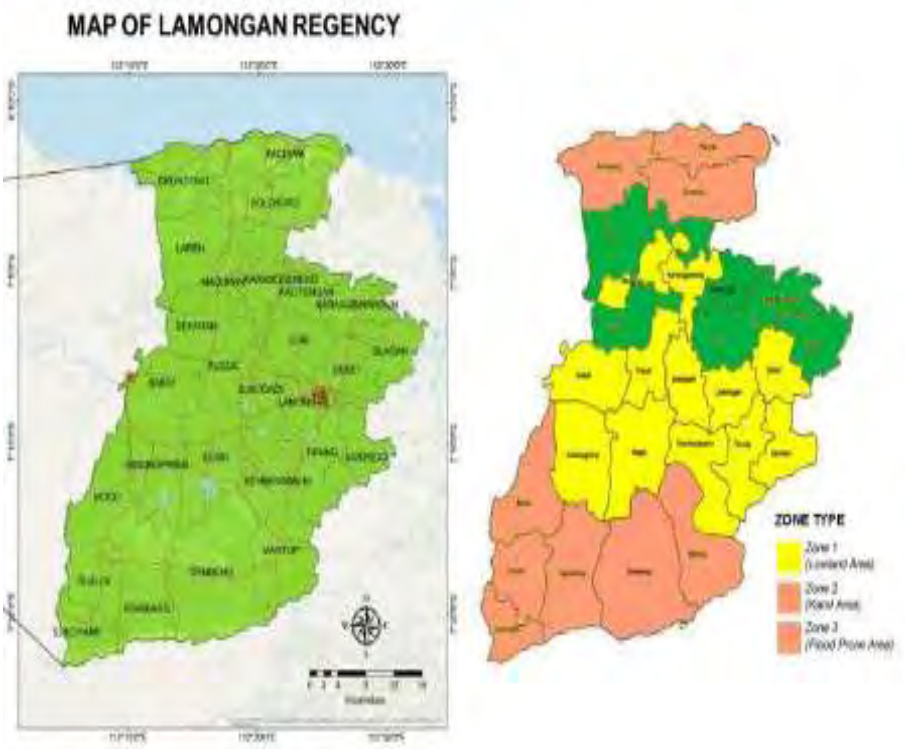

Adopted from (BPS Lamongan, 2021)

Figure 3. Zone Type of Lamongan

The climatic condition of Lamongan Regency is nearly identical to those in Surabaya City, however the average temperature in Lamongan is slightly lower than Surabaya. It's because the development in Lamongan is not as massive as in Surabaya. The average monthly temperature is ranged between 22.44^{O}C to 28.97^{O}C. The minimum and maximum monthly temperature ranges between 22.40^{O}C and 25.10^{O}C and 31.19^{O}C and 33.60^{O}C, respectively. In terms of precipitation, the lowest monthly rainfall in Lamongan Regency is 2.00 mm in September and the maximum monthly rainfall is 589.90 mm in January (BPS Lamongan, 2021).

2.1.3. Bojonegoro Regency

The Bojonegoro Regency is known as the Food and Energy Barn (Agustono, 2021). Astronomically, Bojonegoro is located at 6^{O}59' to 7^{O}37' S and 112^{O}25' to 112^{O}09' E with total area approximately 2307.06 square kilometers. Administratively, Bojonegoro location is adjacent to Tuban regency in the North, Lamongan Regency in the east, Madiun, Nganjuk and Jombang regencies in the south, Ngawi and Blora regencies in the west (BPS Bojonegoro, 2023).

Bojonegoro is the neighboring region of the Lamongan Regency. Topographically, Bojonegoro is dominated by high slope land (Saragih et al., 2018) with altitude ranges around 6.25 msl to 900 msl. The slope distribution is divided by 4 classes, such as 0-8%, 8-15%, 15-25%m and > 25% (see Figure 4). The slope 0-8% extends from the southwest to the southeast part of

Bojonegoro, whereas the slopes 15-25% and > 25% are located in the southern part of the region (Halil, 2018).

Modified from (Halil, 2018)

Figure 4. Slope map of Bojonegoro Regency

According to the study of the Halil (2018), Bojonegoro has average annual precipitation between 1500 to 2000mm per year in the majority of the region's areas and more than 2000 mm in the high altitude areas (Halil, 2018). The surface temperature in Bojonegoro is varied into several categories, there are Category 1 (20 to 30OC) which locate in some districts in the border of Bojonegoro regency. Category 2 (20-35OC) spreads out to almost all districts, and Category 3 (> 35OC) is specifically in the Oil and Gas Mining Industrial areas in the Gayam District (Rendra & Putri Tamara, 2020).

2.1.4. Ngawi Regency

Ngawi Regency is the one of several regions in Java Island whose has not ocean border or called land locked regions. Astronomically, this regency is located at latitude 7O21' to 7O31' S and longitude 110O10' to 111O40 E which has total area approximately 1295.98 square kilometers and divided by 19 district (BPS Kabupaten Ngawi, 2023).

Topographical condition of Ngawi Regency is considerably flat, wavy, hilly to high mountains with an altitude range between 40 to 3031 msl. Comparing to the three previous regions, Ngawi has lower temperature which likely due to its higher altitude. The average monthly temperature is ranged between 24.5OC to 26.7OC and the montly minimum and maximum temperature are about 16.2OC and 31.2OC, respectively (BPS Kabupaten Ngawi, 2023).

Land use in Ngawi Regency was split to the six categories, there are Residential, tourism, and industrial areas (built-up area) make up about 19.26% of the land in Ngawi Regency. Dry cropland makes up about 36.19% of the area, forest makes up about 0.26% of the area, wet cropland makes up about 43.75% of the area, and inland water bodies make up about 0.54% of the area.

Climatological data shows that Ngawi Regency experiences slightly higher precipitation compared to its two neighboring regencies, Lamongan and Bojonegoro. The average monthly precipitation in Ngawi is approximately 319.835 mm, with the maximum reaching about 665 mm per month, and the lowest recorded at approximately 47.4 mm per month (BPS Kabupaten

Ngawi, 2023). However, the results of the study, based on spatio-temporal data analysis revealed that Ngawi has encountered drought hazards in various regions and years. For instance, August 2015 was classified as an extreme drought period, while November 2015 experienced moderate to high drought conditions. Additionally, December 2021 faced a moderate drought situation, with some mountainous areas experiencing extreme drought conditions (Inayah et al., 2023).

2.1.5. Banyuwangi Regency

Banyuwangi is located in eastern tip of Java Island and is the largest region in East Java Province. It is bordered by the Bali Strait to the east, Situbondo Regency to the north, Bondowoso and Jember regencies to the west and Indian Ocean to the south (see Figure 1). Banyuwangi Regency has divided by 24 districts covering a total area of approximately 5782.50 square kilometers. It has lengthy coastline that stretched 175.8 km from the south to east of the region. Geographically, Bayuwangi is located at 7O43' to 8O45' S and 113O53' to 114O38' E (BPS Banyuwangi, 2023). Banyuwangi has a varied topography due to its altitude, which ranges from 0 to more than 1000 msl. The portion of the territory in the east is characterized by the region's flat terrain, while the portion of the region in the west is characterized by the area's step mountainous area (Nuryadi & Agustiarini, 2018). The border area with the Bondowoso Regency in the west is the part of Raung Mt. and Merapi Mt. with the highest altitude approximately 3344 msl and 2799 msl, respectively.

The climate condition of Banyuwangi is categorized as the tropical climate type with two distinct seasons: the wet season (October to April) and the dry season (April to October). The average temperature in year 2022 is 27.1OC, with the maximum and minimum temperature recorded at 34.OC, and 21OC, respectively. For the highland areas, the temperature can be less than 19OC. Total amount of annual precipitation was approximately 1841.3 mm. The dry season in Banyuwangi is caused by modest increase in cloud cover and the low pressure in the northwest of Australia, which result in an increase in wind speed, sea waves and decrease the cloud growth, then the sunlight is not blocked by cloud. This is makes Banyuwangi to be dry, but the air is quite cold due to the heat absorbed by the earth from the morning to the evening, which is then released back into the atmosphere with high intensity at the night (Azmi et al., 2021). According to the Koppen climate classification, the vast majority of Banyuwangi has categorized as wet and dry climate. The wet and dry climate means that rainfall can occur during dry season with the mild and normal rainfall intensity.

2.2 Literature Review

Literature studies were focused on scientific journals, which also sourced from websites that discuss agriculture water management, countries, rainwater intensity in Indonesia, and the typical water consumption in Indonesia. Meanwhile, secondary data related to long-term rainfall is obtained from BMKG. Other data such as irrigation facilities were obtained from the Indonesian statistical data center

3. Results and Discussion

3.1 climate change-related agriculture water management adaptation in Indonesia

3.1.1. Overview Spatio-temporal trends of watershed rainfall-runoff

Trend Rainfall intensity during the rainy season tends to decrease based on rainfall data from 2000 to 2022 (Figure 5). The highest rainfall intensity occurs in February and March each year. Since 2016 the intensity of rainfall has increased but not significantly. Climate change affects the shift of dry and rainy seasons.

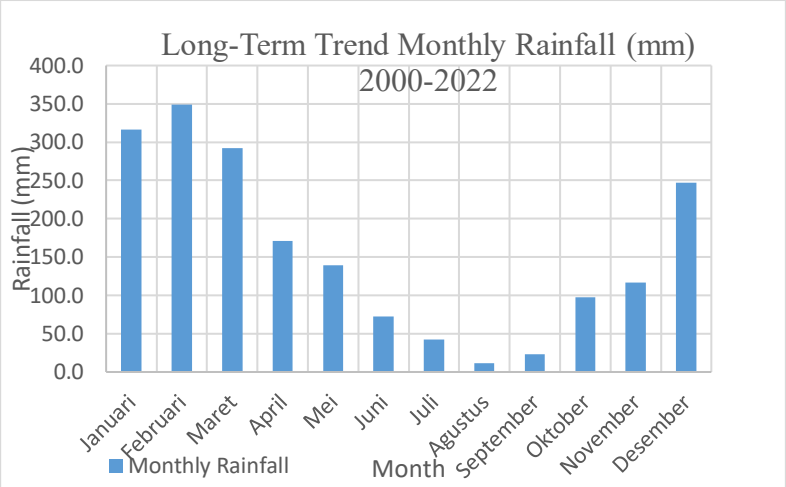

Figure 5. Long-Term Trend Monthly Rainfall (mm) 2000-2022, (Source:BMKG, 2023)

3.1.2. Overview Spatio-temporal trends of temperature

The following temperature trends were obtained using BMKG observation data from 1981-2020(Figure 6). Based on the processing results of temperature trends in Indonesia, in general, the temperature in Indonesia, both the minimum, average and maximum temperatures, has a positive trend with a magnitude that varies around 0.03 °C each year. This can be interpreted that the temperature will increase by 0.03 °C every year so that in 30 years the location will increase by 0.9 °C. Climate change does not have too large an effect on temperature rises in Indonesia. However, climate change causes a shift in the seasons. However, this slight increase in temperature causes a decrease in rainfall intensity. The extreme climate events was a shifting of season, particularly for the planting season, and the time where the water sources were depleted. In terms of the sequence of extreme climate events, that long period of dry season occurred every 8 to 10 years (Widyanti and Dittmann, 2014).

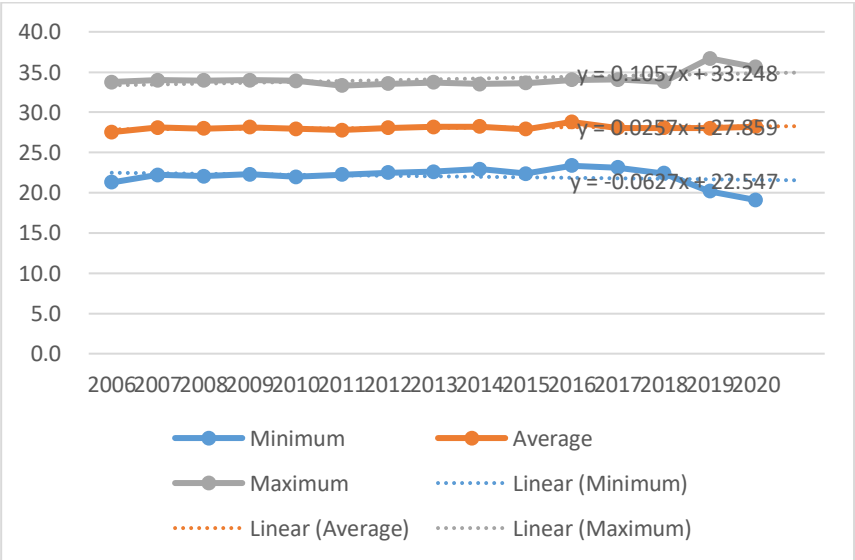

Figure 6 Trends of Temperature (BMKG, 2022)

3.3 Overview of land use and Irrigation facilities

3.3.1 Land use of Surabaya City

As a metropolis area and the significant city development, the majority of Surabaya's land cover consist of built-up areas with 49%, agriculture is 39% and water body/inland water approximately about 15% (Widyastuty et al., 2023). However, only 1704.83 hectares of cropland are still in production and spreads across the western and eastern part of Surabaya (BPS Surabaya, 2023).

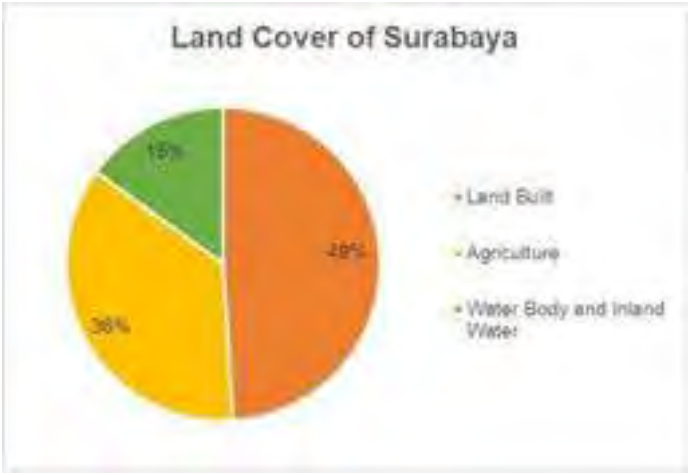

Source: Widyastuty et al (2023)

Figure 7. Land Use of Surabaya

3.3.2 Land use of Lamongan Regenc

According to the data from Statistic Agency of East Java Province, Lamongan's Agriculture production (paddy) in 2022 is ranked in first position over all region in East Java province with total production approximately 531.766,76 tons. It is increasing compared to the year of 2021 (likely due to COVID-19). However, according to the Indonesia Disaster Risk Index published by Badan Nasional Penanggulangan Bencana (BNPB-Disaster Agency of Disaster Countermeasure), Lamongan was categorized as high risk among all districts in term of the severity of the drought (BNPB, 2022).

Figure 8. Zone Type of Lamongan

3.3.3 Land use of Bojonegoro Regency

Related to the Agriculture in Bojonegoro Regency, the diagram of agricultural production of paddy commodity in East Java shows that Bojonegoro Regency occupied the third position in the total amount of paddy production (see Figure 2). If we dig deeper in the historical data, the paddy productivity of Bojonegoro Regency has a significant increment until more than 1 million tons per year between year 2014 and 2015 (Andika, 2021) but the production has declining trend until 2022 by only 412907.22 tons per year as shown in Figure 2. The declining trend of the paddy production likely because the development of Oil and Gas Industry which converted several cropland areas become the oil mining areas (Danugroho, 2022).

3.3.4 Land use of Ngawi Regency

Regarding to the agriculture condition, the center area of Ngawi dominated by a plain area with fertile soil agriculture land. The northern part is dominated by the limestone rock land with low soil fertility. The south part is a hilly and mountainous area with the slope more than 45% (Purnama et al., 2021). According to the data from Statistic of East Java, Ngawi is ranked in the second highest crop production with total annual production in year 2022 approximately 453296.74 tons (BPS Jawa Timur, 2022). However, the study conducted by Muttaqin and Ridho (2022) stated that one of district in Ngawi regency has experienced the crop failure (*gagal panen*) and suffered losses up to 7254 tons in one year crop production (Muttaqin & Ridho, 2022). Another potential disruption of agriculture production can be a soil degradation which could be triggered by anthropogenic activities or natural factors, such as natural hazard or climate change. Mujiyo et al (2019) revealed that the potential for soil degradation in Ngawi Regency is somewhere between low and moderate, particularly in Pitu District. This is because to several parameters, such as soil texture, bulk density, total porosity and soil permeability. Inability of the soil to drain water quickly can lead to an increase in runoff, which in turn can lead to severe soil erosion (Mujiyo et al., 2018). The changing pattern of rainfall which could be triggered by climate change will increase the risk of soil degradation.

3.3.5 Land use of Banyuwangi Regency

Regarding to the Agriculture condition, Banyuwangi has ranked in the sixth place in case of rice production in the East Java province. Annual production recorded in 2022 approximately 267105.77 tons. According to the recorded data from East Java Statistic Agency, there has been significant decrease in rice production between 2018 to 2023. The production decreased from 306073 tons in 2018 to 270467.76 tons in 2020. However, in 2021, the rice production experienced the bounced-back, increasing their productivity to 299536.04 tons, but it declined again to 267105.77 in 2023.

3.3.6 Irrigation Facilities

One of the adaptations of climate change in East Java in facing shifts in the rainy and dry seasons is to build rainwater reservoirs such as reservoirs, ponds or dams. In Indonesia, the collection of rainwater for agricultural irrigation is known as Dam, Reservoir or Dam. One of the largest rice producing cities has the largest number of dams and ponds (Figure 9).

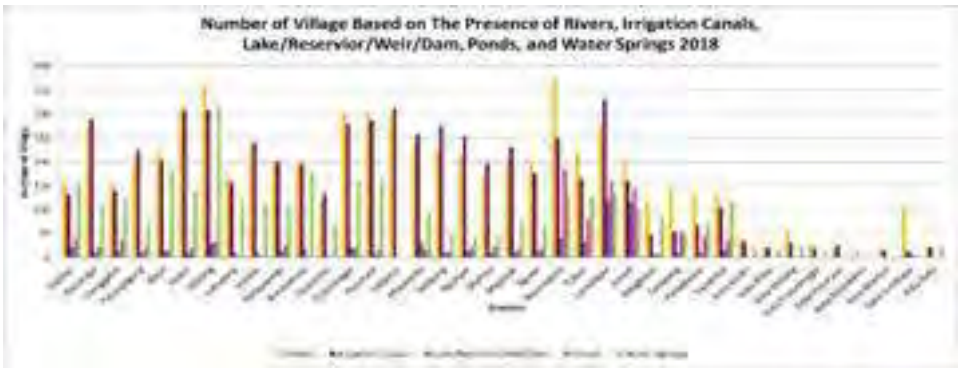

Figure 9. Irrigation Facilities

3.4 Overview of Agriculture management adaptation strategies

Several adaptation steps have been taken by policy makers and the community to deal with climate change disasters. One example of adaptation carried out by the community is as follows. Planting cultivars resistant to drought (cassava, maize, soybean, and groundnut) or doing tumpangsari between those cultivars. Several adaptation measures have been implemented by local farmers, mainly through crop diversification, crop intensifification, and socioeconomic adaptation (Widyanti and Dittmann, 2014).

Meanwhile, several strategies carried out by the government apart from building irrigation facilities are building weather monitoring. BMKG has 22 station climatology, more than 120 meteorological stations, and 31geophysical stations that provide climate data supply and about 5000 cooperation posts (rain post, postal evaporation, climate post, and meteorological station of special agriculture/SMPK). Online observation consists of Automatic Weather Station (AWS), Automatic RainGauge (ARG), and Agriculture Automatic Weather Station(AAWS).

Currently installed and monitored a total of 697 online tools are available divided by about 120 AAWS and the rest is divided almost the same, namely ARG or AWS. AAWS has additional observations of soil conditions in addition to atmospheric weather observations. Besides that, BMKG tools has 34 radar stations that continuously monitor extreme weather events in locations close to main airport

BMKG also has monitoring of using satellite imagery and also observations at sea based on Buoy data in the Pacific Ocean and in the Indian Ocean. Data from the Buoy network is used to monitor the current conditions of regional and global status climate phenomenon conditions.

Conclusions

The effect of climate change on agriculture in East Java is a shift in the rainy and dry seasons. Seasonal shifts affect the planting season because farmers in East Java still depend on the season. One of the adaptations made by the community is the tumpeng sari planting method. In addition, the government is also building irrigation and weather monitoring facilities.

References

Abdullah-Al-Faisal, Abdulla - Al Kafy, Foyezur Rahman, A. N. M., Rakib, A. Al, Akter, K. S., Raikwar, V., Jahir, D. M. A., Ferdousi, J., & Kona, M. A. (2021). Assessment and prediction of seasonal land surface temperature change using multi-temporal Landsat images and their impacts on agricultural yields in Rajshahi, Bangladesh. *Environmental Challenges*, *4*. https://doi.org/10.1016/j.envc.2021.100147

Asare-Nuamah, P., & Botchway, E. (2019). Understanding climate variability and change: analysis of temperature and rainfall across agroecological zones in Ghana. *Heliyon*, *5*(10). https://doi.org/10.1016/j.heliyon.2019.e02654

Agustono. (2021). Peran Sektor Pertanian Dalam Pertumbuhan Dan Stabilitas Produk Domestik Regional Bruto Di Kabupaten Bojonegoro. *SEPA: Jurnal Sosial Ekonomi Pertanian Dan Agribisnis*, *8*(1), 14–21. https://doi.org/https://doi.org/10.20961/sepa.v8i1.48841

Andika, Y. A. (2021). Determinants of Production of Agricultural Commodities of Food Crops in Bojonegoro Regency (Case Study of Farmers Accessing Tani Card and Non Accessing Tani Card). *East Java Economic Journal*, *5*(1), 58–74. https://doi.org/10.53572/ejavec.v5i1.60

Azmi, A. U., Hadi, A. F., Anggraeni, D., & Riski, A. (2021). Naive bayes methods for rainfall prediction classification in Banyuwangi. *Journal of Physics: Conference Series*, *1872*(1), 0–8. https://doi.org/10.1088/1742-6596/1872/1/012028

BMKG. (2022). *Climate Change Projection*.

BNPB. (2022). *Indeks Resiko Bencana Indonesia* (Vol. 1). Badan Nasional Penanggulangan Bencana. https://inarisk.bnpb.go.id/pdf/BUKU IRBI 2022.pdf

BPS. (2022). *Luas Panen, Produksi, dan Produktivitas Padi Menurut Provinsi 2020-2022*. Badan Pusat Statistik Republik Indonesia. https://www.bps.go.id/indicator/53/1498/1/luas-panen-produksi-dan-produktivitas-padi-menurut-provinsi.html

BPS. (2023). *Statistik Indonesia 2023*. Badan Pusa Statistik Republik Indonesia. https://www.bps.go.id/publication/download.html?nrbvfeve=MTgwMThmOTg5NmYwOWYwMzU4MGE2MTRi&xzmn=aHR0cHM6Ly93d3cuYnBzLmdvLmlkL3B1YmxpY2F0aW9uLzIwMjMvMDIvMjgvMTgwMThmOTg5NmYwOWYwMzU4MGE2MTRiL3N0YXRpc3Rpay1pbmRvbmVzaWEtMjAyMy5odG1s&twoadfnoarfeauf=MjAyMy0wNy0zMSAwODozNzozNw%3D%3D

BPS Banyuwangi. (2023). *Kabupaten Banyuwangi dalam Angka 2023* (Issue 1). Badan Pusat Statistik Kabupaten Banyuwangi.

https://banyuwangikab.bps.go.id/publication/2023/02/28/eed06d8c5cd49bc2664fb1f4/kabupaten-banyuwangi-dalam-angka-2023.html

BPS Bojonegoro. (2023). *Kabupaten Bojonegoro dalam Angka 2023*. Badan Pusat Statistik Kabupaten Bojonegoro. https://bojonegorokab.bps.go.id/publikasi.html

BPS Jawa Timur. (2022). *Produksi Padi dan Beras Menurut Kabupaten/Kota di Provinsi Jawa Timur, 2021 dan 2022*. Badan Pusat Statistik Provinsi Jawa Timur.

BPS Kabupaten Ngawi. (2023). *Kabupaten Ngawi dalam Angka 2023*. Badan Pusat Statistik Kabupaten Ngawi. https://ngawikab.bps.go.id/publication/download.html?nrbvfeve=OTc5YzBiYmNlNDI5Mzc2MmFiODQ0YmJi&xzmn=aHR0cHM6Ly9uZ2F3aWthYi5icHMuZ28uaWQvcHVibGljYXRpb24vMjAyMy8wMi8yOC85NzljMGJiY2U0MjkzNzYyYWI4NDRiYmIva2FidXBhdGVuLW5nYXdpLWRhbGFtLWFuZ2thLTIwMjMuaHRtbA%253D%253

BPS Lamongan. (2021). *Kabupaten Lamongan Dalam Angka 2021*. Badan Pusat Statistik Kabupaten Lamongan. https://lamongankab.bps.go.id/publication/2021/02/26/28b8635a338b571c7b2500b3/kabupaten-lamongan-dalam-angka-2021.html

BPS Surabaya. (2023). *Kota Surabaya Dalam Angka 2023*. Badan Pusat Statistik Kota Surabaya. http://bappeda.jatimprov.go.id/bappeda/wp-content/uploads/potensi-kab-kota-2013/kota-surabaya-2013.pdf

Danugroho, A. (2022). Threats To Food Security in The Food and Energi Barn Area: Agricultural Land Function Change in Bojonegoro Regency. *Jurnal Aristo (Social, Politic, Humainora)*, *10*(2), 218–231. https://doi.org/10.24269/ars.v10i2.5056

Fadhliani, Z. (2016). The Impact of Crop Insurance on Indonesian Rice Production. *University of Arkansan, Fayetteville*.

World Bank. (2021). Climate Risk Country Profile: Indonesia. In *World Bank Publications*.

Guo, L. N., She, C., Kong, D. Bin, Yan, S. L., Xu, Y. P., Khayatnezhad, M., & Gholinia, F. (2021). Prediction of the effects of climate change on hydroelectric generation, electricity demand, and emissions of greenhouse gases under climatic scenarios and optimized ANN model. *Energy Reports*, *7*. https://doi.org/10.1016/j.egyr.2021.08.134

Hill, H., Resosudarmo, B. P., & Vidyattama, Y. (2010). Economic geography of Indonesia: location, connectivity, and resources. *Reshaping Economic Geography in East Asia*, *50*(5).

Halil, A. (2018). Sensitivity pattern of drought region in Bojonegoro. *MATEC Web of Conferences*, *229*, 1–6. https://doi.org/10.1051/matecconf/201822902009

Hariyanto, T., Pribadi, C. B., Purwitasari, A., & Kurniawan, A. (2019). Identification of potential drought in Lamongan Regency. *IOP Conference Series: Earth and Environmental Science*, *389*(1). https://doi.org/10.1088/1755-1315/389/1/012009

Inayah, A. M. N., Indriana, R. D., & N., M. I. (2023). Drought Analysis On Ngawi District West Jawa Using The Standardized Precipitation Index (Spi) Method Based On Rainfall Data 2012 To 2021. *International Journal of Progressive Science and Technologies*, *38*(2), 230–237. https://doi.org/http://dx.doi.org/10.52155/ijpsat.v38.2.5322

IndonesiaBaik. (2022). *10 Penghasil Padi Terbesar di Indonesia*. IndonesiaBaik.

IPCC. (2001). Climate Change 2001. Synthesis Report. IPCC Third Assessment Report (TAR). *Ipcc*.

IPCC. (2018). IPCC special report on the impacts of global warming of 1.5°C - Summary for policy makers. In *Ipcc - Sr15*.

Mujiyo, Sumarno, Sudadi, & Murti, R. W. (2018). Assessment of soil degradation in Pitu District, Ngawi Regency. *Journal of Degraded and Mining Lands Management*, *7*(2). https://doi.org/10.15243/jdmlm.2020.072.2049

Muttaqin, M. R., & Ridho, I. N. (2022). The Efforts of Government to Overcome Farmer Losses Due to Crop Failure in The Form of Protection for Farmers in Kwadungan District, Ngawi Regency Based on Laws. *Journal of Research in Social Science And Humanities*, *2*(1), 29–34. https://doi.org/10.47679/jrssh.v2i1.23

Nuryadi, & Agustiarini, S. (2018). Analisis Rawan Kekeringan Lahan Padi Kabupaten Banyuwangi Jawa Timur. *Jurnal Meteorologi Klimatologi Dan Geofisika*, *5*(2), 29–37. https://jurnal.stmkg.ac.id/index.php/jmkg/article/view/56

Nelson, G. C., Rosegrant, M. W., Palazzo, A., Gray, I., Ingersoll, C., Robertson, R. D., Tokgoz, S., Zhu, T., Sulser, T. B., Ringler, C., Msangi, S., & You, L. (2010). Food security, farming, and climate change to 2050: Challenges to 2050 and beyond. IFPRI Issue Brief No. 66. In *IFPRI Issue Brief*.

Purnama, I. L. S., Rahmawati, L., Primacintya, V. A., & Febriarta, E. (2021). The influence of aquifer material to the groundwater potency in Ngawi Regency. *E3S Web of Conferences*, *325*. https://doi.org/10.1051/e3sconf/202132508011

Rendra, M. I., & Putri Tamara, A. (2020). Analysis of Changes in Land Surface Temperature in the Oil and Gas Mining Industry Sector in Bojonegoro Regency. *Jurnal Sains Informasi Geografis*, *3*(2), 87. https://doi.org/10.31314/jsig.v3i2.661

Rudianto, R., Darmawan, V., Isdianto, A., & Bintoro, G. (2022). Restoration of coastal ecosystems as an approach to the integrated mangrove ecosystem management and mitigation and adaptation to climate changes in north coast of East Java. *Journal of Coastal Conservation*, *26*(4), 1–17. https://doi.org/10.1007/s11852-022-00865-4

Research, A., & Agency, D. (2015). *Indonesia's Agricultural Land Resources: Area, Distribution, and Potential Availability* (Agus Fahmuddin, N. Dedi, & H. Edi (eds.)). IAARD Press.

Saragih, I. J. A., Meygatama, A. G., Sugihartati, F. M., Sidauruk, M., & Mulsandi, A. (2018). Study of atmospheric condition during the heavy rain event in Bojonegoro using weather research and forecasting (WRF) model: Case study 9 February 2017. *IOP Conference Series: Materials Science and Engineering*, *332*(1). https://doi.org/10.1088/1757-899X/332/1/012025

Saptutyningsih, E., Diswandi, D., & Jaung, W. (2020). Does social capital matter in climate change adaptation? A lesson from the agricultural sector in Yogyakarta, Indonesia. *Land Use Policy*, *95*. https://doi.org/10.1016/j.landusepol.2019.104189

Wibawa, B. S. S., Maharani, A. T., Andhikaputra, G., Putri, M. S. A., Iswara, A. P., Sapkota, A., Sharma, A., Syafei, A. D., & Wang, Y. C. (2023). Effects of Ambient Temperature, Relative Humidity, and Precipitation on Diarrhea Incidence in Surabaya. *International Journal of Environmental Research and Public Health*, *20*(3). https://doi.org/10.3390/ijerph20032313

Widyastuty, A. A. S. A., Rukmana, S. N., & Feninlambir, H. (2023). Surabaya City Surface Temperature Distribution Based On Land Cover And Vegetation Density. *IOP Conference Series: Earth and Environmental Science*, *1186*(1), 012005. https://doi.org/10.1088/1755-1315/1186/1/012005

INNOVATIVE AGRICULTURAL SOIL AND WATER MANAGEMENT TECHNIQUE UNDER CLIMATE CHANGE

Dr. Shivaji Sangle[1] Dr. Pradeep Bhalage [2] Er Balasaheb Chivate[3] Ms. Shivani Sangle[4]

ABSTRACT

Indian agriculture is facing challenges due to several factors such as increased competition for land, water and labour from non-agricultural sectors and increasing climatic variability. Adaptive actions may be taken to overcome adverse effects of climate change on agriculture. Innovative agricultural practices and technologies can play important role in climate mitigation and adaptation. Further, creating the necessary innovative agricultural technologies and its adoption in agricultural systems will require innovations in policy, institutions and governance according to changing climate. There is a need to investigate and invest in alternate sustainable agricultural methods and approaches tailored to local and agro-climatic conditions which can generate economic benefits for local communities, use natural resources more effectively, and focus on improving health and nutrition simultaneously. Such approaches can emphasize minimizing inputs, and put the focus back on farmers while responding to the changing climate, reversing the deterioration of ecological systems, and increasing farmers' resilience and incomes. Saguna Rice Technique (SRT), now referred as Saguna Regenerative Technique, is a unique new method of cultivation of rice and related rotation crops without ploughing, puddling and transplanting rice on permanent raised beds. SRT is zero tillage, conservation agriculture type of cultivation, an innovative method introduced about 9 years back under leadership of Saguna Rural Foundation, Neral in the state of Maharashtra, India. It is a simple and adoptable technique based on conservation agriculture principal. It is an effective tool for sustainable agriculture, low cost cultivation and improve yield with high net returns. Numerous farmers in different district situated in Maharashtra State, India, has adopted SRT in their own farm and achieved good result. It saves 30 to 40 per cent cost of production, 50 per cent labour, 20 per cent loss of valuable silt and 30 to 40 per cent increase in productivity. This technique promotes zero or minimum mechanical soil disturbance, maintenance of a permanent soil cover and diversification of plant species. It enhances biodiversity and natural biological processes above and below the ground surface, which contribute to increased water and nutrient use efficiency, enhance productivity and sustained crop production. It indirectly and strongly supports soil and water conservation. SRT is helpful to the farmer i.e. end-user, to take initiative for improvement in productivity. It also reduces the irrigation water requirement apart from soil and water conservation.

Key Words: Innovative agricultural technique, Soil-Water Conservation, Saguna Rice Technique, zero tillage Technique, Climate change.

1.0 INTRODUCTION

Indian agriculture is facing challenges due to several factors such as increased competition for land, water and Labour from non-agricultural sectors and increasing climatic variability. Adaptive actions may be taken to overcome adverse effects of climate change on agriculture. Innovative agricultural practices and technologies can play important role in climate mitigation

1 Former Member (Economics), Maharashtra Water Resources Regulatory Authority (MWRRA), Mumbai-400005, (M.S.), India Email: sanglest@yahoo.co.in

2 Professor, Civil Engineering Department, Hi-Tech Institute of Technology, Waluj, Aurangabad, M.S., India Email: pradeep.bhalage@gmail.com

3 Director (Technical), International Commission on Irrigation and Drainage (ICID), Chanakyapuri, New Delhi – 110021, India Email: bachivate@icid.org

4 Full-Time Student, Master of Arts (Economics), Gokhale Institute of Politics and Economics, Pune (M.S), India - 411004 Email: 84shivanisangle@gmail.com

and adaptation. Further, creating the necessary innovative agricultural technologies and its adoption in agricultural systems will require innovations in policy, institutions and governance according to changing climate. There is a need to investigate and invest in alternate sustainable agricultural methods and approaches tailored to local and agro-climatic conditions which can generate economic benefits for local communities, use natural resources more effectively, and focus on improving health and nutrition simultaneously. Such approaches can emphasize minimizing inputs, and put the focus back on farmers while responding to the changing climate, reversing the deterioration of ecological systems, and increasing farmers' resilience and incomes. Saguna Rice Technique (SRT), now referred as Saguna Regenerative Technique, is a unique new method of cultivation of rice and related rotation crops without ploughing, puddling and transplanting rice on permanent raised beds. SRT is zero tillage, conservation agriculture type of cultivation, an innovative method introduced about 10 years back under leadership of Saguna Rural Foundation, Neral in the state of Maharashtra, India. It is a simple and adoptable technique based on conservation agriculture principal. It is an effective tool for sustainable agriculture, low cost cultivation and improve yield with high net returns. Numerous farmers in different district situated in Maharashtra State, India, has adopted SRT in their own farm and achieved good result. It saves 30 to 40 per cent cost of production, 50 per cent labour, 20 per cent loss of valuable silt and 30 to 40 per cent increase in productivity. This technique promotes zero or minimum mechanical soil disturbance, maintenance of a permanent soil cover and diversification of plant species. It enhances biodiversity and natural biological processes above and below the ground surface, which contribute to increased water and nutrient use efficiency, enhance productivity and sustained crop production. It indirectly and strongly supports soil and water conservation. SRT is helpful to the farmer i.e. end-user, to take initiative for improvement in productivity. It also reduces the irrigation water requirement apart from soil and water conservation.

2.0 OBJECTIVE

The main objective of this paper is to study innovative agricultural soil and water management technique under climate change. However, following are the specific objectives:

a) To study innovative Soil and Water conservation techniques.
b) To study Saguna Regenerative Technique (SRT) used for Soil and Water conservation.
c) To study impact of SRT on enhancement of water productivity in Maharashtra State, India.

3.0 METODOLOGY

The present study is relying on both primary and secondary data. Secondary data are collected from various reports, plan documents and information from the research articles, journals and magazines, internet, etc. The primary data are collected from the Saguna Bagh, Neral. Saguna Bagh is an eco-friendly agro tourism rural farm. It is pioneer in adoption of Saguna Rice Technique in the State of Maharashtra, India and doing research on it from last 22 years. The results of three different experiments to judge the improvement in physical soil properties like to drainage, soil loss, and water conservation, conducted by Saguna Bagh are also enumerated.

4.0 NECESSITY OF INNOVATIVE AGRICULTURAL TECHNOLOGIES

There is a need investigate and invest in alternate sustainable agricultural methods and approaches adoptable to local and agro-climatic conditions which can generate economic benefits for local communities, use natural resources more effectively, and focus on improving health and nutrition simultaneously. Such approaches can emphasize minimizing inputs, and put the focus back on farmers while responding to the changing climate, reversing the deterioration of ecological systems, and increasing farmers' resilience and incomes. Addressing the challenges of climate change in agriculture necessitates a holistic approach that involves innovative technologies, supportive policies, strengthened institutions, and effective governance. The agriculture sector can adapt to a changing climate while promoting economic prosperity and safeguarding natural resources for future generations.

Climate Uncertainty: Climate change has led to increased variability in weather patterns, making it challenging for farmers to predict the timing of seasons, rainfall, and temperature

changes. Adaptive actions help farmers become more resilient and better prepared to cope with these uncertainties.

Crop Resilience: Adapting agricultural practices can enhance the resilience of crops to changing climatic conditions. By selecting innovative farming practices and cultivating climate-resilient crop varieties, farmers can improve the chances of successful harvests.

Water Management: Climate change can alter precipitation patterns, leading to more frequent and severe droughts or floods. Implementing adaptive measures, such as water-efficient irrigation systems, rainwater harvesting, and water storage, can help ensure a stable and sustainable water supply for agricultural needs.

Soil Conservation: Extreme weather events and temperature changes can degrade soil health and reduce its fertility. Adaptive actions that focus on soil conservation practices, like reduced tillage, mulching, and cover cropping, can help protect soil structure and nutrient content.

Pests and Diseases: Changes in temperature and humidity can impact the distribution and prevalence of pests and diseases. Adaptive actions, such as integrated pest management and disease-resistant crop varieties, can mitigate the risks posed by these agricultural threats.

Agricultural Diversification: Climate change can affect the suitability of certain crops and cropping patterns. Diversifying crops and adopting multiple cropping systems can spread risks and provide alternative income sources for farmers.

Innovations in Policy: To foster the development and adoption of innovative agricultural technologies, supportive policies are required. Governments and policymakers need to incentivize research and development in agriculture, provide funding for innovative projects, and create a conducive regulatory environment. Policy frameworks can encourage private sector participation, collaboration, and technology transfer to ensure that the benefits of innovation reach farmers effectively.

Innovations in Institutions: Effective institutions are crucial for the successful integration of innovative agricultural technologies into existing systems. Research institutions, extension services, and agricultural advisory bodies play a vital role in disseminating knowledge about new technologies and facilitating their adoption. Strengthening these institutions through capacity building and better outreach can ensure that farmers have access to the latest information and resources.

Innovations in Governance: Climate change is a complex and multidimensional issue that requires a coordinated approach across different levels of governance. Integrated governance mechanisms that involve multiple stakeholders, such as government agencies, research organizations, NGOs, and farmers' associations, can help create a cohesive strategy for promoting and scaling up innovative agricultural technologies. Transparent and accountable governance practices are essential to build trust and ensure the efficient implementation of climate-smart solutions.

Sustainable Agriculture for Economic Benefits: Sustainable agricultural methods not only help mitigate the impact of climate change but also offer economic benefits to local communities. Practices that focus on resource conservation, such as regenerative farming, zero tillage , conservation agriculture , mulching and crop rotation, can lead to cost savings and increased productivity over the long term. By reducing input costs and enhancing yields, farmers can improve their livelihoods and economic stability.

Efficient Use of Natural Resources: As climate change puts pressure on natural resources, it becomes crucial to use them efficiently. Micro irrigation, conserving soil moisture, and conserving Soil organic carbon (SOC) enable farmers to optimize resource use, reducing water and fertilizer wastage. This efficient use of resources contributes to environmental sustainability and resilience in the face of changing climate patterns.

Simultaneous Focus on Health and Nutrition: Climate change can impact food security and nutrition. Innovative agricultural practices that prioritize diverse and nutritious crop cultivation, promote agro-biodiversity, and encourage sustainable livestock management can contribute to improved diets and overall health. Emphasizing nutrition-sensitive agriculture ensures that communities are better equipped to withstand climate-related challenges to food availability and quality.

Knowledge and Technology Transfer: Adaptive actions often involve the dissemination of knowledge about climate-smart practices and the adoption of appropriate technologies.

Effective extension services and training programs can facilitate the uptake of these practices among farmers.

Food Security: Agriculture is the primary source of food for billions of people worldwide. By adapting to climate change, farmers can maintain or even enhance food production, contributing to global food security.

Economic Stability: Agriculture is a significant contributor to the economies of many countries, particularly in rural areas. Adaptation measures can safeguard agricultural productivity, incomes, and livelihoods, supporting overall economic stability.

Environmental Sustainability: Climate change impacts are not limited to agriculture alone. By implementing adaptive actions, farmers can contribute to broader environmental sustainability by reducing greenhouse gas emissions, conserving natural resources, and protecting ecosystems.

5.0 SAGUNA REGENERATIVE TECHNIQUE

Saguna Regenerative Technique (SRT), previously it was named as Saguna Rice Technique, is an innovative method of soil and water conservation. SRT is zero tillage; conservation agriculture type of cultivation, basically invented for rice in Kharif (rainy season) followed by pulses, vegetables and oil seed in successive season. SRT is introduced 10 years back, after 12 years (1999 to 2011) research, under leadership of Saguna Rural Foundation (SRF), Neral in the state of Maharashtra, India. It is a simple and adoptable technique based on conservation agriculture principal. It is fruitfully implemented in Saguan Bagh by Mr. Chandrashekhar Bhadsavale, Founder of SRF and then successfully adopted in 10 different districts of Maharashtra State by more than 3000 farmers under his leadership (Bhadsavale, 2015). Now it is spread over in 27 districts of Maharashtra States and adopted by more than 8000 farmers (Bhadsavale, 2023). The innovator Mr. Chandreshekhar Bhadsavale is honored with various national and state levle awards along with International WatSave Farmer's Award issued by International Commission on Irrigation & Drainage in the year 2016. It is an effective technique for sustainable agriculture, low cost cultivation and improved yield. SRT is a unique new method of cultivation of rice and related crops in rotation without ploughing, puddling and transplanting (rice) on permanent raised beds. Numerous farmers in different district situated in Maharashtra state, India, had applied SRT for se in their own farm and achieved good result. The permanent raised beds used in this method facilitates ample of oxygen supply to root zone area while maintaining optimum moisture condition there. Mr. Chandrashekhar Bhadsawle has made suitable changes in traditional crop cultivation to ease the laborious work of farmers and reduce the cost of cultivation. In the case of paddy cultivation, this technique prevents loss of soil fertility during puddling. In the case of rice and other crops, this technique prevents the loss of the fertile soil layer during heavy rains.

5.1 STEPS OF SAGUNA REGENERATIVE TECHNIQUE

Following are the saguna regenerative technique

Step 1 Preparation raised beds and plantation

At the start of this method good ploughing and tilling has to be done with available residual moisture or by providing irrigation. Desirable or available quantity of any organic manure may be spread over the field. Make it workable using a rotavator or power tiller. Then prepare the raised beds, finish it with top width of bed 1 meter and centre to centre distance 1.36 meter is desirable for growing all types of seasonal crops as shown in figure 1. Raised beds has to prepare only once for permanent use in subsequent season. The same beds will be used again and again to grow various crops in rotation.

Step 2 Punching holes

A special SRT frame of size 100 cms x 75 cms is used to punch holes in to the soil for dibbling the seeds. It can punch 20 holes at 25 x 25 cm in one stroke, when strikes manually over the raised bed. 3–4 days before rain begins, make holes on beds by SRT iron forma (Figure 2).

Step 3 Dropping seeds

Put 3 to 4 treated crop seeds in each hole, press it with mixture of manure or good soil (10 Kg. manure and 400 g. of NPK 15:15: 15). About 20 to 25 kg seeds and 175 kg fertilizer per

hectare land are usually sufficient to get good crop yield (Figure 3). Crop sowing can be done directly into the soil before the onset of good rains.

Step 4 Weed control

On next day after a good rain, a selective weedicide like Goal (Oxyfluorfen 23.5% EC) is sprayed at the rate of 1 ml per liter water (Figure 4).

Step 5 Maintain plant populations and apply fertilizer

At about 4 leaf stage carryout the gap filling by using extra seedlings from nearby hills. 25 to 30 days after sowing, manual weeding has to be done, without walking on beds and apply Dia Ammonium Phosphate (DAP) briskets or one tea spoonful of 15:15:15 NPK in between 4 hills / plants (Figure 5). Within few days the plots will start looking very nice. In case of rice crop to control attack of crabs, press Gliricidia leaves in the crab holes & plug with mud, Keep the bunds clean, and maintain the water levels in the rice plots.

Step 6 SRT Crop Harvesting Method

After the maturity of crop (Figure 6) harvest the crop at proper time. While harvesting cut the plants leaving 2 to 3 inches stem on the beds and their roots beneath the soil. It is very important to leave the roots of previous crop in to soil and spray the plot with weed killer like Glayphoset (15 lit water + 100 ml Glayphoset + about 200 g of sea salt or 150 g of Urea) 2 to 3 days after harvesting. On the same beds the next seasonal crop seed can be planted immediately after the harvest of previous crop. Same raised beds are to be used again and again without any ploughing or cultural operations.

Step 7 Post harvesting and planting in next season

Spraying of Glayphoset has to be done after 2 to 3 days harvesting of paddy. In case of rice crop this technique avoids mud formation and then transplanting of rice. With this technique, seeds can be sown without depending on the erratic behaviour of rainfall. This means that only optimum rainfall is sufficient for best sowing performance. Similarly, frequent dry spells during the cropping season do not cause moisture stress, soil cracking or immediate crop kill.

Soil fertility and crop rotation

Cereals are to be followed by pulses and oil seeds leaving the roots of previous crops in the same spot for slow decay without any agricultural operations (Zero till). This is the most important principal of SRT. It significantly improves the organic carbon and thereby fertility of the soil. Stubbles of 15 cm height should be left in the beds for slow rotting while harvesting the crop. The residual juice in paddy stubble has lot of nutrient is forced to decay at the same place

where a selective weedicide is applied. Thus direct usable forms of nutrients are made available and enhance the growth of the following crops on the same ground.

6.0 KEY FEATURES OF SAGUNA REGENERATIVE TECHNIQUE

Following are the key features of saguna regenerative technique

- **sustainable agriculture**

It is an effective tool for sustainable agriculture, low cost, reduces had work, simple cultivation prevents soil erosion, prevents silt loss, and improve yield with high net returns.

- **Low cost cultivation**

This technique promotes zero or minimum mechanical soil disturbance, It is a zero till _ saves Machines and its thousand liters of fuel which on otherwise used in cultural operations. In case of conventional paddy cultivation lots of labors are required while transplanting rice seedlings in mud, removal of weeds etc.; procurement of labor at right is more costly and very hard. Seed rate and fertilizer dose per ha is significantly less in SRT as there is no wastage, the observations shows that it saves 30 to 40 per cent cost of production

- **Improve yield with high net returns**

Numerous farmers in different district situated in Maharashtra State, India, has adopted SRT in their own farm and achieved good result. Over a period of two years, residual roots of six crops taken over the same field are left in the soil, the soil samples are tested before and after adoption of SRT indicates that, the 0.30 % initial organic carbon level in the soil incredibly rises to 2.5 % (Bhadsavale 2015). Different crops are sown and harvested with SRT over the field plots of Saguna Bag. SRT was first implemented in year the 2013 and then followed continuously. From 2016 onward significantly high number of farmers adopted SRT, by the end of year 2022 more than 8000 farmers adopted this technique. Out of which nearly about 7000 farmers achieved very good yield. The comparison of yield of Rice and Pulses achieved by SRT farmers with other Indian farmer's data is shown in Table 1; and Figure 7 and 8.

- **Enhances biodiversity**

The zero tillage, minimum soil disturbance and accumulated decayed roots of previous crop and weed maintains lot of biomass in the soil, in which vast growth of earthworms, useful bacteria, fungus and millions of other organisms profusely expands and sustains. These are essential for the vigorous growth of crops and plants. Thus SRT enhances biodiversity and natural biological processes above and below the ground surface, maintenance of a permanent soil cover and diversification of plant species.

Table1: Comparison of Yield of Rice and Pulses (Tur) achieved by SRT Farmers with other Indian farmers

Sr. No.	Year	No of SRT Farmers	Rice Average yield Quintals per ha		Pulses TUR Average yield Quintals per ha	
			SRT Farmers	Other Farmers*	SRT Farmers	Other Farmers*
1	2013	30	45	24	10	8
2	2014	30	45	23	10	8
3	2015	30	45	23	10	7
4	2016	800	45	23	12	6
5	2017	2000	45	24	12	9
6	2018	3000	50	25	12	10
7	2019	3500	50	26	12	7
8	2020	4500	50	26	12	9
9	2021	5000	50	26	12.5	9
10	2022	7000	50	27	12.5	9

Source: *Economic survey 2022-23, Government of India. Data retrieved from https://www.indiabudget.gov.in/economicsurvey/doc/stat/tab117.pdf

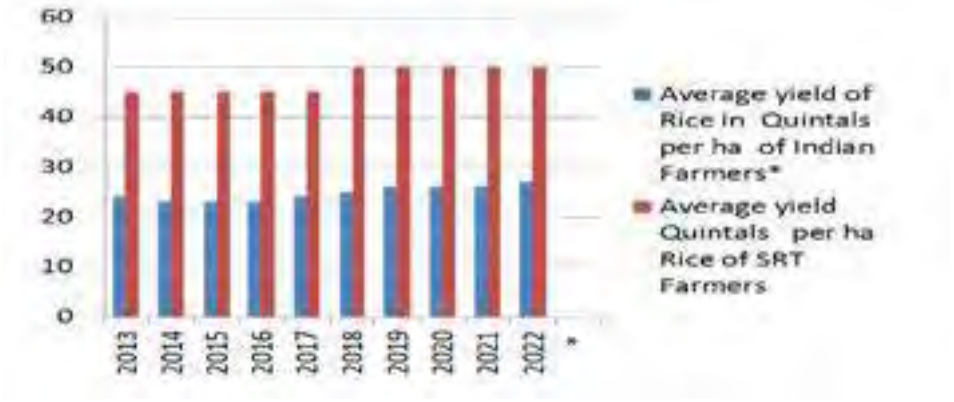

Figure 7: Comparison of Yield of Rice achieved by SRT Farmers with other Indian farmers

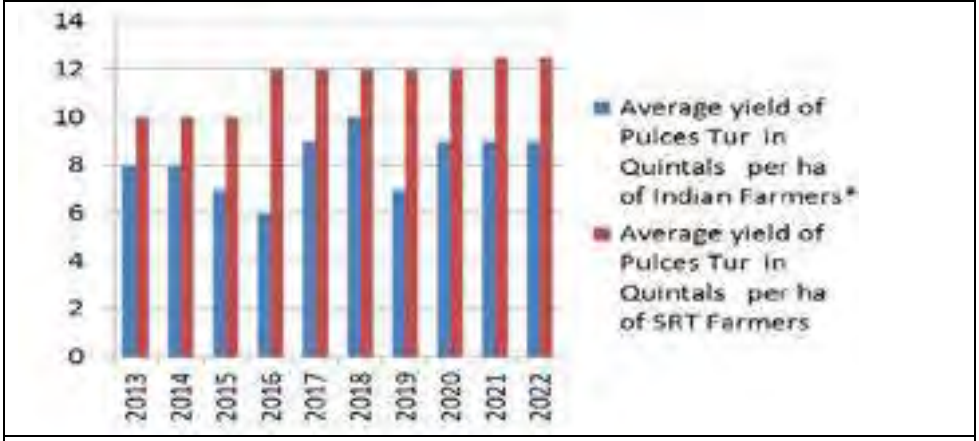

Figure 8: Comparison of Yield of Pulses (Tur) achieved by SRT Farmers with other Indian farmers

Increase in productivity of pulses by SRT was observed in the range of 30 to 50 per cent more.

- **Enhanced productivity and sustainable crop production**

The enhanced biodiversity contribute to increased water and nutrient use efficiency. The inbuilt biomass reduces the requirement of costly fertilizer application. It also improves the quantity as well as quality of the food grains with low input cost. With every additional crops grown, more and more nutriment in the form of biomass is added in to the soil, which recoups the nutrient up taken by the current crops/plants and the soil fertility goes on improving and attends a sustainability level.

- **Prevents soil erosion and silt loss**

On behalf of Saguna Rural Foundation, in the rainy season of year 2022, samples of runoff water from 100 different rice fields were collected and analysed. It is found that the runoff water form SRT field contains negligible amount of silt while samples form non SRT fields, in which power tiller and tractor were used for puddling, contains about 14.13% and 15.21 % Silt respectively (figure 9). It means in non SRT field 15 mm fertile soil layer is getting washed with every 100 mm water depth of runoff, which is very serious problem. This is the major reason for the non SRT fields becoming unproductive. Bigger the tillage machine used for cultivation, higher the loss of silt (figure 10).

Figure 9: Runoff sample for rice fields

Figure 10: Analysis of runoff sample

- **Indirect and strong supports to soil and water conservation**

Vast quantum of microbial activity and high soil organic carbon makes the soil spongy and porous, holds the soil grains together, thereby significantly conserve soil, controls soil erosion. It also increase water infiltration rate and water holding capacity of the soil, thereby water conservation improves. As the availability of soil moisture is more in SRT field, it reduces the irrigation water requirement apart from soil and water conservation.

7.0 IMPROVEMENT IN PHYSICAL PROPERTY OF SOIL BY SRT OVER NON SRT FIELD

Three different experiments to judge the improvement in physical soil properties like drainage, soil loss, and water conservation are conducted and the results are enumerated below.

a) Experiment to check improvement in drainage property od soil conducted on 3 May 2015 at Saguna Bag by Mr. Chandreshekhar Bhadsavale, the Innovator.

Two pieces of PVC pipe of 200 mm diameter and 300 mm length are inserted in the soil up to 100 mm depth, one in an adjoining non SRT farm (Figure 11) and one in SRT Farm (Figure 12) of same soli type. Two litres of water was poured in each pipe. It was observed that Water in the pipe at non SRT farm takes 2 hours to disappear i.e. to get infiltrate in soil while the water in the pipe at SRT farm disappears in only 15 minute.

Figure 11: Non SRT

Figure 12: SRT

Inference

In non SRT farms, due to low organic content and repeated cultural operation, soil becomes very hard thereby reduces the drainage property of the soil.
High organic content developed due to Zero till and crop rotation with SRT, significantly improved the drainage property of soil.

b) Experiment for checking reduction in surface runoff: conducted on 3 May 2015

Undisturbed soil form SRT and Non SRT are kept in two different transparent containers having perforated bottom and both are placed in another slightly big container (Figure 13).

Figure 13: Runoff simulation in Non SRT and SRT field

Very small and equal slope is maintained to each container. Equal amount of water through hanged Plastic glass with perforated bottom are sprinkle over the upper end of the samples to represent the rainfall. V cut at the downstream side of the containers is made to collect the surface runoff. It is observed that:

i) Surface runoff does not occurred with SRT soil sample, all the water get percolates inside the sample and some part of clear water gets collected at the bottom of outside container.

ii) With Non SRT sample considerable surface runoff of turbid colour occurs and water not seen at the bottom of outside container.

Inference

The non-turbid water in SRT sample indicated the presence of sufficient organic matter. It holds the soil grains together and prevents the valuable rich soil layer to wash along the rains. The improved physical properties support the sustainable good yield

In Non SRT sample, significant turbid runoff water clearly indicates the washing of the soil grains. Low vertical movement of water indicates the degraded physical soil properties.

c) Experiment for checking deduction in soil loss with surface runoff conducted on 3 May 2015

Two Glass jars are filled with clean water. Small Undisturbed soil lumps from SRT and Non SRT are kept inside the mouth of the Glass jars along with a wire mesh holder in such a way that they get partially merged in water (Figure 14).

Figure 14 : soil grains dispersion in presence of water simulation in Non SRT and SRT field

It is observed that:

i) SRT soil lump absorbs the water but do not disintegrate. The water in the jar remains clear.

ii) Non SRT soil lump starts disintegration at the moment it absorbs the water, the soil grains starts separation from the lump and water in the jar becomes turbid. In another experiment the runoff water during rains form SRT, Non SRT field are collected separately in two glass beaker and equal amount of portable water is kept in third glass beaker (Figure 15). It is observed with simple eyes that the runoff water from the SRT field is as clear as portable water and the runoff from Non SRT field is significantly turbid.

Figure 15: soil grains dispersion in presence of water in Non SRT and SRT field

Inference

The clear water in the Jar in which non disturbed soil sample from SRT field is partially merged clearly indicated that the soil grains are hold tightly to gather due to presence of organic matter and crop roots, indicates the reduction in soil loss due to presence of sufficient organic matter. The improved physical properties support the sustainable good yield

The turbid water in the Jar in which non disturbed soil sample form non SRT field is partially merged clearly indicated that the soil grains are not hold together due to absences of organic matter and crop roots..

Turbid runoff water in the glass beaker clearly indicated that valuable fertile soil layers form non SRT field get washed along with runoff. And clear water in the glass beaker indicated the

importance of use of SRT to prevent the washing of fertile soil layer again and again. The improved physical properties support the sustainable good yield. Significant turbid runoff water clearly indicates the washing of the soil grains.

8.0 MULTIPLE ADVANTAGES OF SAGUNA REGENERATIVE TECHNIQUE

- For not having to do puddling, transplanting and hand hoeing, saves 30% to 40% cost of production & not requiring transplanting saves 50% treacherous labour.
- Loss of valuable silt (about 20%) during puddling can be prevented thus more fertile land can be handed over to next generation.
- Leaves of rice plants on SRT beds seem to be broader and head more upwards to sunlight than their counterparts in conventional method. They are likely to produce more biomass, means higher yield.
- SRT has ability to bring vigorous uniformity and higher yields in all soil types even in degraded soils and socio-economic groups. Almost all farmers adopting SRT will attain higher yield per unit area.
- Hand hoeing is strictly avoided in SRT. Once again this reduces hard-work and loosening of top soil making it vulnerable for washing away.
- Today's recommend dose of fertilizer can be brought down considerably.
- A good number of earthworms are noticed on SRT beds during high rainfall days attracting unusual birds to SRT plots. This magic is due to suppressing all green growth with glyphosate, which decays and becomes instant food for the worms. Also 'No-Till' prevents destruction of Eelworms life. Thus SRT proves to be Eco-friendly farming. This is big positive gain.
- SRT insists keeping of roots of previous crop in the raised bed. The root network prevents soil from cracking and makes it more spongy. The same roots become valuable source of organic carbon which is uniformly distributed and oxygen pathways to root zone of next crop.
- Avoiding of puddling will drastically reduce diesel consumption, emission of CO_2 over thousands of acres of paddy cultivation. Also SRT being aerobic method it will prevent methane generation. Both CO_2 and methane are responsible for global warming.
- The traumatic shock caused to the rice seedlings during transplanting is avoided in SRT. This reduces possibility of pest & disease problem.
- Rice crop gets ready 8–10 days earlier. Also it saves time required for soil tilling between two crops. This leaves valuable 10–15 days of crop season for the farmer enabling him to take more than one crop in the same plot in a year.
- SRT is feasible for organic farming method.
- Due to excessive water in low-lying plots removing of harvested paddy from the plot for drying can be avoided with SRT raised beds.
- During milling of paddy, SRT will yield higher percentage recovery of grains.
- Non-use of heavy agricultural machinery for tilling in field will prevent compaction and formation of hard pan of lower strata of soil enabling better percolation of water into dipper soil and permanent establishment of earthworms.
- It is possible to get high returns (more than ₹ 5,00,000 per hector per annum) with crop rotation such as Basamati Rice (PS-5) in Kharif (rainy), leafy vegetables in Rabbi (winter), Bold Groundnut (W-66) in Summer, while improving health of the soil.
- This could be the best solution in natural calamities such as hail storm, floods, cyclones, untimely rain-storms, etc. because the crop cycle is shortest (no till) and it involves multiple choices of short-term rotation crops such as pulses, vegetables, onion, sun-flower, groundnuts, and so on.
- Damaged soils can be recovered by SRT, which is caused by lashing, scrubbing & natural calamities, in quickest possible time.

9.0 CONCLUSION

Adaptive actions are essential for the agricultural sector to effectively respond to the challenges posed by climate change. It emphasizes the role of innovative agricultural practices and technologies in climate mitigation and adaptation. These actions can enhance agricultural resilience, ensure food security, and contribute to sustainable development while minimizing the negative impacts of climate change on farming communities and the environment. Innovative agricultural practices and technologies offer a dual benefit in climate mitigation by reducing greenhouse gas emissions and enhancing carbon sequestration, while also supporting climate adaptation by making agriculture more resilient to the challenges posed by a changing climate. By investing in and adopting these innovations, the agricultural sector can play a significant role in combating climate change and ensuring food security and sustainability for the future. To achieve this, there is a need for policy, institutional, and governance innovations to respond to the changing climate. The focus should be on developing sustainable agricultural methods tailored to local conditions, benefiting local communities economically and environmentally. Saguna Regenerative Technique (SRT), previously named as Saguna Rice Technique, is an innovative method based on conservation agriculture, is basically invented for rice in Kharif (Rainy season) followed by pulses, vegetables and oil seed in successive season. SRT is a unique zero tillage and conservation agriculture method successfully adopted by numerous farmers in the State of Maharashtra India. This technique has resulted in cost savings, labor reduction, increased productivity, and improved water and soil conservation. The technique enhances biodiversity, natural processes, and supports sustainable crop production while reducing irrigation water requirements. Overall, SRT is a promising approach to improve agricultural productivity and resilience in the face of climate change.

REFERENCES

Bhadsavle Chandrashekhar (2014), "A zero tillage Conservation agriculture technique for rice based faminig",Data retrieved from http://www.slideshare.net/SRI.CORNELL/1448-a-zero-till-conservation- agriculture-technique-for-rice-based-farming and "Saguna Rice Technique – SRT farming" from https://sagunarice.wordpress.com

Bhadsavle Chandrashekhar (2015), "Zero tillage/Conservation agriculture practices for rice-based farming systems: Insights from India" retrieved from https:// www.youtube.com/watch?v=d-m8mNYfukE&feature=youtu.be

Bhadsavle Chandrashekhar (2015), https://www.youtube.com/ watch?v= Cb2VFFlJiQE,

Bhadsavle Chandrashekhar (2023), "SRT – 'Zero tillage technique' Boon for agriculture" (in Marathi), Published in Vivek Marathi magazine on 22 July, 2023.

Conservation Tillage 2016, "A Management Option for Climate Variability and Change", Southeast Climate, Advancing Extension in Agriculture, retrieved from http://agroclimate.org/wp-content/uploads/2016/03/Conservation-tillage.pdf

FAO 2014. What is Conservation Agriculture? Available from http://www.fao.org/ag/ca/1a.html [Accessed 05/07/2014]

MWIC GOM 1999 - Maharashtra Water and Irrigation Commission (MWIC), June 1999, Water Resources Department, Government of Maharashtra, India

Pradeep Bhalage, Piyush Bhalage, Shivaji Sangle (2016), Mitigating Climate Change with Conservation Agriculture, 2nd World Irrigation Forum WIF2, 6-8 November 2016, Chaing Mai, Thailand

Rattan Lal 2017," Soil Conservation", Reference Module in Life Sciences, Retrieved form https://www.sciencedirect.com/topics/nursing-and-health-professions/tillage

Swift R.S. (2001), Sequestration of carbon by soil, Soil Science, pp. 858–87

Thierfelder C, Wall PC. 2010. Investigating conservation agriculture (CA) systems in Zambia

Zachary Senwo 2021, "What is Soil Organic Carbon (SOC)?", Open Access Government. Retrieved form https://www.openaccessgovernment.org/what-is-soil-organic-carbon- soc/120702/

Zoran I. Mileusnic, Elmira Saljnikov, Rade L. Radojevic, Dragan V. Petrovic 2022, "Soil compaction due to agricultural machinery impact", Journal of Terramechanics, Volume 100, April 2022, Pages 51-60

IMPACTS OF CLIMATE CHANGE ON AGRICULTURAL WATER MANAGEMENT IN TANK CASCADE SYSTEMS IN SRI LANKA

(Eng T J Meegastenna, Former Additional Director General of Irrigation, Sri Lanka)

Abstract:

Approximately 70% of Sri Lanka's dry zone areas rely on tank cascade systems to support irrigated agriculture. These systems enhance food security and increase self-sufficiency in rice production. Dry zones are more conducive to rice cultivation than wet zones. However, during prolonged droughts in the dry zone, the base flow of streams and dry waterspouts is diminished. These intricate, environmentally friendly irrigation systems are based on a series of tanks. They serve to accumulate, preserve, release, and guide water downstream for irrigation.

Climate change significantly impacts agriculture and water management in Sri Lanka, a country heavily dependent on agriculture for economic growth and food security. The dry zone of Sri Lanka predominantly benefits from the 2nd inter-monsoon and the Northwest Monsoon. Climate change has resulted in altered precipitation patterns, including reduced rainfall in the dry zone and intensified rainfall in the wet zone. The tank cascade systems in the dry zone are highly vulnerable, facing numerous challenges during seasonal operations. This has led to reduced water availability for agricultural purposes in areas with agricultural potential in Sri Lanka. Higher temperatures and changing precipitation patterns have elevated water demand for crops and livestock, necessitating increased irrigation. This places additional strain on existing water resources and infrastructure. Climate change has also led to shifts in temperature and rainfall patterns, affecting crop growth and productivity. Some crops may struggle to adapt to these changes, resulting in reduced yields.

The development of tank cascade-associated agriculture will help increase rural income, reduce inequality, and enhance nutritional outcomes through diversification. This approach will facilitate more rapid economic transformation, directing labor away from relatively unproductive primary agricultural production toward sectors of higher productivity, including agro-processing and other agri-business activities. This will contribute to productivity growth and competitiveness within agriculture itself, benefiting those engaged in agriculture. A climate-smart approach to agriculture will connect productivity growth with enhanced resilience to shocks and a reduced climate footprint.

This paper examines the impact of extreme weather events and climate change on agriculture in Sri Lanka's dry zone. It also discusses the adverse effects of the heightened frequency of floods and droughts. Through improved irrigation, agricultural inputs, and practices, the paper highlights the resilience of these areas and their influence on farming communities. These impacts have implications for the country's food security and economic growth, underscoring the necessity for effective adaptation strategies and water management policies.

Keywords: Climate change, dry zone, cascade-associated agriculture, Village tank cascade, climate resilience

Introduction to Tank Cascade Systems and Agricultural Importance in Sri Lanka

Sri Lanka is an island in the Indian Ocean, situated east of the southern tip of the Indian subcontinent, with the Palk Strait separating it. Sri Lanka's coordinates lie between the northern latitude of 5°55' and 9°51', and the longitude of 79°41' to 81°53'. The total land area covers 65,610 km², with inland water spanning 2,905 km², and a coastal line extending 1340 km². Its terrain is primarily low, featuring flat to rolling plains, with mountains in the south-central interior. Elevation distinguishes three zones: the Central Highlands, the plains, and the coastal belt. The coastal belt, situated about thirty meters above sea level, encompasses the island, with sandy beaches constituting much of the coast.

Sri Lanka experiences a tropical and hot climate. The mean temperature varies between a low of 16°C in Nuwara Eliya in the Central Highlands and a high of 32°C in Trincomalee on the northeast coast. The average annual temperature for the country falls between 28°C and 30°C. Sri Lanka witnesses a tropical climate characterized by distinct dry and wet seasons, along

with two monsoons. The "wet zone," encompassing the central mountains and the southwest, receives an average of 2,500 millimeters (mm) of rainfall annually (rising to 5,500 mm in certain areas). On the other hand, the "dry zone," comprising much of the southeast, east, northwest, and northern regions, experiences notably lower annual rainfall (ranging from 1,200 to 1,900 mm). In a typical year, the dry zone receives its rainfall, accounting for about 70% of its annual precipitation, during the Northeast monsoon. Rainfall mechanisms in Sri Lanka include convectional activity, monsoons, and weather systems originating in the Bay of Bengal. Annual rainfall in Sri Lanka ranges from 850 mm to 5500 mm, with an average of 1861 mm. The overall annual rainfall volume is 122 km².

Ancient irrigation systems were designed to facilitate drainage and the capture of excess water from one system to be utilized in a downstream system. This interconnected system of reservoirs is known as a cascade (Sri Lanka Water Resources Development Report, 2010). Functioning as a hydraulic system, it collects and preserves water in a sequential arrangement of tanks, distributing water downstream for various purposes. Agriculture serves as the primary user, forming the backbone of Sri Lanka's rural economy. The tank cascade system, also referred to as the village tank system, represents an ancient Sri Lankan irrigation infrastructure that fulfills basic human needs, provides water for agriculture, sustains floral and faunal communities through water, soil, air, and vegetation, all with human intervention on a sustainable basis. In the north-central dry zone alone, there are 457 identified cascades (Panabokke, 1999). The size and configuration of a cascade are largely determined by topography influenced by geology. Various types of tanks exist within the cascade system, including main tanks, auxiliary tanks, filter tanks, temple tanks, and the terminal major tank. These tanks have distinct functions to optimize water utilization. Upper catchment tanks provide water and filter debris for wildlife. Some tanks serve as storage reservoirs, augmenting water sources for tanks with irrigable areas. Drainage from paddy fields in the upper part of the cascade flows into downstream tanks for reuse in the fields below. This exemplifies the wisdom behind managing drought, flash floods, land degradation, groundwater recharge, and ecosystem enrichment in a tropical environment prone to seasonal water scarcity. This exceptional Cascade Tank System received recognition as a "Globally Important Agricultural Heritage System" (GIAHS) from the Food and Agricultural Organization (FAO) in 2018.

Figure 1: Schematic diagram of Village Tank Cascade System Services

Tank Cascade Systems (TCSs) in Sri Lanka's Dry Zone have evolved as sustainable ecosystems through human interventions, ensuring water availability and various services for people and their surroundings over millennia. The Village Tank Cascade System (VTCS) represents a complex socio-ecological system present in the Dry and Intermediate Zones of Sri Lanka. The VTCS exhibits unique features, not only hydrological, but also in terms of ensuring sustainability and socio-ecological resilience. However, TCSs face vulnerability to global environmental changes, leading to the ongoing deterioration of ecological health and hydro-socio-ecological status. These factors are critical for the food and livelihood security of rural farming communities in the dry zone (Ratnayake, S.S., 2021).

Climate Change and Its Impacts on Precipitation Patterns:

A changing climate leads to changes in the frequency, intensity, spatial extent, duration, and timing of weather and climate extremes. This can result in unprecedented extremes increasing exposure of people and economic assets, which has been a major cause of long-term increases in economic losses from climate-related disasters (IPCC SREX 2012).

Future climate expectations rely on the use of modeling approaches (global climate models), the results of which are synthesized in the assessment reports of the Intergovernmental Panel on Climate Change (IPCC). The Sri Lankan models generally concur in projecting a future increase in both temperatures and precipitations, with a higher level of agreement for temperatures. Precipitation is generally projected to increase in Sri Lanka, although modest drying trends have been observed in recent decades, with a decrease in the number of wet days, possibly due to the delayed offset of the southwest monsoon.

Sri Lanka's climate is considered tropical monsoonal, characterized by significant rainfall variation seasonally and across the three principal climatic zones: the Wet Zone (WZ) in the southwestern region; the Dry Zone (DZ), covering the northern and eastern parts of the country; and the Intermediate Zone (IZ), bordering the central hills. The DZ and IZ, where the majority of Sri Lanka's agro-ecological regions (AERs) are concentrated, are particularly vulnerable to rainfall seasonality and variability (Punyawardena BVR, 2007). According to climate predictions, Sri Lanka's wet areas are becoming wetter, while the dry areas are becoming drier, directly affecting agriculture activities in the WZ and DZ (Marambe B et al, 2004). Annual rainfall is expected to increase by a minimum of +57 mm, with up to +121 mm in the WZ, while droughts will be magnified, particularly in the IZ. Temperature increases will range between +1 and +1.2 °C, with a greater impact in the DZ and IZ.

Sri Lankan agriculture has already felt the effects of extreme weather events and climate changes, including a slow but steady rise in ambient temperature (0.01–0.03 °C per year).

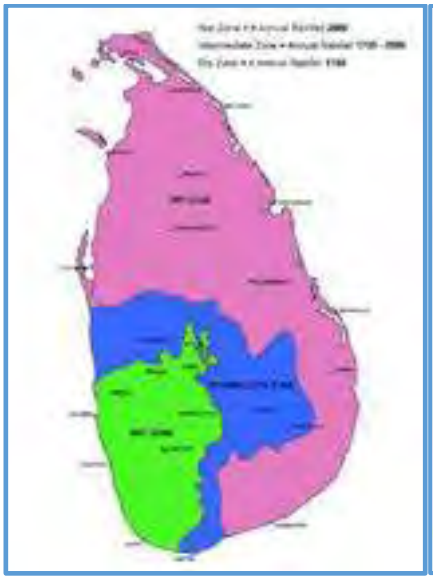

Figure 2: Climatic zones in Sri Lanka

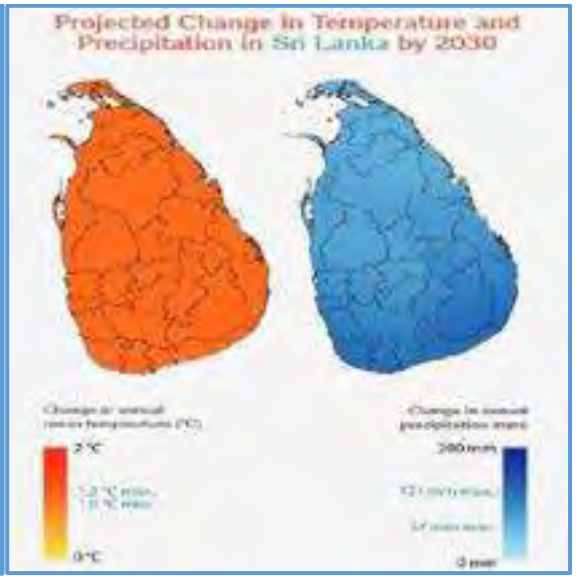

Figure 3: Projected change in Temperature and Precipitation projection in Sri Lanka (Source: CSIAP)

Vulnerability of Tank Cascade Systems to Climate Change:

The demand for water has progressively escalated over time, serving various purposes such as agriculture, drinking, food security, and supporting the needs of the village population. Additionally, the multifaceted role of village tank cascade systems extends beyond these fundamental requirements. These systems also cater to the water needs of village cattle and other living organisms, supplying moisture and a variety of edible grasses essential for cattle and even wild elephants, a significance that becomes pronounced during dry seasons. However, the escalating impacts of climate change, including prolonged dry spells, have led to a significant reduction in water levels within Village Tank Cascade Systems (VTCS) during drought periods. This reduction holds the potential to severely affect the availability of water for daily needs and the livelihoods of rural communities, compounded by the deteriorating quality of water available in the VTCS, often characterized by eutrophication.

Looking forward, the impending impacts of climate change continue to pose a formidable challenge to the agricultural sector as a whole, with particularly acute consequences for smallholder farmers dependent on village tank cascade systems. The observed rise in temperature in recent times, along with projected increases in future climate scenarios, casts a substantial influence on evapotranspiration rates and subsequently augments agricultural water demands.

Adaptation Strategies for Climate-Resilient Agriculture

Tank cascade systems in Sri Lanka's dry zone play a critical role in upholding agricultural productivity and sustaining rural livelihoods. As these systems confront increasing vulnerabilities due to shifting climate patterns, a combination of existing and potential adaptation strategies is imperative to ensure their resilience and continuous functionality.

1. Improved Water Storage and Management:

Existing: Enhancing water storage efficiency in tanks through desilting and rehabilitation programs. However, the costs associated with tank desilting are substantial, warranting detailed operational and flood studies to explore spill raising without affecting upstream fields or downstream water needs. This can expand water-holding capacity and extend water availability during dry periods.

Potential: Implementing advanced water management techniques, such as utilizing seasonal forecasts, employing smart water meters, and adopting real-time monitoring systems, to optimize water distribution and minimize losses.

2. Rainwater Harvesting and Conservation:

Existing: Promoting traditional rainwater harvesting practices that capture and store rainwater for agricultural use during water-scarce periods.

Potential: Introducing rainwater harvesting technologies like capturing rain onset during land preparation, establishing seedbeds prior to planting, and minimizing water discharge from tanks on rainy days. These steps can enhance water availability for irrigation.

3. Diversification of Crop Varieties:

Existing: Encouraging farmers to cultivate a diverse range of crops with varying water requirements and climate adaptability. This mitigates the risk of complete crop failure amid changing weather conditions.

Potential: Researching and developing climate-resistant crop varieties that thrive in the evolving climatic conditions of the dry zone.

4. Efficient Irrigation Techniques:

Existing: Promoting efficient irrigation methods, such as drip irrigation and system modernization, to minimize water wastage and enhance water use efficiency.

Potential: Integrating sensor-based irrigation systems that utilize real-time data to determine precise irrigation needs based on soil moisture levels.

5. Water-Efficient Farming Practices:

Existing: Educating farmers within VTCS about water-efficient agricultural practices, including mulching, cover cropping, increased crop densities, and intercropping. These practices reduce evaporation and soil moisture loss.

Potential: Adopting precision agriculture techniques that leverage satellite imagery and remote sensing to optimize water and nutrient application at a micro-level.

6. Climate-Resilient Infrastructure Development:

Existing: Ensuring the maintenance and proper functioning of existing tank infrastructure, including embankment repairs and sluice gate maintenance, to prevent water leakage and enhance water retention.

Potential: Upgrading infrastructure with climate-resilient designs capable of withstanding extreme weather events. This entails stronger embankments, flood control structures, and implementing watershed management and catchment protection programs to reduce the impact of flash floods and tank siltation issues.

7. Community-Based Water Management:

Existing: Encouraging community involvement in seasonal planning and water management decisions, fostering cooperation and equitable water resource distribution among farmers.

Potential: Establishing community-based water user associations at the village tank cascade level, enabling collaborative management of operations, water allocation, and maintenance activities.

8. Climate Information and Advisory Services:

Existing: Disseminating weather forecasts and climate information to farmers, enabling informed decisions about planting, irrigation, and other agricultural activities.

Potential: Integrating climate adaptation advice and strategies into advisory services to empower farmers to proactively respond to changing conditions.

9. Research and Capacity Building:

Existing: Supporting research initiatives investigating the impacts of climate change on tank cascade systems and exploring effective adaptation measures.

Potential: Investing in training programs and capacity-building workshops for farmers, extension workers, and policymakers to ensure the effective implementation of adaptation strategies.

By integrating a combination of these existing and potential adaptation strategies, the long-term resilience of tank cascade systems in Sri Lanka's dry zone can be bolstered. These strategies not only mitigate the immediate impacts of climate change but also contribute to the sustainable development of agricultural practices better suited to evolving climatic conditions.

Economic and Social Implications of Climate-Resilient Agriculture:

Climate-resilient agriculture, coupled with effective management of tank cascade systems, offers substantial economic benefits to rural communities and the broader economy. These benefits will be described as follows.

- Enhanced Agricultural Productivity: Implementing climate-resilient practices, such as efficient irrigation and crop diversification, can lead to higher and more stable crop yields. This, in turn, increases farmers' incomes and contributes to overall food security.
- Reduced Risk of Crop Losses: By adapting to changing climate conditions, farmers can mitigate the risks of crop failures due to extreme weather events, such as droughts or floods. This stability in production ensures a consistent income source for farmers.
- Increased Employment Opportunities: Climate-resilient agriculture often requires additional labor for tasks like water management, monitoring, and implementing new practices. This can lead to increased rural employment and improved livelihoods.

- Value Addition and Agribusiness Growth: Adapting to climate change often involves adopting new technologies and practices, which can drive innovation and promote agribusiness development. Climate-resilient practices can also lead to improved product quality, resulting in higher market prices.

Rural Income Growth and Nutritional Outcomes:

- Increased Rural Income: Climate-resilient agriculture, when combined with effective water management through tank cascade systems, can lead to increased agricultural productivity. This translates to higher income for rural farming communities. The reliable water supply from tank cascade systems ensures consistent crop production, enabling farmers to generate a more stable income throughout the year.
- Diversification and Income Stability: Climate-resilient practices encourage farmers to diversify their crops and income sources. This diversification not only reduces the risk of income fluctuations due to climate variability but also provides a safety net against market price fluctuations for specific crops.
- Nutritional Improvements: Increased agricultural productivity and income can improve access to diverse and nutritious foods for rural households. Farmers can allocate more resources to growing a variety of crops, contributing to better dietary diversity and improved nutritional outcomes, particularly for vulnerable populations.

Broader Economic Transformation and Growth:

- Multiplier Effects: Improved agricultural productivity and increased rural income stimulate local economies. Increased spending by farmers can lead to the growth of local markets and the development of downstream sectors, such as transportation, retail, and services.
- Agri-Business Development: As climate-resilient agriculture gains prominence, there is a potential for the growth of agri-businesses that provide climate-adapted technologies, seeds, equipment, and services. This contributes to economic diversification and employment opportunities beyond traditional farming.
- Resilience to Shocks: By integrating climate-smart practices, farming communities become more resilient to climate-related shocks. This resilience enhances the stability of rural economies, reducing the impact of extreme events on livelihoods and preventing long-term economic setbacks.

In conclusion, embracing climate-resilient agricultural practices and optimizing tank cascade systems in Sri Lanka's dry zone has significant economic and social implications. These implications range from increased agricultural productivity and rural income to improved nutritional outcomes and broader economic growth. By fostering resilient farming practices, communities can enhance their adaptive capacity to climate change, achieve sustainable economic development, and ensure food security for the present and future generations.

Case Studies and Success Stories:

Plan International initiated a village tank cascade development program, selecting two cascades in the driest part of the north-central province from 2001 to 2004. The villagers within these cascades were limited to a single season of tank-irrigated paddy cultivation during the wet season with the northeast monsoon. These tanks had accumulated significant silt over time, resulting in reduced storage capacities. Rather than focusing solely on desilting, Plan International emphasized enhancements in the water delivery system. This included the renovation of field canals, reinforcement of tank bunds, spills, and sluices where necessary, as well as limited reforestation efforts. Additionally, improvements were made in home gardening practices, and efforts were made to strengthen the management capacities of farmer organizations. While the Plan International's efforts did not achieve monumental success, they provided valuable insights into the managerial and operational intricacies of cascade-based tank development.

In more recent years, between 2013 and 2015, the International Union for Conservation of Nature (IUCN) initiated a village tank cascade development program in the north-central province. One cascade with 22 minor tanks was selected for this tank cascade-based irrigation development program. The project encompassed various interventions, including desilting

selected tanks, enhancing both main and field canals, incorporating water management structures with measuring devices, improving the drainage canal system, renovating tank bunds, and implementing capacity development programs for members of farmer organizations. While the outcomes of the projects did not fully meet expectations and the overall project impacts fell short of the desired standards, this initiative served as a valuable learning experience for future stakeholders engaging in this mode of development.

Conclusion and Future Outlook:

The convergence of climate-resilient agriculture and efficient management of village tank cascade systems presents a promising path towards sustainable development in Sri Lanka's dry zone. The interplay of these strategies yields a host of economic, social, and environmental benefits, forging a pathway that addresses the challenges posed by changing climate patterns.

Conclusion:

Climate change continues to exert profound impacts on agricultural practices and water management systems in Sri Lanka's dry zone. The reliance on village tank cascade systems, intricately linked with agriculture, necessitates innovative approaches to adapt and mitigate these challenges. The exploration of case studies and success stories reveals that while not all endeavors have yielded desired outcomes, they provide invaluable insights for future endeavors. Adapting village tank cascade systems and embracing climate-resilient agricultural practices yield a multifaceted range of benefits that extend well beyond the fields.

Improved water storage and management, rainwater harvesting, crop diversification, efficient irrigation techniques, and climate-resilient infrastructure collectively enhance agricultural productivity, income stability, and employment opportunities. These strategies bolster the capacity of farming communities to confront climate variability and extreme events, ultimately fostering resilience and safeguarding livelihoods. Furthermore, the positive ripple effects of enhanced rural income on local economies and agribusiness development demonstrate the potential to transform the broader economic landscape.

Future Outlook:

As Sri Lanka's dry zone navigates the evolving challenges of climate change, the outlook remains promising through the synergy of climate-resilient agriculture and village tank cascade systems:

1. **Technology Integration:** Continued integration of technology, such as real-time monitoring systems, sensor-based irrigation, and precision agriculture techniques, will optimize resource utilization, improve yields, and enhance sustainability.
2. **Community Empowerment:** Strengthening community involvement in seasonal planning, water management decisions and the adoption of climate-resilient practices will foster ownership, cooperation, and equitable distribution of resources.
3. **Research and Development:** Investment in research initiatives to understand the complex interactions between climate change, village tank cascade systems, and agriculture will refine adaptation strategies and inform policy decisions.
4. **Capacity Building:** Empowering farmers, extension workers, and policymakers with knowledge and skills in climate-resilient practices ensures effective implementation and long-term success.
5. **Sustainable Partnerships:** Collaborative efforts among government agencies, non-governmental organizations, research institutions, and local communities are pivotal to holistic climate adaptation and sustainable development.
6. **Scaling Up:** Learning from past experiences, scaling up successful interventions, and tailoring strategies to specific local contexts will amplify the positive impacts on livelihoods and economies.

In conclusion, the future trajectory of climate-resilient agriculture and tank cascade systems in Sri Lanka's dry zone is one of dynamic adaptation, innovation, and collaboration. By harnessing the economic and social benefits offered by these strategies, rural communities can

thrive in the face of climate challenges, ensuring food security, income growth, and sustainable development for generations to come.

References:

CSIAP, 2019: Climate Smart Agriculture in Sri Lanka, file:///D:/ICID/CSA%20in%20Sri%20Lanka.pdf

Dharmasena, P.B. Cascaded Tank-Village System: Present Status and Prospects. In Agricultural Research for Sustainable Food Systems in Sri Lanka; Springer: Singapore, 2020; pp. 63–75.

FAO. "Globally Important Agricultural Heritage Systems" (GIAHS). 2021. Available online: http://www.fao.org/giahs/en/ (accessed on 26 January 2021).

Imbulana K A U S, Wijesekera N T S. Nepune B R, Aheeyar M M M, Nanayakkara V K , 2010: Sri Lanka Water Resources Development Report, Ministry of Irrigation and Water Resources Management, Sri Lanka

IPCC, 2012: Managing the Risks of Extreme Events and Disasters to Advance Climate Change Adaptation. A Special Report of Working Groups I and II of the Intergovernmental Panel on Climate Change [Field, C.B., V. Barros, T.F. Stocker, D. Qin, D.J. Dokken, K.L. Ebi, M.D. Mastrandrea, K.J. Mach, G.-K. Plattner, S.K. Allen, M. Tignor, and P.M. Midgley (eds.)]. Cambridge University Press, Cambridge, United Kingdom and New York, NY, USA, 582 pp

Jayawardena S, Thanuja Darshika and Roshan Herath, 2016: Center for Climate Change Studies, Observed Climate trends, future climate change projections and possible impacts for Sri Lanka, Department of Meteorology, Sri Lanka

Marambe B; Silva P; Weerahewa J; Pushpakumara G; Punyawardena R; Pallawala R, 2014: Enabling policies for agricultural adaptations to climate change in Sri Lanka. In: Handbook of Climate Change Adaptation. Leal W. (ed.). Springer-Verlag Berlin Heidelberg. (Available at: http://link.springer.com/ reference work entry/10.1007/978-3-642-40455-9_108-2).

Panabokke, C.R.; Sakthivadivel, R.; Weerasinghe, A.D. Evolution, Present Status and Issues Concerning Small Tank Systems in Sri Lanka; International Water Management Institute: Colombo, Sri Lanka, 2002.

Punyawardena BVR. 2007. Agro-ecology (Map and Accompanying Text). National Atlas of Sri Lanka. 2nd ed. Colombo: Survey Department.

Punyawardena BVR. 2011. Country report, Sri Lanka. Workshop on Climate Change and its Impacts on Agriculture. Seoul, Republic of Korea (Available at: http://www.adbi.org/files/2011.12.13.cpp.day1.sess1.13. country.paper.sri.lanka.pdf).

Ratnayake, S.S.; Kumar, L.; Dharmasena, P.B.; Kadupitiya, H.K.; Kariyawasam, C.S.; Hunter, D. Sustainability of Village Tank Cascade Systems of Sri Lanka: Exploring Cascade Anatomy and Socio-Ecological Nexus for Ecological Restoration Planning. Challenges 2021, 12, 24. https://doi.org/10.3390/challe12020024

Tennakoon M U A, 2017: Cascade Based Tank Renovation for Climate Resilience Improvement, Ministry of Disaster Management, Sri Lanka

NON-INTRUSIVE TECHNOLOGY FOR IRRIGATION AND DRAINAGE DISCHARGE MEASUREMENT

Yen-Cheng Lin [1],Hao-Che Ho [2)]

ABSTRACT

The effects of climate change have made the availability of water resources unpredictable. Discharge has therefore become a key factor in irrigation and drainage systems management. Accurate discharge measurement not only reduces water wastage but also improves the efficiency of water management. The most common method to estimate the discharge in a channel is to use ultrasonic wave instruments that are installed above the weir. However, this single-point measurement is vulnerable to environmental factors, leading to distorted readings. In recent years, using non-intrusive methods to measure hydrological data has become a mainstream development. For instance, Large-Scale Particle Image Velocimetry (LSPIV) can measure surface velocity and estimate discharge using imaging techniques. Nevertheless, there are two major obstacles. Firstly, it uses the direct cross-correlation algorithm to measure, which is susceptible to environmental noise. Secondly, the LSPIV method can only measure surface velocity. Therefore, this study uses the LSPIV framework as a basis and introduces a convolutional neural network (CNN) model to develop an innovative image surface velocity measurement method. Along with the velocity obtained from this method which is used to derive the two-dimensional bathymetry by using the Leap-frog scheme in a pre-defined grid by solving the continuity equation.

The experiments in this study were conducted using a quadcopter drone in a river. The Ryskin and Leal (RL) orthogonal grid was used to improve the data resolution near the banks. And the ground truth data were measured by ADCP for analysis. The results show that the proposed method significantly improves the velocity measurement capability compared to the conventional LSPIV method. Furthermore, the average error of bathymetry was only 11%. Thus, there is every indication that the proposed method was effective in measuring surface velocity and bathymetry in the field. This innovative hydrological measurement method has non-intrusive, digital, and low-cost characteristics, which could increase the measurement coverage points and improve the management of irrigation and drainage systems.

Keywords: LSPIV, convolutional neural network, shallow water equations, bathymetry, non-intrusive method

1. Introduction

Discharge is a key parameter for open channel flow dynamics. Traditional methods involve measuring water levels, establishing rating curves, and estimating discharge based on real-time water level measurements (Juracek, 1798). Acoustic Doppler Current Profilers (ADCP) divide the river cross-section into blocks, measure water depth and flow velocity, and calculate discharge using the velocity-area method (Herschy, 1993). However, during extreme events, the rating curve approach lacks high discharge measurements, leading to uncertainty and risks during flood events (Sivapragasam et al., 2005; Kuczera, 1996).

Non-intrusive methods like Large-Scale Particle Image Velocimetry (LSPIV) have practical applications in hydrological measurement. LSPIV accurately calculates discharge at stream cross-sections (Bradley et al., 2002) and performs well in low velocity flows (Meselhe et al., 2004). LSPIV is suitable when velocities fall below other instrument limits (Le Coz et al., 2010; Kantoush et al., 2011). However, the accuracy of LSPIV measurements can be influenced by environmental factors such as light reflections and shadows.

[1] Graduate Student, Department of Civil Engineering, National Taiwan University, Taipei, Taiwan, d10521010@ntu.edu.tw
[2] Assistant Professor, Department of Civil Engineering, National Taiwan University, Taipei, Taiwan, haocheho@ntu.edu.tw

In recent years, AI and computer vision, particularly convolutional neural networks (CNNs), have emerged as powerful tools in image recognition tasks. CNNs process images directly as input, eliminating the need for pre-processing image features. They can automatically adjust the weights of convolutional filters to acquire kernels suitable for image recognition. By reducing the number and complexity of parameters, CNNs enhance tolerance to image distortion, rotation, and panning. CNNs have found applications in various fields, including transportation, agriculture, and medicine (Hao et al., 2018; Ma et al., 2021). In this study, we utilized a CNN as an alternative to the traditional LSPIV algorithm for the recognition of granular images representing a flow field, aiming to improve the accuracy of velocity measurement.

Regarding bathymetry estimation, (Johnson et al. 2016) utilized LSPIV to estimate discharge by measuring instantaneous surface velocities and establishing the relationship between integrated length and water depth. This relationship can be derived from a large amount of experimental data. However, in-situ measurements often face challenges related to low resolution and inaccurate surface velocity. To overcome challenges of low resolution and inaccurate surface velocity, this study aims to solve the continuity equation and invert bathymetry using surface velocity measured by CNN as the boundary condition. The continuity equation represents first-order nonlinear hyperbolic partial differential equations that accurately depict physical phenomena (Gao et al., 2016; Ferrolino et al., 2020), requiring numerical approximation.

The Leapfrog Method, initially introduced by Mesinger and Arakawa in 1976 for shallow water equations, has proven effective in simulating real flow conditions (Mesinger et al., 1976). (Zhou, 2002) further improved the Leapfrog method by implementing a semi-implicit staggered time grid system, doubling its computational efficiency. However, the semi-implicit scheme reduces the convergence of the equation. To design a numerical method capable of effectively simulating real flow conditions, Stelling (Stelling et al., 2003) introduced the explicit staggered grid scheme for the Leapfrog Method in shallow water equations. This method is particularly suitable for rapidly changing flow transition zones, such as hydraulic jumps.

To assess the feasibility of using surface velocity as a boundary condition to solve the continuity equations and obtain the bathymetry, this study conducted experiments using a quadcopter drone in a river. The Ryskin and Leal (RL) orthogonal grid (Ryskin & Leal, 1983) was employed to improve data accuracy, and the ground truth data were measured by ADCP for analysis. The surface velocities obtained from the images were used to discretize the derivatives of the continuity equation in space between adjacent points and approximate the water depth at each grid point. Finally, the accuracy and feasibility of the method were evaluated by comparing the measured bathymetry.

2. Methods

2.1 Image preprocessing

To enable the computer to track the movement of the particles, a number of pre-processing steps are required on the image. The first step is to greyscale the three-channel RGB image. This is then orthorectified using the coordinates on the screen. This allows the points to calculate the true displacement of the particle features in the image. In addition, the drone is susceptible to wind effects that cause the continuous image itself to shift. This has a serious impact on the accuracy of the measurement. Therefore, this study uses Scale-invariant feature transform (SIFT), a machine vision algorithm widely used in object recognition, robot map perception and navigation, image stitching, 3D modelling, gesture recognition, image tracking and so on. It can be used to detect and characterize local features in images and extract their position, scale and rotation invariants by finding extreme points in the spatial scale.

2.2 LSPIV algorithm

The LSPIV method employs the Direct Cross-Correlation (DCC) algorithm as the image matching method, specifically for tracking the features of surface seeding. This method involves defining an Interrogation Area (IA) sub-image and delineating a Searching Area (SA). By doing so, the computer is capable of locating the most similar candidate sub-images (Figure 1) within the image at time t+1, thereby determining the displacement. The DCC algorithm calculates the cross-correlation between two corresponding IAs in space by evaluating the

difference in brightness distribution. The cross-correlation is computed using the following equation:

$$r_{AB} = \frac{\sum_{i=1}^{M}\sum_{j=1}^{N}(A_{ij} - \overline{A_{ij}})(B_{ij} - \overline{B_{ij}})}{\sqrt{\sum_{i=1}^{M}\sum_{j=1}^{N}(A_{ij} - \overline{A_{ij}})^2 \sum_{i=1}^{M}\sum_{j=1}^{N}(B_{ij} - \overline{B_{ij}})^2}} \quad [1]$$

where i , j are image coordinates; M , N are width and height for sub-images; A_{ij} , B_{ij} are pixel intensity at location (i , j) for sub-image A and B; $\overline{A}_{ij}$, $\overline{B}_{ij}$ are average pixel intensity.

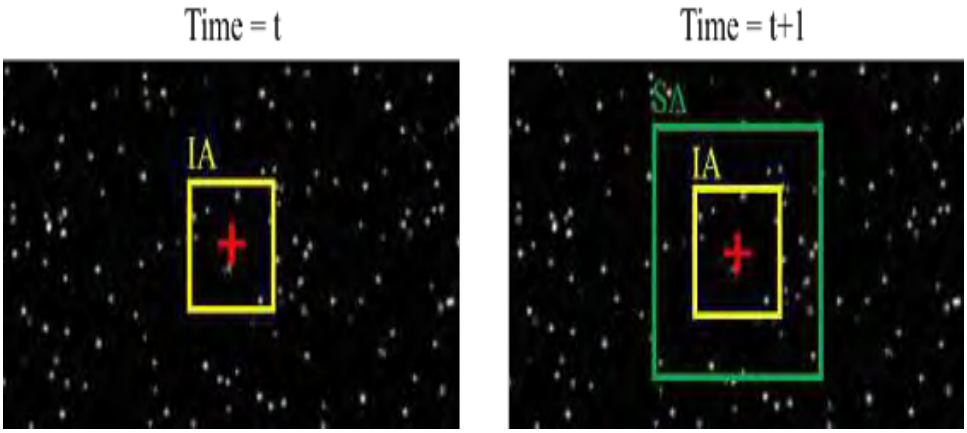

Figure 1. The definition of IA and SA

The calculation of particle displacement involves obtaining the cross-correlation matrix between sub-image A at time t and each matching sub-image B at time t+1. The peak value within the matrix indicates the location of the matching sub-image B that exhibits the highest correlation with sub-image A at time t+1. The distance between sub-images A and B can be interpreted as the displacement distance of the particle movement.

2.3 Convolutional Neural Network (CNN) algorithm

Regarding the CNN framework, we investigated a configuration consisting of two convolutional layers, a maximum set layer, a fully-connected layer, and an output layer. The depth of the convolutional layer plays a crucial role in determining the diversity of the extracted features. Insufficient depth may result in an inadequate number of features being extracted, impeding the completion of the recognition task, whereas excessive depth increases training time. To strike a balance, we opted for a two-layer structure with varying depths, as depicted in Figure 2.

In this study, we employed the Rectified Linear Unit (ReLU) as the activation function. The use of ReLU offers several advantages in deriving flow measurements. Firstly, it aligns with the signal transmission mechanism of biological neurons, which remain inactive until a certain intensity threshold is surpassed, subsequently emitting weak signals. Secondly, during error transmission, the gradient of the error needs to be computed with respect to bias and propagated backward. Notably, when employing ReLU as the output function, the error gradient does not vanish. Thirdly, the ReLU function causes the output of certain neurons to become zero, thereby promoting sparsity among active neurons in the network, mirroring biological mechanisms.

Lastly, ReLU offers computational simplicity and imposes reasonable computational overhead. Consequently, we utilized ReLU as the activation function in the CNN architecture for all subsequent analyses.

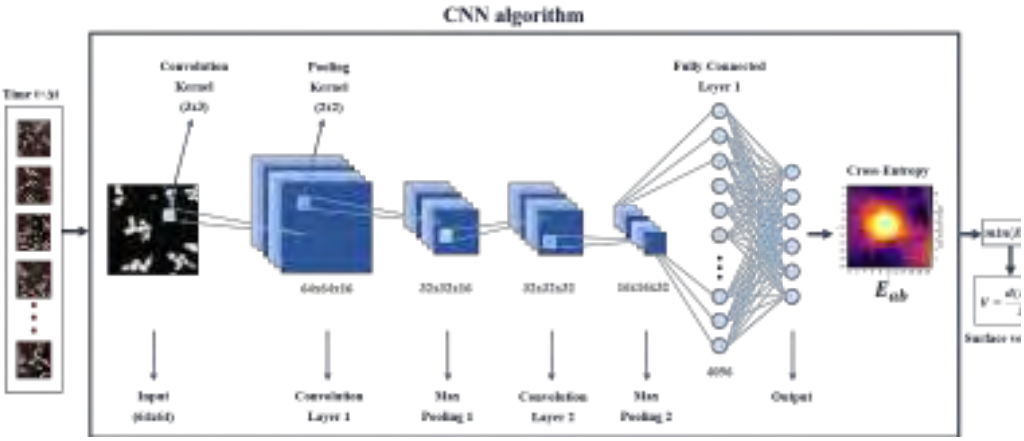

Figure 2. CNN framework

2.4 Combined with the differential equation

This study applies the continuity equation of the shallow water equation to estimate the distribution of water depth using a two-dimensional velocity field. Shallow water currents, which are predominant in rivers, are characterized by considerably larger horizontal and velocity scales compared to vertical scales. The flow is assumed to be stable; therefore, the aforementioned equation can be simplified as equation 2 and applied to estimate the water depth for this study.

$$H\left(\frac{\partial u}{\partial x}+\frac{\partial v}{\partial y}\right)+u\frac{\partial H}{\partial x}+v\frac{\partial H}{\partial y}=0 \qquad [2]$$

2.5 Leapfrog method

To numerically solve the partial differential equation, the Leapfrog Method, a finite difference method, was employed in this study. This method operates on four spatially interleaved grids and replaces the continuous differential operator in the original equation with a discretized differential operator based on spatial discretization, resulting in a discrete approximation. The accuracy of the numerical analysis relies on the grid density. In this research, the Arakawa C-grid (Figure 3) was adopted for numerical computation, and the water depth at the grid points was determined using the two-dimensional velocity field measured by LSPIV.

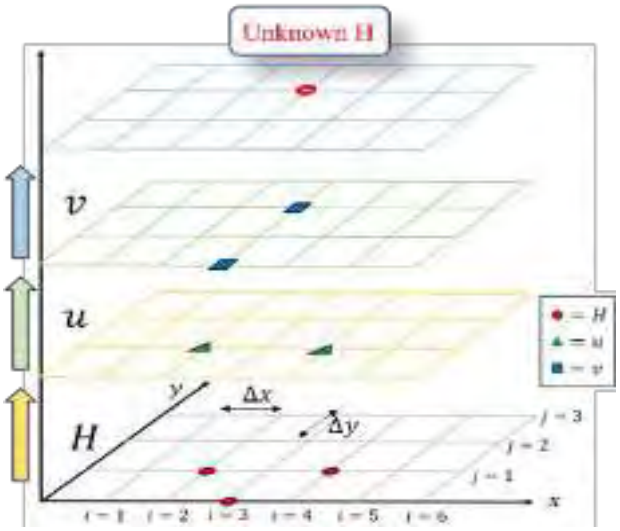

Figure 3. The demonstration of Arakawa C-grid for numerical calculation

Under the condition of steady flow, the two-dimensional continuity equation (Eq. 3) can be discretized into a first-order leapfrog format using finite difference method to solve for the water level. The equation can be expressed as follows:

$$(Hu)_{i+1,j} - (Hu)_{i-1,j} = -\frac{\Delta x}{\Delta y}\left[(Hv)_{i,j+1} - (Hv)_{i,j-1}\right] \quad [3]$$

Equation 4 has second order accuracy in both the x and y directions and provides a numerical solution for the two-dimensional continuity equation. To solve for water depths at each grid point, specific boundary conditions were applied in this study. The upstream boundary water depth (H_u) was set equal to the initial water depth (H_0), while the sidewall water depth (H_w) was defined as $\partial H_w / \partial y = 0$. To ensure convergence and stability in the numerical analysis, the Courant-Friedrichs-Lewy (CFL) condition played a crucial role. This condition establishes an interdependent relationship between the range of parameter values derived from initial conditions and the chosen approximation method for all grid points. By constraining the maximum step size of the grid spacing, the CFL condition guarantees numerical stability.

3. Experimental Setup

To verify the feasibility of non-intrusive methods for velocity and bathymetry measurements. This study was carried out in the field in a river. Continuous imagery was acquired using a drone with real-time kinematic (RTK) capability, which provides realistic coordinates in the images for image orthorectification. In addition, a Ryskin and Leal (RL) orthogonal grid was used in this study, which, unlike a conventional rectangular grid, can significantly improve the resolution of river banks. Leaves and branches were chosen as tracers because they can be clearly seen in the images. And because it is a natural material, it does not pollute the environment.

The study also used the ADCP to measure four river cross sections. Each section was measured more than five times. The results were used as a benchmark for comparison and analysis.

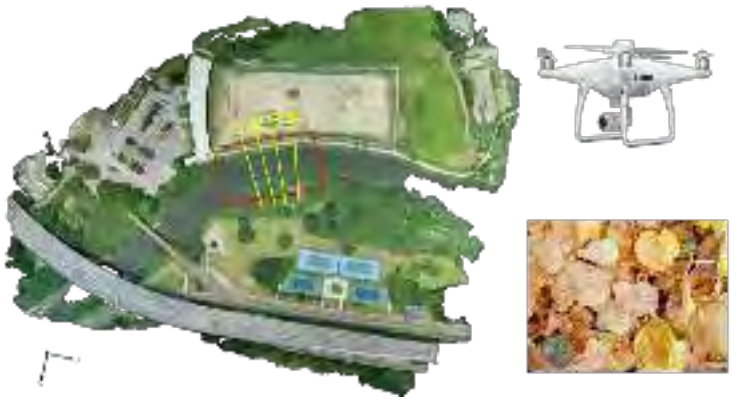

Figure 4. Field experiment setup

4. Results and Discussions

4.1 Comparison of Velocity Measurement Results

The comparison between the surface velocity calculation results obtained from the DCC method and the CNN method reveals the superior measurement capabilities of the CNN approach, which is capable of capturing a more comprehensive flow field. Unlike the traditional single-point measurement method, the CNN method can discern variations in flow velocity both inside and outside the river. On the other hand, the DCC method is susceptible to the influence of light and shadow, leading to errors in the measurements (Figure 5). The analysis results, using the root-mean-square error (RMSE) as the error metric, are presented in Table 1. These results indicate that the CNN method achieves an approximately 5-8% improvement in

accuracy compared to the DCC method. Furthermore, employing the SIFT algorithm for image stabilization contributes to error reduction. These findings demonstrate the potential of non-intrusive measurement methods in rapidly acquiring extensive 2D velocity field data.

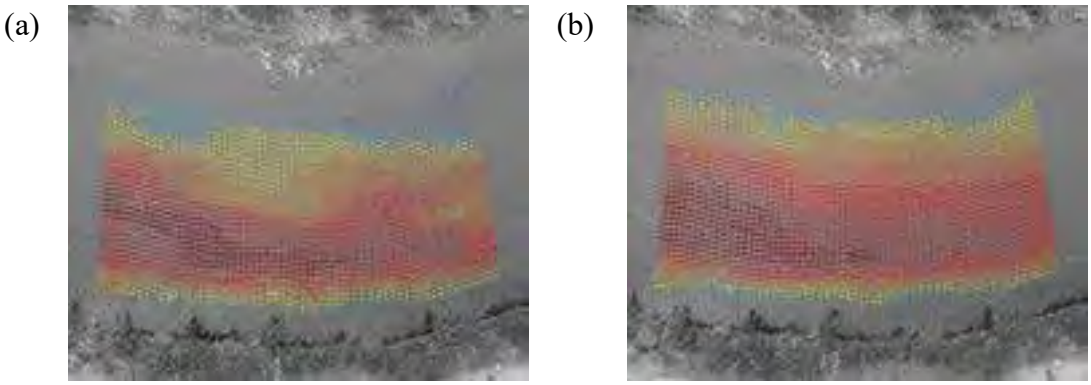

Figure 5. Surface velocity measurement results (Grid: 40x60)
(a) DCC method; (b) CNN method;

Table 1. Surface velocity measurement results (Grid: 40x60)

	Non-stabilized		Stabilized	
	DCC	CNN	DCC	CNN
Section1	26.07%	22.10%	19.98%	21.35%
Section2	25.06%	17.59%	20.78%	15.57%
Section3	35.14%	25.70%	31.35%	22.67%
Section4	30.32%	18.76%	28.80%	20.24%
Average	29.14%	21.03%	25.22%	19.95%

4.2 Bathymetry measurements

After obtaining the surface flow velocities using the CNN method, the bathymetry measurements from Section 1 of the ADCP were employed as the boundary condition for inverting the two-dimensional bathymetry using the leap-frog method. Different grid densities were utilized to validate the numerical analysis.

Figure 6 illustrates the results of the 3D bathymetric inversion, which are satisfactory regardless of the grid size: 10x15, 20x30 and 40x60. In addition, the detailed error data of the bathymetry inversion of sections 2-4 with ADCP measurements are shown in Table 2. The result shows that this approach can capture substrate trends. Apparently, the image technique combined with solving the bathymetry continuity equation effectively reveals the variation of the bed surface elevation, with an average accuracy of about 90% in this study.

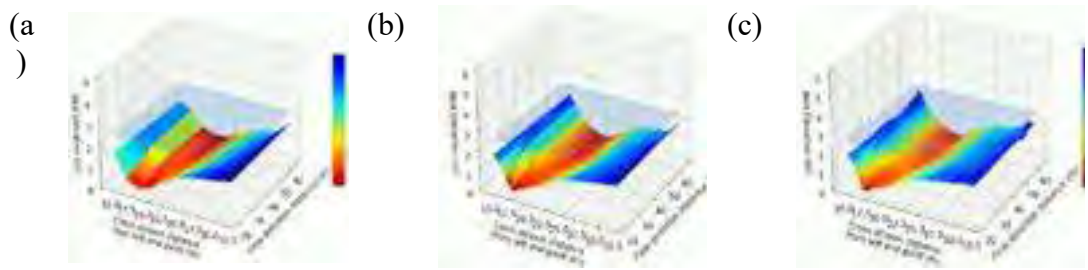

Figure 6. Bathymetry measurement of different girds (a)10x15; (b)20x30; (c)40x60

Table 2. Bathymetry measurement results

	Grids		
	10x15	20x30	40x60
Section2	12.69%	13.77%	13.73%
Section3	8.97%	9.39%	10.52%
Section4	7.54%	10.15%	9.45%
Average	9.73%	11.1%	11.23

5. Conclusions

The traditional methods for estimating discharge and measuring bathymetry have limitations and uncertainties, particularly during extreme events and in low-velocity flows. The use of LSPIV has gained popularity as a non-intrusive method for measuring hydrological data, but it is susceptible to environmental factors that can affect its accuracy. In this study, the CNN model was introduced to improve the accuracy of velocity measurements obtained through LSPIV. The CNN-based method demonstrated superior measurement capabilities compared to the traditional LSPIV method, as it could capture a more comprehensive flow field, both inside and outside the river. The CNN method showed approximately 10% improvement in accuracy, reducing errors caused by environmental factors such as light reflections and shadows. Furthermore, this study successfully applied the surface velocities obtained from the CNN method to derive two-dimensional bathymetry by solving the continuity equation. The results showed that the proposed method effectively estimated bathymetry with an average accuracy of approximately 90%. The three-dimensional bathymetry inversions based on different grid densities demonstrated satisfactory results, capturing the variation trend of the substrate.

In conclusion, this innovative hydrological measurement method, combining LSPIV with a CNN model, offers a promising solution for accurate and efficient measurement of surface velocity and bathymetry in rivers. It overcomes the limitations of traditional methods, provides improved measurement capabilities, and has the potential to enhance water management in the face of unpredictable water resources due to climate change. The non-intrusive, digital, and low-cost characteristics of the method make it suitable for increasing the measurement coverage points and improving the management of irrigation and drainage systems.

References

Bradley, A. A., Kruger, A., Meselhe, E. A., & Muste, M. V. (2002). Flow measurement in streams using video imagery. Water Resources Research, 38(12), 51-1.

Ferrolino, A., Mendoza, R., Magdalena, I., & Lope, J. E. (2020). Application of particle swarm optimization in optimal placement of tsunami sensors. PeerJ Computer Science, 6, e333.

Fujita, I., & Komura, S. (1994). Application of video image analysis for measurements of river-surface flows. Proceedings of hydraulic engineering, 38, 733-738.

Gao, L., Zhang, L. M., Chen, H. X., & Shen, P. (2016). Simulating debris flow mobility in urban settings. Engineering Geology, 214, 67-78.

Hao, W., Bie, R., Guo, J., Meng, X., & Wang, S. (2018). Optimized CNN based image recognition through target region selection. Optik, 156, 772-777.

Herschy, R. (1993). The velocity-area method. Flow measurement and instrumentation, 4(1), 7-10.

Johnson, E. D., & Cowen, E. A. (2016). Remote monitoring of volumetric discharge employing bathymetry determined from surface turbulence metrics. Water Resources Research, 52(3), 2178-2193.

Juracek, K. E. (1798). Geomorphic changes caused by the 2011 flood at selected sites along the lower Missouri River and comparison to historical floods. US Geological Survey Professional Paper.

Kantoush, S. A., Schleiss, A. J., Sumi, T., & Murasaki, M. (2011). LSPIV implementation for environmental flow in various laboratory and field cases. Journal of Hydro-environment Research, 5(4), 263-276.

Ma, J., Jiang, X., Fan, A., Jiang, J., & Yan, J. (2021). Image matching from handcrafted to deep features: A survey. International Journal of Computer Vision, 129(1), 23-79.

Meselhe, E. A., Peeva, T., & Muste, M. (2004). Large scale particle image velocimetry for low velocity and shallow water flows. Journal of Hydraulic Engineering, 130(9), 937-940.

Mesinger, F., & Arakawa, A. (1976). Numerical methods used in atmospheric models.

Sivapragasam, C., & Muttil, N. (2005). Discharge rating curve extension–a new approach. Water Resources Management, 19(5), 505-520.

Stelling, G. S., & Duinmeijer, S. A. (2003). A staggered conservative scheme for every Froude number in

rapidly varied shallow water flows. International journal for numerical methods in fluids, 43(12), 1329-1354.

Zhou, W. (2002). An alternative leapfrog scheme for surface gravity wave equations. Journal of Atmospheric and Oceanic Technology, 19(9), 1415-1423.

Le Coz, J., Hauet, A., Pierrefeu, G., Dramais, G., & Camenen, B. (2010). Performance of image-based velocimetry (LSPIV) applied to flash-flood discharge measurements in Mediterranean rivers. Journal of hydrology, 394(1-2), 42-52.

Kuczera, G. (1996). Correlated rating curve error in flood frequency inference. Water resources research, 32(7), 2119-2127.

Ryskin, G., & Leal, L. G. (1983). Orthogonal mapping. Journal of Computational Physics, 50(1), 71-100.

EVALUATION OF THE EFFECT OF INSTALLING ICT DEVICES FOR PADDY IRRIGATION FROM THE VIEWPOINT OF PADDY WATER TEMPERATURE MANAGEMENT

Masaomi Kimura[1], Wenpeng Xie[2], Katsunori Shimomura[3] and Yutaka Matsuno[4]

ABSTRACT

Improving the productivity of paddy rice cultivation per unit labor cost of farmers is essential for addressing future challenges such as the aging of the farming population and a decline in the number of successors. According to several statistical analyses, labor associated with daily water management, including the operation of inlet and outlet gates or valves for irrigation and drainage of paddy fields, constitutes a significant proportion of the total labor time required for paddy rice cultivation.

Recent advancements in technology have facilitated the modernization of irrigation practices in the field of water management for paddy cultivation, resulting in a reduction of labor associated with daily water management. One such solution is the implementation of ICT smart automated sluice gates, which allow for remote control and automatic scheduling of irrigation and drainage in paddy fields. While the benefits of such automated gates in reducing labor costs are evident, they also offer the added advantage of enabling paddy water temperature management. With climate change leading to increased concerns over high-temperature damage to rice grains, particularly in Japan, the ability to manage paddy water temperature is a valuable tool for farmers seeking to mitigate the effects of excessively high water temperatures during hot summers.

Field experiments were conducted in a paddy plot in Japan, where an ICT automated sluice gate (Paditch Gate, Enowa Co., Ltd.) was installed at the inlet. This study presents the experimental findings, including the spatio-temporal variation of paddy water temperature and the effect of scheduled water management using ICT automated gates on reducing water temperature aiming to mitigate high-temperature damage to rice grains under global warming conditions.

1. Introduction

Climate change and global warming pose significant threats to sustainable agriculture worldwide, impacting the spatio-temporal variation of available water resources and causing yield losses in staple food crops such as wheat and rice. In humid subtropical Asian regions, extreme high temperatures during the summer season not only reduce yields but also degrade the quality of rice grains, primarily through the restriction of grain growth due to reduced enzyme activity related to starch synthesis. High-temperature damage results in inadequately filled grains, causing cracking and the formation of milky-white kernels (chalky grains), which are expected to worsen with future global warming. Studies have shown that the occurrence of chalky grains increases when the average temperature in the 20 days after heading exceeds 26°C, and that high temperatures in the first 10 days after heading lead to an increase in cracked grains (Chiba et al., 2017). Additionally, high night-time temperatures during the grain-ripening period have been found to be more detrimental to rice grain weight than high daytime temperatures (Morita et al., 2005). Several effective measures have been proposed and recommended by governments (Tsurita et al., 2013) to prevent this type of damage, including variety development, soil management, modification of planting methods, and water and

[1] Associate Professor, Faculty of Agriculture, Kindai University, Japan, mkimura@nara.kindai.ac.jp
[2] JSPS Research Fellow, Institute of Industrial Science, the Univertity of Tokyo, Japan.
[3] CEO, Enowa Co., Ltd., Japan.
[4] Professor, Faculty of Agriculture, Kindai University, Japan.

fertilizer management. Among these, paddy water management (Chiba et al., 2017; Nishida et al., 2018) is one of the simplest methods for farmers to implement (Kimura et al., 2022).

On the other hand, future projections for Japanese rice farmers, estimated by several institutes using various statistical data, indicate that the Japanese rice farming industry faces complex and serious challenges such as an aging farming population and a decreasing number of successors. As such, enhancing the productivity of paddy rice per unit labor cost of farmers is crucial for addressing these challenges. According to several statistical analyses, labor associated with daily water management, including the operation of inlet and outlet gates for irrigation and drainage of paddy fields, constitutes a significant proportion of the total labor time required for paddy rice cultivation.

In recent years, technical innovation in the field of water management for paddy cultivation has shown steady progress, enabling a reduction in labor associated with daily water management. One such solution is the implementation of ICT smart automated sluice gates, which allow for remote control and automatic scheduling of irrigation and drainage in paddy fields. While the benefits of such automated gates in reducing labor costs are evident, they also offer the added advantage of enabling control over ponding water temperature in paddy fields. Given that high-temperature damage to rice grains is a major concern in Japan, the ability to control water temperature in paddy fields is a valuable tool for farmers seeking to mitigate the effects of excessively high water temperatures during hot summers.

In this study, field experiments were conducted in a paddy plot located in Japan, where an ICT automate gates was installed at the inlet. The experimental findings, including the spatio-temporal variation of ponding water temperature and the effect of scheduled water management using ICT automated gates on reducing water temperature, will be presented. This paper also describes numerical models that represent the mechanisms of water temperature variation in paddy ponding water by combining a heat balance model among air-rice plants-water-soil with 2-dimensional flow analysis models.

2. Methods

2.1 Field experiments

An observation paddy plot was selected in Toyama Prefecture, Japan. An ICT smart automated sluice gate (Paditch Gate, Enowa Co., Ltd.) was installed at the inlet of the plot (**Figure 1**) to allow the paddy farmer to remotely control the gate and manage irrigation at arbitrary times. The plot has access to a relatively cool and large amount of irrigation water from its mountainous basin.

The Paditch Gate also has a scheduled operation function that can be set through a website. We examined various gate opening schedules, such as simultaneous opening for 2.5 days, 6-hour openings every 30 hours (e.g., 0 am to 6 am on the first day, 6 am to 12 pm on the second day, 12 pm to 6 pm on the third day, etc.), and 3-hour openings every 30 hours (e.g., 0 am to 3 am on the first day, 6 am to 9 am on the second day, 12 pm to 3 pm on the third day, etc.).

Figure 1. Paditch Gate (ICT smart automated sluice gate) installed at the observation plot.

To understand the spatio-temporal variation of ponded water temperature in the experimental plot, ten temperature loggers (HOBO MX2201, Onset) were deployed. The locations where they were placed are shown in **Figure 2**. An auto-capturing camera (TLC 200, Brinno) was installed at the paddy inlet, aimed at the ICT automated gate, to capture the situation around the gate every 30 minutes as well as the temperature and depth loggers (HOBO U20, Onset) that were installed at inlet and outlet as illustrated in **Figure 2**. Temperature loggers (TR-52i, T&D) were also installed, as shown in **Figure 3**, 10 cm and 20 cm below the soil surface at locations No.1, 4, and 7 as well as inlet and outlet to measure the spatio-temporal variation of soil temperature beneath the ponded water.

Meteorological data, including air temperature, relative humidity, atmospheric pressure, wind speed, and solar radiation, were collected during the observation period using a weather station (ATMOS 41, Meter) installed at the plot, as shown in **Figure 4**.

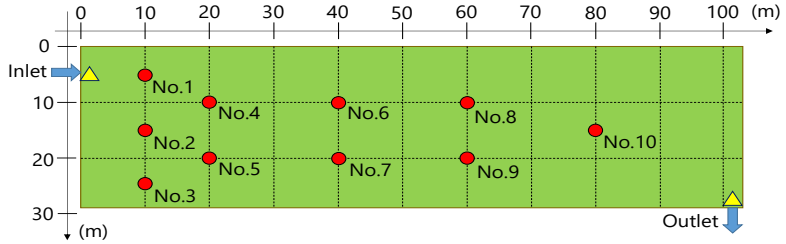

Figure 2. Observation points for temperature and depth of ponded water in the plot.

Figure 3. Temperature loggers installed in the experimental paddy plot for temperature measurement of ponded water and soil.

Figure 4. Weather station and environmental sensors installed at the plot.

2.2 Numerical models

In this section, we describe the numerical algorithms developed by the authors (Xie et al., 2021; Xie et al., 2022) to simulate temperature distributions of paddy ponding water and evaluate the efficiency of decreasing ponding water temperature using automated sluice gates. **Figure 5** shows a schematic diagram of the numerical models (layer model), which consist of three parts: rice leaves, water body, and underground soil.

The basic equation for the heat balance of leaf surface is given as;

$$\frac{\partial T_c}{\partial t} = \frac{R_{nc} - H_c - lE_c}{c_c \rho_c l_c LAI} \tag{1}$$

where, T_c is plants community temperature, R_{nc} is net radiation to the vegetation layer, H_c and lE_c are sensible heat flux and latent heat flux to the vegetation layer, respectively. c_c is specific heat of leaves, ρ_c is leaf density, l_c is leaf thickness and LAI is leaf area index.

The net radiation R_{nc} can be expressed by following equation;

$$R_{nc} = (1 - f_v)\{(1 - \alpha_c)S + L_{da} + L_{uw} - L_{uc} - L_{dc}\} \tag{2}$$

where, S is solar radiation, α_c is albedo of vegetation, L_{dc} and L_{da} are downward long wave radiation of plants and atmosphere, respectively. L_{uc} and L_{uw} are upward long wave radiation of plants and water, respectively. f_v is radiation transmittance of vegetation which is expressed by

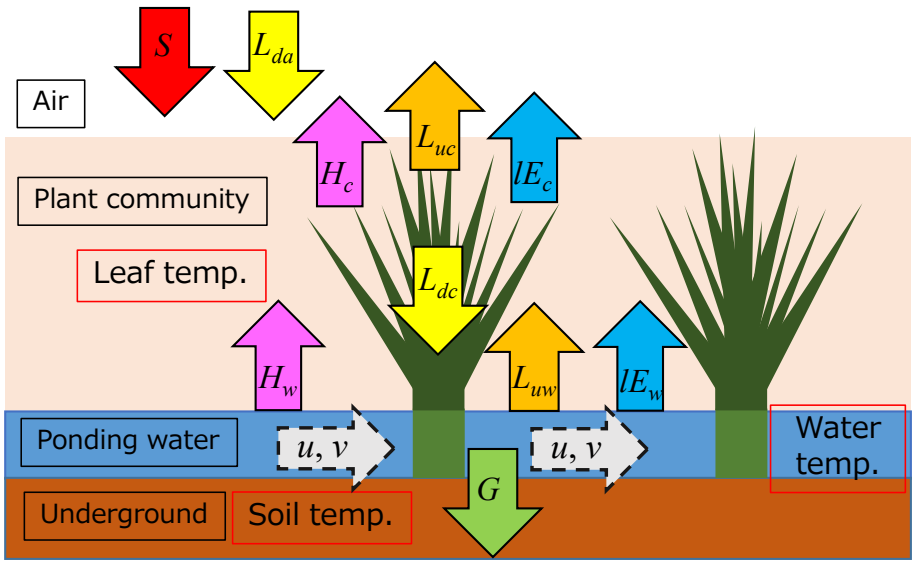

Figure 5. Schematic diagram of the numerical models for thermal energy exchange, considering the flow velocity of ponding water in a paddy plot.

the following equation;

$$f_v = \exp(-k \cdot LAI) \tag{3}$$

where, k corresponds to the extinction coefficient.

The basic equation for the heat balance of water body is given as;

$$\frac{\partial T_w}{\partial t} + u\frac{\partial T_w}{\partial x} + v\frac{\partial T_w}{\partial y} = D_w\left(\frac{\partial^2 T_w}{\partial x^2} + \frac{\partial^2 T_w}{\partial y^2}\right) + \frac{R_{nw} - H_w - lE_w - G}{\rho_w c_w h} \tag{4}$$

where, T_w is ponded water temperature, u and v are the components of x and y axis of flow velocity of ponded water, respectively, which are determined by solving the shallow water

equations considering the resistance of rice bunches represented by drag coefficients (Kimura et al., 2015). D_w is diffusion coefficient of water temperature, R_{nw} is net radiation to the water surface, H_w and lE_w are sensible heat flux and latent heat flux to the water body layer, respectively. ρ_w and c_c are density and specific heat of water, respectively, and h is ponded water depth.

The net radiation to water surface R_{nw} can be determined by following equation;

$$R_{nw} = f_v\left\{(1-\alpha_w)(1-\alpha_c)S + L_{da}\right\} + (1-f_v)L_{dc} - L_{uw} \tag{5}$$

where, α_w is albedo of water.

To calculate the heat flux to the ground G, the vertical soil temperature distribution is estimated by following equation.

$$\frac{\partial T_g}{\partial t} = D_g \frac{\partial^2 T_g}{\partial z^2} \tag{6}$$

where, T_g is soil temperature, D_g is thermal conductivity of paddy soil and z is depth from the soil surface. In this study the upper boundary condition was set as water temperature and the lower boundary condition was set as the annual average air temperature of the observation field.

From the soil temperature distribution, the soil heat flux G was calculated by following equation.

$$G = c_g \rho_g \int_0^D \frac{\partial T_g}{\partial t} dz \tag{7}$$

where, c_g and ρ_g are specific heat and density of soil, respectively, and D corresponds to the damping depth.

3. Results and discussion

The time series of observed water depth inside a box pool upstream of the ICT automated gate, as well as the ponded water depth near inlet and outlet of the paddy plot, are shown in **Figure 6**. The decrease in water depth in the box pool corresponds to the duration when the ICT automated gate was open. The results confirmed the effectiveness of the ICT automated gate in terms of remote and scheduled paddy water management. It should be noted that the effectiveness of deploying ICT automated gates strongly depends on the availability of irrigation water at the installation point, such as water pressure in pipelines or water levels in open channels.

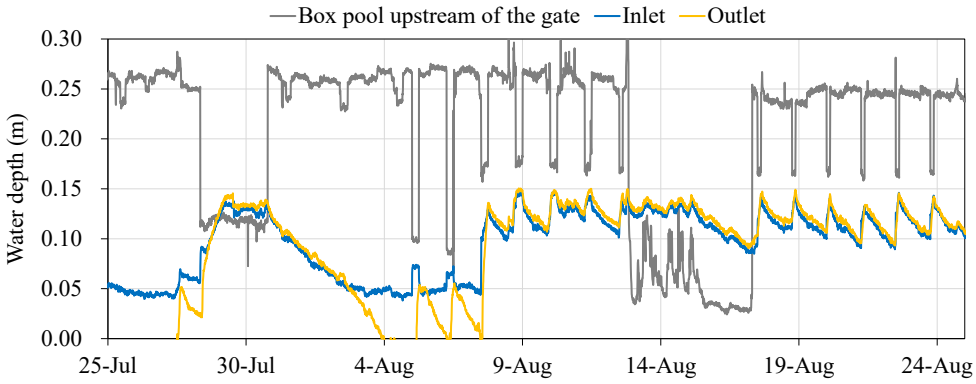

Figure 6. Observed water depth inside a box pool upstream of the ICT automated gate and the ponded water depth near inlet and outlet of the paddy plot.

The time series of water temperature obtained at the observation points inside the paddy plot are illustrated in **Figure 7**. The variation in water temperature showed a tendency for the ponding water to be cooler closer to the inlet point of the paddy fields. As a result, it was revealed that the water temperature near the inlet was more easily lowered during the gate

opening period compared to other positions. The efficiency of suppressing rising water temperatures was assumed to be relatively higher in paddy fields where cooler irrigation water is available.

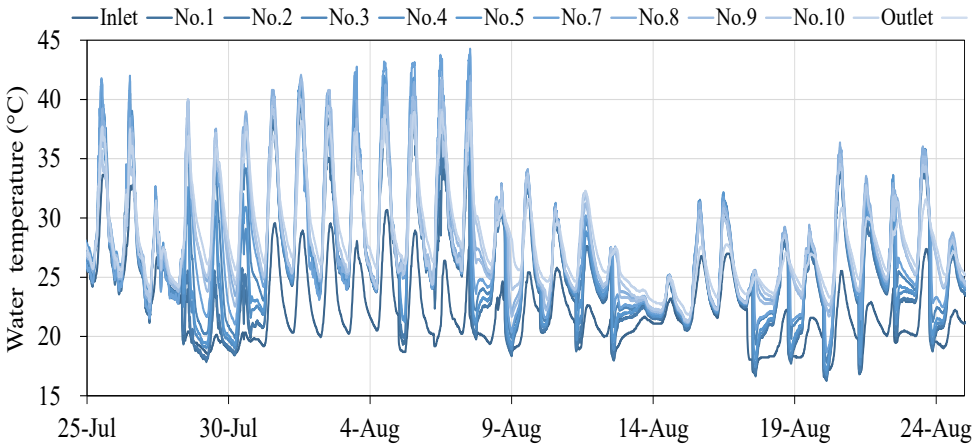

Figure 7. Time series of ponded water temperature at the observation points inside the paddy plot.

The spatio-temporal distribution of soil temperature measured at No.1, 4, 7 as well as the inlet and outlet of the experimental paddy plot are illustrated in **Figure 8**. They showed a similar trend to the ponded water temperature, which suggests that deploying an ICT automated gate could be an effective strategy for mitigating high-temperature damage to rice grains while also saving on labor costs.

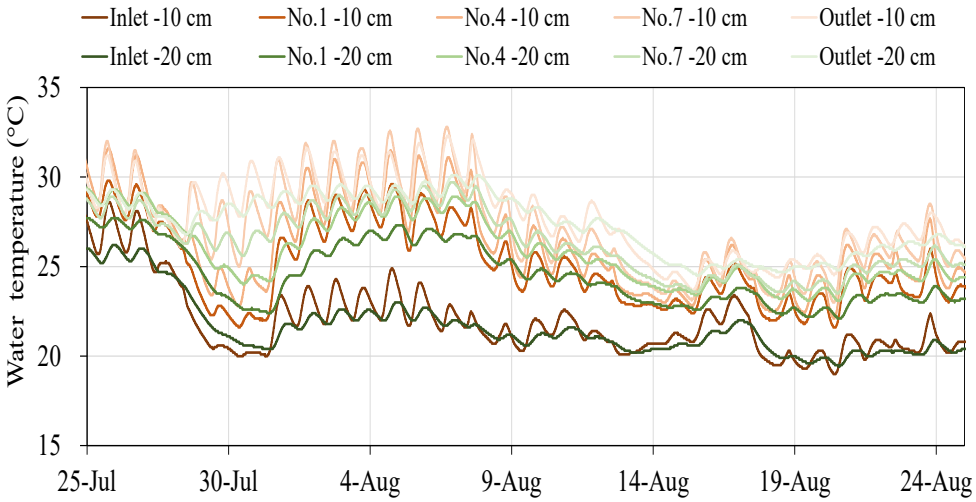

Figure 8. Time series of ponded water temperature at the observation points inside the paddy plot.

The simulation models proposed for heat exchanges in paddy fields have been validated using observed ponded water temperatures from the same experimental paddy plot in 2017 and 2018, as reported by Xie et al. (2022). **Figure 9** illustrates the relationship between the measured and simulated ponded water temperatures. The simulated water temperature shows good agreement with the observed data from 2017 and 2018, with mean Root Mean Square Errors (RMSE) of 1.67°C and 1.39°C, respectively. Therefore, our focus will be on validating the two-dimensional distribution model of ponded water and soil temperature using data obtained in 2021.

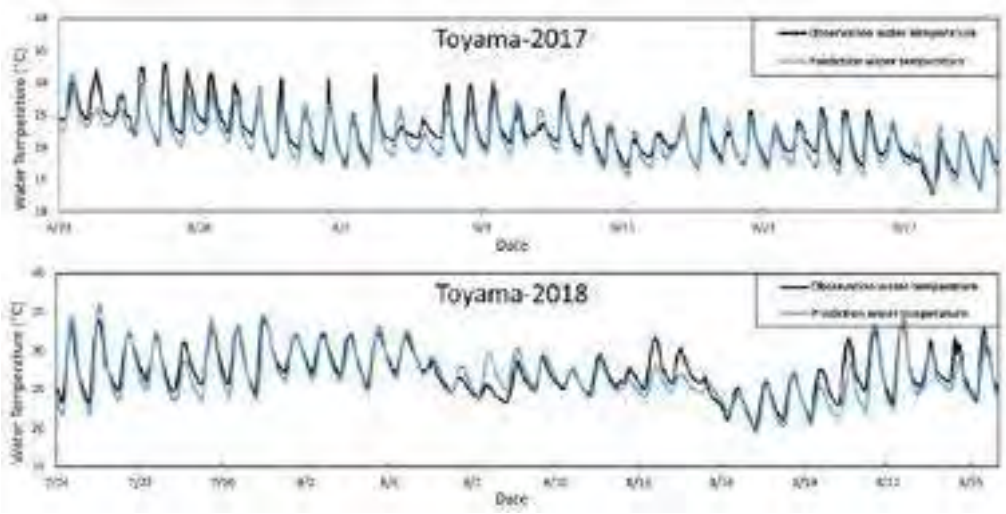

Figure 9. Validation results of the proposed simulation models for heat balances in paddy fields. (Xie et al., 2022)

4. Conclusions

In this study, field experiments were conducted in a paddy plot in Japan, where an ICT automated gates was installed at the inlet to clarify the additional function of the gates in terms of ponding water temperature control. The results showed the reliability of remote scheduled ICT automated gate management. However, the efficiency of deploying the ICT automated gates strongly depends on the availability of irrigation water at the installed point, such as water pressure in pipelines or water level in open channels. The observed variation in ponding water temperature suggested the possibility of temperature management in the thermal environment of paddy plots, which may contribute to deciding on an adaptation strategy against high-temperature damage to rice grains through paddy water management controlled by ICT automated sluice gates in the future. Further quantitative analysis regarding the effect of scheduled paddy water management on decreasing ponding water temperature rise is ongoing, and the results and findings will be reported.

REFERENCES

Chiba, M., Terao, T., Watanabe, H., Matsumura, O., Takahashi, Y., 2017. Improvement in rice grain quality by deep-flood irrigation and its underlying mechanisms. Japan Agricultural Research Quarterly 51.2: 107-116.

Kimura, M., Kobayashi, S., Mitsuyasu, M., Xie, W., Iida, T., 2022. Simulation model of water temperature variation in dual-purpose canals considering return flow from upstream paddy fields. Irrigation and Drainage 71.S1: 138-154.

Kimura, M., Kouketsu, H., Iida, T., Kubo, N., 2015. A calculation method for two-dimensional ponding water flow on a paddy field plot with rice plants, Irrigation, Drainage and Rural Engineering Journal 83.1: 47-58.

Morita, S., Yonemaru, J., Takanashi, J., 2005. Grain growth and endosperm cell size under high night temperatures in rice (*Oryza sativa* L.). Annals of Botany 95: 695-701.

Nishida, K., Yoshida, S., Shiozawa, S., 2018. Theoretical analysis of the effects of irrigation rate and paddy water depth on water and leaf temperatures in a paddy field continuously irrigated with running water. Agricultural Water Management 198: 10-18.

Tsurita, I., Prabhakar, S.V.R.K., Sano, D., 2013. Approaches to climate change adaptation: a case study of agricultural initiatives in Japan. In: Ha, H. & Dhakal, T. (Eds.) Governance approaches to mitigation of and adaptation to climate change in Asia. United Kingdom: Palgrave Macmillan: 87-102.

Xie, W., Kimura, M., Iida, T., Kubo, N., 2021. Simulation of water temperature in paddy fields by a heat balance model using plant growth status parameter with interpolated weather data from weather stations. Paddy and Water Environment 19.1: 35-54.

Xie, W., Kimura, M., Asada, Y., Iida, T., Kubo, N., 2022. The development of a hybrid model to forecast paddy water temperature as an alert system for high-temperature damage. Irrigation and Drainage 71.S1: 124-137.

ANALYZING THE IMPACT OF AGRICULTURAL WATER TRANSFER MECHANISMS ON WATER RESOURCE ALLOCATION EFFICIENCY AND BENEFITS IN TAIWAN UNDER CLIMATE CHANGE

Guan-Yu Lin[1], Ya-Wen Chiueh[2]*

Climate change is causing an increase in the frequency of droughts and floods in Taiwan, which has adverse effects on the allocation of water resources. Due to the competition between industrial and public water users, agricultural water resources are often compromised, resulting in negative impacts on agricultural production and the environment. Balancing the needs of people, industries, and ecological environments is a crucial challenge for Taiwan in the face of climate change. Economic experiments have been shown to be effective in evaluating alternative policies quickly and predicting market outcomes before policy implementation. Therefore, we conducted three economic experiments to analyze the impact of various agricultural water diversion or trading mechanisms on the efficient and effective use of agricultural environmental water. The study aims to demonstrate the differences in water allocation benefits between the non-drying and drying seasons and between water usage that considers agri-environmental water and that which does not. It also aims to demonstrate the differences in water allocation benefits between water usage that considers agri-environmental benefits and that which does not, as well as policy that supports environmental water retention and that which does not support it. The goal is to establish a fair and efficient mechanism for managing and allocating agricultural water resources in drought periods in Taiwan. The anticipated findings of this study will contribute to the efficient and effective allocation of water resources, especially during periods of drought, and aid in the development of policies that balance the needs of various stakeholders and promote sustainable development.

Key words： Agricultural water transfer, Economic experiment, Water resource allocation, Climate change

Introduction

Taiwan's rainfall is concentrated in the summer, with low precipitation in the winter. Due to its narrow and elongated shape and the distribution of high mountains in the central region, most of its rivers are on seasonal rivers. Not only does the water volume fluctuate greatly between the summer and winter seasons, but also the storage of fresh water is challenging. Under the impact of climate change, Taiwan's precipitation may become more unstable. For instance, from 2020 to 2021, Taiwan experienced an unusual drought situation. From June to September 2020, there was little rainfall due to the influence of an extremely strong subtropical high-pressure system. The following autumn and winter were also affected by La Niña, resulting in below-average rainfall. By May 2021, the precipitation remained low, affecting around 74,000 hectares of farmland that required compensation for water stoppage. Miaoli, Taichung, and northern Changhua regions are implementing 61-day rotational water supply. Under the influence of climate change, how to allocate water resources while considering the needs of the public, various industries, and the ecological environment has become a crucial challenge Taiwan is currently facing.

According to Article 24 of the Water Act, water rights obtained but not used for more than two years shall be deemed forfeited upon investigation and public announcement by the competent authority. The Taiwan Water Corporation, managed by the Water Resources Agency, MOEA, also faces performance pressure in fulfilling consumer water service contracts. Therefore, Taiwan currently faces challenges in water resource allocation and management, both during non-drought periods and drought periods.

Chiueh (2002) pointed out that water resource transactions during non-drought periods often adopt terms such as "channel borrowing fees" or "construction usage fees" to circumvent water laws, resembling an underground market. During drought periods, Taiwan often holds government-initiated meetings to coordinate the water stoppage of farmlands. The Council of Agriculture, Executive Yuan, subsidizes the area of farmland under water stoppage for farmers, and agricultural water is then redirected to support the industrial sector. Chen (2003) pointed

[1] Taiwan Research Institute on Water Resources and Agriculture[1],
[2] National Tsing Hua University, Taiwan

out that in Taiwan, those capable of using water more efficiently cannot obtain water rights through a cost-sharing mechanism. This water resource management model does not follow a user-pay principle, and it lacks social justice.

The existing Water Law has not clearly regulated the form of water resource allocation during drought periods. The order of priority of Water Consumption Purposes is explicitly defined in Article 18 of the Water Law, which includes domestic and public water supply, agricultural water use, hydropower, industrial water use, water transportation, and other purposes. However, the competent authority, Water Resources Agency, MOEA, has the discretion to consider specific waterways or government-designated industrial areas and request approval from central authorities for any necessary changes. It can be understood that the current Water Law does not take into account environmental water usage and environmental base flow factors, and the priorities of Water Consumption Purpose do not implement.

Currently, due to the regular of the Water Law, Taiwan still lacks a complete water resource trading management mechanism. However, the Intergovernmental Panel on Climate Change (IPCC) proposed water market development as a hope to improve water resource utilization efficiency in 2008 (Bates, et al., 2008). In response to climate change, some countries have amended their past water resource management regulations and established water rights trading markets. For instance, Australia began water market development under the Council of Australian Government (COAG) in 1994, and in 1991, California in the United States established the Drought Water Bank (DWB) in the Colorado River Basin to address drought issues (Chiueh, 2005; Möller-Gulland & Donoso, 2016; Macaulay, 2009). Therefore, designing a comprehensive water resource trading management mechanism and incorporating environmental water rights targets into the regulations offer hope to improve Taiwan's current water resource utilization efficiency.

The findings from laboratory research can be a robust method for studying economic theories before conducting real-world experiments (Smith, 1976). Moreover, experimental economics allows for replicable and swift evaluation of alternative policies, providing insights into market outcomes before policy implementation (Tisdell, 2011; Tisdell et al., 2004). This study aims to design an economic experiment by drawing on the water resource management experiences of countries like Australia, Colorado in the United States, and Chile. The goal is to explore whether integrating environmental water rights targets into the water market system within a fully competitive market setting can enhance water resource allocation efficiency during drought periods in Taiwan. The research seeks to establish Taiwan's water resource management system from the standpoint of mechanism efficiency. The research objectives can be summarized as follows:

1. Through economic experiments, we aim to compare the water resource allocation efficiency of monetizing environmental water benefits during both non-drought and drought periods under a market mechanism in Taiwan.
2. Using economic experiments, we seek to compare the water resource allocation efficiency of providing subsidies for environmental water during both non-drought and drought periods under a market mechanism in Taiwan.

Experimental Hypotheses

Experimental Mechanism Assumptions

In response to Taiwan's current industrial development , the increase in water demand for industrial use is driven by the growth of the manufacturing and business sectors. As the adaptability of the agricultural industry is higher than the industry, water resources can be reallocated to improve usage efficiency. However, the existing Water Law in Taiwan does not clearly specify the base flow or targets for environmental water retention, leading to a lack of emphasis on environmental benefits amidst industrial development improvements. Hence, this study employs an economic supply-demand model to design experiments for analysis, drawing inspiration from the water banking systems in the United States and water markets in Australia.

Experimental area setup

To provide practical guidance for policy-making, we assume a hypothetical area H, taking reference from the Hsinchu area, which is a high economically valuable water resources

conflict area. The primary water supply facilities in this region include Baoshan Reservoir, Second Baoshan Reservoir, Shangping Weir, and Longen Weir. The Shangping Weir was incorporated as a subsidiary facility of the Second Baoshan Reservoir in 2014 by the Ministry of Economic Affairs. Both Baoshan Reservoir and Second Baoshan Reservoir serve as public water supply sources, catering to the water needs of the Hsinchu region's residents and the Hsinchu Science Park. On the other hand, Longen Weir provides water for agricultural and industrial purposes.

Based on data from the Water Resources Agency, the average annual water withdrawal for agricultural purposes between 2007 and 2017, excluding the drier year of 2014, was 33,517.3 million tons. Due to the reuse of water between upper and lower sections in agricultural usage, and the challenge of collecting data on river flow usage, this study only considers the water intake from weirs for agricultural purposes.

Both Baoshan Reservoir and Second Baoshan Reservoir serve as water sources for the Hsinchu Science Park. As a result, industrial and public water usages are combined for calculation. The average total water consumption for industrial use in the Hsinchu region, excluding the drier year of 2014, between 2007 and 2017, was 15,097.1 million tons. As the reuse of recycled water depends on the characteristics of each factory and their respective industrial conditions, this study does not consider the use of recycled water for industrial purposes.

The water usage for agricultural and industrial purposes in the Hsinchu area, obtained from dam intakes, is shown in Figure 1.

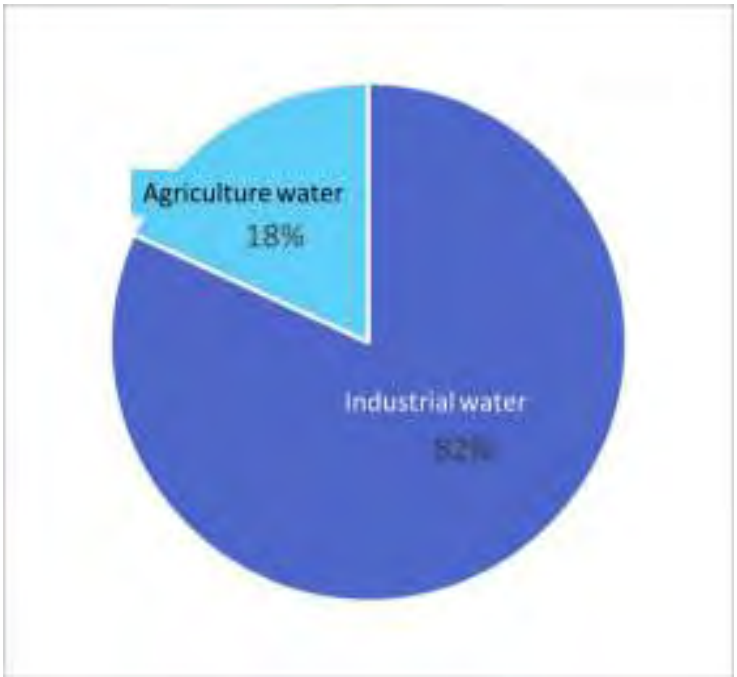

Average Water Usage Proportion from Dam Intakes in the Hsinchu Region during Non-Drought Years (2007-2017)

This study adopts the Tennant method Mean Annual Flow (MAF) method from hydrology, which suggests the following standards for ecological flow maintenance: 10% of poor habitat, 30% of satisfactory or moderate habitat, and 60% for good habitat. These percentages represent the minimum environmental flow required to sustain different ecological conditions. Additionally, taking into account observations from 22 New Zealand rivers by Jowett (1997), larger rivers should maintain 10% to 20% of their monthly average flow, while smaller rivers should maintain 20% to 30% of their monthly average flow (Water Resources Agency, Ministry of Economic Affairs, 2014; Jowett, 1997).

Considering the assumed region H in this study has only one major river, we will use 12% as the minimum required water amount for environmental production and maintenance.

This research assumes an area, H, with an area of 100,000 square meters. The water resource trading characteristic is a monopolistic market, where all water resources are owned by the agricultural sector. There is a river running through the area, and a reservoir is set up to intercept all the water flow for agricultural and industrial use in the region. The infrastructure for water resource allocation and transportation is well-established, and there are no topographical differences or water loss issues during water transportation.

During the drought period, the available water supply is 10,000 tons. The water requirement to maintain normal agricultural production is 1,800 tons, while the industrial water demand is 8,200 tons. To ensure the normal functioning of the environment, the water requirement is set at 12% based on Tennant's Mean Annual Flow (MAF) method (1976) and Jowett's (1997) recommended river base flow, amounting to 1,200 tons.

The allocatable water during the drought period is determined according to the operation guidelines of the Disaster Emergency Response Team of the Water Resources Agency, Ministry of Economic Affairs (2016), which defines a Level 1 drought as a shortage of public water supply exceeding 30% and agricultural water supply shortage exceeding 50%. Thus, it is assumed that the total allocatable water during the drought period is 6,640 tons. The schematic diagram of Area H is shown in Figure 2.

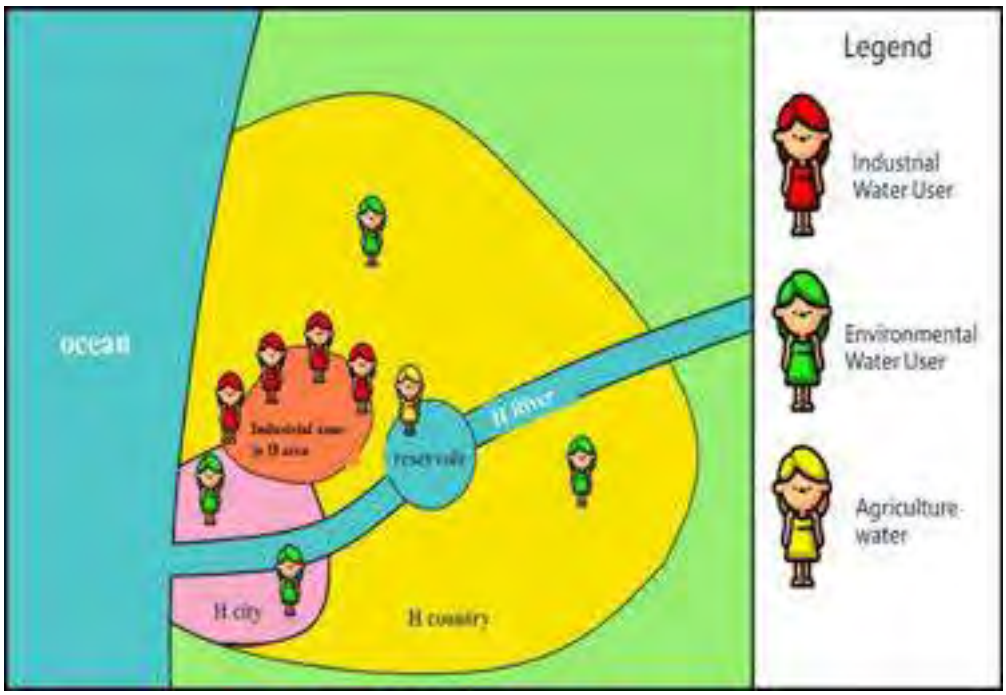

Figure 2: Schematic Diagram of Area H

Experimental Role Assumptions

The water use efficiency for each water consumption purpose in Region H is assumed based on data and previous studies in the Hsinchu area. For agricultural water use efficiency, it is calculated based on the rice yield and rice value in the Hsinchu region from 2013 to 2017, as well as the irrigation water volume for rice cultivation from the Water Resources Agency's water use statistics database during the same period. On average, the value of each ton of water used for rice cultivation in the Hsinchu region is NT$3.0331. Chen (2003) also pointed out that the average agricultural water use efficiency in Taiwan is NT$3.2 per ton of water. For industrial water use efficiency, Chiueh (2015) used the contingent valuation method to estimate that the willingness to pay for each ton of water in the industrial sector during a drought period is NT$28. The environmental water use efficiency is estimated based on Qu (2014), considering the non-market benefits per kilogram of rice for both the agricultural sector and the general

public, which amounts to NT$29.67. Additionally, the non-market benefit per ton of water for rice production, with a water footprint of approximately 3.4 cubic meters per ton, is NT$8.73 (Chapagain & Hoekstra, 2004; Qu, 2014). In summary, this study assumes that the average water use efficiency for agricultural water in Region H is NT$3 per ton, the average efficiency for industrial water use is NT$26 per ton, and the environmental water use efficiency is NT$9 per ton.

The role assignment for each water user in the experiment is summarized in Table 1, and the experimental hypothetical region map is depicted in Figure 2.

Table 3: Summary of Experimental Role Information

Water User Type	Supply/demand	name	Non-drought-year Allocable Water Quantity (tons)	Drought-year Allocable Water Quantity (tons)	Water Quantity Required for Sustaining Normal Production (tons)	Water Benefit (NTD)	Per Capita Water Purchase Funds (in dollars)	User Instructions
Agriculture water	supplier		10,000	6,640	2,000	3		Irrigation Association Organization in H area
Industrial Water User	demander	A、B、C、D	0	0	2,000	26	50,000	Industrial businesses in H area
Environmental Water User		E	0	0	600	9	6,750	EPA in H County
		F	0	0	600		6,750	EPA in H city
		G	0	0	0		6,750	NGO in H area
		H	0	0	0		3,375	NGO in H area

Experimental Design

To understand the impact of incorporating environmental water rights on the allocation of water quantity, water price, and benefits in Taiwan, this study is divided into three stages: the first stage is the "non-monetized environmental water benefits" experiment, the second stage is the "monetized environmental water benefits" experiment, and the third stage is the "monetized environmental water benefits with water subsidy" policy sensitivity experiment. The experimental framework is illustrated in Figure4. To achieve the design similar to the Australian water market mechanism, this study assigns clear property rights and transferable rights to agricultural, industrial, and environmental water users. However, as explained in the previous section, the water market characteristics in region H involve a monopolistic market structure, which means that in the experiment, agricultural water users can sell water resources while industrial and environmental water users can purchase water resources.

Before the experiment begins, the participants will be informed of the user roles they will be assigned, along with relevant information such as their water requirements, benefits, and water purchasing funds. They will be clearly instructed that the goal of the experiment is to "maximize their own water benefits." Industrial water users can bid for water resources in units of 500 tons during each market period, while environmental water users can bid for 150 tons of water. The water allocation for environmental users is divided into four equal parts based on their required water volume for maintaining production. Each user can submit five different prices to purchase water in each round, allowing them the opportunity to increase their benefits. If a water user's bids secure four parts of the required water, they can maintain their expected benefits for the year. If all five bids are successful, they will increase their benefits for that round. The defined benefits in this experiment can be represented by the following formula

$$U = (B - P) * V$$ Formula 1

In which, U = User's overall utility; B = User's water benefit; P = Water purchase price for the user; V = Water volume purchased by the user.

The market in this experiment is a monopoly market for agricultural water, where if users bid higher than the water benefit of agricultural users, they will choose to sell water resources until all the water resources are sold out.

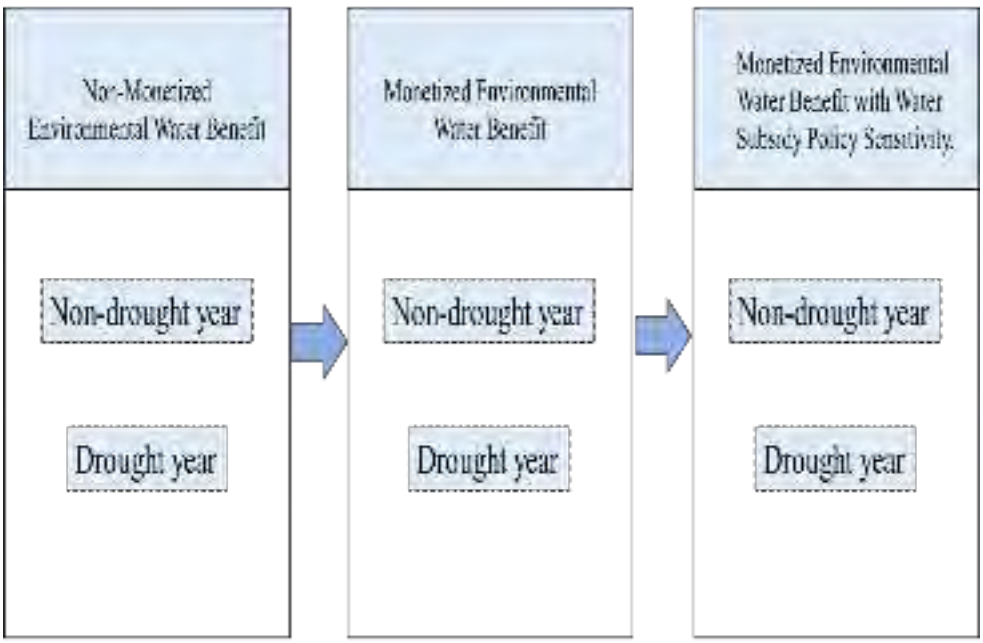

Figure 3: Experimental Framework

Study Participants

Laboratory experiments are known for their replicability and ability to rapidly evaluate alternative policies, providing market results before policy implementation (Tisdell, 2011; Tisdell et al., 2004). In laboratory experiments, it is common to use students as participants, although this convenience sampling method has been criticized for its limited representativeness of the general public (Broadbent et al., 2017; Levitt and List, 2007; Loomis, 2011). However, recent studies by Falk et al. (2013) have found that both student and non-student samples exhibit similar behavioral patterns (Broadbent et al., 2017; Falk et al., 2013).

For this study, the targeted participants are undergraduate and graduate students majoring in environmental resource management or related fields at a national university in Hsinchu. All of them have taken courses in principles of economics and environmental resources.

Implementation Process

The experiment consists of three stages: Stage 1 "Non-Monetized Environmental Water Benefit," Stage 2 "Monetized Environmental Water Benefit," and Stage 3 "Monetized Environmental Water Benefit with Water Subsidy Policy Sensitivity." As the market operates as a monopoly, the experiment organizers take on the role of agricultural water users responsible for selling the water resources and calculating transaction prices.

The experiment is divided into three stages: Preparation Stage, Trading Stage, and Settlement Stage, each with specific procedures as illustrated in Figure 4 below:

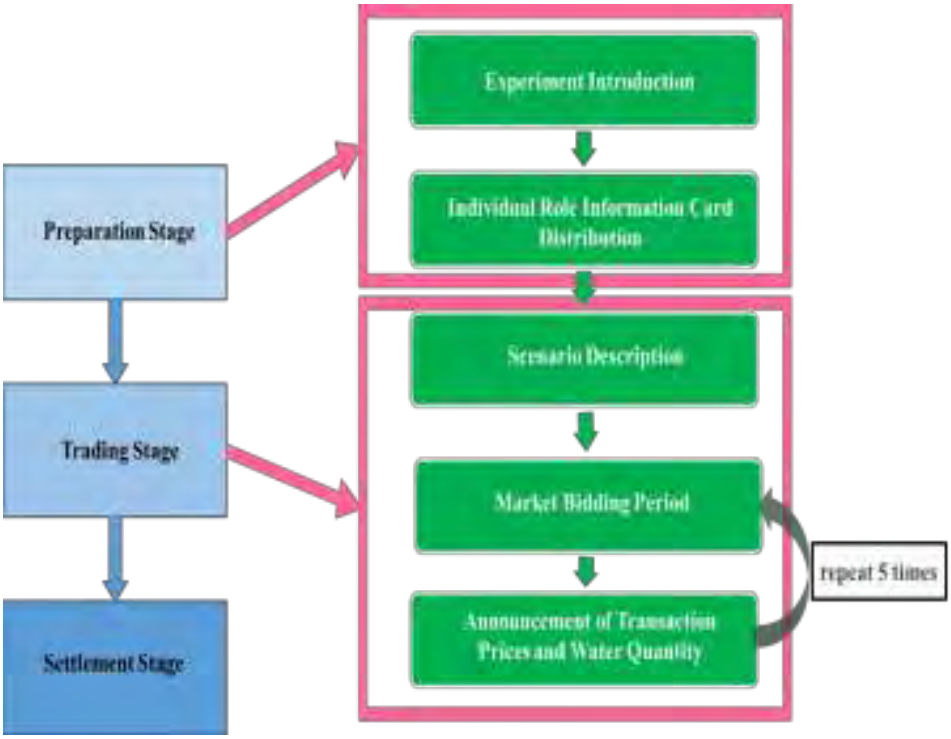

Figure 4: Illustration of the Three Stages

Preparation Stage: Participants are informed of their roles, water needs, benefits, and purchasing budgets.

Trading Stage: Participants, including agricultural and industrial water users, as well as environmental water users, submit their bids for water resources.

Settlement Stage: The experiment organizers determine the water transactions based on the highest bids, and participants' benefits are calculated accordingly.

The detailed procedures for each stage will be explained to the participants before the experiment begins.

Stage 1: Preparation Stage

I. Experiment Introduction: Provide a background explanation of the experiment, including Taiwan's current water resource management and allocation, the environmental benefits of water use, a brief overview of previous research on water use efficiency, the water resource usage and allocation in the Hsinchu area, and the assumptions of this experiment. The experiment introduction presentation is provided in Appendix 1.

II. Individual Role Information Card Distribution: Hand out role information cards and bidding record sheets to participants, and explain the role information. The role information card includes the role's objectives, water use benefits, water needs, and purchasing budget, as shown in Appendix 2. The bidding record sheet is presented in Appendix 3.

Stage 2: Trading Stage

I. Scenario Description: Describe the detailed situation of the experiment, including whether it is a non-drought year or a drought year, the available water allocation for the current year, and the trading rules for water use benefits among all players.

II. Market Bidding Period: Participants, based on their roles, can purchase different amounts of water each time. Industrial water users can buy 500 metric tons per bid, while environmental water users can buy 150 metric tons. Each participant submits five different bidding prices. The experiment organizer, acting as the seller, sorts all the bidding prices from high to low and sells

water resources to those whose bids exceed the agricultural water use benefit. The highest bidders are given priority to purchase water resources until all water resources are sold.

III. Announcement of Transaction Prices and Water Quantity: The transaction prices and water quantities are announced on the projection screen, providing participants with reference for modifying their bids in the next round.

Stage 3: Settlement Stage

Settle the benefits obtained by all players in the current scenario stage and proceed to the next scenario stage of the experiment.

Results

The experiment consists of six groups, divided based on whether it is a non-drought year or a drought year, whether the environmental water use benefits are monetized or not, and whether there is a water purchase subsidy. The details are shown in Table 2. The study conducted a total of three experiments, each with 8 participants. All participants had received training in environmental resource management-related courses at tertiary institutions. Among the participants, 12 were male and 12 were female, resulting in a total of 24 participants in this experiment.

Table 2 Experimental Scenarios

Scenario Coding	Scenario Description	Allocatable water quantity
S1	Non-drought year water market with non-monetized environmental water benefits.	10,000
S2	Non-drought year water market with non-monetized environmental water benefits.	6,640
S3	Non-drought year water market with monetized environmental water benefits.	10,000
S4	Non-drought year water market with monetized environmental water benefits.	6,640
S5	Non-drought year water market with monetized environmental water benefits.	10,000
S6	Non-drought year water market with monetized environmental water benefits.	6,640

The average bidding of each water user type in the experiment is shown in Table 3. The average amount of water purchased by each water user type in each scenario is presented in Table 4. Additionally, Table 5 illustrates the average water purchase price of each water user type in different scenarios.

Table 3 Average Bidding of Each Water User Type in Each Scenario

						(**Unit: New Taiwan Dollars (NTD**)
Water User Type	**S1**	**S2**	**S3**	**S4**	**S5**	**S6**
Industrial Water User	13.05	14.97	13.11	16.41	16.58	20.23
Environmental Water User (Governance)	6.07	6.54	7.70	8.62	9.87	11.57
Environmental Water User (NGO)	2.27	0.91	5.69	6.37	8.97	11.39

Table 4: Average Purchased Water Volume for Each User Type in Each Scenario

						(**Unit：tons**)
Water User Type	**S1**	**S2**	**S3**	**S4**	**S5**	**S6**
Industrial Water User	8,800	6,166.67	8,800	6,133.33	8,933.33	6,000
Environmental Water User (Governance)	830	380	780	370	610	260
Environmental Water User (NGO)	240	10	350	50	390	310

Table 5: Average Purchased Water Price for Each User Type in Each Scenario

（Unit: New Taiwan Dollars (NTD）						
Water User Type	**S1**	**S2**	**S3**	**S4**	**S5**	**S6**
Industrial Water User	14.16	18.07	14.07	18.58	17.21	22.48
Environmental Water User (Governance)	8.95	13.94	9.55	17.54	12.18	19.03
Environmental Water User (NGO)	7.17	22	8.94	15.8	15.69	21.58

Industrial Water Bidding Behavior Analysis

Regardless of whether the environmental water benefits are monetized or under environmental water purchasing subsidies, there are significant differences in bidding behavior for industrial water users between non-drought and drought periods. Due to the reduced available water during drought periods, the bidding prices are higher compared to non-drought periods. There are also notable differences in bidding behavior during drought periods based on whether the environmental water benefits are monetized, with higher bidding prices observed when the benefits are monetized. Additionally, if there are incentives for environmental water use, there are significant differences in bidding behavior for both drought and non-drought years, with higher bidding prices for those who receive water purchasing subsidies. In summary, it can be inferred that by monetizing the environmental water benefits and implementing increased subsidies for environmental water use, industrial water users can raise their bidding prices within their affordable cost range to ensure the security of their production water supply.

Table 6 Paired Sample t-Test for Industrial Water Users' Bidding Behavior

Paired Sample Test								
	Paired Differences					T	df	Significance (two-tailed)
	Mean	Deviation Standard	Standard Error of Mean	95% confidence interval of the difference				
				upper bound	lower bound			
ln-s1-price - ln-s2-price	-1.923	6.360	.367	-2.646	-1.201	-5.238	299	.000***
ln-s3-price - ln-s4-price	-3.307	5.319	.307	-3.911	-2.702	-10.767	299	.000***
ln-s5-price - ln-s6-price	-3.653	5.340	.308	-4.260	-3.047	-11.850	299	.000***
ln-s1-price - ln-s3-price	-.057	5.261	.304	-.654	.541	-.187	299	.852
ln-s2-price - ln-s4-price	-1.440	6.189	.357	-2.143	-.737	-4.030	299	.000***
ln-s3-price - ln-s5-price	-3.470	4.985	.288	-4.036	-2.904	-12.058	299	.000***
ln-s4-price - ln-s6-price	-3.817	6.678	.386	-4.575	-3.058	-9.900	299	.000***

Note: * indicates P<0.1; ** indicates P<0.05; *** indicates P<0.01. The significance level in this study is set at P<0.05.

Analysis of Environmental Water Bidding Behavior

In the context of environmental water benefit monetization and providing environmental water subsidies, there are significant differences in bidding behavior for governance environmental water users between drought and non-drought years. The bids are higher during drought years, likely due to the limited available water allocation. In both non-drought and drought years, there are also significant differences in bidding behavior depending on whether the environmental water benefit is monetized. In the monetized scenario, bids are consistently higher compared to the non-monetized scenario. Furthermore, in the case of governance environmental water users receiving subsidies, there are also significant differences in bidding behavior between different scenarios. The paired-sample t-test results for the bidding behavior of governance environmental water users in different scenarios are shown in Table 7.

Table 7 Paired-sample t-test for Bidding Behavior of Governance Environmental Water Users

	Paired Differences					T	df	Significance (two-tailed)
	Mean	Deviation Standard	Standard Error of Mean	95% confidence interval of the difference				
				upper bound	lower bound			
EPA-s1-price - EPA-s2-price	-.467	6.177	.504	-1.463	.530	-.925	149	.356
EPA-s3-price - EPA-s4-price	-.927	6.511	.532	-1.977	.124	-1.743	149	.083*
EPA-s5-price - EPA-s6-price	-1.700	6.147	.502	-2.692	-.708	-3.387	149	.001**
EPA-s1-price - EPA-s3-price	-1.620	4.316	.352	-2.316	-.924	-4.597	149	.000***
EPA-s3-price - EPA-s5-price	-2.173	5.059	.413	-2.990	-1.357	-5.261	149	.000***
EPA-s2-price - EPA-s4-price	-2.080	6.278	.513	-3.093	-1.067	-4.058	149	.000***
EPA-s4-price - EPA-s6-price	-2.947	7.852	.641	-4.213	-1.680	-4.596	149	.000***

Note: * indicates P<0.1; ** indicates P<0.05; *** indicates P<0.01. The significance level in this study is set at P<0.05.

From the bidding behavior of Environmental NGO Water Users, it can be observed that, in the private sector, the willingness to purchase environmental water was relatively low before the environmental water benefits were monetized. Additionally, under the condition of non-monetized benefits, there were lower bids during drought periods compared to non-drought periods. This can be attributed to the limited available water during drought years, as observed from their bidding behavior in non-drought scenarios, where insufficient funds and lack of water benefits resulted in a decreased willingness to purchase private sector environmental water. However, after the monetization of environmental water benefits, the private sector's willingness to bid for environmental water increased significantly.

Moreover, the provision of water purchase subsidies for environmental water greatly boosted the private sector's willingness to bid for such water. The results of the paired-sample t-test for the Environmental NGO Water Users' bidding behavior are shown in Table 8.

Table 8 Paired-sample t-test for Environmental NGO Water Users' Bidding Behavior

	Paired Differences					T	df	Significance (two-tailed)
	Mean	Deviation Standard	Standard Error of Mean	95% confidence interval of the difference				
				upper bound	lower bound			
GG-s1-price - GG-s2-price	1.360	3.461	.283	.802	1.918	4.813	149	.000***
GG-s3-price - GG-s4-price	-.673	4.535	.370	-1.405	.058	-1.818	149	.071*
GG-s5-price - GG-s6-price	-2.413	5.872	.479	-3.361	-1.466	-5.033	149	.000***
GG-s1-price - GG-s3-price	-3.420	4.947	.404	-4.218	-2.622	-8.467	149	.000***
GG-s3-price - GG-s5-price	-3.280	6.715	.548	-4.363	-2.197	-5.983	149	.000***
GG-s2-price - GG-s4-price	-5.453	5.281	.431	-6.305	-4.601	-12.648	149	.000***
GG-s4-price - GG-s6-price	-5.020	8.036	.656	-6.316	-3.724	-7.651	149	.000***

Note: * indicates P<0.1; ** indicates P<0.05; *** indicates P<0.01. The significance level in this study is set at P<0.05.

Purchasing Price Analysis

In order to understand whether there are significant differences in the purchasing prices of water resources among different types of water users in three scenarios - "non-drought and drought periods," "monetization of environmental water benefits," and "availability of environmental water purchase subsidies," this study conducted independent samples t-tests for the purchasing prices of water resources obtained in the experiment, categorized by industrial water users and environmental water users, and analyzed them separately based on the scenarios.

Table 9 Independent Samples t-test Results of Purchasing Prices of Different Water Users in Different Scenarios

Water User Type	**S1-S2**	**S3-S4**	**S5-S6**	**S1-S3**	**S3-S5**	**S2-S4**	**S4-S6**
Industrial Water User	Significant Difference	Significant Difference	Significant Difference	Significant Difference	Significant Difference	Significant Difference	Significant Difference
Environmental Water User	Significant Difference	Significant Difference	Significant Difference	Significant Difference	Significant Difference	Significant Difference	Significant Difference

Result

Regarding the bidding behavior of industrial water users, it is evident that under the condition of monetizing the environmental water benefits and providing environmental water purchase subsidies, industrial water users have the capability to offer higher bids to secure their production needs. However, in the scenario with environmental water purchase subsidies, the water benefit results are compromised, indicating that in the absence of monetized environmental water benefits, the industrial water usage neglects the environmental benefits, which goes against the principles of social equity and justice.

Observing the bidding behavior of the governance for environmental water, it can be understood that despite having lower environmental water benefits, the governance still needs to bid as it is responsible for ensuring the minimum water quantity required for production. However, due to the industrial and commercial orientation, the monetary benefit of industrial water is much higher than that of environmental water. Consequently, the market is skewed

towards industrial water users, leading to a decline in the benefits of protecting environmental water, and making it difficult for the governance to fulfill the task of maintaining the minimum water quantity required for production. On the other hand, for private sector environmental water users, the observation of bidding behavior reveals that monetizing the environmental water benefits significantly increases their bids, indicating that if environmental water can be traded in the market, its benefits need to be clearly defined to motivate the private sector to retain and use environmental water. Additionally, if policies aim to encourage the private sector to purchase environmental water to enhance environmental quality, subsidies can be employed to increase their willingness to purchase water.

Analyzing the results of the purchased water prices, it is evident that there are significant differences in purchased water prices between non-drought and drought periods, with prices being higher during drought periods. In conjunction with the statistical analysis of purchased water quantities, it can be observed that regardless of whether the environmental benefits are monetized or environmental water purchase subsidies are provided, there is no significant difference in the total purchased water quantities between industrial water users and environmental water users. However, during non-drought and drought periods, the presence of environmental water purchase subsidies leads to significant differences in the overall social benefits.

Conclusion

Regarding the bidding behavior of industrial water users, it was found that under the scenarios of monetized environmental water benefits and the provision of water subsidies for environmental water, industrial water users have the capability to offer higher bids to secure their production needs. However, it was observed that when environmental water benefits were not monetized, industrial water users tended to undervalue environmental water during drought periods compared to non-drought periods. This neglect of environmental benefits contradicts the principles of social equity and justice.

Analyzing the bidding behavior of governance environmental water users, it was evident that these users must bid for water even if the environmental water benefits are relatively lower. This is due to their responsibility to maintain the minimum water quantity required for essential production tasks. However, because industrial and commercial interests prevail, the monetary benefits derived from industrial water usage outweigh the monetary benefits of environmental water. Consequently, water resources are allocated more towards industrial water users, leading to diminished benefits for environmental water and making it difficult for the governance to fulfill its obligation of maintaining the minimum water quantity for environmental and agricultural needs.

As for the bidding behavior of private sector environmental water users, it was observed that monetizing environmental water benefits significantly increased their willingness to offer higher bids. This highlights the importance of clearly defining the benefits of environmental water when it becomes a tradable commodity, as it can stimulate the private sector to retain environmental water. Additionally, providing water subsidies for environmental water significantly elevated the bidding behavior of private sector users. Therefore, to encourage private sector water users to invest in environmental water and enhance environmental quality, implementing subsidy policies to boost water purchasing intentions is recommended.

As for the bidding behavior of NGO environmental water users, it was observed that monetizing environmental water benefits significantly increased their willingness to offer higher bids. This highlights the importance of clearly defining the benefits of environmental water when it becomes a tradable commodity, as it can stimulate the NGO to retain environmental water. Additionally, providing water subsidies for environmental water significantly elevated the bidding behavior of NGO users. Therefore, to encourage NGO water users to invest in environmental water and enhance environmental quality, implementing subsidy policies to boost water purchasing intentions is recommended.

As noted above, Taiwan's current water resource management lacks the establishment of environmental water rights as specified under the Water Act's Water Consumption Purpose categories. The absence of proper retention of agricultural and environmental water jeopardizes the country's food security and environmental health. Furthermore, in a market-oriented economy, the overwhelming monetary benefits of industrial water lead to disproportionate water resource allocation towards industrial water users. To enhance water

resource allocation efficiency in Taiwan, the implementation of a water banking system similar to California's drought water banking system is suggested. This system activates water resource trading mechanisms during water scarcity and pre-reserves the minimum water quantity required for environmental and agricultural needs. Alternatively, a permanent water banking system based on basin management principles, similar to Idaho's approach, may better improve water resource allocation efficiency compared to a completely free-market water system.

Moreover, the findings from observing the bidding behavior, purchased water prices, and purchased water quantities of public and private sector environmental water users suggest that providing water subsidies significantly positively impacts their bidding behavior. Therefore, it is recommended to promote the benefits of retaining environmental water in policies, mainstream the advantages of maintaining environmental water, and enhance the willingness of both public and private sector users to voluntarily retain and use environmental water. This will ultimately enhance environmental quality and social welfare.

The current water resource trading system in Taiwan is constrained by the regulations of the Water law, making it difficult to conduct water resource transfers transparently and efficiently. Additionally, during non-drought periods, the limitations imposed by Article 24 of the Water law may lead to potential water rights losses. Furthermore, the lack of a fair mechanism for water users to bear corresponding costs during water resource transfers hinders efforts to improve water resource allocation efficiency during drought periods. To address these issues, revising the regulations governing water resource transfers under the Water law and establishing cross-county/city government mechanisms or institutions for water resource management in major watersheds are recommended. These mechanisms should facilitate water resource allocation based on demands, enhance water management flexibility, and perform functions such as policy formulation or revision, policy adjustment promotion, and acting as a communication role.

Furthermore, environmental water rights should be explicitly defined and regulated in the law to ensure their claimable rights. This will facilitate the formal inclusion of environmental water in the water resource management mechanism and enable its function in maintaining environmental system health and improving environmental quality. Drawing inspiration from the Australian Water Partnership's recommendations regarding water resource management mechanisms, it is essential to ensure that such mechanisms or institutions operate effectively and contribute to maintaining a balance between water resource allocation efficiency, social equity, and environmental protection.

References

Council of Agriculture, Executive Yuan. (2014). Explanation of the first crop paddy suspension compensation operation in 2015. Retrieved from https://www.coa.gov.tw/ws.php?id=2502565

Ke, A. (2006). The Study on Water Right Transaction of Taiwan. Master's thesis, Institute of Economics, National Sun Yat-Sen University, Kaohsiung City. Retrieved from https://hdl.handle.net/11296/58ptt5

Chen, C. D., Chu, J. R., Hsu, H. H., Lu, M. M., Sui, C. H., Chou, C., ... Yang, C. D. (2014). Projection of Climate Change Over Taiwan Using Statistical Downscaling Scheme. Atmospheric Sciences, 42(3), 207-251.

Chen, M. J. (2003). Economic Issues of Irrigation Water Right and Water Market in Taiwan. Agriculture and Economics, (30), 1-26.

Chiueh, Y. W. (2002). Economic Issues of Water Market and Water Bank in Taiwan. Doctoral dissertation, National Taiwan University, Taipei City. Retrieved from https://hdl.handle.net/11296/q9gk84

Chiueh, Y. W. (2005). Changes and achievements in the US water rights system and reflections on Taiwan's water rights system. Journal of Hsinchu Teachers College, (20), 201-218. doi:10.7044/JNHCTC.200506.0201

Chiueh, Y. W. (2008). Market structure analysis of water resource allocation by agricultural water associations. Agriculture and Economics, (41), 45-72. doi:10.6181/agec.2008.41.02

Chiueh, Y. W. (2005). Reforms of Australia's water resource management system and regulations for agricultural water transactions. Retrieved from http://www.rest.org.tw/zh_tw/Download

Chiueh, Y. W. (2015). Status and reflections on irrigation water resource trading in Australia. Retrieved from http://www.rest.org.tw/zh_tw/Download

Chiueh, Y. W. (2015). Regulations for agricultural water transactions and water market information in Australia. Retrieved from http://www.rest.org.tw/zh_tw/Download

Chiueh, Y. W. (2014). Evaluate the Economic Cost of Irrigation Water Supply Stability and Drought Lost in Changing Environment and Society (I). Final Report for Ministry of Science and Technology Research Project (No. MOST 103-2625-M-134-001), unpublished.

Water Resources Agency, MOEA. (2017). Basic planning for water resources management in Northern Taiwan. Sustainable Engineering Exclusive Website. Retrieved from http://eem.wra.gov.tw/default.asp

Water Resources Planning Institute. (2014). Study on the determination and promotion strategy of river environmental flow under climate change (Project No. MOEAWRA1030250), unpublished.

Bates, B., Kundzewicz, Z., & Wu, S. (2008). Climate change and water. Intergovernmental Panel on Climate Change Secretariat.

Chiueh, Y. W., & Huang, C. C. (2015). The Willingness to Pay by Industrial Sectors for Agricultural Water Transfer During Drought Periods in Taiwan. Environment and Natural Resources Research, 5(1), 38.

Garrido, A. (2007). Designing water markets for unstable climatic conditions: Learning from experimental economics. Review of Agricultural Economics, 29(3), 520-530.

Hung, M. F., Shaw, D., & Chie, B. T. (2014). Water trading: locational water rights, economic efficiency, and third-party effect. Water, 6(3), 723-744.

Zetland, D. (2013). All-in-Auctions for water. Journal of environmental management, 115, 78-86.

Hansen, K., Kaplan, J., & Kroll, S. (2014). Valuing options in water markets: a laboratory investigation. Environmental and Resource Economics, 57(1), 59-80.

Broadbent, C. D., Brookshire, D. S., Coursey, D., & Tidwell, V. (2017). Futures contracts in water leasing: An experimental analysis using basin characteristics of the Rio Grande, NM. Environmental and Resource Economics, 68(3), 569-594.

Möller-Gulland, J., & Donoso, G. (2016). A typology of water market intermediaries. Water International, 41(7), 1016-1034.

Smith, V. L. (1976). Experimental economics: Induced value theory. The American Economic Review, 66(2), 274-279.

Tisdell, J. G. (2011). Water markets in Australia: an experimental analysis of alternative market mechanisms. Australian journal of agricultural and resource economics, 55(4), 500-517.

Cherry, T. L., & McEvoy, D. M. (2013). Enforcing compliance with environmental agreements in the absence of strong institutions: An experimental analysis. Environmental and Resource Economics, 54(1), 63-77.

Murphy, J. J., Dinar, A., Howitt, R. E., Rassenti, S. J., & Smith, V. L. (2000). The Design of`Smart"Water Market Institutions Using Laboratory Experiments. Environmental and Resource Economics, 17(4), 375-394.

Parkhurst, G. M., Shogren, J. F., & Crocker, T. (2016). Tradable set-aside requirements (TSARs): conserving spatially dependent environmental amenities. Environmental and Resource Economics, 63(4), 719-744.

Leroux, A., & Crase, L. (2010). Advancing water trade: A preliminary investigation of Urban-Irrigation options contracts in the Ovens basin, Victoria, Australia. Economic Papers: A journal of applied economics and policy, 29(3), 251-266.

Wheeler, S., Garrick, D., Loch, A., & Bjornlund, H. (2011). Incorporating Temporary Trade with the Buy-Back of Water Entitlements inAustralia (No. 1101). Centre for Water Economics, Environment and Policy, Crawford School of Public Policy, The Australian National University.

Ancev, T. (2015). The role of the commonwealth environmental water holder in annual water allocation markets. Australian Journal of Agricultural and Resource Economics, 59(1), 133-153.

Falk, A., Meier, S., & Zehnder, C. (2013). Do lab experiments misrepresent social preferences? The case of self-selected student samples. Journal of the European Economic Association, 11(4), 839-852.

Schwabe, K., Nemati, M., Landry, C., & Zimmerman, G. (2020). Water markets in the Western United States: Trends and opportunities. Water, 12(1), 233.

Nelson, R. (2022). Water rights for groundwater environments as an enabling condition for adaptive water governance. Ecology and Society, 27(2).

Acharyya, A. (2019). Groundwater pricing and groundwater markets. Groundwater Development and Management: Issues and Challenges in South Asia, 471-488.

Wheeler, S. A., Zuo, A., Xu, Y., Haensch, J., & Seidl, C. (2020). Water market literature review and empirical analysis. Report Prepared for the Australian Competition and Consumer Commission (ACCC).

PRODUCTIVITY AND EFFICIENCY ANALYSIS OF PADDY RICE MANAGEMENT PRACTICES UNDER EXTREME WEATHER EVENTS IN TAIWAN

Yu-Chuan Chang[1],Ching-Tien Chen[2], Sheng-Fu Tsai[3] and Ming-Tee Hung[4]

ABSTRACT

In order to adapt the current water management practices to extreme weather events and to economic growth in Taiwan, a field experiment was conducted to evaluate the effect of different water management practices on crop productivity and water storage capacity. The results revealed that the shallow intermittent irrigation (SII) increased potential yield of rice during the dry season, and deepwater intermittent irrigation (DII) increased effective rainfall and percolation during rainy season. Further, the results from evaluating productivity and water storage capacity point out that SII water management can save input resources in first cropping season, while DII provided more water storage capacity in second cropping season.

It is concluded that in Taiwan, water-saving irrigation practices can be applied with high potential yield during the first cropping season when the crop can efficiently raise input resource productivity by the promotion of System of Rice Intensification (SRI). On the other hand, instead of having farmers operate their paddy fields without controlling water in the second cropping season, when plenty of water is available in rivers, farmers should be encouraged and subsidized by the government to sustain their paddy fields as shallow retention ponds through deepwater management practices in that season.

RÉSUMÉ ET CONCLUSIONS

Keywords: System of rice intensification, deepwater management practice, intermittent irrigation, farmer water management practice

1. Introduction

The coming global food crisis is not only a result from the increasing world population, but also from the shortage of water and arable land cause in the climate change and economic growth. That means the vulnerability of agriculture should be examined, the adapting capacity to climate change will decline and the competition for water, labor and land resources between sectors will become keener due to the economic globalization. In the case of irrigated agriculture, sustainable development strategies must be taken up as well as environmental changes.

The performance of water management practice of paddy field affects the vulnerability and the adapting capacity for local food security. Typical water management in paddy fields, with submergence only for required periods and under water ponding depth control in a paddy lot, is based on a sufficient supply of water, improvement of the drainage system, and land consolidation (Mizutani et al., 1999). Since the rice production in paddy fields requires so much water that it is under constant pressure to conserve water. Therefore, the traditional concept is to apply only the minimum amount of water required for the growth of rice, and to use the most efficient irrigation method that minimizes the evaporation, percolation and runoff from the paddy fields.

1 Professor, Department of Tourism and LeisureManagement, Hsing Wu University, No. 101, Sec.1, Fenliao Rd., LinKou Township, New Taipei City 24442, Taiwan; E-mail: e06033@gmail.com

2 Associate Professor, Department of Civil and Water Resources Engineering, National Chiayi University, No.300, Syuefu Rd., Chiayi City 60004, Taiwan, ctchen@mail.ncyu.edu.tw

3 Director-General, Irrigation Agency, Council of Agriculture, Executive Yuan, No. 5, Ln. 45, Sec. 1, Beixin Rd., Xindian Dist., New Taipei City 231002, Taiwan

4 Divison director, Irrigation Management Division, Irrigation Agency, Council of Agriculture, Executive Yuan, No. 5, Ln. 45, Sec. 1, Beixin Rd., Xindian Dist., New Taipei City 231002, Taiwan

In the past years, the intermittent irrigation is regarded as a crisis factor for system of rice intensification (SRI), an integrated crop management technology developed by the Fr. Henri de Laulanie in Madagascar. The constituent practices were: (i) transplanting very young seedlings, (ii) transplanting single seedlings in hills at wider spacing, and (iii) application of intermittent irrigation during the vegetative growth stage so as to develop a greater root system (Stoop et al, 2002; Uphoff, 2007; Sato et al., 2011). The incredible yield increases have been achieved using few external inputs and less water and seed than conventional rice production systems (Namara et al, 2004; Sato and Uphoff, 2007; Sinha and Talati, 2007).

In intermittent irrigation, irrigation water is applied to obtain flooded conditions after a certain number of days have passed after the disappearance of ponded water. The number of days of nonflooded soil in intermittent irrigation before irrigation is applied can vary from 1 day to more than 10 days. The suggestion from the website of SRI-Rice is recommend as only a minimum of water is applied during the vegetative growth period, and thereafter only a thin layer of water is maintained on the field during flowering and grain-filling. Alternatively, to save labor time, some farmers flood and drain (dry) their fields in 3-5 day cycles with good results. Best water management practices depend on soil type, labor availability and other factors, so farmers should experiment on how best to apply the principle of having moist but well-drained soil while their rice plants are growing (SRI International Network and Resources Center, 2012). Some researchers have reported a yield increase using intermittent irrigation (Zhang and Song 1989, Stoop et al 2002), recent work indicates that this is the exception rather than the rule (Belder et al 2004, Cabangon et al 2004, Tabbal et al 2002).

The rapid industrialization, economic growth and rise in living standard resulted in a dramatic increase in water demands by the domestic and industrial water users in Taiwan. This imposes an additional pressure to the agricultural sector, presently using about 80% of available water resources, to sharply curtail the water use and a substantial reduction in paddy field acreage is imminent. Under such an environment, some of the concepts that were unconceivable before begin to appear logical and worth exploring.

During the last 50-60 years, limited labour and increasing production costs led to expansion of the size of field plot and the precipitation of agricultural mechanization in Taiwan. For poverty alleviation in rural area, the policy of agriculture input subsidy is practiced for decades. However, it might also cause the farmers to waste the input resources without attempting to save the use. For most rice farmers, there is no deliberate choice to save water as they are just confronted by a lack of water. Because of the labour scarcity in Taiwan, the farmer always used to practice the submerge water management in paddy field for labor saving and the intermittent irrigation only implement in drought season. On the other hand, when considering effective and sustained weed control, integrated weed management with proper water control is used. Most of farmers believe the increase of the ponding depth will result in better weed control. Some researches advise the best ponding depth is 20 cm for weed control (Bhagat, Bhuiyan, and Moody, 1996) and the ponding depth shouldn't higher the plant height after the productive tiller stage, but there is no significant drop in yield between 40% and 70% of plant height (Shih, 1977).

Rainfall in Taiwan is abundant, but has a very uneven distribution over time. About 78% of the rainfall runs directly to the ocean without being utilized (Chang et al., 2007). There has been a recent increase in the risk of flood disaster in rainy season owing not only to the changes in frequency and intensity of rainfall, but also to changes in land use and modernization of agriculture leading to the expansion of impervious areas and shortening of the arrival time of floods. The storage of rainfall in paddy fields by the bunds is like an effective rainwater cistern system during the wet months, which forms individual ecosystems and maintains a farmland wetland (Hayase, 1994; Lee et al., 1995; Sekiya, 1992). Considering the water storage capacity of paddy field, the potential benefits of increased application of water to paddy fields were investigated in Taiwan from 1998. A conceptual model was developed to represent the hydrologic system of the paddy field (Chang et al., 2001). Field experiments were also performed for the impact on water productivity (Chang et al., 2007). Those investigation shows that deepwater management is good for water storage capacity and rice production at the same time. In general, rice production, irrigation water, effective rainfall and percolation increase under deepwater management practice (DMP) and the runoff coefficient decreases. The water productivity results show that even though the volume of irrigation water had increased, DMP can still generate high water productivity. However, for improving the productivity of high quality rice cultivation in DMP is being addressed in Japan with ponding

depth to 25 cm (Kiyochika, 1994). It is advisable to keep the third leaf blade above the surface of the water for better rooting (Kiyochika Hoshikawa, 1989).

The overproduction results in diminished profit from intensive agriculture result of depressed prices in Taiwan for decades. High labour and capital outlays enforce some of farmers turn to extensive agriculture and the others try to increase the efficiency of input resources to find more profit. Under the above-mentioned conditions, paddy rice field seems to subsist in a variable management practices. In consideration of increasing the productivity and water storage capacity of paddy fields, three blocks of farm field were designed to investigate the effects of deepwater management and basic SRI principle (Sato, Yamaji and Kuroda, 2011) on rice crop performance, productivity and water storage capacity.

2. Methods and materials

2.1 Design and Treatments

The cases being studied are fields where farmers apply water management practice based on experience; rice variety TG11 (hybridize by Oryza Stiva) was grown in field under farmer's practice (FP) in A block, deepwater intermittent irrigation (DII) in B block and shallow intermittent irrigation (SII) in C block during crop season (Jan 24 to June 17 for first crop season and July 22 to Nov 8 for second crop season, 2013).

In FP, the adjusted water depth in the paddy field is made in accordance with the stage of growth of rice. Desirable depths for transplanted rice are (a) 3-5 cm during the stand establishment, (b) 3-8 cm during the tillering stage with a mid-season drainage at the maximum tillering stage, (c) 5-10 cm during the panicle formation stage, (d) gradual drainage for 2-3 weeks after full flowering stage. DII applies the intermittent irrigation based on DMP for the whole stages, which increase the irrigation depth not more than 40% of plant height and the maximum depth is 25 cm. SII applies the intermittent irrigation based on SRI for the whole stage which decrease the irrigation depth to 1~2 cm excluding the flower stage. For each block, three different transplanting spacing were applied, including single seedling, low density and high density in table 1.

2.2 Crop, water and productivity measurement

At harvest, the total plants for each block in different transplanting spacing were taken for determining yield components such as tiller number, number of grains per panicle, weight of 1000 grains and grain yield.

To help evaluate the efficiency of input resources under SRI and deepwater management practice, productivity of capital, labor and irrigation water were introduced. The production costs were recorded and accounted into three different transplanting spacing based on the design and treatment on fields, which were separated into labor and material input resources during the whole stage. The analysis of water budget was also conducted to figure out the water storage capacity and irrigation water productivity improvement of the paddy field. A rain gauge and a U.S. Weather Bureau Class A Land Pan were installed to record the rainfall and evaporation, respectively. The evapotranspiration was estimated using the crop coefficients and the reference crop water recommended by FAO under nonrestricting soil conditions based on Penman- Monteith equation (Allen et al., 1998). Flow gauges and standard 90° V-notch weirs were placed to measure the irrigation water and drainage discharge, respectively. The water depth in the paddy field was maintained by earth levees, the height of which had been raised to 30 cm in order to control the overflow from levees. Field water tubes were installed at the paddy fields to record the water depth.

2.3 Calculations and statistical analysis

Statistical analysis consisted of two-factor analysis of variance (ANOVA) using SPSS v.20 with crop season, transplanting spacing and water management practice as main factors. The level of confidence was set at 95%. The improvement in water storage capacity was compared with the effective rainfall, percolation and runoff coefficient. In order to figure out if the DII and SII were good for productivity, productivity of capital (kg grain US$-3 capital), labor (kg grain hour-1 labor) and irrigation water (kg grain m-3 water) were calculated as grain yield divided by total capital, labor and irrigation water input respectively.

Table 1. Transplanting spacing in blocks

Description	Single seeding	Low density	High density
Transplanting method	hand	machine	machine
Seedling	very young	very young	very young
Number of seedlings (no.)	1	3~5	>5
Spacing			
a. Row (cm)	25.0	30.0	30.0
b. Line (cm)	25.0	24.0	18.0
c. Transplant Density (no./m^2)	16.0	41.7	92.6
Weed frequency (times)	2~4		
Fertilizer (kg/ha)	N=83, P=21 and K=41		

3. Results

3.1 Yield components

1. Tiller number

The numbers of tiller were among 14-30. The results of the two-factor analysis of variance showed the tiller number was significantly different both in crop seasons and transplanting spacing but not in water management practices, at the 5% level. The numbers of tiller were among 14-30 and 15-23 in first and second crop season respectively after harvest. Compared to the high density which the farmers adopted, the low density under FP reached the greatest tiller number: 30 (22% increased) in first crop season and 23 (40% increased) in second crop season (Fig. 1). Single seedling showed the highest tiller number decrease: 42% decreased in first crop season and 8% decreased in second crop season.

2. Number of grains per panicle

The number of grains per panicle (NGPP) was among 79-151. The results of the two-factor analysis of variance showed the NGPP was significantly different in transplanting spacing but not in crop seasons and water management practices, at the 5% level. The NGPP were among 109-151, 79-145 and 84-118 in single, low density and high density respectively. Compared to the high density, the average NGPP increased 30% and 11% in single seedling and low density respectively. The greatest NGPP was found at single seedling under SII water management: 151 (50% increased) in second crop season (Fig. 1). Low density under DII showed the lowest NGPP: 79 in first crop season.

3. Weight of 1000 grains

The weight of 1000 grains (WkG) was among 18.8-27.9 g. The results of the two-factor analysis of variance on the WkG showed a significant difference in crop season but not in water management practices and transplanting spacing, at the 5% level. The WkG were among 18.8-24.1 g and 21.7-27.9 g in first and second crop season respectively. The average WkG in first crop season was 21.74 g, which was lower than the 24.37 g in second crop season. The greatest WkG was found at low density under DII water management: 26.2 g in second crop season (Fig. 1). Low density under DII showed the lowest WkG: 18.8 g in first crop season.

4. Grain yield

Grain yield was about 3.6-8.4 t/ha after harvest. The results of the two-factor analysis of variance showed the grain yield was significantly different in crop season but not in water management practices and transplanting spacing, at the 5% level. The grain yield was among

4.1-8.4 t/ha and 3.6-5.1 t/ha in first and second crop season respectively. The average grain yield in first crop season was 5.57 t/ha, which was higher than the 4.34 t/ha in second crop season, which was explained as low temperature pattern and increasing damage of pests, diseases, weeds and flood implied a higher risk of yield losses in second crop season. The greatest grain yield was found at low density under SII water management: 8.446 in first crop season (Fig. 1). Single seedling under DII showed the lowest grain yield: 3.61 t/ha in second crop season.

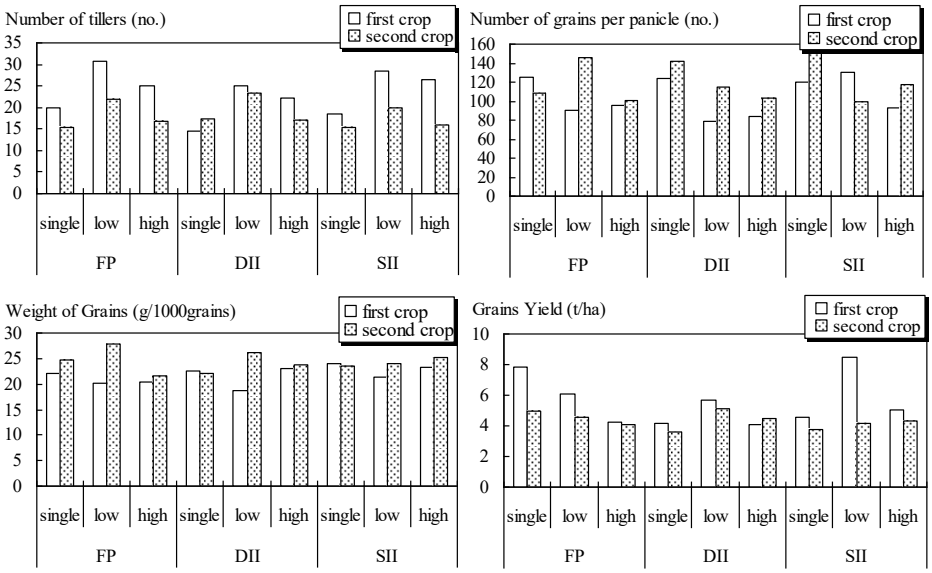

Figure 1. Effects of the water management practices on yield components.

3.2 Production Cost

Fig. 2 showed the production cost of three different transplanting spacing for two crop seasons. The total production cost was 1948-2180 US$/ha and 2102-2335 US$/ha in first and second crop season respectively. The production cost increased 7.09-7.93% in second crop season compared to first crop season owing to the increased application of pesticide and fertilizer. The labor input resource only occupied 8.43%-9.70% of production cost at low and high density seedling transplanted by machine, which increased to 22.84%-24.46% at single seedling transplanted by hand owing to the high labor cost in Taiwan. Looking at the adaptation of farmer over different water management practices, SII field was complained by the farmer on additional work of leveling for achieving even distribution in small amount of water.

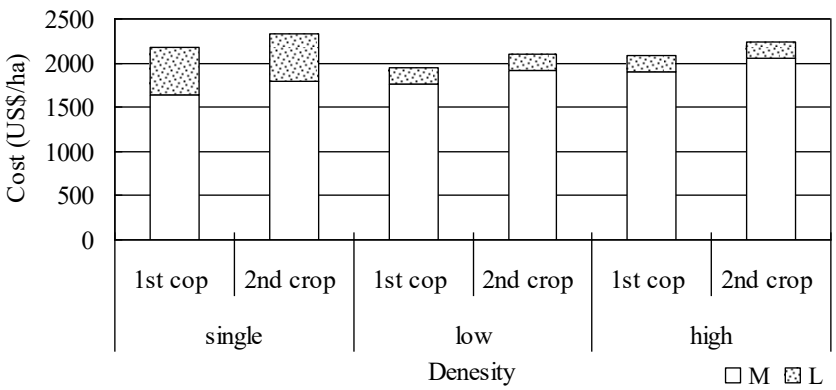

Figure 2. Effects of the transplanting spacing on production cost

3.3 *Water storage capacity*

Table 2 showed the water budget of different field blocks under different water management practices for two crop seasons. The total input water in first crop season was 758-2471 mm, and 87.47%-96.16% of the water came from irrigation and the rest was rainfall. In second crop season, the total input water was 587-1261 mm, and 35.09%-53.29% of the water came from irrigation and the rest was rainfall. Evapotranspiration occupied 30.51%-99.47% of total output water in first crop season and 34.89-74.96% in second crop season. Percolation from ground surface was 0.53%-69.49% of the total output water in first crop season and 25.04%-66.10% in second crop season. Drainage from field wasn't measured in first crop season and which was 85-293mm in second crop season. The runoff coefficients that corresponded to different water management practices were 0.22, 0.13 and 0.43 under FP, DII and SII respectively, which decreased 42% under DII and increased 101% under SII compared to FP. Among the water management practices, SII provided a water saving option with low irrigation water need and minimal percolation losses in first crop season, while DII made the paddy field become a rainwater cistern with high effective rainfall, high percolation (potential recharge) and low runoff coefficient in second crop season.

Table 2. Volume of water budget on three water regimes in two crop seasons

Item	First crop			Second crop		
	FP	DII	SII	FP	DII	SII
Growth period (days)	145	145	145	110	110	110
Field requirement (mm)	1934	2471	758	1055	1261	587
Irrigation water need (mm)	1839	2376	663	527	672	206
Effective rainfall (mm)	95.2	95.2	95.2	528	589	381
Evapotranspiration(mm)	754	754	754	440	440	440
Percolation(mm)	1180	1717	4	615	821	147
Drainage (mm)	0	0	0	146	85	293

*The amount of rainfall was 95mm and 674mm in first and second crop season respectively.

3.4 *Productivity*

Due to the lack of single transplanted machine in Taiwan, the change in transplanting spacing of DMP and SRI affected total production cost and productivity of capital (Pc) and labor (Pl). The Pc and Pl is defined as the amount of weight of grains over total capital and labor input. The results of the two-factor analysis of variance showed Pc was significantly different in crop seasons but not in water management practices and transplanting spacing, and Pl was significantly different in water management practices but not in crop seasons and transplanting spacing, at the 5% level. In general, the Pc was among 1.67-4.04 kg/US$ and the Pl was among 25.63-148.96 kg/hr as show in Fig. 3. Among the crop seasons, the average Pc decreased 26.98% in second crop. The maximum Pc was obtained at low density under SII in first crop season with Pc: 4.04 kg/US$. The minimum Pc was found at single seedling under SII in second crop season with Pc: 1.67 kg/US$. Among the water management practices, DII increased Pl along 46.38-104.17% and 107.06-192.85% in first and second crop season respectively where SII increased Pl along 63.39-204.50% and 115.14-148.26% in first and second crop season respectively. In general, the Pl under SII was higher than other water management practices in first crop season, while the Pl under DII was higher then others in second crop season. The maximum Pl was obtained at low density under SII in first crop season with Pl: 148.96 kg/hr. The minimum Pl was found at high density under FP in second crop season with Pl: 25.63 kg/hr.

The changes in irrigation depth also affected total water use and irrigation water productivity (Pi). The Pi is defined as the amount of weight of grains over cumulative weight of water inputs

by irrigation. In general, Pi was among 1.71-21.03 kg/m3 as show in Fig. 3. The results of the two-factor analysis of variance showed the Pi was significantly different both in crop seasons and water management practices, at the 5% level. In general, the Pi increased 59.58-238% in second crop season. Among the water management practices, DII decreased the Pi along 25.71-58.60% and 12.43-42.46% in first and second crop season respectively, where as SII increased Pi along 60.60-285.95% and 95.04-170.24% in first and second crop season respectively. The maximum Pi was obtained at high density under SII in second crop season with Pi: 21.03 kg/m3. The minimum Pi was found at high density under DII in first crop season with Pi: 1.71 kg/m3.

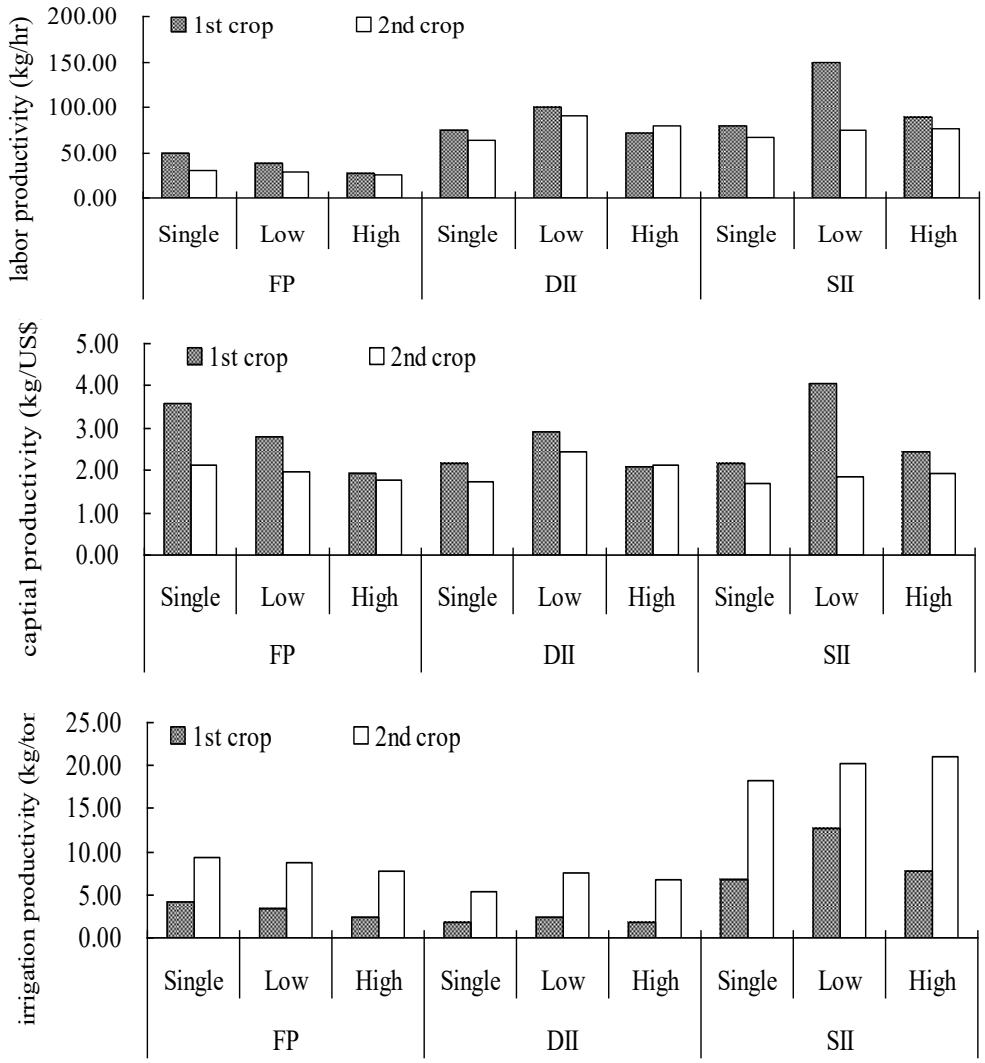

Figure 3.Productivity of labor, capital and irrigation water.

4. Discussions

Based on these facts and other figures, it can be concluded that among the transplant transplanting spacing, the high density seedling of farmer's practice in Taiwan didn't resulted in high rice grain yield as compared to single seedling and low density. On the contrary, because of the competition of plant root, populous seedling always accompany with high amount of fertilizer and pesticide which may result in high production cost and low productivity of labor

and capital. However, the farmers of the experiment field are willing to decrease the density of transplant seedling after the practice of single seedling of SRI.

On the other hand, the high yield in the first crop season results form the trend of tempeture provides the farmer a good chance to grow paddy rice in Taiwan. Unfortunately, heavycompetition for water resource between different sectors (city, industry) and decreasing rainfall pattern are causing waterscarcity in this period. According the results of this research, the water management practice of SRI provides a response option to water scarcity with high productivity of irrigation, low irrigation water need and minimal percolation losses. In this case, water savings byfarmers can be a voluntary and deliberate choice oftheir own result from the potential of high grain yield. Although there are certain debate over the additional labor input of SRI method comparing withconventional practice, yet the SRI method in Taiwan present a water saving management practice is no doubt in first crop season.

In contrast to first crop season, the low rice yield and high production cost always lead the farmers to abandon their paddy field in second crop season, which results in the increase of runoff load in the downstream during rainy season. To overcome these problems, making use of paddy fields as aflood control system instead of rice production has been highlighted in second crop season. Different from first crop season, it is hard to practice SII under heavy rain season and small amount of irrigation always leads to very high irrigation water productivity levels, because rainfall supplies the most water need for crop growth. However, compared the water budget of different water management practices, efficient rainfall increased 11.551%, percolation increased 33.50% and drainage decreased 41.78% under DII in second crop season. Considering the capacity of flood detention in paddy fields, the runoff coefficient under DII decreased41%. It was reasonable to conclude that the DII provided more water storage capacity during growth season. From the viewpoint of effective utilization of water resources, it is meaningless to save water during second crop season. On the contrary, if the excess water is available in rivers, it should be timely delivered to the rice fields to increase the efficient rainfall, maintain adequate percolation and replenish groundwater, without having to follow the strict water conservation measures.

5. Discussions

The overproduction results in diminished profit from intensive agriculture result of depressed prices in Taiwan for decades. High labour and capital outlays lead to the reduction of arable land and the waste of water. Increasing the efficiency of input resources to find more profit for the farmers is imminent. The performance of water management practice of paddy field affects the vulnerability and the adapting capacity for local food security. The review of literature showed it seems to subsist in a variable management practices in paddy rice field. In consideration of increasing the productivity and water storage capacity of paddy fields, and adapting water management practice to the climate change and economic growth, three blocks of farm field were designed to investigate the effects of deepwater management and basic SRI principle on rice crop performance, productivity and water storage capacity in this paper.

The results showed that in Taiwanwater saving irrigation practices can be applied with high potentialyieldduring first crop season when the crop can efficiently compensate highlabor, capital and irrigation water productivityby the promotion of SRI under low labor, capital and water input. However, although the SRI still can generate high productivity in second crop season, but low temperature patternand increasing damage of pests, diseases, weeds and flood implied a higher risk of yield losses and narrows the range to exploit labor, capitaland irrigation water productivity of SRI. From the viewpoint of productivity and effective utilization of water resources, it seems meaningless to achieve high yields based onthe prescriptive use of fertilizers (and pesticides) without economically warrant in second crop season. On the contrary, if the excess water is available in rivers, the farmer should be encouraged and subsided by the government to sustain the paddy field as a shallow detention pond through deepwater management practice in second crop season, instead of letting the farmer abandoned their paddy field without controlling.

In addition to providing a technology improvement, the SRI also provides a chance to reexamine the difficulty between the theory of scientist and the practice of farmer based on some simple principles. Facing the double exposure of climate change and globalization, the SRI reminds the people need to pay more attention on the system of less input resources and more agricultural production in Taiwan.

Acknowledgments

This research was supported by Chi-Seng Water Management and Development Found and Caremed Supply Inc.. We would like to thank Mr. Tony Liu, the chairman of Caremed Supply Inc., for providing useful comments and essential equipment on the manuscript.

REFERENCES

Allen R. G., Pereira L. S., Raes D., and Smith M.. 1998. Crop Evapotranspiration - Guidelines for Computing Crop Water Requirements, FAO, Rome, Italy.

Belder P, Bouman BAM, Spiertz JHJ, Cabangon R, Guoan L, Quilang EJP, Li Yuanhua, Tuong, TP. 2004. Effect of water and nitrogen management on water use and yield of irrigated rice. Agric. Water Manage, 65:193-210.

Bhagat RM, Bhuiyan SI, Moody K. 1996.Water, tillage and weed interactions in lowland tropical rice: a review. Agric. Water Manage. 31: 165–184.

Chang YC, Kan CE, Lin GF, Chiu CL, Lee YC. 2001. Potential benefits of increased application of water to paddy fields in Taiwan. Hydrological Processes, 15: 1515–1524.

Chang YC, Kan CE, Chen CY and Kuo SF. 2007. Enhancement of water storage capacity in wetland rice fields through deepwater management practice. Irrigation and Drainage, 56: 79–86.

Cabangon RJ, Tuong TP, Castillo EG, Bao LX, Lu G, Wang GH, Cui L, Bouman BAM, Li Y, Chongde Chen, Jianzhang Wang. 2004. Effect of irrigation method and N-fertilizer management on rice yield, water productivity and nutrient-use efficiencies in typical lowland rice conditions in China. Rice Field Water Environ, 2:195-206.

Hayase Y. 1994. Evaluation of paddy fields for flood control and a proposal of their enhancing project. Journal of the Japanese Society of Irrigation Drainage and Reclamation Engineering, 62(10): 943–948 (in Japanese).

Kiyochika Hoshikawa. 1989. The Growing Rice Plant—An Anatomical Monograph. Nobunkyo: Tokyo; 83–84.

Kiyochika S. 1994. The Technology of Increasing Rice Produce. Ie No Hika Association: Tokyo; 52–133 (in Japanese).

Kuo CH. 1994. Irrigation in Taiwan. In Proceedings of the Sino-Japanese Workshop on Agricultural Engineering, Taipei, Taiwan: 1–5 (in Chinese).

Lee YC, Kan CE, Chang YC. 1995. A preliminary strategy of Taiwan water resources usage: a case study in Chia-Nan area. Journal of Taiwan Water Conservancy, 43(3): 1–18 (in Chinese).

Mizutani M., Hasagawa S., Koga K., Goto A., Murty VVN. 1999. Advanced Paddy Field Engineering. The Japanese Society of Irrigation, Drainage and Reclamation Engineering (JSIDRE): 393

Namara R E, Weligamage P, Barker R. 2004. Prospects for adopting system of rice intensification in Sri Lanka: A socioeconomic assessment. IWMI Research Reports. Colombo: International Water Management Institute: 75.

Sato S., Yamaji E., Kuroda T.. 2011. Strategies and engineering adaptions to disseminate SRI methods in large-scale irrigation systems in Eastern Indonesia. Paddy Water Environ, 9: 79–88.

Sato S, Uphoff N. 2007. A review of on-farm evaluation of system of rice intensification (SRI) methods in eastern Indonesia. CAB Reviews: Perspectives in Agriculture, Veterinary Science, Nutrition and Natural Resources. Wallingford: Commonwealth Agricultural Bureau International.

Sekiya S. 1992. Functions of Paddy Fields. Ie No Hika Association: Tokyo: 644 (in Japanese).

Shih CC. 1977. Primary study on damage to paddy rice by water inundation. Symposium on Environment Impact of Rainstorms, Taiwan; 189–222.

Sinha S K, Talati J. 2007. Productivity impacts of the system of rice intensification (SRI): A case study in West Bengal, India. Agric Water Manage, 87: 55–60.

Stoop W, Uphoff N, Kassam A. 2002. A review of agricultural research issues raised by the system of rice intensification (SRI) from Madagascar: opportunities for improving farming systems for resource-poor farmers. Agric. Syst. 71:249-274.

SRI International Network and Resources Center. 2012. SRI Methodologies. Retrieved August 1, 2012, from http://sri.ciifad.cornell.edu/aboutsri/methods/index.html.

Tabbal DF, Bouman BAM, Bhuiyan SI, Sibayan EB, Sattar MA. 2002. On-farm strategies for reducing water input in irrigated rice: case studies in the Philippines. Agric. Water Manage. 56:93-112.

Uphoff N.. 2007. The system of rice intensification: using alternative cultural practices to increase rice production and profitability from existing yield potentials. International Rice Commission Newsletter, No. 55. Food and Agriculture Organization, Rome

Zhang W., Song S.T.. 1989. Irrigation model of water saving-high yield at lowland paddy field. International Commission on Irrigation and Drainage, Seventh Afro-Asian Regional Conference, 15-25 October 1989. Tokyo, Japan. I-C: 480-496.

BIG DATA FOR TARGETED IRRIGATION INVESTMENTS IN PEOPLE, CLIMATE, AND NATURE

Anton Urfels, Andrew McDonald, Saral Karki, Emma Karki, Krishna Kafle, Hari Sankar Nayak, Laura Arenas Calle, Gokul Paudel, Timothy Krupnik, Sonam Sherpa, Virender Kumar, Syed Adil Mizan

Structured Abstract

Introduction(100 words)

Irrigation is emerging as a crucial climate adaptation option for agriculture. But current investments are often poorly aligned with agronomic opportunities, farmers' investment capacities, and the natural resource base to support increased water abstraction. At the same time, recent advances in computational sciences and digital technologies can substantially support spatial targeting of irrigation investments across large landscapes. Being interconnected, complex, and open – agricultural water systems require a holistic approach for successful modeling and management. Addressing global water and food grand challenges requires integrating big data on agronomy, water systems, and socio-technical aspect of irrigation.

Methodology(100 words)

Specifically, this new generation of irrigation targeting champions (i) transdisciplinary across agriculture, hydrology, irrigation technologies, and social science (ii) fusion of datasets from remote sensing, survey data, and simulation models (iii) machine learning and participatory approaches to continuously improve and ground-truth predictions. Here we illustrate such an approach by providing insights from largely groundwater dependent Eastern India. We combine large-scale agricultural production surveys piloted in South Asia (n: >40k) combined with machine learning, environmental analytics on (>1k observation wells), and participatory approaches. Importantly, we showcase the importance of feedbacks loops participatory and quantitative analytics.

Analysis and results(50 words)

Our results indicate that large water yield gaps prevail. But co-limiting factors vary across the region. At the same time, farmers' incentives to invest in irrigation are low due to small farm sizes. The large monsoon-driven groundwater recharge poses especially high risks in the dry season and in the South.

Conclusions and recommendations(100 words)

Our results suggest that effectively enhancing climate resilience and food security will rely on spatially varying co-investments for enabling low-cost agronomic practices such as timely crop planting as well as irrigation. To achieve this funders and policy makers leverage big data for evidence-based and adaptive decision-making and investment targeting. This can substantially increase the effectiveness of investments in irrigation while safeguarding against maladaptive irrigation expansion and the participatory approaches help to co-develop strong governance mechanisms and co-define sustainability (ground)water management strategies. Altogether, leveraging big data can provide diagnostics and solutions for irrigation investments that caters to people, nature, and climate:

Keywords (5): machine learning; groundwater; human-environment systems; sustainability science

Introduction

Climate change is increasing the frequency of drought and dry spells across the globe (IPCC, 2023), resulting in increased stress of crops for food production. To increase the resilience of agricultural production systems against this increasingly erratic rainfalls, countries and global financial institutes are investing heavily in irrigation to provide farmers with a more secure and stable source of water when rainfall does not suffice – with e.g. the world bank having 6.4 billion USD pipelined for irrigation investments and 213 active irrigation investment projects (*Projects*, n.d.). However, investments in irrigation do not have a strong track record in delivering returns on investments when compared to the expected returns. For example, it was found that only 13% of the designed area of medium and large irrigation schemes in Africa was being irrigated (Higginbottom et al., 2021). The build-neglect-rebuild cycle has long been discussed in the academic literature (Huppert et al., 2003; Suhardiman & Giordano, 2014), and is an infamously difficult problem to address. Nevertheless, some 60% of global food production comes from the only 30% of globally irrigated areas – showcasing the importance of irrigation for global food security (Molden, 2007).

Given the strong contribution of irrigated agriculture to food security and the increasing pressures these system face, a more targeted approach to investing in irrigation is necessary. Here, we present examples of how agronomic and environmental data stacks can be used to provide planner and policymakers with relevant and updated information on where investments are most likely to pay of while being unlikely to cause severe impacts on groundwater irrigation.

Irrigation is emerging as a crucial climate adaptation option for agriculture. But current investments are often poorly aligned with agronomic opportunities, farmers' investment capacities, and the natural resource base to support increased water abstraction (Bo et al., 2022; Puy et al., 2022; Schmitt et al., 2022). At the same time, recent advances in computational sciences and digital technologies can substantially support spatial targeting of irrigation investments across large landscapes (McDonald et al., 2022; Urfels et al., 2022). Being interconnected, complex, and open – agricultural water systems require a holistic approach for successful modeling and management (Urfels et al., 2023). Addressing global water and food grand challenges requires integrating big data on agronomy, water systems, and socio-technical aspect of irrigation.

Specifically, this new generation of irrigation targeting champions (i) transdisciplinary across agriculture, hydrology, irrigation technologies, and social science (ii) fusion of datasets from remote sensing, survey data, and simulation models (iii) machine learning and participatory approaches to continuously improve and ground-truth predictions. Here we illustrate such an approach by providing insights from largely groundwater dependent Eastern India. We combine large-scale agricultural production surveys piloted in South Asia (n: >40k) environmental analytics on (>1k observation wells), and participatory approaches. Here, we present how outputs from these approaches can jointly inform planning and targeting of irrigation investments.

Methods

In this paper, we utilize two major data sources: first of all, we use data from the Landscape Crop Assessment Survey (LCAS) that has been developed by the Cereal Systems Initiative for South Asia (CSISA) in cooperation with Krishi Vigyan Kendra Knowledge Network (KvK) and Indian Council of Agricultural Research (ICAR) (Singh et al., 2019). Additionally, we use groundwater level data that has been collected by the Central Ground Water Board (CGWB) of India that is part of the Ministry of Jal Shakti, Department of Water Resources.

To understand where irrigation is most likely to pay off the most, we construct a random forest yield prediction model from the LCAS dataset (Breiman, 2001; McDonald et al., 2022; Urfels et al., 2021). Random forest models have been shown to provide robust predictions while allowing for some degree of interpretability. But instead of using the model for diagnostic purposes, we here apply it for predictions of the yield increase when farmers add one additional irrigation. The main drawback of using random forest models is that their accuracy declines substantially when moving beyond the observed data in the training dataset (Hastie et al., 2001). Increasing irrigation number by a single unit (1 application), thus ensures that our predictions are within the model's effective inference space.

Next, we collate the groundwater levels across Bihar. However, the time series are not without gaps and we therefore investigate the continuity of the time series. We find that ~40% of observation wells contain more than 70 observation and are thus suitable for time series analysis. We thus subset the observation wells to wells with at least 70 observations and remove the remaining ones. To determine the trend in water levels, we use a linear regression analysis of the dry season water levels that are measured during the month of May – before the monsoon starts.

Lastly, we consider both the expected increase in yield from additional irrigation and the current trends of groundwater decline to delineate areas where investments in irrigation are most likely to benefit farmers without endangering nature and other water users.

Results and discussion

Our results indicate that large water yield gaps prevail. But co-limiting factors vary across the region. At the same time, farmers' incentives to invest in irrigation are low due to small farm sizes. The large monsoon-driven groundwater recharge poses especially high risks in the dry season and in the South. Figure 1, provides an overview of the where providing one additional irrigation might have the largest impact on yield in Bihar, Nepal, and Eastern Uttar Pradesh. It is evident that there is a clear spatial structure to the opportunity of irrigation. We can see that the areas in Southern Bihar are unlikely to see dramatic increases in yield with additional irrigation, except for the easternmost parts. The largest response is concentrated in the central regions and eastern most parts. While In Nepal, some parts in the West have the largest likely response.

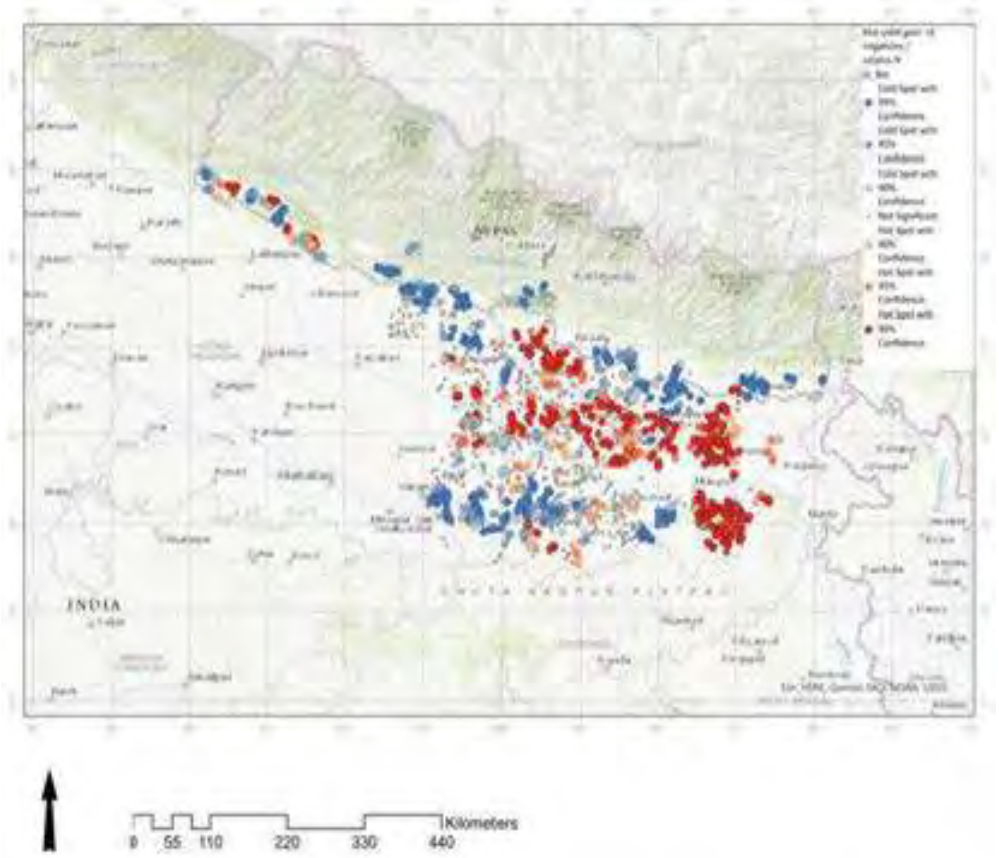

Figure 1. Benefit of providing one additional irrigation to rice in. Red areas are clusters with a high yield response and blue areas are clusters with a low yield response.

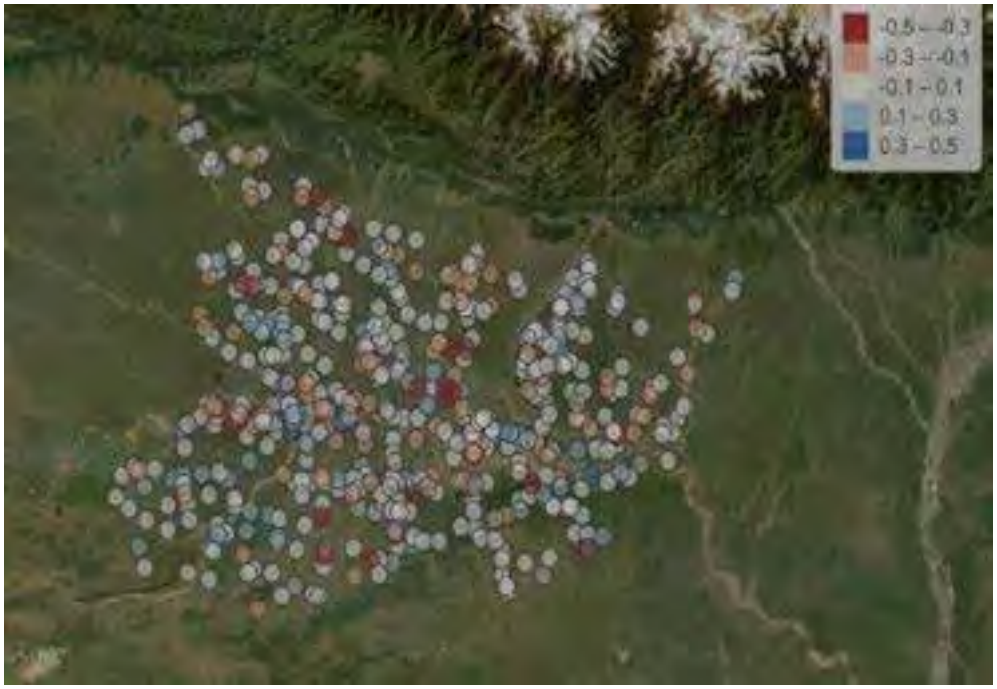

Figure 2. Trend in dry season groundwater levels in m/year.

Next, we consider the groundwater levels in the study area – focusing on Bihar. Figure 2, shows the trends of groundwater levels over the last 20 years. Importantly, what we see is that there is no clear spatial demarcation of trends but nearby areas might experience opposing groundwater trends. This patterns is likely due to the multi-layered nature of the aquifer caused by the highly active morpho dynamic river systems with immense sedimentation and discharge loads of substantial annual amplitude.

Lastly, we conducted a series of focus group discussion in Nepal and Bihar where we elicited farmers response to the advice to increase their irrigation by one single application. However, we found that farmers were very reluctant to increase the numbers of irrigation they provide – citing increased risk of lodging as a key factors that they expect to result from additional irrigation. Future studies need to further investigate these behavioral aspects and validate our results with field trials.

As a result, we recommend that irrigation investments are targeted and designed in a two-stage manner. Irrigation development and irrigation-led intensification need to be targeted on a place by place basis focusing on areas of highest likely return. That is, first, the areas of the largest defined response in yield should be targeted. Next a diagnostic approach to what the most important interventions should be can be deployed to map, understand and benchmark existing irrigation schemes for surface and groundwater irrigation. Next the aquifer should be studied and local areas without existing decline should be identified for investing first. Areas that are experiencing decline in groundwater levels might still benefits from investments in irrigation for more equitable and productive use. But cautions is needed here to not further deplete the resource base and identify mechanisms to halt the ongoing decline. Lastly, interventions should be rolled on in a targeted manner to tackle the identified issues and improve both resilience of agricultural production and sustainability of the water resources.

Conclusion

Our results suggest that effectively enhancing climate resilience and food security will rely on spatially varying co-investments for enabling low-cost agronomic practices such as timely crop planting as well as irrigation. To achieve this funders and policy makers leverage big data for evidence-based and adaptive decision-making and investment targeting. This can substantially increase the effectiveness of investments in irrigation while safeguarding against maladaptive irrigation expansion and the participatory approaches help to co-develop strong governance

mechanisms and co-define sustainability (ground)water management strategies. Altogether, leveraging big data can provide diagnostics and solutions for irrigation investments that caters to people, nature, and climate.

References

Bo, Y., Jägermeyr, J., Yin, Z., Jiang, Y., Xu, J., Liang, H., & Zhou, F. (2022). Global benefits of non-continuous flooding to reduce greenhouse gases and irrigation water use without rice yield penalty. *Global Change Biology*, *28*(11), 3636–3650. https://doi.org/10.1111/gcb.16132

Breiman, L. (2001). Random Forests. *Machine Learning*, *45*(1), 5–32. https://doi.org/10.1023/A:1010933404324

Hastie, T., Friedman, J., & Tibshirani, R. (2001). *The Elements of Statistical Learning*. Springer. https://doi.org/10.1007/978-0-387-21606-5

Higginbottom, T. P., Adhikari, R., Dimova, R., Redicker, S., & Foster, T. (2021). Performance of large-scale irrigation projects in sub-Saharan Africa. *Nature Sustainability*, *4*(6), Article 6. https://doi.org/10.1038/s41893-020-00670-7

Huppert, W., Svendsen, M., & Vermillion, D. L. (2003). Maintenance in Irrigation: Multiple Actors, Multiple Contexts, Multiple Strategies. *Irrigation and Drainage Systems*, *17*(1), 5–22. https://doi.org/10.1023/A:1024940516158

IPCC. (2023). *Climate Change 2023: Synthesis Report. Contribution of Working Groups I, II and III to the Sixth Assessment Report of the Intergovernmental Panel on Climate Change []. IPCC, Geneva, Switzerland, pp. 35-115, doi:* IPCC. 10.59327/IPCC/AR6-9789291691647

McDonald, A. J., Balwinder-Singh, Keil, A., Srivastava, A., Craufurd, P., Kishore, A., Kumar, V., Paudel, G., Singh, S., Singh, A. K., Sohane, R. K., & Malik, R. K. (2022). Time management governs climate resilience and productivity in the coupled rice–wheat cropping systems of eastern India. *Nature Food*, *3*(7), Article 7. https://doi.org/10.1038/s43016-022-00549-0

Molden, D. (Ed.). (2007). *Water for Food Water for Life: A Comprehensive Assessment of Water Management in Agriculture*. Routledge. https://doi.org/10.4324/9781849773799

Projects. (n.d.). [Text/HTML]. World Bank. Retrieved September 8, 2023, from https://projects.worldbank.org/en/projects-operations/projects-list

Puy, A., Sheikholeslami, R., Gupta, H. V., Hall, J. W., Lankford, B., Lo Piano, S., Meier, J., Pappenberger, F., Porporato, A., Vico, G., & Saltelli, A. (2022). The delusive accuracy of global irrigation water withdrawal estimates. *Nature Communications*, *13*(1), Article 1. https://doi.org/10.1038/s41467-022-30731-8

Schmitt, R. J. P., Rosa, L., & Daily, G. C. (2022). Global expansion of sustainable irrigation limited by water storage. *Proceedings of the National Academy of Sciences*, *119*(47), e2214291119. https://doi.org/10.1073/pnas.2214291119

Singh, A. K., Craufurd, P., Mcdonald, A., Singh, A. K., Kumar, A., Singh, R., Singh, B., Singh, S., Kumar, V., & Malik, R. (2019). *New frontiers in agricultural extension—Volume 1*. CIMMYT. https://repository.cimmyt.org/handle/10883/20738

Suhardiman, D., & Giordano, M. (2014). Is There an Alternative for Irrigation Reform? *World Development*, *57*, 91–100. https://doi.org/10.1016/j.worlddev.2013.11.016

Urfels, A., Mausch, K., Harris, D., McDonald, A. J., Kishore, A., Balwinder-Singh, van Halsema, G., Struik, P. C., Craufurd, P., Foster, T., Singh, V., & Krupnik, T. J. (2023). Farm size limits agriculture's poverty reduction potential in Eastern India even with irrigation-led intensification. *Agricultural Systems*, *207*, 103618. https://doi.org/10.1016/j.agsy.2023.103618

Urfels, A., McDonald, A. J., van Halsema, G., Struik, P. C., Kumar, P., Malik, R. K., Poonia, S. P., Balwinder-Singh, Singh, D. K., Singh, M., & Krupnik, T. J. (2021). Social-ecological analysis of timely rice planting in Eastern India. *Agronomy for Sustainable Development*, *41*(2), 14. https://doi.org/10.1007/s13593-021-00668-1

Urfels, A., Montes, C., Balwinder-Singh, Halsema, G. van, Struik, P. C., Krupnik, T. J., & McDonald, A. J. (2022). Climate adaptive rice planting strategies diverge across environmental gradients in the Indo-Gangetic Plains. *Environmental Research Letters*, *17*(12), 124030. https://doi.org/10.1088/1748-9326/aca5a2

EFFECTS OF FULVIC ACID APPLICATION ON DRY MATTER ACCUMULATION AND YIELD OF IRRIGATED MAIZE

WU Jiabin [1] QIN Ziyuan[1] WANG Biyu[2]

Abstract

In order to explore the dry matter accumulation and yield formation of maize under different irrigation quotas and fulvic acid application modes, this study set two irrigation quotas (W1:25 mm; W2:30 mm) and three fulvic acid application levels (H0:0; H1:45; H2: 67.5 kg/hm ²) , A total of 6 treatments were conducted to study the effects of fulvic acid application on the growth and development characteristics, dry matter accumulation, water and nitrogen utilization efficiency, yield, and correlation of irrigated maize. The results showed that both high irrigation quota (W2) and application of fulvic acid could improve the accumulation and formation rate of dry matter in maize. Under W2 irrigation treatment, application of fulvic acid could significantly increase the plant height, stem diameter, and leaf area index of maize during maturity, while under W1 irrigation treatment, the leaf area index of maize was significantly increased. High irrigation quota treatment of corn has the characteristics of long duration of rapid growth period and high growth rate, which is conducive to the accumulation of dry matter in corn. Under different irrigation quotas, corn yield increases with the increase of fulvic acid application rate. Taking into account various indicators, W2H1 treatment is the optimal water and fulvic acid application management mode for maize in the study area.

Key words: irrigation quota; fulvic acid; maize; dry matter accumulation; yield

Introduction

Corn is the main grain crop in China, accounting for approximately 36% of the total grain output[1]. With the increasing population, increasing corn yield in limited arable land has become one of the important challenges faced by China's agricultural production, and resource based water scarcity is the primary factor restricting agricultural production in arid and semi-arid areas[2]. Otog Front Banner, Ordos City, Inner Mongolia, is located in the northwest inland arid area of China. Agriculture and animal husbandry are intertwined, and the ecological environment is very fragile. The per capita water resources are less than 1/4 of the average level of China, and the water resource utilization efficiency is less than 1/2 of developed countries[3]. It is estimated that due to periodic or unpredictable drought, agricultural production of about 1/3 of cultivated land is limited[4]. In order to improve Agricultural productivity of cultivated land with limited water resources, it is necessary to carry out research on efficient utilization of water resources, stable crop yield and increased crop production.

Drip irrigation, as an advanced water-saving irrigation technology, has many advantages such as water-saving, increasing yield, improving quality, reducing ineffective surface evaporation, and improving soil conditions in crop root zones. It has been widely applied in the western region of Inner Mongolia[5-7]. At present, the actual irrigation quota of Otog Front Banner is about 2700 m³/hm², In recent ten years, the proportion of Farm water is close to 90%, but with the acceleration of urbanization and industrialization in China, Farm water is bound to be occupied, and the contradiction of "water reduction and grain increase" is prominent[8]. Studies have shown that adequate water conditions can promote the growth rate of vegetation population, extend the accumulation time of dry matter, and help yield formation[9]. Moderate water deficit significantly reduces the total water consumption, while the effect on corn dry matter accumulation and yield formation was not significant[10]. Overall, reducing irrigation quotas is not conducive to crop yield increase, while moderate reduction of irrigation combined with soil improvement, crop growth regulators, and reasonable dense planting can compensate for the negative effect of crop productivity decline caused by water reduction.

[1] Yinshanbeilu Grassland Eco-hydrology National Observation and Research Station, China Institute of Water Resources and Hydropower Research, Hohhot 010020, China;
[2] Research Center of Fluid Machinery Engineering and Technology, Jiangsu University, 212013, China)

As an excellent biological stimulant, fulvic acid promotes plant growth by regulating the "plant soil fertilizer" system, enhancing stress resistance, promoting crop nutrient absorption, improving soil microbial community structure, and increasing yield[11]. El Mekser et al. showed that the application of fulvic acid can significantly reduce the growth period of maize from sowing to tasseling, and significantly increase plant height and yield[12].

Currently, there are more studies on the dry matter accumulation and yield of maize with different irrigation quotas, while there are relatively few studies on the coupled application of fulvic acid. Whether fulvic acid application can further enhance water and nitrogen utilization as well as dry matter accumulation and yield of maize under the appropriate irrigation quotas needs to be explored.

This study conducted field experiments to analyze the effects of fulvic acid application under different irrigation quotas on the growth and development characteristics, dry matter accumulation and accumulation rate, yield and related traits, and water and nitrogen utilization efficiency of corn. The aim is to provide theoretical basis and technical reference for the study of water-saving and yield increasing planting methods of corn in the region.

1 Materials and Methods

1.1 Overview of the experimental area

The experiment was conducted in 2022 at the Ordos Irrigation Experimental Station in Inner Mongolia (38 ° 7 ′ 37 ″ N, 107 ° 31 ′ 5 ″ E). The test area belongs to temperate Continental climate, with long cold winter, short hot summer, drought and little rain, strong wind and more sand, which is a typical distribution area of aeolian sandy soil. The multi-year average temperature is 7.9 ℃, the multi-year average evaporation is 2497.9mm, and the multi-year average precipitation is 260.6mm. The precipitation from June to September accounts for 60~90% of the annual precipitation. The multi-year average Sunshine duration are 2958h, and the annual frost free period is about 171d.

The maximum depth of the frozen soil layer is 1.54m. The soil at 1m depth in the test area is sandy soil, the Field capacity is 22.86%, and the buried depth of groundwater level is 1.2~2.0 m. Before the experiment, the basic physical and chemical properties of the topsoil (0-20 cm) were as follows: pH value 8.21, organic matter mass fraction 10.37g/kg, alkali hydrolyzed nitrogen mass fraction 76.9 mg/kg, available phosphorus mass fraction 14.56 mg/kg, and available potassium mass fraction 121.3 mg/kg.

1.2 Design of experiments

The maize variety "Yidan 81", which has been planted and promoted for many years in Otog Front Banner, was used as the test material. The experiment was a 2-factor randomized group design, with two irrigation quotas (25 and 30 mm, respectively W1 and W2), three levels of fulvic acid application (0, 45 and 67.5 kg/hm², respectively H0, H1 and H2), and a total of six treatments (W1H0, W1H1, W1H2, W2H0, W2H1, W2H2) with three replications for each treatment. A total of 18 plots were arranged in randomized blocks, with each test plot covering an area of 50 m² (5 m×10 m), and a 1 m wide isolation zone was set between each plot to eliminate mutual interference.

The planting density of corn in the experimental field was 4500 plants/mu. The bottom fertilizer of the experimental field was 75 m³/hm² of rotted cow dung applied by integrated agricultural machine, and the base fertilizer was 450 kg/hm² of compound fertilizer with N:P2O5:K2O of 15-20-10, which was applied to the soil in layers with sowing. Nitrogen fertilizer for the test was urea (containing 46% N), following the principle of front control, middle promotion, and back supplementation, and was applied in three times during the fertility period, totaling 240 kg/hm² (the ratio of application during the pulling stage, male pumping stage, and grouting stage was 4:3:3), and drip irrigation was used to apply fertilizer along with the water.

The experiment was sown on April 29, 2022, with 66,700 seedlings/hm², harvested on September 25, with a full-life span of 150 d. Drip irrigation was applied nine times, and xanthate was applied three times in the seedling and nutrient growth stages, with H1 and H2 flushed with drip irrigation each time at 15 and 22.5 kg/hm², respectively, and the water intake pipe of each plot was connected with a small water meter.

1.3 Measurement Items and Methods

1.3.1 Determination of irrigation water volume

After sowing corn, record the date of each drip irrigation and use a small water meter to calculate the water volume for each irrigation in each plot.

1.3.2 Determination of Plant Dry Matter Quality

Three maize plants were randomly selected from each experimental plot during the seedling stage, jointing stage, tasseling stage, filling stage, and maturity stage. They were killed in a drying oven at 105 ℃ for 0.5 hours, then dried at 80 ℃ to a constant mass, cooled to room temperature, and the dry matter mass of the plants was measured using an electronic balance with an accuracy of 0.01 g.

1.3.3 Determination of growth indicators

Three maize plants were randomly selected from each experimental plot during the seedling, jointing, tasseling, filling, and mature stages for growth index measurement. The plant height was measured with a tape measure, covering the maximum distance from the stem base to the maize growth point; The stem diameter shall be measured with a Vernier scale with an accuracy of 0.01 mm. The middle part of the first stem node of the aboveground part shall be selected for the measurement at the seedling and jointing stages. After the heading stage, the stem diameter in the middle of the stem node where the ear position is measured shall be added and the average value shall be calculated; The leaf area index is calculated using the LI-3000C portable leaf area meter, which is the ratio of total leaf area to unit land area.

1.3.4 Yield and related shape determination

Randomly select 1m² of each experimental plot during the maturity period for yield measurement. After threshing, measure the moisture content of the seeds, and calculate the yield based on the 14% moisture content of the seeds. Simultaneously measure indicators such as corn ear diameter, ear length, number of grains per ear, effective ears per unit area, 100 grain weight, and bald tip.

1.4 Calculation method

The Logistic growth equation was used for Nonlinear regression fitting of Cumulant of dry matter of maize[13], as follows:

$$y=a/(1+be^{-kt}) \quad (1)$$

Where y is the cumulant of dry matter of corn (kg/hm ²), a is the potential maximum dry matter value of corn(kg/hm²), b is the regression parameter related to cumulant of dry matter of maize(b>0), k is the growth rate of cumulant of dry matter(k<0), t is the time after corn sowing(d).

By taking the derivative of the logistic function and calculating its eigenvalue equation, three key points can be obtained, with the abscissa corresponding to the initial peak period (T_1, d), peak period (T_2, d), and peak period (T_3, d), as well as the fastest growth rate (Vmax, kg/hm) ²· d) The growth process fitted by the logistic curve can be divided into gradually increasing period (0-T_1), rapidly increasing period (T_1-T_3), and slowly increasing period (T_3~∞) using the initial and final stages. The eigenvalue equations are

$$T_1=(\ln b-1.317)/k \quad (2)$$

$$T_2=\ln b/k \quad (3)$$

$$T_3=(\ln b+1.317)/k \quad (4)$$

$$\Delta T = T_3 - T_1 \quad (5)$$

$$V_{max}=ak/4 \quad (6)$$

$$IWUE=Y/I \quad (7)$$

$$PFP=Y/N \quad (8)$$

Where, ΔT is the duration of rapid growth period(d), Y is the corn yield(kg/hm²), I is the irrigation volume per unit area(mm), N is the nitrogen rate(kg/hm²).

1.5 Data Analysis

Excel 2019 and Origin 2022 were used for data processing and plotting, and SPSS 27.0 was used for statistical analysis. Multiple comparisons between treatments were conducted using the Duncan method in One Way ANOVA.

2 Results and Analysis

2.1 Effects of Fulvic Acid Application on Maize Growth and Development under Different Irrigation Quotas

The effects of applying fulvic acid under different irrigation quotas on maize plant height, stem diameter, and leaf area index are shown in Figure 1. The experimental results showed that during the mature period, the application of fulvic acid under W2 treatment significantly increased the plant height, stem diameter, and leaf area index of maize ($P<0.05$), while under W1 treatment, the application of fulvic acid had no significant effect on the plant height and stem diameter of maize ($P>0.05$), and had a significant effect on the improvement of leaf area index ($P<0.05$). The variation trend of corn plant height under different treatments is basically the same. From the jointing stage to the tasseling stage, the corn plant height rapidly increases, and then the increase in plant height tends to stabilize. The plant height reaches its maximum value during the filling stage, and decreases slightly during the mature stage. Under the W2 treatment, the corn plant height increased by an average of 10.58% compared to the W1 treatment, while under the H2 treatment, the corn plant height increased by 4.05% and 4.14% compared to the H0 and H1 treatments, respectively.

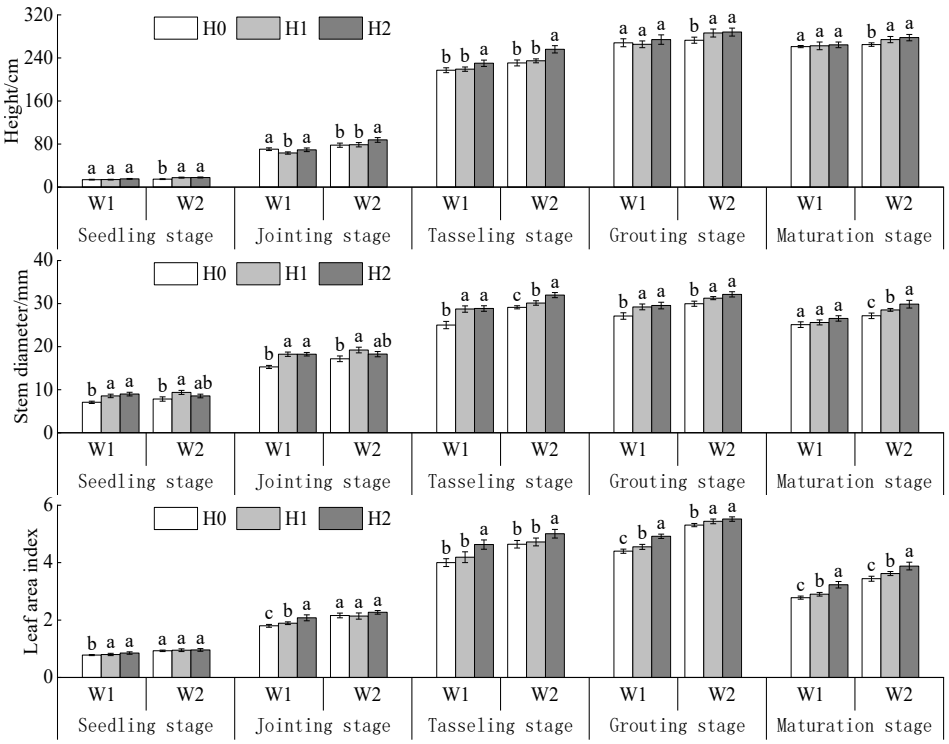

Fig.1 Effects of fulvic acid application on growth characteristics of maize under different irrigation quotas

The trend of corn stem diameter change is similar to that of plant height. During the filling period, the stem diameter reaches its maximum value, with an average stem diameter of 29.88mm for each treatment. Under W2 treatment, the corn stem diameter increases by an average of 9.54% compared to W1 treatment. The corn stem diameter increases with the increase of fulvic acid dosage, and the plant height of H1 and H2 treatments increases by 7.08% and 0.86% compared to H0 treatment, respectively. The variation trend of maize leaf area index from seedling stage to filling stage is similar to that of plant height. After reaching its maximum value during the filling stage, the leaf area index significantly decreases as the growth period progresses. The leaf area index decreases by 29.71% to 36.82% from filling stage to mature stage in different treatments. The leaf area index of maize under W2 treatment increased by an average of 14.66% compared to W1 treatment. The leaf area index of maize increased with the increase of fulvic acid dosage. The leaf area index of maize under H1 and H2 treatment increased by 2.38% and 9.99% compared to H0 treatment, respectively.

2.2 Effect of application of fulvic acid on dry matter accumulation in maize under different irrigation quotas

The effect of application of fulvic acid on dry matter accumulation in corn under different irrigation quotas is shown in Figure 2. The results showed that the increase range of dry matter Cumulant of maize in different treatments gradually decreased with the advance of growth period, and the increase range of dry matter accumulation from filling stage to maturity stage was the smallest, with an average of 15.34%. The addition of fulvic acid can promote the accumulation of dry matter in corn, but there is no significant difference in dry matter accumulation between H1 and H2 ($P>0.05$). Under the same irrigation quota, the dry matter accumulation of maize under H1 and H2 treatments was consistently higher than that under H0 treatment. During the filling and ripening stages, the dry matter accumulation of maize under H1 and H2 treatments was significantly higher than that under H0 treatment ($P<0.05$), with an increase of 7.40% to 11.56%. Under the same application amount of fulvic acid, the dry matter accumulation of corn in W2 treatment was higher than that in W1 treatment at all growth stages. The average increase in growth stages of H0, H1, and H2 treatments was 9.17%, 11.89%, and 11.01%, respectively.

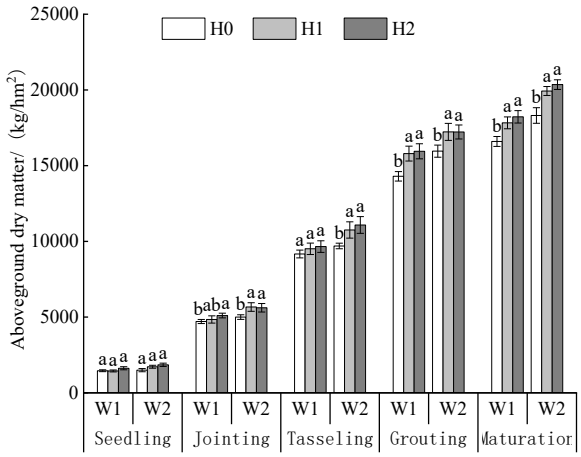

Fig.2 Effects of fulvic acid application on dry matter accumulation in maize under different irrigation quotas

The Logistic growth equation fitting and model effectiveness evaluation of Cumulant of dry matter above ground of maize are shown in Table 1. The consistency index of the Logistic growth model for aboveground dry matter of maize under different treatments ranged from 0.9988 to 0.9993, the efficiency coefficient ranged from 0.9760 to 0.9858, and the Coefficient of determination R^2 ranged from 0.9904 to 0.9943. The evaluation of model effectiveness showed that the effect of fitting the process of dry matter accumulation of maize with the Logistic growth equation was better, and the predicted value of the model was in good agreement with the measured value. The fitting results indicate that the theoretical maximum accumulation of aboveground dry matter in maize under different irrigation quotas is 17472.77~21605.19 kg/hm

for each treatment of fulvic acid application ², Under the same irrigation quota, the theoretical maximum value of dry matter accumulation in the aboveground part of corn increases with the increase of the amount of fulvic acid applied, among which the theoretical maximum value of dry matter accumulation in W2H2 treatment is 2.50%~23.65% higher than other treatments.

Tab.1 Logistic growth equation fitting and model validity of aboveground dry matter of maize accumulation

handle	Dry matter accumulation logistic equation	Model Validity		
		AI	EF	R^2
W1H0	$y=17472.77/(1+78.89e^{-0.049t})$	0.9990	0.9805	0.9922
W1H1	$y=18646.38/(1+120.22e^{-0.053t})$	0.9992	0.9841	0.9937
W1H2	$y=19304.17/(1+88.36e^{-0.049t})$	0.9992	0.9835	0.9934
W2H0	$y=19277.31/(1+99.49e^{-0.051t})$	0.9993	0.9858	0.9943
W2H1	$y=21078.77/(1+79.71e^{-0.049t})$	0.9993	0.9855	0.9942
W2H2	$y=21605.19/(1+70.8e^{-0.047t})$	0.9988	0.9760	0.9904

The first derivative of the logistic growth equation was obtained to obtain the curve of the accumulation rate of aboveground dry matter in maize under different irrigation quotas, as shown in Figure 3. The variation curve of the aboveground dry matter accumulation rate of corn is a single peak curve, which shows a trend of first increasing and then decreasing with the advancement of the days after maize emergence. Under the same irrigation quota, the average accumulation rate of dry matter in maize treated with H1 and H2 was higher than that in H0 treatment. In the middle and late stages of growth, the accumulation rate of aboveground matter in maize increased with the increase of yellow fulvic acid application amount. The average accumulation rate of maize aboveground parts under W2 treatment was higher than that under W1 treatment with the same amount of fulvic acid applied.

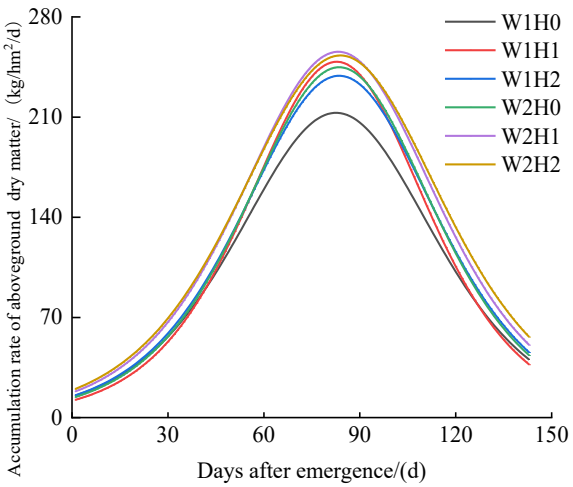

Fig.3 Effects of fulvic acid application on dry matter accumulation rate of maize under different irrigation quotas

The second derivative of the logistic growth equation was obtained, and the main characteristic values of the accumulation process of aboveground dry matter in maize under different irrigation quotas were obtained as shown in Table 2. Under different irrigation quotas, the average rapid increase period of dry matter accumulation rate in the aboveground part of corn treated with fulvic acid application was 53.17 days, and the maximum increase rate of dry matter accumulation in the aboveground part was 90.28 days. The time difference in the fastest

growth rate among different treatments is relatively small. Under W2 treatment, the peak period of dry matter accumulation was advanced with the increase of fulvic acid application amount. The peak period of dry matter accumulation rate in H1 and H2 treatments was on average 1.51 and 1.81 days earlier than that in H0 treatments, respectively. During the rapid growth period, the application amount of fulvic acid is 45 kg/hm² At the same time, the maximum growth rate of aboveground dry matter in maize under various irrigation quotas reached its maximum value, with the maximum growth rate of aboveground dry matter in W2H1 treatment being 255.63 kg/(hm²d) Compared with other treatments, it has increased by 1.77% to 18.83%.

Tab.2 Main characteristic values of aboveground dry matter of maize accumulation process

handle	Main characteristic values of dry matter accumulation				
	T_1/d	T_2/d	T_3/d	ΔT/d	$Vmax$/(kg·hm^{-2}·d^{-1})
W1H0	62.59	89.60	116.62	54.03	212.95
W1H1	65.10	89.79	114.48	49.38	248.65
W1H2	63.94	90.55	117.16	53.22	238.84
W2H0	64.63	90.55	116.48	51.85	244.82
W2H1	63.11	90.26	117.41	54.30	255.63
W2H2	62.82	90.93	119.04	56.22	253.05

2.3 Effect of Fulvic Acid Application on Corn Yield under Different Irrigation Rations

The effects of application of fulvic acid under different irrigation quotas on maize yield and related traits are shown in Table 3. The experimental results showed that under different irrigation quotas, the yield of corn increased with the increase of fulvic acid application rate, and the yield of W2H2 treatment was the highest, at 10464.34kg/hm², There was no significant difference in yield between W2H1 and W2H2 treatments (P>0.05). Under the same irrigation mode, the application of fulvic acid significantly increased maize yield. The average increase in maize yield under W1 and W2 treatments with fulvic acid application was 4.19% and 4.74% higher than that under H0 treatment, respectively. From the perspective of corn yield related trait indicators, the effective ears per unit area, number of grains per ear, and ear diameter are directly proportional to the amount of fulvic acid applied. The average values of 100 grain weight and ear length are 34.25g and 22.36cm, respectively. High irrigation quotas have a promoting effect on 100 grain weight and ear length, while the average value of corn bald tip is 0.51cm, indicating significant variability. The average yield and related shapes of maize under W2 treatment were higher than those under W1 treatment, indicating that high irrigation quotas have a positive effect on maize growth and yield formation. The effective panicle per unit area, number of grains per panicle, 100 grain weight, panicle diameter, and yield all increase with the increase of fulvic acid application rate. From this, it can be seen that the appropriate application of fulvic acid under high irrigation quotas can increase storage capacity by forming sufficient large ears, thereby increasing maize yield.

Tab.3 Effects of fulvic acid application on yield and related traits of maize under different irrigation quotas

Treament	Effective panicle per unit area /10^4·hm^{-2}	100 grain weight /g	Number of grains per spike / grain	Spike length /cm	Balding tip /cm	ear diameter /cm	production /kg·hm^{-2}
W1H0	6.11c	33.14c	466.35d	21.15c	0.49b	5.42c	9017.12e
W1H1	6.29b	34.67b	474.44d	21.27c	0.51b	5.42c	9168.13d
W1H2	6.35ab	33.23c	496.11c	22.51b	0.00c	5.52b	9621.37c
W2H0	6.39a	35.28a	496.94c	23.41a	0.97a	5.45bc	9947.85b
W2H1	6.44a	34.45b	514.76b	22.66b	0.56b	5.51b	10374.38a
W2H2	6.47a	34.71b	532.28a	23.17a	0.53b	5.71a	10464.34a

Note: Different Minuscule in the table indicate significant differences between treatments (P<0.05)

2.4 Effect of Fulvic Acid Application on Water and Nitrogen Utilization of Maize under Different Irrigation Quotas

The effect of fulvic acid application on water and nitrogen utilization in maize under different irrigation quotas is shown in Figure 4. The experimental results showed that the irrigation water use efficiency of W1 treatment was significantly higher than that of W2 treatment ($P<0.05$), and there was no significant difference in irrigation water use efficiency under W1 treatment ($P>0.05$). Under W2 treatment, the application of fulvic acid significantly improved the irrigation water use efficiency ($P<0.05$). The W1H2 treatment has the highest irrigation water use efficiency, at 4.07kg/m³, which is 0.60%~11.56% higher than other treatments. Under the same irrigation quota, the nitrogen fertilizer partial productivity increases with the increase of the amount of fulvic acid applied. The difference in nitrogen fertilizer partial productivity under W1 treatment is not significant ($P>0.05$), while under W2 treatment, the addition of fulvic acid treatment is significantly higher than that under H0 treatment. At the same application rate of fulvic acid, the nitrogen fertilizer partial productivity of W2 treatment was higher than that of W1 treatment, and the nitrogen fertilizer partial productivity of W2 treatment significantly increased by 8.76%~13.16% compared to W1 treatment ($P<0.05$).

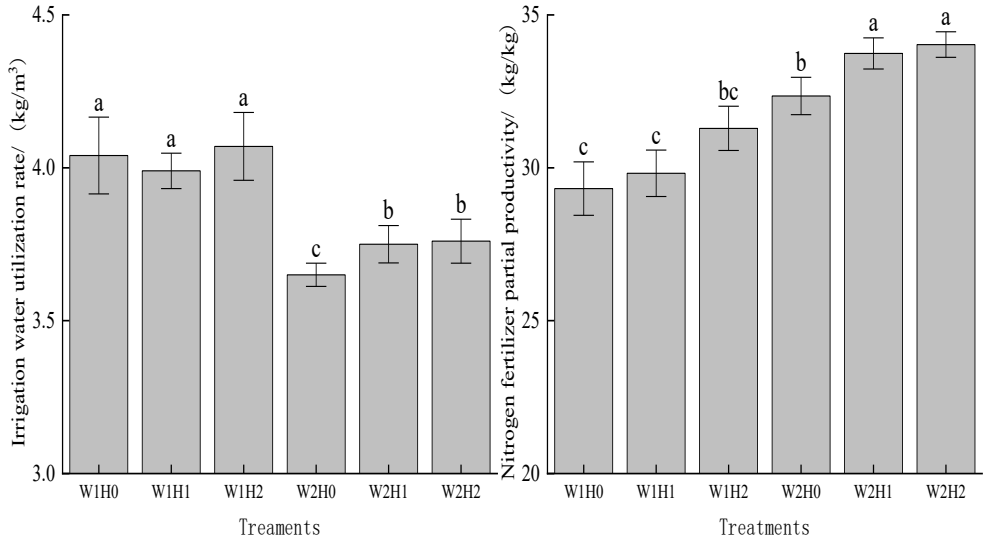

Fig.4 Effects of fulvic acid application on water and nitrogen utilization of maize under different irrigation quotas

2.5 Yield correlation analysis

The correlation between corn yield and yield related traits, as well as the dry matter quality of mature corn, is shown in Table 3. There was a highly significant positive correlation ($P<0.01$) between maize yield and effective ears per unit area, number of grains per ear, ear length, ear diameter, and dry matter mass, while there was a significant positive correlation ($P<0.05$) between maize yield and 100 grain weight.

There was no significant correlation ($P>0.05$) between maize yield and bald tip; There is a highly significant positive correlation between effective panicles per unit area and 100 grain weight, number of grains per panicle, panicle length, panicle diameter, and dry matter mass ($P<0.01$); There was a highly significant positive correlation between 100 grain weight and bald tip ($P<0.01$), as well as a significant positive correlation with spike length and dry matter quality ($P<0.05$);

There is a highly significant positive correlation between the number of grains per spike and spike length, spike diameter, and dry matter quality ($P<0.01$); There was a highly significant positive correlation between ear length and dry matter quality ($P<0.01$), and a significant positive correlation with ear diameter ($P<0.05$); There is a highly significant positive correlation between ear diameter and dry matter quality ($P<0.01$).

Tab.3 Maize yield correlation analysis

	Production	Effective panicle per unit area	100 grain weight	Number of grains per spike	Spike length	Balding tip	Ear thickness	Dry mass
Production	1							
Effective panicle per unit area	0.906**	1						
100 grain weight	0.516*	0.598**	1					
Number of grains per spike	0.960**	0.914**	0.433	1				
Spike length	0.861**	0.856**	0.536*	0.808**	1			
Balding tip	0.287	0.168	0.784**	0.091	0.327	1		
Ear thickness	0.652**	0.607**	0.192	0.803**	0.484*	-0.169	1	
Dry mass	0.936**	0.908**	0.485*	0.968**	0.700**	0.115	0.764**	1

3 Discussion

The plant height, stem diameter, and leaf area of corn are indicators that measure the growth status of corn, and are also important factors determining the formation of grain yield. Under different irrigation quotas and fulvic acid application treatments, there are differences in field soil moisture and crop physiological status, which in turn affect the growth and development indicators of corn[14]. The results of Chen Tingting's research on the maize irrigation system in the Ningxia Yellow River Diversion Irrigation Area show that within a certain range, the irrigation quota is directly proportional to the maize plant height, and the leaf area first increases and then decreases with the increase of irrigation quota[15]. Liu Shichang et al. have shown that biochemical potassium fulvic acid can lead to early tasseling of corn, promote plant height in the later stages of maize growth, and significantly improve stem diameter throughout the entire growth period[16]. This study shows that high irrigation quotas and the application of fulvic acid have a certain promoting effect on maize plant height, stem diameter, and leaf area index. This is because the study area has a high evaporation to drop ratio and is located in a sandy soil distribution area. The field water holding capacity is poor, and high irrigation quotas can better meet crop water needs. At the same time, the application of fulvic acid can promote root growth, enhance root water absorption capacity, and improve crop stress resistance, However, the significant characteristics of maize growth characteristics in different growth periods under different treatments are different from the previous research results, which may be related to different climatic conditions, soil type, application amount of fulvic acid, irrigation methods and other factors in the study area.

The Cumulant of dry matter above ground of maize is an important indicator reflecting crop production capacity[17]. The proper coupling of water and fulvic acid can significantly change the CUSUM of dry matter and the distribution proportion in different organs, promote the growth of crop roots, and improve the utilization ratio of water and fertilizer of crops[18]. The results of this study indicate that high irrigation quotas and the application of fulvic acid can promote the accumulation of dry matter in the middle and late stages of maize growth. This is because the application of fulvic acid under high irrigation quotas can increase the leaf area index of maize relatively greatly, increase the ability of maize population to capture light energy, delay the senescence of maize leaves in the later stage, and ensure high photosynthetic capacity, thus increasing the accumulation of dry matter in the middle and late stages of maize. Meanwhile, there was no significant difference in dry matter accumulation between the H1 and H2 fulvic acid application treatments in this study ($P>0.05$), indicating that under the current two irrigation quotas, the promotion effect of lower fulvic acid application rates on dry matter accumulation in maize has reached a good level. Previous studies have shown that corn varieties, irrigation quotas, fertilizer levels, meteorological factors, and the addition of modifiers can all affect the process of dry matter accumulation in crops, while logistic growth equations can change the relevant fitting parameters[19].

In this study, from the perspective of the change process of dry matter accumulation rate in corn, the application of fulvic acid under different irrigation quotas has a relatively small impact on the trend of dry matter accumulation rate. The change of dry matter accumulation rate in corn with the number of days after emergence is still a single peak curve, and it first increases and then decreases with the number of days after emergence. The fitting effect of the Logistic growth model of maize dry matter under different irrigation quotas of fulvic acid application was better, and the dry matter accumulation parameters were different, leading to differences in the corresponding peak, peak, peak and end periods, Cumulant and accumulation rate. Zhu Qi Chao et al. showed that the cumulant of plant dry matter was in direct proportion to the time when the maximum growth rate occurred, and inversely proportional to the duration of the rapid growth period[20]. This is different from the research results in this paper. In this study, the maximum growth rate of dry matter cumulant among different treatments has little difference, which occurs in 89 and 90 days after emergence. Under high irrigation quota, the rapid growth period of dry matter accumulation of maize increases with the increase of fulvic acid application. The higher dry matter accumulation treatment does not reflect the short duration of the rapid growth period, which indicates that the application of fulvic acid has little impact on the occurrence time of the maximum growth rate of dry matter, It may prolong the duration of the rapid growth period of corn, which is more conducive to the accumulation of dry matter in the middle growth stage of corn. Compared with W1 treatment, the rapid increase period of dry matter accumulation rate under W2 treatment increased by about 2 days, with the fastest growth rate increasing by an average of 7.58%. This indicates that high irrigation quota has the characteristics of long duration and high growth rate during the rapid increase period, which is conducive to the accumulation of dry matter in corn.

In addition, the simulation of dry matter accumulation in corn in this article takes the days after maize emergence as the independent variable, and there are differences in climate conditions under different hydrological year types. Only relying on the days after maize emergence for simulation may result in bias, as the heat accumulation required for different growth stages of corn is relatively fixed. Research on crop dry matter accumulation simulation based on effective accumulated temperature is gradually increasing. Four different types of effective accumulated temperature of farmland air temperature and crop canopy temperature were used as independent variables to carry out logistic simulation on the cumulant of corn dry matter, and a logistic normalization model of corn dry matter was established, which achieved good simulation accuracy[21]. However, there is no unified method to carry out the logistic simulation analysis of corn dry matter at present, which is also the direction of the next step to continue and improve the work.

4 Conclusion

(1) During the mature period, the application of fulvic acid under W2 treatment can significantly improve the plant height, stem diameter, and leaf area index of maize ($P<0.05$), while W1 has a significant impact on the improvement of leaf area index ($P<0.05$). The average stem diameter and leaf area index of corn increase with the increase of fulvic acid application rate.

(2) The application of fulvic acid can promote the accumulation of dry matter in maize, but there is no significant difference in dry matter accumulation between H1 and H2 treatments ($P>0.05$). Under the same application amount of fulvic acid, the dry matter accumulation of maize under W2 treatment was higher than that under W1 treatment at all growth stages. The average increase in dry matter of maize under H0, H1, and H2 treatments was 9.17%, 11.89%, and 11.01%, respectively.

(3) The accumulation rate of aboveground dry matter in maize shows a trend of first increasing and then decreasing as the days after maize emergence advance. Under the same irrigation quota, the average accumulation rate of dry matter in maize under H1 and H2 treatments was higher than that under H0 treatment. The average accumulation rate of maize aboveground parts under W2 treatment was higher than that under W1 treatment with the same amount of fulvic acid applied. Under W2 treatment, the peak period of dry matter accumulation advanced with the increase of fulvic acid application amount.

(4) Under different irrigation quotas, the yield of corn increases with the increase of fulvic acid application rate, with the highest yield of 10464.34kg/hm² under W2H2 treatment, There was no significant difference in yield between W2H1 and W2H2 treatments ($P>0.05$). The appropriate amount of fulvic acid under high irrigation quotas can increase storage capacity by forming sufficient large ears, thereby increasing maize yield. The irrigation water use efficiency

of W1 treatment was significantly higher than that of W2 treatment ($P<0.05$), and there was no significant difference in irrigation water use efficiency under W1 treatment ($P>0.05$). Under W2 treatment, the application of fulvic acid significantly improved irrigation water use efficiency ($P<0.05$).

Funding:

This research was funded by the research grants from Special Fund Project for Transformation of Scientific and Technological Achievements in Inner Mongolia (Grant No. 2021CG0003).

Reference:

1. You Y, et al., Dynamic changes in biomass accumulation and forage quality of silage corn after tasseling stage. Pratacultural Science. 2022. **39**(09): p. 1849-1860.
2. Cao, X., et al., Unravelling the effects of crop blue, green and grey virtual water flows on regional agricultural water footprint and scarcity. Agricultural Water Management, 2023. **278**.
3. Zhang J, Effects of enclosure on degraded grassland community and soil chatacteristics in Etoukeqian Banner. 2021, Inner Mongolia Agricultural University.
4. Zhang, F., et al., Towards sustainable water management in an arid agricultural region: A multi-level multi-objective stochastic approach. 2020. **182**.
5. Cao, Z., et al., Hydro-agro-economic optimization for irrigated farming in an arid region: The Hetao Irrigation District, Inner Mongolia. Agricultural Water Management, 2023. **277**.
6. Yu, Y., et al., Mechanisms underlying nitrous oxide emissions and nitrogen leaching from potato fields under drip irrigation and furrow irrigation. 2022. **260**.
7. Cao X, et al., The effect of drip fertigation with Yellow River water on water consumption and yield of summer maize. Journal of Irrigation and Drainage. 2022. **41**(03): p. 33-39.
8. Yin, D., et al., Matching supply and demand for ecosystem services in the Yellow River Basin, China: A perspective of the water-energy-food nexus. Journal of Cleaner Production, 2023. **384**.
9. Wei B, et al., Effects of coupling of irrigation and nitrogen application as well as planting density on photosynthesis and dry matter accumulation characteristics of maize in oasis irrigated areas.Scientia Agricultura Sinica. 2019. **52**(03): p. 428-444.
10. Zhou Y., et al., Research on the growth, yield and water use efficiency of sticky maize under water and fertilizer regulation. Agricultural Research in the Arid Areas. 2014. **32**(03): p. 114-118+126.
11. Brazien, Z., V. Paltanaviius, and D.J.E.R. Aviienyt, The influence of fulvic acid on spring cereals and sugar beets seed germination and plant productivity. 2021(3): p. 110824.
12. El-Mekser, H.K.A., E.O.M. Mohamed, and M.A.M.J.w.a.s.j. Ali, Influence of humic acid and some micronutrients on yellow corn yield and quality. 2014.
13. Qin Z, et al., Effect of water and nitrogen coupling on rice yield and nitrogen absorption and utilization in black soil. Transactions of the Chinese Society of Agricultural Machinery. 2021. **52**(12): p. 324-335+357.
14. Xu C, et al., Study on yield formation and irrigation yield potential of maize under irrigation quota condition.Water Saving Irrigation. 2020(05): p. 22-26+31.
15. Chen T, Effects of irrigation quotas on growth, yield and water use of maize in Yellow River irrigation ares of Ningxia. 2022, Ningxia University.
16. Liu S, et al., Effects of biochemical fulvic acid potassium on maize growth. Heilongjiang Agricultural Sciences. 2022(09): p. 51-55.
17. Ishaque, W., et al., Short-term effects of tillage and residue management practices on dry matter yield and fate of 15 N-urea in a continuous maize cropping system under subtropical conditions. 2018. **182**: p. 78-85.
18. Liu, X., et al., Integrated application of inorganic fertilizer with fulvic acid for improving soil nutrient supply and nutrient use efficiency of winter wheat in a salt-affected soil. 2022. **170**: p. 104255.
19. Darroch, B.A., et al., Grain Filling in Three Spring Wheat Genotypes: Statistical Analysis. 1990. **30**(3).
20. Zhu Q, et al., Effects of nitrogen rates on dry matter accumulation and nutrient absorption of rice under film mulch with drip irrigation. Xinjiang Agricultural Sciences. 2013. **50**(03): p. 433-439.
21. Cai J, et al., Simulation of maize dry matter accumulation in normalized logistic model with different effective accumulated temperatures in field. Transactions of the Chinese Society of Agricultural Machinery. 2020. **51**(05): p. 263-271.

MACHINE LEARNING AND REMOTE SENSING-BASED WATER MANAGEMENT PLATFORM FOR SUSTAINABLE AGRICULTURE IN ASIAN DELTAS (MARSWM-ASIA)

Takanori NAGANO[1], Natsuki YOSHIKAWA[2], Masaomi KIMURA[3], Yoshitaka MOTONAGA[4], Lan Thanh HA[4] Budi Indra SETIAWAN[5]

Abstract

Rice is a staple food of many Asian countries. Productive rice cultivated areas are often situated in deltas which are subject to increased occurrence of severe flood damage and saltwater intrusion due to climate change today. The project “Development of Machine Learning and Remote Sensing-based Water Management Platform for Sustainable Agriculture in Asian Deltas” (MARWAM-Asia, 2021-2024) is a scientific project among Japan, Vietnam and Indonesia to develop and share a GIS-based "Integrated Water Management Platform" to assist operators of water management facilities for adaptive management of agricultural water in Asian deltas.

For the development of the platform, the following five elemental technologies are being developed and integrated by the collaboration of partner countries; (1) remote sensing techniques that prioritize risk mitigation zones and evaluate crop growth and damages; (2) sensor networks based on ICT to monitor real-time hydrological state; (3) physical models to generate a number of input data fed to machine learning model as training data; (4) machine learning (ANN) model to quickly produce quasi-real-time forecasting of water levels and saltwater states; (5) GIS-based visualizing application to display current states and forecasting results on PCs and hand-held devices.

1. Introduction

River deltas in the Asian monsoon countries are major agricultural areas. While their flat topography, fine-grain soil and abundant available water make them suitable for rice production, deltas are inherently vulnerable to water related risks such as flood drainage and saltwater intrusion. To mitigate these risks agricultural organizations installed control facilities and set management rules. However, facilities and management rules are becoming increasingly complicated over time in most cases, and thereby they are still manually operated based on experiences.

In recent years, disaster risk management is becoming more important in deltas due to rapid urbanization and increase of extreme weather events. With sea-level rise in the future, unprecedented extreme events are expected to increase. Therefore, integration of real-time observation and more sophisticated adjustments of facility operations will be required.

The purpose of this project is to develop and share integrated water management system for deltas among Japan, Vietnam and Indonesia which are under different environment and development stage. The project goal is to introduce smart water facility operations based on real-time observations and predictions to secure agricultural production through mitigation of flood and saltwater damages and damages attributed to other water related hazards.

[1] Graduate School of Agricultural Science, Kobe University
[2] Faculty of Agriculture, Niigata University
[3] Faculty of Agriculture, Kindai University
[4] Institute of Water Resources Planning (IWRP), Vietnam
[5] Bogor Agricultural University, Indonesia

2. Materials and methods

2.1 Study areas

Kemda District (9,623 ha) and Nishikanbara District (13,266 ha) in Niigata prefecture, Japan, Xuan Thuy District (13,455 ha) in Nam Dinh province, Vietnam and Pusakanegara District in Suban regency, West Java, Indonesia were chosen for the model development and simulations.

2.2 Models and approaches

Smarter water management in this project means adaptive management (change of management rules based on observations) and decision support for water structure operations. Monitoring of the state of vast delta requires remote sensing by satellite sensors and on-the-ground sensor networks. Decision support system is a GIS based platform which integrates and visualizes observation data and model calculations on hand-held devices. The final image of the system is illustrated in Figure 1.

2.2.1 Flood damage reduction

A physical inland flood analysis model developed by Yoshikawa et al. (2013) was first calibrated to study areas using observed and field surveyed data. Its outputs are used for training Long Short Term Memory (LSTM) neural network model (Kimura et al., 2019), which estimates hydrological state of the delta much quicker than the physical model in response to short-time forecast of rainfall.

In creating the training data, we used the physical model to calculate the inundation locations and depths within the analysis area, and used a large amount of simulated torrential rainfall data as the input data. As for the method of generating the simulated rainfall waveform, the recurrence period is obtained from an arbitrary total rainfall amount based on the Cleveland-type probable rainfall intensity formula, and a model rainfall is created in which all n-hour rainfall amounts satisfy this recurrence period. A number of patterns of rainfall waveforms with different peak appearance times were created. Based on the created simulated rainfall waveform, the calculation results of the drainage analysis simulation model were prepared as learning data. A simulated rainfall of 200mm to 500mm for 3 days was given as rainfall of a scale that causes flooding.

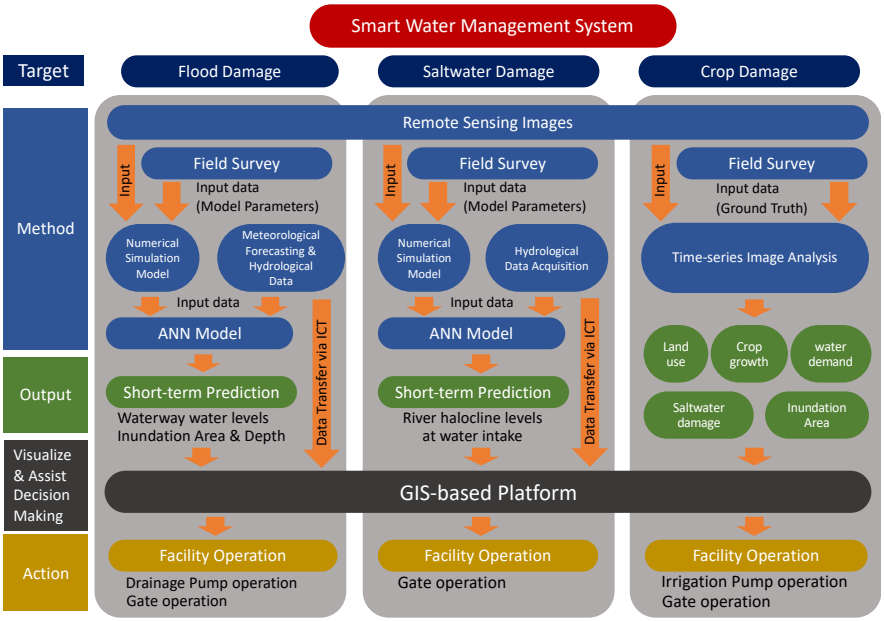

Figure 1 The scheme of smart water management system to be developed in MARSWM-Asia

2.2.2 Saltwater damage reduction

One dimensional two-layer unsteady flow model which predicts saltwater intrusion, developed by Liu et al. (2017) was calibrated to the study area (Shinkawa River in Niigata, Japan). The model simulates longitudinal saltwater halocline depth in response to various scenarios of tidal level and river runoff. The outputs were used to train neural network (NN), recurrent neural network (RNN) and LSTM model, respectively, because neural network models estimate saltwater halocline location in a quick response to observed tidal levels and runoffs.

2.2.3 Land use and crop growth monitoring

Experts from participating countries worked together to develop time-series analysis of satellite images (Sentinel-1: synthetic aperture radar image, Sentinel-2: optical image) to monitor, i) land use, ii) crop growth at farm-parcel scale. The analysis is planned to extend to iii) flooding detection and iv) salt damage detection. For providing agricultural information for a long term, land use should be classified based on the field boundaries. In this project, Field boundary detection was carried out with use of recent Setninel-2 images. Rice and non-rice cultivation was carried out with 3 different methods. The first was a monthly composite approach (Fatchurrachman et al., 2022) combined with k-means classification.

The second is a simple threshold approach to detect lowering of backscatter coefficient at transplantation stage (Chen et al, 2022). The third was a difference time warp approach combined with k-means method (Chen et al, 2022).

2.2.4 Sensing system and communication network infrastructure

For realizing precise water management in deltas, large number of sensors need to be installed efficiently in wide areas and reliable communication network is necessary for data retrieval and redistribution. The sensor node was designed to use Raspberry Pi. I2C for communication, and OpenVPN was used for communication with the server using a 4G line. The use of OpenVPN ensures confidentiality of data and handshakes that combine push, pull, and interactive types can be performed.

2.2.5 Data management platform

Data to be handled by the integrated water management platform comprises, i) data from existing observation systems, ii) data from newly installed sensors, iii) outputs of ANN model and iv) near-real-time land surface analysis by remote sensing. The web application framework by Django has a database function, and using that database function, the table structure would be recreated, considering various data formats, exchange methods, and relationships between data.

3. Results and discussions

3.1 Flood damage reduction

A comparison on inundation depth simulated by physical model and LSTM is shown in Figure 2. Evaluation of the simulation with the optimized model showed that the Nash-Sutcliffe coefficient of the hydrograph of flood water was 0.8 or more in all cases, and sufficient accuracy could be secured as a flood prediction model. In addition, the calculation time per case was about 2 seconds, which was 1/600 of the 20 minutes for the inland flood analysis model. This indicates that it will be a powerful tool for real-time prediction, which is the goal of this research.

3.2 Saltwater damage reduction

As shown in Figure 3, LSTM had the best fit and reproduced the results of numerical calculations. In addition, it was shown that the calculation time for saltwater intrusion can be reduced to about 6% by using machine learning.

3.3 Land use and crop growth monitoring

Figure 4 shows the clarity of rice-non rice detection using the parcel boundary data. Three different approaches performed relative well in Niigata (Japan) and Xuan Thuy (Vietnam) with total accuracy above 80% because size of parcels were relatively large (>0.15 ha). In Pusakanegara (Indonesia) however, field boundary detection was difficult because of small parcel size. Monthly composite approach and Difference Time Warp approach were more robust in detecting multiple rice cultivation in Xuan Thuy.

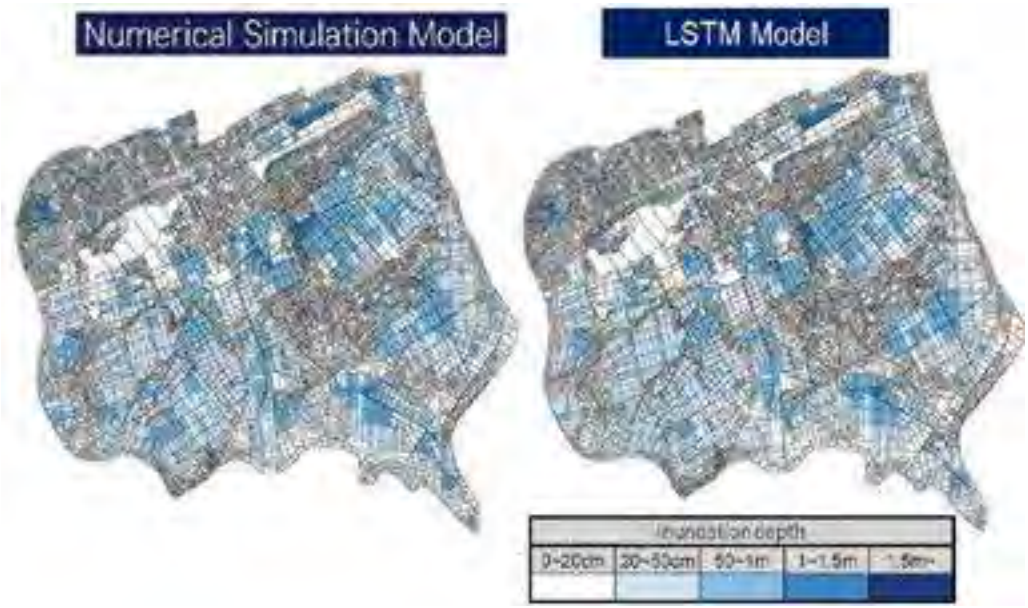

Figure 2 Comparison of simulated inundation depth at Kameda District after simulated rainfall of 500 mm/3days.

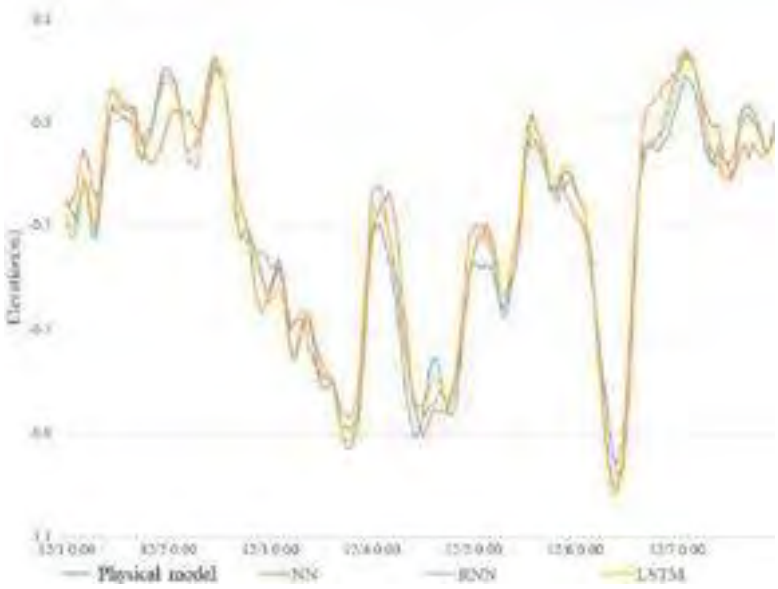

Figure 3 Change of height of Salt-freshwater interface at a pumping station in Shinkawa River simulated by the physical model, neural network (NN), recurrent neural network (RNN) and long and short term memory (LSTM), (Sato and Yoshkawa, 2022).

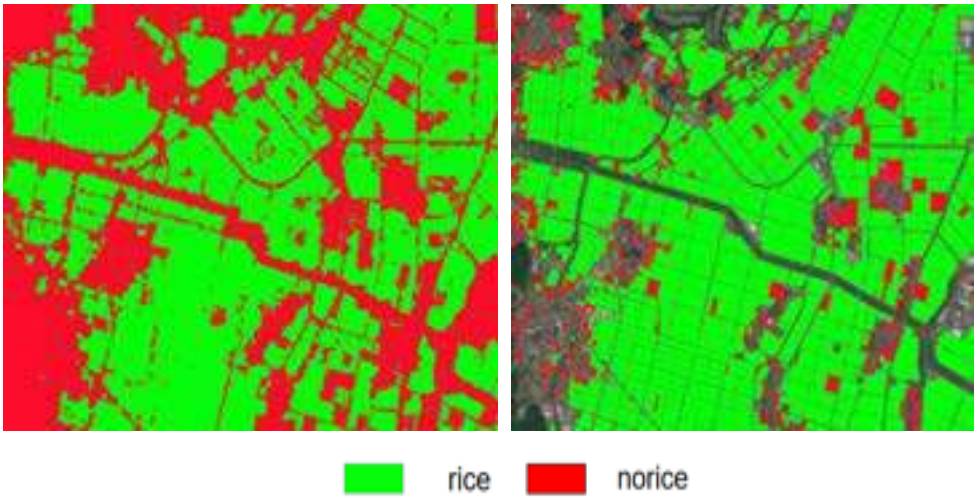

Figure 4 A comparison of rice and non-rice classification in Kameda District in Niigata, Japan with use of Sentinel-1 images by pixel based approach(left) and object (parcel) based approach (Chen et al., 2022)

3.4 Sensing network, communication and data management system

The development of sensing network, communication and data management system remains to be at laboratory level and only partially implemented in the study field. Figure 5 shows the image of the integrated water management platform which runs on a hand-held device.

Figure 5 The image of data integration visualized on the integrated water management platform.

4. Ending remark

The ultimate goal of this project is to implement this water management platform and share among stakeholders in Asian countries. The platform will reduce inundation and saltwater damages on crops. The degree of damage mitigation can be quantitatively presented through high-speed computation by the combination of the physical model and ANN model. As water disasters are projected to increase in the future, the introduction of this platform will accelerate the change in water management in Asian deltas from experience-based to objective information-based which will secure sustainable agricultural production for farmers.

References

Chen, S., Nagano, T., Yoshikawa, N. (2022): Development of field-specific discrimination method for various paddy rice, PAWEES 2022 Conference in Fukuoka.

Fatchurrachman, Rudiyanto, Soh, N.C.; Shah, R.M., Giap, S.G.E., Setiawan, B.I., Minasny, B. (2022): High-Resolution Mapping of Paddy Rice Extent and Growth Stages across Peninsular Malaysia Using a Fusion of Sentinel-1 and 2 Time Series Data in Google Earth Engine. Remote Sens. 2022, 14, 1875. https://doi.org/10.3390/rs14081875

Kimura, M., Okumura,N., Azechi I., Takano Y., Yoshikawa N. (2019): Examination of the effect of preliminary operation of drainage pumping stations on the reduction of inundation damage inside low-lying agricultural area. Journal of Japan Society of Civil Engineers, Ser. B1 (Hydraulic Engineering) 75(2) I_1309 - I_1314

Liu H., Yoshikawa N., Tamaki S (2017): Effective method of removing saltwater wedge for preserving agricultural water quality, Paddy and water environment. 15(2), 331-341, DOI: 10.1007/s10333-016-0552-0

Sato, H. and Yoshikawa, N. (2022): Prediction of Saltwater Wedges by Machine Learning" , PAWEES 2022 Conference in Fukuoka

Yoshikawa, N., Miyadu, S., Abe, S., Misawa, S. (2013): Development of method for creating topographically adjusted cells and preparing geometric attribute data for inundation analysis model, 284, 185-191. (in Japanese)

A DATA-DRIVEN APPROACH TO ESTIMATE HYDROGEOLOGICAL PARAMETERS AND GROUNDWATER WITHDRAWAL: CASE STUDY IN CHOUSHUI AQUIFER

Hua-Ting Tsen[1], Hwa-Lung Yu[a]

Abstract

The Choushui alluvial fan in the midwestern of Taiwan is one of the most excellent aquifers in the country. Its abundant and convenient groundwater resources are one of the indispensable reasons for the prosperity of agriculture and industry in this area. However, the ever-increasing water demand has also led to the long-term over-pumping of water, causing to the problem of land subsidence which also has involved with personal safety due to the highspeed railway crossing through. Although the plenty of uncensored pumping well increasing the obstacle of groundwater management, the Choushui alluvial has relative complete groundwater observation network with hourly recording data. Therefore, this study proposes a framework for estimating groundwater withdrawal and spatial distribution based on water level data. It consists of three parts: (1) pumping signal extraction, (2) estimation of hydrogeological parameters and (3) spatial and temporal estimation of water pumping.

The groundwater level is composed of signals from many stimuli which have different frequencies and spatial characteristics., e.g. rainfall, lateral inflow and pumping, etc. In order to extract the pumping signal from the mixed water level, Empirical Mode Decomposition method (EMD) and Empirical Orthogonal Function (EOF) was respectively used in the decomposition of water level signal and the exploration of spatial and temporal patterns of the decomposed sub-signals. Furthermore, to estimate hydrogeological parameters, i.e., storage coefficients, this study proposed the use of impulse response function to represent the impact of pumping on the water levels. Two observation wells in the Choushui alluvial fan are selected to verify the proposed method. The storage coefficients of the two selected observation wells from the pumping test are 3.95×10^{-4} and 1.465×10^{-3}, respectively. The estimated results of this project are 4.52×10^{-4} and 3.54×10^{-3}, respectively. According to definition of storage coefficient, the groundwater withdrawal can be derived by the product of pumping trend and the storage coefficient. In addition, the spatial estimation was used to estimate groundwater withdrawal to unobserved location. The algorithm was applied to second aquifer of the Choushui alluvial fan in 2018, the estimated groundwater withdrawal is 218.24 million tons.

Keywords: Pumping signal extraction, Hydrogeological parameters estimation, Groundwater withdrawal estimation, Time series decomposition

1. Introduction

Groundwater depletion is a pressing concern, especially in regions where its heavy reliance leads to over-extraction (Pang et al., 2023). Taiwan exem-
plifies this challenge with over 120,000 illegal wells and insufficient monitor-

ing systems, hindering accurate assessment and regulation of groundwater use (Bouwer, 2000, 2002; Gourbesville, 2008).

Traditionally, groundwater demand has been investigated through costly and limited survey-based approaches or through physically-based numerical models like MODFLOW (Harbaugh, 2005). Both these methods face constraints, including high uncertainties in estimation (Wagener et al., 2001) and unrepresentative findings in specific study areas. Geostatistical methods, though useful in understanding the environmental variables' heterogeneous nature, have been complemented by the application of data-driven

[1] Department of Bioenvironmental Systems Engineering, National Taiwan University, Taipei, Taiwan

approaches to groundwater level (GWL) signals (Chiles and Delfiner, 2012). Techniques such as wavelet method, empirical mode decomposition (EMD), and its variant Ensemble EMD (EEMD), have been applied to decompose time series and understand nonstationary processes (Daubechies, 1988; Huang et al., 1998). Furthermore, unsupervised feature extraction like independent component analysis (ICA) has identified key features in groundwater variations (Longuevergne et al., 2007).This study introduces a data-driven approach for spatiotemporal pumping pattern derivation and estimation in Taiwan's Choushui River aquifer from 2008 to 2019. It innovatively combines the Hilbert-Huang transform (HHT) method with empirical orthogonal function (EOF) analysis to iden tify and retrieve signals related to pumping activities, offering a promising solution to the complexities of groundwater monitoring and management.

2. Materials and method

2.1. Pumping Signal Extraction

The methodology entails applying the Hilbert-Huang Transform (HHT) to break down the groundwater time series into intrinsic mode functions (IMFs) and a residual component. The EEMD method helps to resolve the mode-mixing issue, allowing for the identification of IMFs related to specific signals. Given a GWL time series at space location **s**, denoted as $z(\mathbf{s},t)$, EMD splits it into a sum of IMFs $c_j(t)$ and a residual $r(t)$:

$$z(\mathbf{s},t) = \sum_{j=1}^{k} c_j(\mathbf{s},t) + r(\mathbf{s},t) \quad (1)$$

Here, the residual $r(\mathbf{s},t)$ signifies the trend of the time series, while $c_j(\mathbf{s},t)$ is a defined Hilbert spectrum or IMF. Its complex form or ana lytic signal, $c^H_j(\mathbf{s},t)$, takes the form $c^H_j(\mathbf{s},t) = c_j(\mathbf{s},t) + iH\{c_j(\mathbf{s},t)\} = a_j(\mathbf{s},t)e^{iR\ \omega j(\mathbf{s},t)dt}$, where $\omega_j(\mathbf{s},t)$ and $a_j(\mathbf{s},t)$ are the instantaneous frequency and amplitude of the analytic signal, respectively. The Mean Shift Clustering (MSC) method is used for frequency clas- sification, followed by the EOF method to identify primary spatiotemporal patterns of GWL changes linked to the same forcings. Exploration continues into the spatial distribution characteristics of EOF to distinguish groundwater responses to various external forcings. The EOF method decomposes a spatiotemporal random field into a set of orthogonal spatial functions or empirical orthogonal functions (EOFs), along with their corresponding temporal projections or expansion coefficients (ECs), as illustrated in previous studies (Hannachi et al., 2007; Yu and Chu, 2010; Yu and Lin, 2015). The EOF decomposition for the IMF, as classified by the MSC method, $c_{j,\text{class}}(\mathbf{s},t)$, can be represented as:

$$Nn\ c_{j,\text{class}}(\mathbf{s},t) = \sum_{n=1}^{X} u_n(\mathbf{s})\kappa_n(t),\ \text{class} = 1,\ldots,N_{\text{class}} \quad (2)$$

In this expression, N_n is the number of decomposed spatiotemporal modes, N_{class} is the total number of classes identified from the results ofthe MSC method, and $u_n(\mathbf{s})$ and $\kappa_n(t)$ are the EOFs and corresponding ECs, respectively. It should be noted that the leading EOFs can account for a significant proportion of the observed variances in the original spatiotemporal dataset (Hannachi et al., 2007). Typically, singular value decomposition (SVD) is employed for EOF analysis. The study further involves the reconstruction of recharge-associated GWL fluctuations and the estimation of spatiotemporal pumping flow rate using the obtained IMFs. Techniques such as ordinary kriging are applied to determine the distribution of the pumping rate.

2.2. Hydrogeological Parameter Estimation

In the context of extracting groundwater from a confined aquifer, the

Impulse Response Function (IRF) is symbolized by $\theta_w(t)$, which characterizes the alteration in drawdown as a function of instantaneous withdrawal. The expression for $\theta_w(t)$ in the context of pump-induced confined flow is given by

$$\theta_w(t) = -\frac{1}{4\pi Tt}\exp\left(-\frac{r^2}{4Dt}\right) \quad (3)$$

where D is the hydraulic diffusivity, defined as T/S, and r is the radial distance between the pumping well and the observation well. The cumulative drawdown during continuous pumping can be computed using the Theis well function, equivalent to its unit response function as follows:

$$\Theta_w(t) = -\frac{1}{4\pi T} W(u) \tag{4a}$$

$$u = \frac{r^2}{4Dt} \tag{4b}$$

where $W(u)$ is the well function, defined as $W(u) = \int_u^\infty e^{-y}/y\,dy$. The Theis drawdown solution is given by $s(t) = Q\Theta_w(t)$, and for a variable pumping rate $q(t)$, the drawdown value can be found $s(t) = \int_0^t q(t)\theta_w(t-\tau)d\tau$.

Equations (3) and (4) convey that the drawdown IRF generally needs information on the relative spatial positions between pumping and observation wells. Sometimes, especially in regions without adequate groundwater management practices, the pumping locations and rates may be unknown. In groundwater numerical modelling, the study area is typically divided into

grids with uniform hydrogeological parameters and characteristics like pumping, injection, and recharge. This study emphasizes pumping as the principal factor affecting the groundwater flow system. Assuming spatial uniformity in pumping activities around an observation well can be useful, even if the exact locations are not known. Based on this assumption, the IRF in relation 86 to spatially equivalent instantaneous pumping in a confined aquifer can be 87 expressed as:

$$\sum_{i=1}^{n} \theta_i(t) \approx \theta_{w,e}(t) = \frac{\int_0^{2\pi}\int_0^R \theta(t) r\,dr\,d\theta}{\int_0^{2\pi}\int_0^R r\,dr\,d\theta} \tag{5}$$

where R denotes the equivalent radius, and $\theta_{w,e}$ is referred to as an equivalent IRF (EIRF). For $\theta(t) = \theta_{w,e}(t)$, the corresponding EIRF in a confined aquifer can be derived as:

$$\theta_{w,e}(t) = \frac{De^{-R^2/4Dt} - D}{\pi R^2 T} \tag{6}$$

Additionally, the drawdown for spatially equivalent pumping rate $Q_e(t_m)$ at discrete time intervals can be described as:

$$se(tk) = \mathrm{X}\ Qe(tm)\Delta\Theta w,e(tk-m+1) \tag{7}$$
$$m=1$$

where

$$\Theta_{w,e}(t) = \frac{D}{\pi R^2}\left(\frac{t}{T}e^{-R^2/4Dt} - \frac{t}{T} - \frac{R^2}{4T}W\left(\frac{R^2}{4Dt}\right)\right), \tag{8}$$

and $\Delta\Theta_{w,e}(t_m) = \Theta_{w,e}(t_m) - \Theta_{w,e}(t_{m-1})$, and $\Theta_{w,e}(t)$ represents the pumpingassociated equivalent unit response function (EURF). Finally, the calculation of pump-induced drawdown, based on Eq. (??), requires the EURF $\Theta_{w,e}(t)$ and the time series of pumping rate $Q(t_m)$. To determine pumping activities from drawdown observations, if the drawdown $\Delta s(t_m) = s(t_m) - s(t_{m-1})$, then the pumping process of $Q_e(t_m)$ can be defined as $Q\Delta s(t_m)/\Delta t$, where Q is a constant pumping rate

.

2.3. Spatiotemporal Estimation of Water Extraction

This study employed the HHT to decompose $\hat{z}(\mathbf{s},t)$ and extract the IMFs corresponding to common pumping activities in the study area, such as those with frequencies of one to seven days. These are referred to as pumping-associated signals, denoted by $\hat{c}^{P}(\mathbf{s},t)$. The spatiotemporal variation in GWL due to pumping activities can be estimated by summing these pumping-associated signals. The total signal can be represented as

$$\hat{z}^{P}(\mathbf{s},t) = \sum_{n}^{N^{P}} \hat{c}_{n}^{P}(\mathbf{s},t)$$

where N^{P} is the number of pumping-associated IMFs. Based on the identified pumping-associated GWL variation, the spatiotemporal pumping flow rate can be obtained by calculating the rate of groundwater 112 head drawdown over time:

$$Q(\mathbf{s},t) = S(\mathbf{s})A(\mathbf{s}) \frac{\hat{z}^{P}(\mathbf{s},t_l) - \hat{z}^{P}(\mathbf{s},t_u)}{t_l - t_u}, \quad t_u \le t \le t_l \qquad \textbf{(9)}$$

In this equation, $S(\mathbf{s})$ refers to the elastic storage coefficient, representing the volume of water released from storage for each unit decline in hydraulic head in the aquifer. The symbol $A(\mathbf{s})$ denotes the area size corresponding to the drawdown change, while t_u and t_l are the temporal instances at the local maxima and minima of the pumping-associated GWL variation, respectively. The corresponding drawdown between these two instances is $\hat{z}^{P}(\mathbf{s},t_l) - \hat{z}^{P}(\mathbf{s},t_u)$. The flow rate $Q(\mathbf{s},t)$ was estimated solely at locations of groundwater wells. To deduce the pumping rate distribution across the entire study area, the ordinary kriging method was initially applied to estimate the pumping- induced GWL change rates, specifically $[\hat{z}^{P}(\mathbf{s},t_l)-\hat{z}^{P}(\mathbf{s},t_u)]/(t_l - t_u)$, in both

space and time. Subsequently, the spatial distribution of storage coefficients was taken into account to estimate the spatiotemporal distribution of pumping rates.

2.4. Study Area

The Choshui River flows through an alluvial fan demarcated by the Tai- wan Strait to the west, the Central Mountain Ridge to the east, the Wu River to the north, and the PeiKang River to the south (Figure 1). Com- posed mainly of unconsolidated sediments like gravel, sand, and clay, the alluvial fan originates from the rock formations of the Western Foothills and the Central Range, which include diverse rock types such as slate, shale, metamorphic quartzite, sandstone, and mudstone.

In the upper segment of the alluvial fan, gravel and coarse sand are predominant, whereas the lower portion consists mainly of soil and fine sand. The fan receives an average annual rainfall of about 2460 mm, with 78% falling between May and Octo- ber, aligning with the plum rain and typhoon seasons.

The Choshui River's annual runoff amounts to roughly 6.08 billion tons. Encompassing an area of approximately 1,800 km^2, the alluvial fan is divided into proximal, mid- le, and distal regions, each characterized by unique hydrological properties. Sediment thickness ranges from 750 to 3000 m, and mean grain size decreases

from east to west. While the proximal fan mainly recharges the aquifer, the middle and distal fan regions show a pattern of diminishing permeability eastward. The hydrogeological structure of the area includes four aquifers situated at varying depths, separated by three aquitards, comprised of low- permeability sediments, such as clay to fine sand. As surface water is limited, groundwater within the alluvial fan is essential for irrigation, aquaculture, domestic, and industrial uses.

Figure 1: Geographical map of the Choshui river alluvial fan.

3. Results and Discussion

Two observation wells located in the Choushui alluvial fan have been 152 selected to validate the proposed method, which pertains to the estimation of groundwater withdrawal. Groundwater withdrawal refers to the extraction of water from the ground, a process that is often regulated to prevent negative impacts on the environment. The proposed method in question involves the application of specific coefficients and algorithms to better gauge this extraction. The storage coefficients for the two selected observation wells were determined from the pumping test and found to be 3.95×10^{-4} and 1.465×10^{-3}, respectively. These coefficients are essential variables in the hydrogeological study as they represent the ability of an aquifer to release water. In comparison, the project's estimated results for these coefficients

are 4.52×10^{-4} and 3.54×10^{-3}, respectively, illustrating the predictive capability of the method.

According to the definition, the storage coefficient is a measure that allows the calculation of groundwater withdrawal. It can be derived from the product of the pumping trend and the storage coefficient itself. This relationship provides a vital link between observed data and the withdrawal prediction, adding robustness to the estimation process.

In addition to the analysis based on storage coefficients, spatial estimation was employed to extend the understanding of groundwater withdrawal to unobserved locations within the aquifer system. This spatial analysis allows for a more complete view of the system, enhancing the ability to make informed decisions on water management. The proposed method and algorithm were specifically 174 applied to the second aquifer of the Choushui alluvial fan in 2018. The 175 estimated groundwater withdrawal, as calculated, was 218.24 million tons.

176 This quantification not only serves as a validation of the methodology but 177 also provides valuable insights into the state of the aquifer, enabling better planning and management. In conclusion, the research introduces a comprehensive method that in- volves both analytical and spatial tools to estimate groundwater withdrawal in the Choushui alluvial fan. By employing storage coefficients derived from observation wells and spatial estimation techniques, this approach offers a nuanced understanding of groundwater dynamics. It could potentially be applied to other alluvial systems, contributing to the broader field of water 185 resource management.

4. Conclusions

The Choushui alluvial fan, situated in the midwestern region of Taiwan, stands as one of the most vital aquifers in the nation, supplying abundant groundwater resources. These resources are indispensable for the thriving agriculture and industry in the area. However, the region has not been immune to challenges. The incessant growth in water demand has led to long-term over-pumping, resulting in land subsidence. This issue has also raised concerns about personal safety, especially with the presence of a high-speed railway crossing the area. Although the plethora of uncensored pumping wells has added to the complexities of groundwater management, the Choushui 196 alluvial fan benefits from a relatively comprehensive groundwater observation 197 network with hourly recording data. In response to these challenges, this study has introduced a robust frame work for estimating groundwater withdrawal and spatial distribution based on water level data.

This framework is tripartite, encompassing (1) the ex201 traction of the pumping signal, (2) the estimation of hydrogeological parameters, such as storage coefficients, and (3) spatial and temporal estimation of 203 water pumping. Key to this approach was the utilization of the Empirical Mode Decom- position method (EMD) and Empirical Orthogonal Function (EOF), enabling the decomposition of the water level signal and the exploration of spatial and temporal patterns within the decomposed sub-signals. Additionally, the innovative use of the impulse response function helped in representing the impact of pumping on water levels, aiding in the precise estimation of hydro210 geological parameters.

The method was verified through the analysis of two observation wells in the Choushui alluvial fan, yielding accurate storage coefficients that were consistent with the results from the pumping test. Spatial estimation techniques were also employed to extrapolate groundwater withdrawal to unobserved locations. The application of this methodology to the second aquifer in 2018 216 revealed an estimated groundwater withdrawal of 218.24 million tons. groundwater dynamics of the Choushui alluvial fan but also provides a scientifically rigorous framework that could be instrumental in better water management.

The innovative techniques applied in this research hold significant promise for addressing the challenges of over-pumping and land subsidence, thereby contributing to the sustainable development and safety of the region. It is a remarkable step towards understanding and managing the complex in- terplay of factors that govern groundwater behavior in one of Taiwan's most crucial aquifers.

References

Bouwer, H., 2000. Integrated water management: emerging issues and chal228 lenges. Agricultural water management 45, 217–228.

Bouwer, H., 2002. Integrated water management for the 21st century: prob-

lems and solutions. Journal of Irrigation and Drainage Engineering 128, 231 193–202.

Chiles, J.P., Delfiner, P., 2012. Geostatistics: modeling spatial uncertainty.

volume 713. John Wiley & Sons.

Daubechies, I., 1988. Orthonormal bases of compactly supported wavelets. Communications on pure and applied mathematics 41, 909–996.

Gourbesville, P., 2008. Challenges for integrated water resources manage237 ment. Physics and Chemistry of the Earth, Parts A/B/C 33, 284–289.

Hannachi, A., Jolliffe, I.T., Stephenson, D.B., 2007. Empirical orthogonal

functions and related techniques in atmospheric science: A review. Inter240 national Journal of Climatology: A Journal of the Royal Meteorological 241 Society 27, 1119–1152. doi:https://doi.org/10.1002/joc.1499.

Harbaugh, A.W., 2005. MODFLOW-2005, the US Geological Survey mod243 ular ground-water model: the ground-water flow process. volume 6. US 244 Department of the Interior, US Geological Survey Reston, VA, USA.

Huang, N.E., Shen, Z., Long, S.R., Wu, M.C., Shih, H.H., Zheng, Q.,

Yen, N.C., Tung, C.C., Liu, H.H., 1998. The empirical mode decom-

position and the hilbert spectrum for nonlinear and non-stationary time 248 series analysis. Proceedings of the Royal Society of London. Series A: 249 mathematical, physical and engineering sciences 454, 903–995. doi:https: 250 //doi.org/10.1098/rspa.1998.0193.

Longuevergne, L., Florsch, N., Elsass, P., 2007. Extracting coherent regional
information from local measurements with karhunen-loève transform: Case
study of an alluvial aquifer (rhine valley, france and germany). Water 254 resources research 43. doi:https://doi.org/10.1029/2006WR005000.

Pang, M., Du, E., Zheng, C., 2023. A data-driven approach to exploring the 256 causal relationships between distributed pumping activities and aquifer 257 drawdown. Science of The Total Environment , 161998.

Wagener, T., Boyle, D.P., Lees, M.J., Wheater, H.S., Gupta, H.V.,
orooshian, S., 2001. A framework for development and application of 260 hydrological models. Hydrology and Earth System Sciences 5, 13–26. 261 doi:https://doi.org/10.5194/hess-5-13-2001.

Yu, H.L., Chu, H.J., 2010. Understanding space–time patterns of ground-
water system by empirical orthogonal functions: a case study in the
choshui river alluvial fan, taiwan. Journal of Hydrology 381, 239–247. 265 doi:https://doi.org/10.1016/j.jhydrol.2009.11.046.

Yu, H.L., Lin, Y.C., 2015. Analysis of space–time non-stationary patterns
f rainfall–groundwater interactions by integrating empirical orthogonal 268 function and cross wavelet transform methods. Journal of Hydrology 525,
585–597. doi:https://doi.org/10.1016/j.jhydrol.2015.03.057.

OPTIMIZATION METHOD FOR LARGE-SCALE PARTICLE IMAGE VELOCIMETRY APPLIED IN DRAINAGE FACILITIES

Cheng-Wei Wu [1], Hao-Che Ho[2]

ABSTRACT

The discharge measurement and real-time monitoring can efficiently reduce the serious impact on food production and livelihoods due to the disparity in water resources under the climate change. Discharge measurement is usually costly, therefore non-contact measurement methods with the low-cost and accurate advantages have become mainstream in recent years. Large-Scale Particle Image Velocimetry (LSPIV) is a non-contact measurement method applied in the outdoor. It crops the image in a video into several small pieces of Interrogation Area (IA), and the surface flow velocity is obtained by tracking the displacement of particle features in the next image using Direct Cross-Correlation (DCC). However, LSPIV can be easily affected by the size of IA. Small IA results in insufficient internal information to track, while large IA does not show all the details of the velocity field. Therefore, in this study, we use PIVlab to generate artificial velocity field images, while information entropy is used to quantify the characteristic statistics of different IA sizes. Furthermore, we use statistical methods to calculate the relationship between the cross-correlation degree and entropy index of two matching IA. Finally, the entropy index can be used to determine the most suitable IA size. In order to verify the application potential of the method, several field trials were conducted in the Jingmei River in Taipei City, Taiwan. The measurement results were compared with the Acoustic Doppler Current Profiling (ADCP) data to improve the accuracy of flow measurement in irrigation and drainage channels and to optimize the efficiency of water supply. The research results demonstrate that the entropy method is a promising approach for quantifying particle information in LSPIV. It exhibits good accuracy, with RMSE values controlled below 0.9 in the u-direction and 2.5 in the v-direction in artificial particle images. Furthermore, the performance of the entropy method is enhanced by considering the grayscale around pixels. This improvement results in approximately a 50% enhancement in quantifying particle information. The observed phenomenon confirms that incorporating the surrounding image intensity contributes to the extraction of seeding in the entropy calculation.

1. Introduction

Under the influence of climate change, the disparity between water resources abundance and scarcity has significantly affected food production and domestic water supply. Accurate flow monitoring is essential to effectively reduce water shortage risks. Taiwan, located in a subtropical climate region, experiences dramatic fluctuations in river water levels due to its island-like climate and steep terrain. Using the Rating-curve to estimate channel flow can result in significant errors during high-flow events. Traditional flow measurement methods are costly and time-consuming, requiring substantial manpower. Consequently, non-contact measurement methods have gradually become mainstream in recent years. One of the most used non-contact measurement methods is Large-Scale Particle Image Velocimetry (LSPIV) (Fujita et al.). LSPIV utilizes image recognition technology to track changes in features within images, thereby calculating the two-dimensional surface flow velocity of rivers. In the image recognition process, computers need to recognize the pattern of the object under test. By comparing the stored patterns with the images frame by frame, the computer identifies the most likely position of the object under test, thereby achieving image recognition. The LSPIV algorithm segments the images into equally sized sub-images called Interrogational Areas (IAs) as patterns of the fluid. It employs Direct Cross-Correlation (DCC) to recognize the position of

1 Graduate Student, Department of Civil Engineering, National Taiwan University, No.1, Section 4, Roosevelt Rd, Da'an District, Taipei City, 10617, r10521326@ntu.edu.tw.

2 Assistant Professor, Department of Civil Engineering, National Taiwan University, No.1, Section 4, Roosevelt Rd, Da'an District, Taipei City, 10617, haocheho@ntu.edu.tw

the pattern in the next time frame, and finally calculates the instantaneous surface flow velocity of that point by measuring the pattern's displacement. However, the size of the IA has a significant impact on the calculation results of LSPIV. An excessively small IA leads to an insufficient number of particles for matching within its coverage area, while an excessively large IA prevents the presentation of detailed changes in the flow field.

In recent years, there have been numerous image processing methods available, and Information Entropy is one approach that utilizes the distribution of brightness intensity in an image to extract its features. Information entropy is characterized by its ability to quantify the amount of information in an image(Shannon, 1948). When there is a higher seeding in the image, the information entropy is greater, and vice versa. Due to its suitability for quantifying particle information in images, information entropy has also been used as a method for image recognition.

In the past, there were no formalized approaches to determine the pattern of the fluid, often resulting in the use of empirical rules or trial and error to determine the size of the IA in fluid image recognition. In this study, we attempt to utilize the quantifying ability of information entropy to measure the amount of particle information in IAs of different sizes. This can provide an indicator for LSPIV to select the appropriate IA size, replacing the previous use of empirical rules and trial and error. From a Eulerian perspective, the study quantifies the change in information entropy as the IA size increases at fixed locations within the flow field. To enhance the reliability of this method, we use PIVlab to generate 12 synthetic particle images for testing. These images include four different particle density distributions and three different particle sizes. We compare the differences and stability of LSPIV results using the information entropy method and the previous empirical rules. Additionally, to enhance the particle information extraction ability of the information entropy method, we consider the average intensity of the surrounding pixels as an additional parameter and analyse its influence. Finally, to validate its practicality, we apply the method to a field experiment. The aim is to establish an IA size selection criterion for LSPIV based on the information entropy method and achieve a certain level of accuracy in the calculation results.

2. Artificial Image and study area description

In this study, there are a total of 13 experimental cases, including 12 synthetic particle image cases and 1 independent field experiment case. The synthetic particle images consist of 4 different particle densities and 3 different particle sizes, resulting in a total of 12 images with different parameter settings. These images were designed to simulate the capture of leaf particles on a natural river using unmanned aerial vehicle (UAV) imaging. To validate the practicality of the method, this study applied the information entropy method to a real field experiment, and using leavies as the tracer particles.

2.1 Artificial particle Image

PIVlab (Thielicke & Stamhuis, 2014) is a software tool based on MATLAB that provides a graphical user interface and programming capabilities. PIVlab offers various functionalities including complete PIV analysis workflow, image preprocessing and post-processing, surface flow velocity analysis, and synthetic particle image generation. During the generation of synthetic particle images, PIVlab allows users to adjust parameters such as the number of particles, particle diameter, and random variation. Additionally, there are five built-in flow fields available for selection, enabling adjustments of flow velocity, vortex radius, and vortex position in different flow fields. When generating particle image patterns, PIVlab employs a Gaussian intensity distribution to determine the brightness of each particle. The formula for the Gaussian intensity distribution is as follows:

$$I(x,y) = I_0 \exp\left[\frac{-(x-x_0)^2-(y-y_0)^2}{\frac{d_p{}^2}{8}}\right] \quad (2.1)$$

Where, I represents the Gaussian intensity, I_0 is the peak intensity, and d_p is the particle diameter. The center of the particle is located at (x_0, y_0). In this study, synthetic particle images were generated using PIVlab. These images aimed to simulate scenarios found in natural river channels.The image size was set to 1500×600 pixels, and the flow velocity was set to 4 pixels/frame. Four different particle density levels were considered: 0.006, 0.011, 0.017, and 0.022 particles per pixel (ppp). Additionally, three different particle diameters were included: 3,

4, and 5 pixels. While the simulated flow field in this study is a steady uniform flow (linear shift flow) as shown in **Error! Reference source not found.**. The parameters were arranged and combined to create a total of 12 different combinations of synthetic particle images. These parameters include particle density, particle size. By arranging these parameters, the study generated a comprehensive set of synthetic particle images to evaluate the performance of the information entropy method for LSPIV.

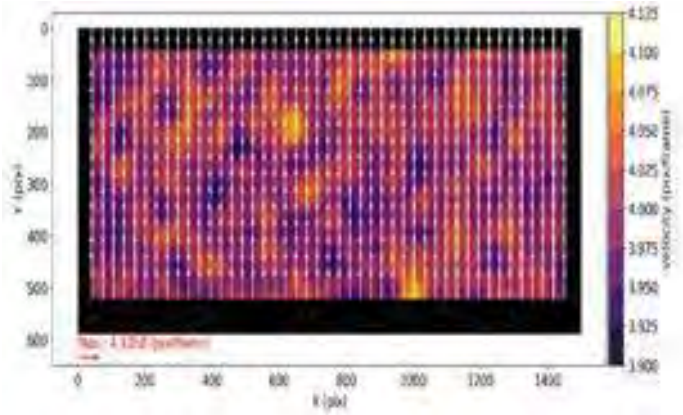

Figure 2.1 Linear shift flow surface velocity results

2.2 Field experiment

The Jingmei River originates from Nanshikeng in Yongding River, located within the territory of New Taipei City. It converges with Xindian River in Wansheng, Taipei City. The main stream of the river has a total length of 29.6 kilometers, covering a watershed area of 120.43 square kilometers. In the past, the Liugongjun and the Wulixue River, which were used for irrigating the farmland in present-day Taipei City, originated from this river. Although they are currently less utilized for irrigation, they still serve as important water sources and provide the river channel. In this study, this river section was selected as the field experiment measurement segment, as shown in Figure 4.1. In terms of measurement, ADCP measurements were used as a reference for comparison with LSPIV.

Figure 2.2 Linear shift flow surface velocity results

In terms of measurement, this study conducted ADCP measurements on four cross sections of the Jingmei River. Each cross section was measured four times, and the average values were obtained. The measured data represents the average flow velocity across the cross section. Therefore, the log-law method was used to calculate the water velocity profile. In this method, without considering the wake effect, the relationship between flow velocity and water depth is related to the shear stress of the bed and the kinematic viscosity of the fluid(Cebeci, 2012). The formula for the log-law is as follows:

$$\frac{u}{u^*} = \frac{1}{\kappa}\ln\left(\frac{zu^*}{\nu}\right) + C \quad (2.2)$$

$$u^* = \sqrt{\frac{\tau_w}{\rho}} \quad (2.3)$$

In the equation, u and z represent the velocity component in the x-direction and the position parameter, respectively. κ is the Von Kármán constant. u* is the shear velocity, which is influenced by the shear stress (τ_w) acting on the bed and the fluid density (ρ). ν represents the kinematic viscosity of the fluid. C is a general constant. The ADCP estimation results and the locations of the cross sections are shown in the **Figure 2.3**.

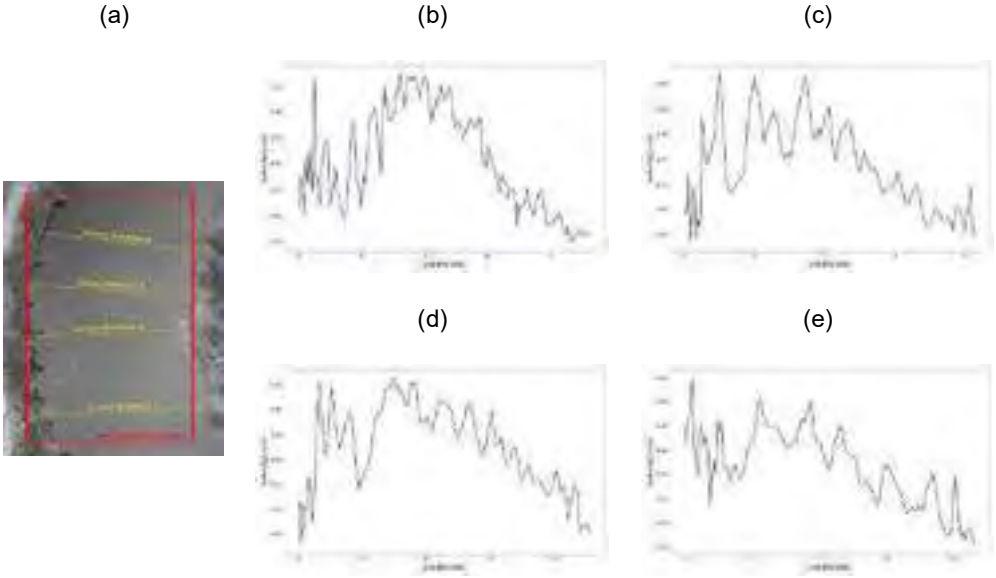

Figure

3. Methodology

In

3.1 Information entropy

In this study, information entropy is used as a method to quantify the patterns within the IA and provide an indicator for IA selection in LSPIV. The formula for information entropy is as HY = $\sum_{j=0}^{2^{\beta}-1} p(x_j)I(x_j)$ (3.1).

$$H(Y) = \sum_{j=0}^{2^{\beta}-1} p(x_j)I(x_j) \quad (3.1)$$

In the formula, H represents the information entropy, Y represents the IA, x_j represents the information within the IA, which we refer to as entropy parameters in this study. β represents the image depth, and in this study, we use 8-bit depth images, which means grayscale images with intensity values ranging from 0 to 256. $p(x_j)$ and $I(x_j)$ represent the probability of occurrence and the variable associated with $x_j$within the entire IA, respectively. Shannon aimed to distinguish events with high and low probabilities within entropy and thus defined the entropy variable as follows (Shannon, 1948):

$$I(x) = -\log_2(p(x)) \quad (3.2)$$

In traditional information entropy, the image intensity of each frame in the image is used as the entropy parameter, as shown in x0= $\{u_{i,j}\}_{j=1,2,\dots,h}^{i=1,2,\dots,w}$ (3.3).

$$x_0 = \{u_{i,j}\}_{j=1,2,\dots,h}^{i=1,2,\dots,w} \tag{3.3}$$

In the formula, x_0 represents the entropy parameter, u represents the image intensity of a single frame in the image, and w and h represent the width and height of the image, respectively. In order to improve the ability of this method to capture information from the surrounding pixels of each frame, this study considers the average image intensity around pixels. The definition of it is as follows:

$$u_{i,j}{}^{neighbour}(n) = \sum_{k=i-n}^{i+n}\sum_{m=j-n}^{j+n} u_{k,m} - u_{i,j} \tag{3.4}$$

Where, $u^{neighbour}$ represents the surrounding image intensity, and n represents the size of the surrounding range. The second type of entropy parameter used in this study considers both u and u^(neighbour) as factors (Liu & Zheng, 2021). In this study, it is referred to as x_n as shown in xn= $\{u_{i,j}, u_{i,j}{}^{neighbour}(n)\}_{j=1,2,\dots,h}^{i=1,2,\dots,w}$ (3.5).

$$x_n = \{u_{i,j}, u_{i,j}{}^{neighbour}(n)\}_{j=1,2,\dots,h}^{i=1,2,\dots,w} \tag{3.5}$$

This study uses information entropy to quantify particle information within the IA (Interrogation Area) and employs LSPIV as an indicator for IA selection. The following steps are followed:

(1) Selection of candidate IA options: In this study, IA sizes are chosen based on empirical rules, including five options: {16 pixels, 32 pixels, 64 pixels, 96 pixels, 128 pixels}.

(2) Extraction of sub-images corresponding to the IA size: Retrieve the sub-images of the corresponding IA size with each grid as the center.

(3) Calculation of information entropy for each sub-image: The information entropy matrix is computed according to the following equation:

$$\overline{H}_{IA\times1}(i,j) = \sum_{t=0}^{T} H(X_{IA\times1}(i,j,t))/T \tag{3.6}$$

In the equation, $\overline{H}_{IA\times1}$ represents the target information entropy matrix, where i and j denote the grid positions horizontally and vertically, respectively. $\overline{H}_{IA\times1}$(i, j, t) represents the sub-image at time t, corresponding to the five different IA sizes. And T is the total number of image frames.

The result of information entropy matrix, as shown in

Figure **3.1**, reveals a turning point at the 64-pixel position as the IA size increases. Subsequently, the slope of the IA entropy values decreases. This indicates that beyond an IA size of 64 pixels, there is a significant decrease in the amount of particle information gained. Moreover, increasing the IA size may introduce errors due to the neglect of flow velocity details in LSPIV. Based on these observations, the study selects the point of slope change as the optimized IA size. This inflection point is determined using the second derivative, as shown in the following equation:

$$\begin{aligned} H'(IA_x) &= \frac{H(IA_{x+1}) - H(IA_x)}{IA_{x+1} - IA_x} \\ H''(IA_x) &= \frac{2(H'(IA_x) - H'(IA_{x-1}))}{IA_{x+1} - IA_{x-1}} \\ IA_{selected} &= MAX\{H''(IA_x)\}_{x=32,64,96} \end{aligned} \tag{3.7}$$

In the equation, $IA_{selected}$ denotes the finally selected IA size. H(IA) represents the entropy value corresponding to the IA size, $\overline{H}$'(IA) and $\overline{H}$''(IA) represent the first and second derivatives of H(IA), respectively, and x represents the candidate IA sizes. After determining the most

suitable IA size for each grid, statistical methods will be applied to select the most frequently occurring IA size as the input parameter for LSPIV.

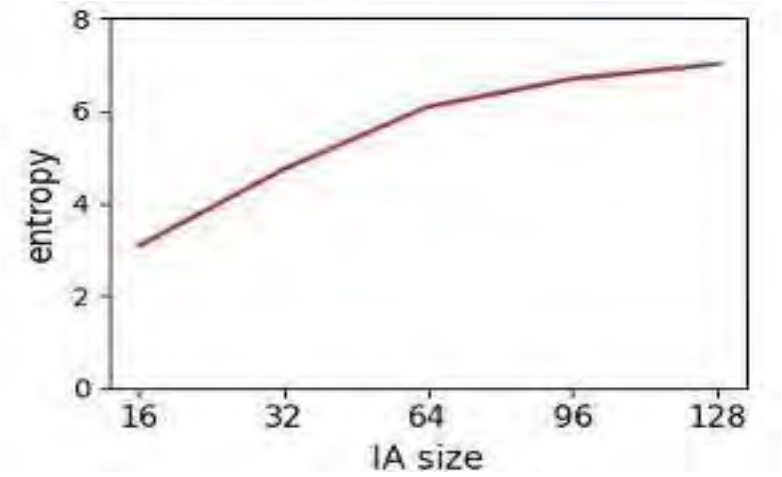

Figure 3.1 The relationship between IA size and information entropy

3.2 Large-Scale Image Particle Velocimetry

The application of Particle Image Velocimetry (PIV) at real scales in field measurements was first introduced by Fujita in 1994, known as Large-Scale Particle Image Velocimetry (LSPIV). Fujita installed a fixed camera on the right bank of the Nagara River, capturing continuous water surface images at 30 frames per second. He utilized features such as floating leaves, bubbles, and ripples generated from the riverbed to the water surface. Although these ripple patterns underwent rapid fluctuations, they exhibited minimal deformation over short periods of time. By incorporating ground reference points (GRPs) placed on both banks and applying image orthorectification techniques, surface flow velocities could be calculated using PIV. The research findings demonstrated the practical feasibility of LSPIV in field flow measurements (FUJITA & KOMURA, 1994). Subsequently, the LSPIV technique continued to mature, and in 1998, Fujita further conducted flow velocity measurements in three large-scale hydraulic model tests. Although there were still several unresolved challenges when applying LSPIV for outdoor flow measurements, such as strong reflections and uneven brightness caused by direct sunlight or obstructions on the water surface, insufficient density of feature points, reduced tracer visibility due to strong winds affecting floating objects, and distortion in image orthorectification. However, through appropriate parameter adjustments, the impact of these interferences could be mitigated ((Fujita et al., 1998); (Creutin et al., 2002); (Zhang et al., 2013)).

In the LSPIV algorithm, the input for image recognition is the sub-images, and the determination of the IA size is a crucial objective in this study. Traditional LSPIV methods divide the target image into several blocks of IA-sized sub-images. However, in this study, a grid-based approach is employed, where sub-images are extracted at each grid point. The IA size is determined using a combination of empirical rules and information entropy methods. Once the sub-images are extracted, they are compared with the corresponding SA in the next frame using the Direct Cross-Correlation (DCC) method. The correlation coefficient is calculated using the following formula:

$$r_{AB} = \frac{\sum_{i=1}^{M}\sum_{j=1}^{N}(A_{ij}-\bar{A})(B_{ij}-\bar{B})}{\sqrt{\sum_{i=1}^{M}\sum_{j=1}^{N}(A_{ij}-\bar{A})^2 \sum_{i=1}^{M}\sum_{j=1}^{N}(B_{ij}-\bar{B})^2}} \quad (3.8)$$

Here, r_{AB} represents the correlation coefficient between the sub-images A and B. A and B are the extracted sub-images and SA sub-images, respectively. i and j denote the coordinates within the sub-images, while M and N represent the width of the sub-images. A_{ij} and B_{ij} denote the pixel intensities of A and B at the (i, j) position, respectively, and $\bar{A}$ and $\bar{B}$ represent the average pixel intensities of A and B, respectively. The correlation coefficients obtained from the

pixel-wise comparisons are recorded in a matrix called the correlation matrix. In the LSPIV algorithm, the IA's most likely position is determined by finding the peak value in the correlation matrix, and its coordinates indicate the most probable position of the sub-image in the next frame. By comparing the distance and time difference between sub-images in consecutive frames, we can calculate the surface flow velocity at the grid point. The formula for calculating the surface flow velocity is as follows:

$$v(t) = \frac{pos_{IA}(t+\Delta t) - pos_{IA}(t)}{\Delta t} \quad (3.9)$$

Where, v(t) represents the surface flow velocity at time t, Δt is the time difference between frames, $pos_{IA}(t+\Delta t)$ and $pos_{IA}(t)$ denote the positions of the IA at times t+Δt and t, respectively.

4. Results and discussion

In this study, the information entropy method was tested on artificially generated particle images with varying degrees of particle density and particle size. A total of 12 different artificial particle images were included, consisting of four different particle density levels and three different particle sizes. **Table 4.1** represents the proportions of different IA sizes determined in all grids without considering the surrounding image intensities, while **Table 4.**2 represents the proportions of different IA sizes determined in all grids after considering the surrounding image intensities. It can be observed that IA sizes of 32 pixels consistently account for approximately 0.65 or more of the total distribution.

The second-highest proportion is occupied by IA sizes of 64 pixels, representing approximately 0.25 of the distribution. Furthermore, the results show that after considering the surrounding image intensity, although the IA size of 32 pixels still has the highest percentage, the percentage of 64-pixel IA has slightly increased. It has risen from the original range of 24-28% to 25-33%, with an improvement of approximately 5%.

Table 4.1 The proportion of each IA size selected by information entropy method(w/o considering grayscale around pixels s)

Particle radius (pixel)	Particle radius (pixel)	IA Size		
		32	64	96
3	.006	.69	.26	.05
3	.011	.69	.26	.05
3	.017	.71	.22	.06
3	.022	.70	.22	.08
4	.006	.67	.26	.07
4	.011	.70	.24	.05
4	.017	.68	.26	.06
4	.022	.68	.26	.07
5	.006	.66	.28	.06
5	.011	.67	.26	.06

5	.017	.69	.24	.07
5	.022	.68	.26	.06

Table 4.2 The proportion of each IA size selected by information entropy method(w/ considering grayscale around pixels)

Particle radius (pixel)	Particle radius (pixel)	IA Size		
		32	64	96
3	.006	.65	.27	.09
3	.011	.61	.30	.09
3	.017	.64	.27	.09
3	.022	.67	.24	.09
4	.006	.61	.29	.10
4	.011	.67	.25	.08
4	.017	.64	.27	.09
4	.022	.62	.28	.11
5	.006	.60	.30	.09
5	.011	.63	.28	.09
5	.017	.63	.28	.09
5	.022	.62	.27	.11

To validate the effectiveness of the IA determined by the information entropy method, this study evaluated 12 artificial particle images using Root Mean Square Error (RMSE). The results are shown in **Table 4.3** and **Table 4.4**. The RMSE will be evaluated separately in the u and v directions. The research results indicate that the RMSE can be kept below 0.9 in the u direction and below 2.5 in the v direction. The difference compared to the empirical method is approximately 0.5 to 2.4.

Table 4.3 RMSE_u comparison of IA selected by Thumb rule and information entropy method

Particle radius (pixel)	Particle radius (pixel)	Selected size of IA					
		Thumb rule					information entropy method
		16	32	64	96	128	
3	.006	0.607	0.642	0.026	0.017	0.012	0.642
3	.011	0.441	0.645	0.020	0.013	0.009	0.645
3	.017	0.830	0.636	0.025	0.017	0.013	0.636

3	.022	0.849	0.050	0.022	0.014	0.010	0.050
4	.006	0.736	0.866	0.116	0.018	0.012	0.866
4	.011	0.811	0.455	0.029	0.019	0.014	0.455
4	.017	0.867	0.449	0.026	0.016	0.011	0.449
4	.022	0.763	0.158	0.027	0.017	0.013	0.158
5	.006	0.681	0.417	0.031	0.020	0.014	0.417
5	.011	0.577	0.065	0.026	0.015	0.011	0.065
5	.017	0.671	0.104	0.028	0.018	0.014	0.104
5	.022	0.439	0.260	0.030	0.018	0.014	0.260

Note. $\mathbf{RMSE_u}$= Root Mean Square Error in u direction.

Table 4.4 $\mathrm{RMSE_v}$ comparison of IA selected by Thumb rule and information entropy method

Particle radius (pixel)	Particle radius (pixel)	Selected size of IA					
		Thumb rule					information entropy method
		16	32	64	96	128	
3	.006	3.801	2.444	0.299	0.018	0.015	2.444
3	.011	3.568	1.699	0.151	0.013	0.050	1.699
3	.017	3.338	1.230	0.023	0.014	0.010	1.230
3	.022	3.182	0.477	0.022	0.014	0.010	0.477
4	.006	3.838	2.507	0.451	0.157	0.013	2.507
4	.011	3.687	1.576	0.023	0.015	0.011	1.576
4	.017	3.329	1.002	0.027	0.017	0.012	1.002
4	.022	3.078	0.470	0.025	0.016	0.011	0.470
5	.006	3.854	2.424	0.367	0.022	0.015	2.424
5	.011	3.530	1.336	0.031	0.020	0.015	1.336
5	.017	3.292	0.808	0.028	0.017	0.012	0.808
5	.022	3.046	0.479	0.028	0.017	0.013	0.479

Note. $\mathrm{RMSE_v}$= Root Mean Square Error in v direction.

4.2 Field experiments result

In this section, field experiments will be presented to demonstrate the application of the information entropy method. After determining the IA using the information entropy method, it will be compared with the IA determined by the conventional empirical method in LSPIV. The

evaluation will be based on the average relative error. The calculation method for the average relative error is as follows:

$$\overline{Err} = \frac{\sum_1^n \frac{|V_{PIV,n} - V_{ADCP,n}|}{V_{ADCP,n}} \times 100\%}{n} \quad (4.1)$$

Where, $\overline{Err}$ represents the average relative error, V_{PIV} and V_{ADCP} denote the surface velocities measured by LSPIV and ADCP respectively, and n represents the number of measurement points.

Table 4.5 shows the IA ratio before and after considering grayscale around pixels, as well as the final decided IA size. It can be observed that the IA sizes of 32 pixels and 64 pixels are very close to each other. Prior to considering grayscale around pixels, the IA size of 32 pixels had the highest ratio. However, after considering grayscale around pixels, the IA size of 64 pixels had the highest ratio. The comparison results between LSPIV and ADCP are shown in **Figure 4.1**. It can be observed that the IA sizes determined by the information entropy method have an average relative error of less than 21%. Although the error is relatively high, it is only about 5% higher compared to the empirical method. Moreover, considering grayscale around pixels can reduce the relative error by approximately 5% and control it below 15%. The larger errors are primarily attributed to the inherent measurement errors of ADCP. When combined with the errors of LSPIV, these errors can propagate and amplify, resulting in larger overall errors. Hence, the error propagation effect contributes to the generation of relatively larger errors.

Table 4.5 The IA ratio before and after considering grayscale around pixels and the final decided IA size.

	IA Size			IA size with the highest ratio
	32	64	96	
W/o considering grayscale around pixels	.493	.410	.097	32
W/ considering grayscale around pixels	.498	.500	.002	64

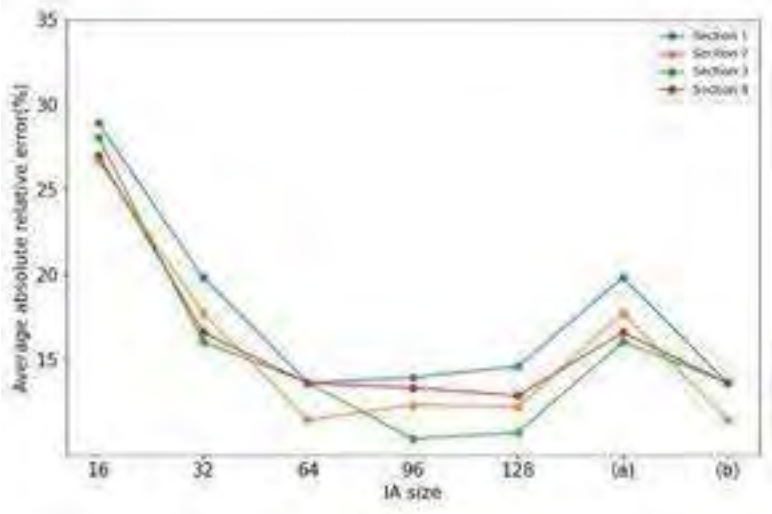

Figure 4.1 Comparison of LSPIV result and ADCP measurements in four cross sections

(a) IA size selected by information entropy method w/o considering grayscale around pixels,

(b) IA size selected by information entropy method w/ considering grayscale around pixels

Figure 4.2 shows the information entropy results before and after considering grayscale around pixels. It can be observed that after considering grayscale around pixels, there is a significant improvement in the information entropy value, with an approximate increase of 50%. Additionally, the lines in the figure appear to converge more closely. This phenomenon confirms that the image intensity around the pixels contributes to enhancing the effectiveness of information entropy in seed point recognition.

(a) (b)

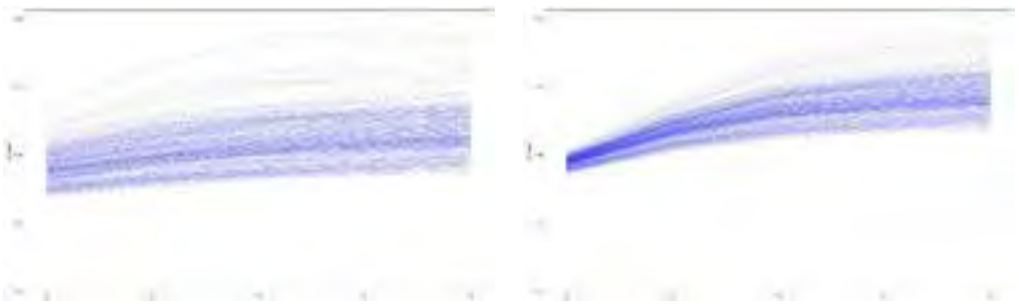

Figure 4.2 The effect of surrounding pixels intensity on information entropy results

(a) information entropy results w/o considering grayscale around pixels

(b) information entropy results w/ considering grayscale around pixels

5. Summary and conclusions

This study demonstrates that the information entropy method can effectively quantify particle information within the IA and serve as an indicator for LSPIV selection. In artificial particle images, the RMSE in the u and v directions can be controlled below 0.9 and 2.5., Furthermore, when considering the grayscale around pixels, the information entropy method shows an improvement of approximately 50% in quantifying particle information. In field experimental images, the accuracy of the entropy method is approximately 80%, and its performance is about 5% worse than the empirical method in terms of error comparison. However, after considering the grayscale around pixels, the accuracy of the entropy method can be improved by approximately 5%, indicating its potential as an algorithm for selecting IA parameters in LSPIV. After analysing and discussing the research findings, the following three conclusions are proposed:

(1) The accuracy of the entropy method can be affected by external factors such as image noise and flow turbulence. These factors should be carefully considered and mitigated to improve the performance of the method.

(2) Considering the grayscale around pixels enhances the performance of the entropy method. It leads to approximately a 50% improvement in quantifying particle information. This phenomenon confirms that incorporating the surrounding image intensity contributes to the extraction of seeding in the entropy calculation.

(3) The entropy method is a promising approach for quantifying particle information in LSPIV. It demonstrates good accuracy with RMSE values controlled below 0.9 in the u-direction and 2.5 in the v-direction in artificial particle images.

REFERENCES

Cebeci, T. (2012). *Analysis of turbulent boundary layers*. Elsevier.

Creutin, J., Muste, M., & Li, Z. (2002). Traceless quantitative imaging alternatives for free-surface measurements in natural streams. Hydraulic Measurements and Experimental Methods 2002,

FUJITA, I., & KOMURA, S. (1994). Application of video image analysis for measurements of river-surface flows. *Proceedings of hydraulic engineering*, *38*, 733-738.

Fujita, I., Muste, M., & Kruger, A. (1998). Large-scale particle image velocimetry for flow analysis in hydraulic engineering applications. *Journal of hydraulic Research*, *36*(3), 397-414.

Liu, G., & Zheng, X. (2021). Fabric defect detection based on information entropy and frequency domain saliency. *The Visual Computer*, *37*(3), 515-528.

Shannon, C. E. (1948). A mathematical theory of communication. *The Bell system technical journal*, *27*(3), 379-423.

Thielicke, W., & Stamhuis, E. (2014). PIVlab–towards user-friendly, affordable and accurate digital particle image velocimetry in MATLAB. *Journal of open research software*, *2*(1).

Zhang, Z., Wang, X., Fan, T., & Xu, L. (2013). River surface target enhancement and background suppression for unseeded LSPIV. *Flow Measurement and Instrumentation*, *30*, 99-111.

THE IMPACT OF CLIMATE CHANGE ON URBAN HEAT ISLAND AND THUNDERSTORM PATTERNS IN TAIPEI

Yuan-Chien Lin[1*], Siti Talitha Rachma[1]

Abstract

Due to the impact of climate change in recent years, the average surface temperature of Earth has been rising specifically in several urbanized cities all over the world. This study aims to understand the Urban heat islands (UHIs) impact in the Taipei basin on thunderstorms in order to be a considerable input for future urban development. The initial step involves using the Hilbert Huang Transform (HHT) to uncover specific details about the UHI by analyzing the non-linear relationship trends in both the time domain and frequency domain. The obtained HHT trend results are then utilized to compare the UHI trends across different stations. Next, the main spatial pattern of thunderstorm events in the Taipei basin is extracted using Empirical Orthogonal Function (EOF) analysis. The findings indicate that urbanization in the Taipei basin has led to an increase in UHI intensity ranging from 0.2 to 1.1℃ over the past 20 years, largely influenced by climate change.

The EOF analysis reveals a significant 42.36% rise in thunderstorm occurrences in urban areas of the Taipei basin since 1998, in contrast to other regions. This suggests that the growing UHI might be contributing to the surge in thunderstorms within urban areas, and it's worth noting that rainstorms are no longer confined solely to metropolitan regions.

Keywords: urban heat island, thunderstorm, Hilbert-Huang Transform, empirical orthogonal function

Introduction

In recent decades, there has been a rapid increase in the world's population and urbanization. The growth of global population in cities and urban regions is projected to be approximately 50% higher than in rural areas. According to the United Nations' 2018 forecast, by 2050, cities are expected to accommodate 68% of the world's population [1]. This substantial growth in urban population has raised concerns about health and safety in future metropolitan areas worldwide. Consequently, extensive research has been conducted to understand the potential factors that could compromise the safety and livability of human settlements, particularly urban areas. This research includes investigating the causes of urban risks, the influencing conditions, and the implementation of policies to minimize or prevent adverse effects [2].

These concerns stem from the broader context of excessive and uncontrolled urbanization, which has widespread negative implications on psychological, social, economic, and environmental aspects of human well-being and quality of life in urban settings. For instance, high levels of urbanization have been found to be strongly associated with multidimensional poverty, encompassing various factors such as education, healthcare, living conditions, and environmental conditions, in addition to monetary indicators [3]. The competition for limited resources in highly urbanized areas, combined with inadequate municipal planning and governance, has resulted in social and economic hardships, potentially leading to mental health issues and even suicides. Such disparities have been linked to increased suicide rates in cities like Taipei [4].

While the effects of urbanization on social, economic, and physicochemical aspects have been widely studied, its impact on the environment has received relatively less attention. Natural resources, considered as public goods, are susceptible to the tragedy of the commons, wherein individuals, companies, and governments believe their consumption of these resources has no significant impact on the environment [5]. Climate, which is also a public good, is less tangible and often overlooked in terms of its impact on human life, despite being crucial for quality of life [6]. This study specifically focuses on climate because urbanization has various implications for climate, including contributing to global warming, particularly evident in metropolitan areas, resulting in the urban heat island (UHI) effect. This UHI phenomenon affects other climate variables such as precipitation, humidity, and temperature [7] [8] [9] [10].

[1] Department of Civil Engineering, National Central University

* Corresponding Author: yclin@ncu.edu.tw

The present study aims to explore the relationship between UHIs and afternoon thunderstorms in Taipei. Afternoon thunderstorms are of particular interest due to their potential indirect links to negative consequences that could harm the quality of life in urban areas, similar to the tragedy of the commons concept discussed earlier. Some studies suggest that afternoon thunderstorms can lead to adverse effects like mercury contamination, extreme floods, landslides, accidents, and fatalities [11] [12] [13].

To investigate this relationship, the study proposes the use of the Hilbert-Huang Transform (HHT) and Empirical Mode Decomposition (EMD) to analyze time series data of UHIs and thunderstorms. This innovative approach will help identify underlying patterns and relationships between UHIs and afternoon thunderstorms in Taipei. By combining meteorological observations and numerical modeling, the research aims to gain a comprehensive understanding of the spatial and temporal dynamics of UHIs and thunderstorms in the metropolitan area. The findings from this study are expected to be valuable for urban planners and policymakers, providing insights that can inform decision-making and mitigation strategies to address the impacts of UHIs and thunderstorms in urban environments.

Materials and Methods

Taipei as the study area

Taipei, depicted in Figure 1, serves as the capital city of Taiwan and is situated in the northern part of the island, specifically at the northeastern edge of the Taipei basin. It shares boundaries with New Taipei City, together forming the Taipei–Keelung metropolitan area. As per the Taiwan Ministry of Interior, the city's population surpassed 2 million people in 2019. Taipei is geographically defined by the convergence of three rivers - Keelung, Dahan, and Xindian - which join to form the Tanshui river that runs through the city. Notably, the winding course of the Keelung River is the most prominent among these waterways. The urban area is nestled amid mountains, resembling a shallow and wide bowl, with some parts even being below sea level.

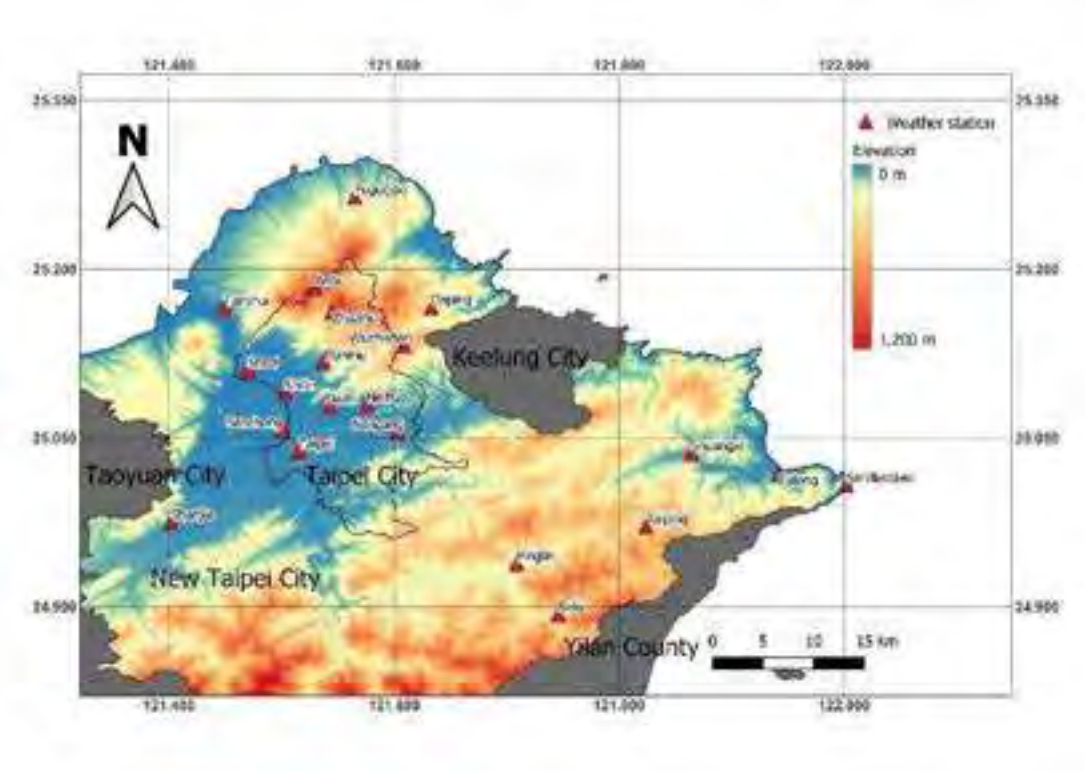

Figure 1. Map of the study area and CWB stations

Taipei experiences a humid subtropical climate, with an average temperature of 22.7 degrees Celsius. January is the coldest month, while July registers the highest temperatures. Interestingly, prior research indicates that while cities at higher elevations typically experience urban heat peaks during winter, Taipei encounters such heat peaks throughout summer, particularly around midday [26]. This subtropical climate is heavily influenced by the

movement of airflows and the East Asian monsoon, with Taipei witnessing two monsoon seasons - one from October to March and another from May to June [27].

In terms of rainfall, Taipei received an average of 2,405 mm of rainfall annually in 2015, providing an adequate water supply from multiple sources. However, it experiences a higher number of dry days compared to wet days, particularly during the monsoon season. Taipei's climate is susceptible to extreme weather events, especially when Pacific storms sweep through during the summer, resulting in approximately three or four typhoons hitting Taiwan each year. Typhoons bring heavy rain and strong winds, posing risks to Taipei's ecosystems, including crop damage, floods, landslides, and waterborne diseases. Additionally, during the summer months, convective afternoon thunderstorms are frequent in Taipei due to elevated seasonal temperatures, leading to intense but brief periods of heavy rainfall. These climatic conditions can contribute to increased rainfall levels, causing excessive runoff and, in some cases, flash floods. Moreover, evidence indicates that Taipei's temperature has risen by 1.4 degrees Celsius over the past century [27].

Data collection and pre-processing

In this research, hourly temperature and rainfall data were collected from 21 ground sites operated by the Central Weather Bureau (CWB) and depicted in Figure 1. These meteorological stations are strategically located across the Taipei basin, and the study covers a time span of 20 years, from 1998 to 2017. Among the 21 stations, eight were situated in metropolitan areas, while the remaining stations were in rural regions, as indicated in Table 1.

Table 1. Weather station list of the study area

No.	Station Number	Station Name	Elevation(m)	Station Status
	466920	Taipei	6.3	Urban
	C0A980	Shezi	11	Urban
	C0A9A0	Dazhi	24	Urban
	C0A9C0	Tianmu	35	Urban
	C0A9E0	Shilin	26	Urban
	C0A9F0	Neihu	35	Urban
	C0A9G0	Nangang	42	Urban
	C0A9I0	Sanchong	18	Urban
	C0A520	Shanjia	48	Rural
	C0A530	Pinglin	300	Rural
	C0A540	Sidu	401	Rural
	C0A550	Taiping	422	Rural
	466900	Tanshui	19	Rural
	466910	Anbu	825.8	Rural
	466930	Zhuzihu	607.1	Rural
	C0A860	Daping	362	Rural
	C0A870	Wuzhishan	685	Rural
	C0A880	Fulong	6	Rural
	C0A890	Shuangxi	40	Rural
	C0A920	Fuguijiao	196	Rural
21	C0A970	Sandiaojiao	96	Rural

Following the completion of the temperature and rainfall data, the hourly temperature data are utilized to generate the UHI intensity index in the Taipei region using the following equation:

$$UHI = T_U - \mu T_R \quad (1)$$

where T_U is the hourly observed temperature of each urban station and μT_R is the mean of the hourly temperature of all the rural stations, expressed by ºC.

Typically, Taiwan experiences two distinct monsoon seasons: the winter/northeast monsoon from September to April, which influences precipitation during the cold season, and the summer/southwest monsoon from May to August, which affects precipitation in the warm season [28]. Precipitation patterns in Taiwan can be categorized into five main types: winter (December to February), spring transition (March and April), mei-yu season (mid-May to mid-June), typhoon season (mid-July to August), and fall regime (September to November). However, in recent times, these boundaries have become less distinct, resulting in years with insufficient rainy seasons or typhoons leading to droughts. On the other hand, there has been an increase in severe afternoon/evening thunderstorms during the summer, causing short-term heavy rainfall and flash flood events. Moreover, the spatial-temporal patterns or durations of these afternoon/evening thunderstorms have also undergone recent changes.

The focus of this study is to identify afternoon/evening thunderstorms (rainstorms) specifically in the Taipei area while excluding other factors. Consequently, the hourly rainfall data during the typhoon season (July to September) will not be considered in this analysis. For the purpose of defining afternoon/evening thunderstorm events, any day with at least 10 mm of cumulative rainfall recorded at any station between 11:00 AM and 9:00 PM Local Standard Time (LST) will be classified as such [29].

Method of analysis: Hilbert-Huang Transform (HHT)

The HHT employs Empirical Mode Decomposition (EMD) for signal decomposition, setting it apart from traditional Fourier transform and wavelet methods, as it does not rely on predefined basis functions or their relationships with the original signal. Instead, the decomposition process is based on the fundamental assumption that data at a given time instant can consist of multiple simple oscillation modes with significantly different frequencies, all active simultaneously.

EMD is a data-driven signal decomposition technique that sequentially extracts normal or quasi-harmonic zero-mean values from high-frequency to low-frequency signals. It acts as an adaptive binary filter resembling a wavelet. Each extracted component is known as an intrinsic mode function (IMF) and meets the following criteria: (1) The number of extrema and zerocrossings in the entire dataset can be the same or differ by no more than one, and (2) The mean value of the envelope is defined at each data point using the local maxima, while the local minima are set to zero [30].

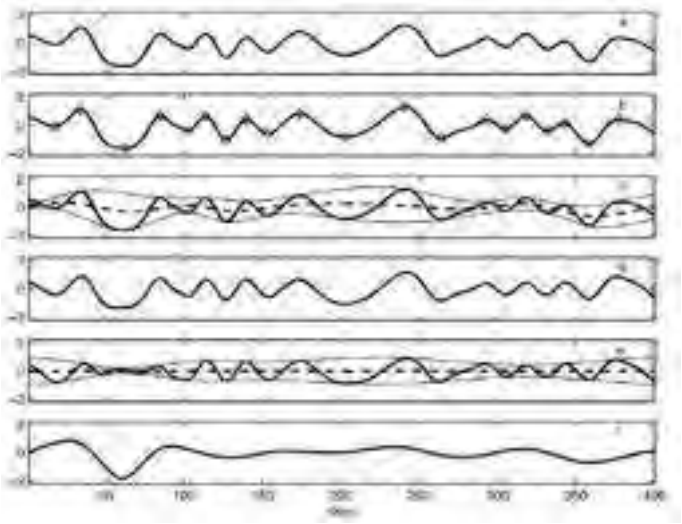

Figure 2. The sifting process of EMD: (a) original signal; (b) identified maxima (diamond) and minima (circles) superimposed on the original signal; (c) upper and lower envelope (thin solid line) and their mean (dashed line); (d) prototype of IMF (the difference between the bold solid line and dashed line in Figure 3c) that is to be refined; (e) upper and lower envelope (thin

solid line) and their mean (dashed line) of a refined IMF; and (f) remain signal after IMF is subtracted from the original signal [30].

Each function can be disassembled using the following IMF definition throughout the verification phase. Figure 2 depicts an example of obtaining IMF from any time series. Figures 3(a) and 3(b) show the original signal data x(t) as thick solid lines. The process of shifting begins with the identification of all local extrema (see Figure 2(b), where diamonds and the minima mark the maxima is marked by circles). Then, as demonstrated by the thin solid line in Figure 2(c), link all local maxima (minima) using cubic splines to build the upper (below) envelope. As seen in Figure 2(c), the upper and lower envelopes often cover all of the data in between. In Figure 2(c), their average value is represented by a dashed line as m_1. The difference between the input and m_1 is the first proto mode, h_1, shown in figure 2(d),

$$h_1 = (t) - m_1 \quad (2)$$

Because of the design, it is assumed that h_1 matches to the IMF definition. However, this is not always the case since moving the local zero from the rectangular to the curvilinear coordinate system may result in additional extrema, necessitating further modifications. That is why the filtering operation, as described before, must be repeated. This filtering procedure has two objectives: (1) to remove the background wave propagating in the IMF, and (2) to make the wave profile more symmetric. To guarantee that the recovered signal matches the IMF's criterion, the filtering procedure should be done as many times as feasible. h_1 can only be viewed as the original IMF throughout the iteration process, and it will be processed as data in the following iteration:

$$h_1 - m_{11} = h_{11} \quad (3)$$

After k times of iterations,

$$h1(k-1) - m1k = h1k; \quad (4)$$

the estimated local envelope symmetry condition is satisfied, and h_{1k} becomes the IMF c_1, in other words,

$$c_1 = h_{1k}, \quad (5)$$

which is the first IMF is expressed in Figure 2(e).

This shifting procedure may remove low-frequency waves, symmetry from the waveform, and isolate high-frequency IMF from the present residual signal. In each IMF's shifting procedure, the SDk determined from two successive shifting results:

$$\equiv \sqrt{\frac{\sum_{t=0}^{T}[h_k(t)-h_{k-1}(t)]^2}{\sum_{t=0}^{T} h_{k-1}^2(t)}}, \quad (6)$$

must be smaller than a predetermined value. The first IMF should contain the smallest scale or the shortest period of the signal that can be extracted from the data by,

$$(t) - c_1 = r_1 \quad (7)$$

As illustrated in Figure 2(d), the residual component, or residue, r_1, still contains significant periods of variance. The residue is then treated as fresh data (new signal), and the filtering procedure described above is repeated to produce a lower IMF frequency. This procedure may be repeated on every following, r_j, the end result being,

$$\begin{aligned} &r_1 - c_2 = r_2 \\ &\cdots \\ &rn-1 - cn = rn \end{aligned} \quad (8)$$

When the residue (r_n) is turned into a monotonic function or a function with just one extremum, the decomposition process is terminated and the IMF cannot be retrieved. If we combine equations (7) and (8), we get,

$$x(t) = \sum_{j=1}^{n} c_j + r_n \quad (9)$$

As a result, the original signal data are fragmented into *n*-IMFs and a residue, r_n, which can be either the adaptive trend or a constant, is produced. Because the EMD approach only employs information pertaining to local extreme values, it does not require a constant mean or zero references. As a result, the sorting process yields zero references for each IMF. EMD avoids eliminating the trend by not requiring a zero reference, resulting in low-frequency components in the resultant spectrum.

The Hilbert-Huang Transform (HHT) technique is a powerful signal processing method that has proven valuable in analyzing diverse physical phenomena, including climate data. When investigating the intricate and multifaceted relationship between urban heat islands and thunderstorm activity, the HHT method offers several advantages that make it particularly wellsuited for this task.

To begin with, the HHT method excels at decomposing time series data into its individual components using empirical mode decomposition (EMD). This ability is especially valuable when dealing with complex systems like the atmosphere, where relevant signals may be obscured by noise or other irrelevant features. By breaking down the time series into its constituent parts, the HHT method can provide clearer insights into the underlying dynamics governing a specific phenomenon, such as the influence of urban heat islands on thunderstorm activity.

Furthermore, the HHT method is adept at analyzing nonlinear and nonstationary data, which are common characteristics of atmospheric data. The adaptiveness and data-driven nature of the EMD algorithm used in the HHT method allow it to handle signals with diverse characteristics. In contrast, traditional Fourier-based methods often rely on assumptions of linearity and stationarity, which may not accurately capture the complexities present in atmospheric data. Moreover, the HHT method facilitates the analysis of phase relationships between different components of a time series, which is crucial in understanding the underlying dynamics of a system. In the context of urban heat islands and thunderstorm activity, where temperature and humidity gradients play a pivotal role, studying the phase relationships between these signals using the HHT method could offer valuable insights into how urban heat islands impact thunderstorm activity.

Lastly, the HHT method has demonstrated successful applications across various climate data studies, including investigations of temperature trends, rainfall patterns, and extreme weather events. This underscores the method's versatility and reliability, suggesting it as a valuable tool for analyzing the influence of urban heat islands on thunderstorm activity. In summary, the HHT method's capabilities in decomposing time series, handling nonlinear and nonstationary data, analyzing phase relationships, and its track record in climate data analysis make it a highly suitable and promising approach for studying the impact of urban heat islands on thunderstorm activity.

Method of analysis: Empirical Orthogonal Function (EOF)

EOF calculates spatial-temporal data by reducing the data's dimension into spatial patterns and lowering all of the information into basic information that will clarify the incomplete fluctuation rates [31]. The spatial patterns resulted from a mechanism known as EOFs, whereas the temporal patterns are known as PCs.The primary goal of EOF was to accomplish spatial-temporal data decomposition *X (t, s)*, where *t* is temporal (time) and *s* is spatial (space) position, as

$$X\ (t,) = \sum^{M}{}_{k=1}\ (t)(\mathbf{s}) \qquad (10)$$

where *M* is the number of modes present in the field, $u_k(\mathbf{s})$ is an optimum set primary spatial 234 function, and $c_k(t)$ is temporal expansion function (time). The EOF/PCA approach, in its application, aims to identify a new set of variables that capture the majority of the observed 236 variation in the data through a combination of the original variables utilizing the linear 237 combination to achieve the goal.

The value of the spatial-temporal field *X (t, s)* at time *t* and spatial position s is recorded in the gridded dataset. For *i* = 1,n and *j* = 1, …p, the value of the field at discrete time t_i and grid 240 point s_j is denoted $x_{ij.}$ The data matrix then represents the observed field: a

$$X = (x_1, x_2, \ldots, x_n)^T = \begin{matrix} x11 & x12 & \ldots & x1p \\ (x^{21}{:}x^{22}{:} & \ldots{:} & & x^{2:p}) \\ x_n1 & x_n2 & \ldots & xnp \end{matrix} \qquad (11)$$

where $x_t = (x_{t1}, x_{t2}, \ldots, x_{tn})^T$, $t = 1, \ldots n$, indicated the value of the map or field at t time. Then, denote the $\bar{x_i}$ the field's temporal average with the i'*th* spatial grid point. This temporal average is 244 accompanied by:

$$\bar{x_i} = \frac{1}{n} \sum_{k=1}^{n} x_{ki} \quad (12)$$

The climatology of the field is determined by,

$$\bar{x} = (\bar{x}_{.1}, \ldots, \bar{x}_{.p}) = \frac{1}{n} 1_n^T X \quad (13)$$

where $1_n = (1, \ldots 1)^T$ is the column vector of the length *n* contained only ones. The anomaly part 249 of the climatology is calculated by *(t, sk)*, *t* = 1,…n, and *k* = 1,…*p*, by:

$$250\ x'_{tk} = x_{tk} - \bar{x}_{.k} \quad (14)$$

Or in matrix form as shown below,

$$X' = X - 1_n \bar{X} = (I_n - \frac{1}{n} 1_n 1 T_n)\ X = HX \quad (15)$$

Once the anomaly matrix is found (equation 15), the covariance of the sample matrix is determined by:

$$S = \frac{1}{n} X^T X, \quad (16)$$

which contained the covariance, s_{ij}, *i*, *j* = 1,…*p*, between the time series of the field at any pair of 257 the grid points (s_j, s_j), as shown below,

$$sij = [S]_{ij} = \frac{1}{} \sum_{n} \quad nt=1\ xtixtj. \quad (17)$$

The goal of EOF/PCA analysis is to discover uncorrelated linear combinations of the individual variables that explain the most variation, or to find a unit-length direction $u = (u_1, \ldots, u_p)^T$ in which Xu has the most variability. This was quickly followed by,

$$\max(u^T S u), \text{ s.t. } u^T u = 1 \quad (18)$$

Therefore, EOFs are obtained as the solution to the eigenvalue problem:

$$Su = \lambda^2 u \quad (19)$$

The k'th EOF is simply the k'th eigenvectors u_k of *S*. The corresponding eigenvalue λ^2_k, *k* 266 = 1,…*p* is then,

$$\lambda 2_k = u T_k S u_k = \frac{1}{n} \| X u_k \| 2 \quad (20)$$

It also provides a measure of the variance of data calculated in the direction u_k. The 269 eigenvalues are generally sorted in decreasing order as $\lambda^2_1 \geq \lambda^2_2 \cdots \geq \lambda^2_p$ after determining the 270 eigen components of the sample covariance matrix *S* in equation 18. Typically, the variance is 271 stated as a percentage as:

$$272\ \frac{}{} \%\ 100\lambda^2 \quad . \quad (21)$$
$$\sum k=1\ \lambda k$$

The projection of the anomaly field *X* onto k'th EOF $u_k = (u_{k1}, u_{k2}, \cdots, u_{kp})^T$, in other words $a_k = Xu_k$ is the k'th PC whose elements $a_{tk}, t = 1, \cdots n$, are given by:

$$a_{tk} = \sum_{j=1}^{p} x_{tj} u_{tj} \quad (22)$$

Usually, in a practical calculation, calculating the covariance (equation 16) and solve the eigenvalue problem (equation 19) is not necessary since the matrix could be calculated using linear algebra named as the singular value decomposition (SVD). Any $n \times p$ data matrix type could be decomposed as:

$$X = A\Lambda U^T \quad (23)$$

Results

UHI trend in Taipei area

Since 1985, urban warming in Taipei has been observed, with a warming rate of 1.57°C per 100 years. In comparison, other cities in low latitudes might experience a more pronounced warming trend, reaching 1.74°C per 100 years [32]. This section employs the Hilbert-Huang Transform (HHT) analysis to investigate the Urban Heat Island (UHI) intensity in the Taipei area over the past two decades. Initially, the UHI intensity in the region was calculated by subtracting the urban temperature from the rural temperature to assess the degree of heat increase. Given that UHI data is nonlinear and nonstationary, the HHT method was utilized to analyze its trend. HHT is renowned for its effectiveness in analyzing datasets with nonstationary and nonlinear characteristics. This technique yielded hourly UHI intensity values from the collected meteorological data, enabling an understanding of the temperature rise over the last 20 years by examining the increasing or decreasing trend of UHI intensity in Taipei.

However, the original data stream at times remains convoluted with seasonal components or other influencing factors. Figure 3 illustrates an example of an HHT result from one station in Taipei. As evident in Figure 3(a), the time series of UHI intensity from 1998 to 2017 did not show a discernible increasing or decreasing trend due to the dominance of seasonal or other components. To isolate the trend, it became necessary to extract these components, resulting in several signals until only the residual remained, as shown in Figure 3(e).

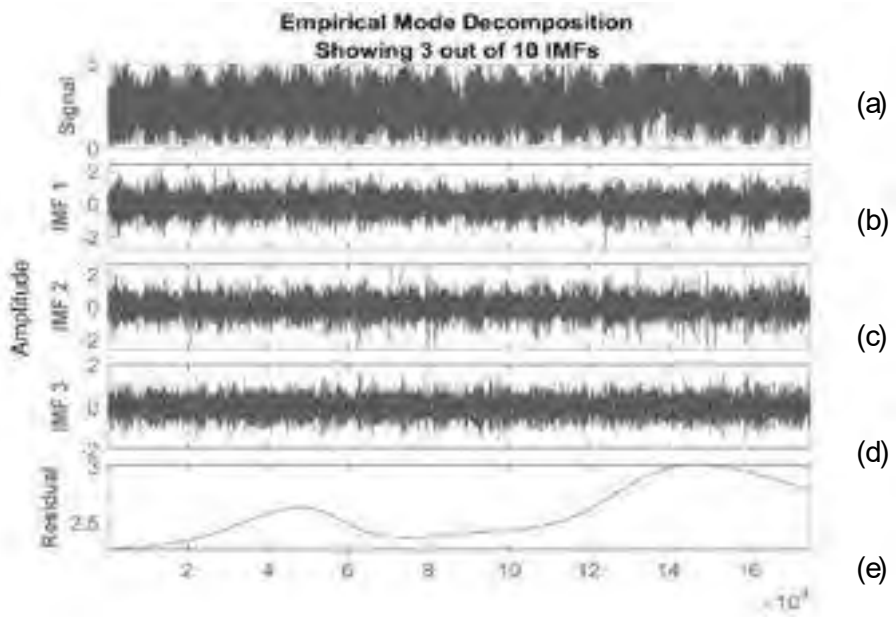

Figure 3. One of the HHT results from 8 stations in Taipei, (a) UHI intensity original signal, (b) (c) (d) The first 3 IMFs out of 10 IMFs total, (e) The residual or trend of the UHI intensity in one of a station in Taipei.

The residual results of the HHT analysis indicate that the majority of stations in Taipei have exhibited an increasing trend in UHI intensity, as depicted in Figure 4. However, there are exceptions, such as the Sanchong

station (Figure 4(a)) and the Neihu station (Figure 4(b)), which have shown a decreasing trend in recent years. It can be argued that while the overall trend of UHI intensity in Taipei's urban regions is generally increasing, there are variations in the warming rate across different stations, ranging from 0.2 to 1.1°C over the past 20 years, as shown in Figure 5, encompassing all areas of Taipei city station.

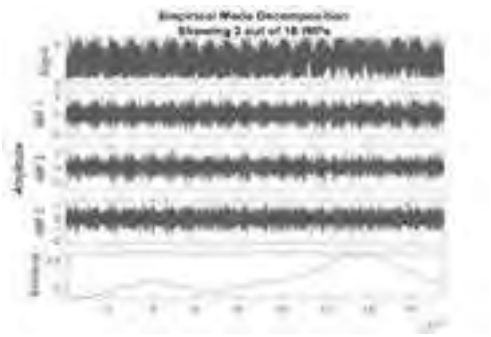

(a) Sanchong

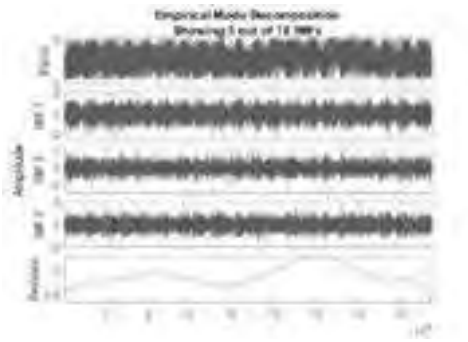

(b) Neihu

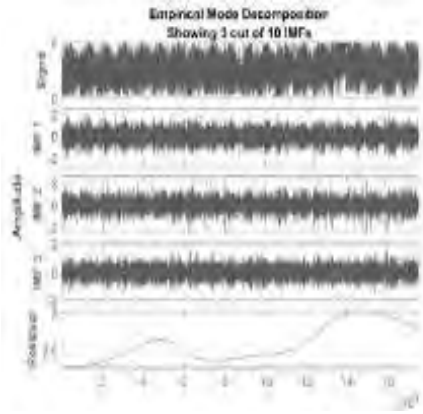

(c) Nangang

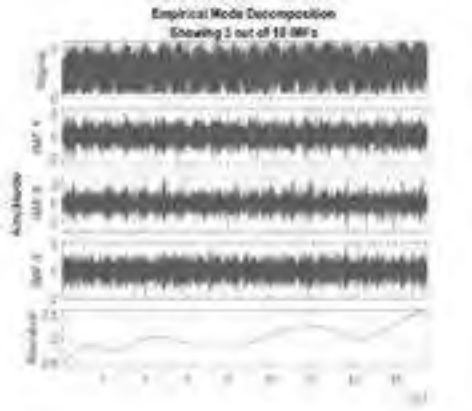

(d) Shilin

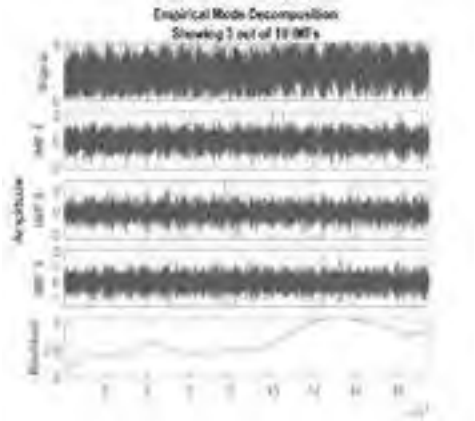

(e) Dazhi

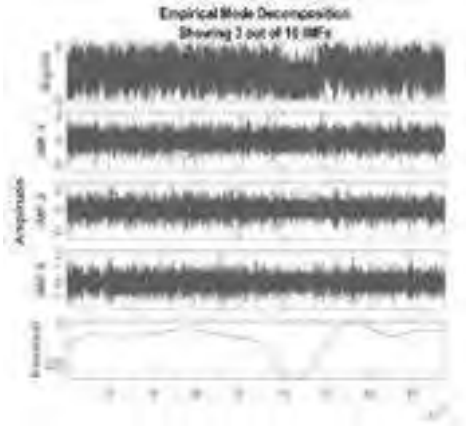

(f) Tianmu

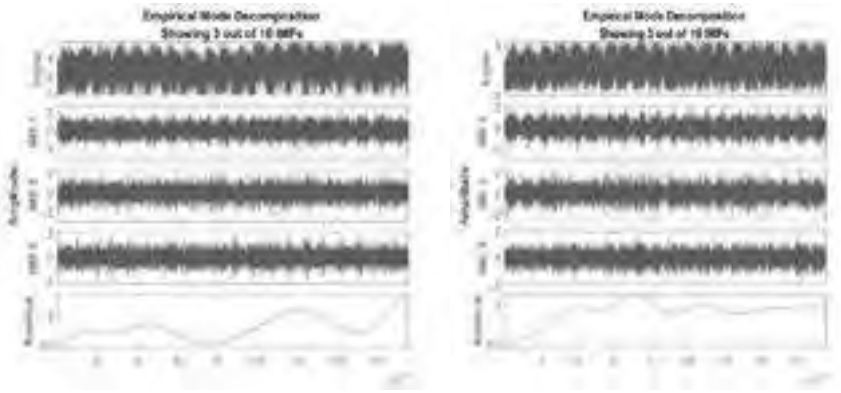

(g) Shezi (h) Taipei

Figure 4. (a) to (h) is UHI trend result from HHT analysis for each station, with the y-axis shown as amplitude or the magnitude of UHI and the x-axis shown as the timestamp

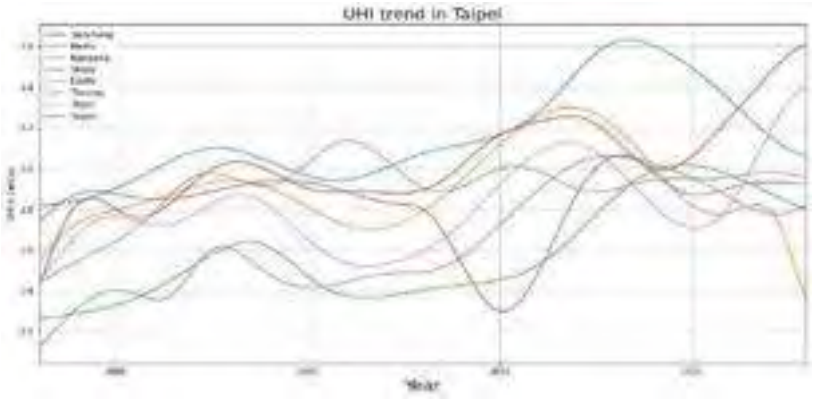

Figure 5. UHI trend result from HHT analysis

Yearly distribution, trend, and spatial variations of thunderstorms

Between 1998 and 2017, there were a total of 225 thunderstorm occurrences in the Taipei basin, primarily concentrated during the mei-yu season compared to other seasons (Figure 6). During the first ten years (1998-2007), there were 100 thunderstorm incidents, and this number increased to 125 during the subsequent decade, indicating a 25% increase in thunderstorms in the Taipei area over the two decades

.

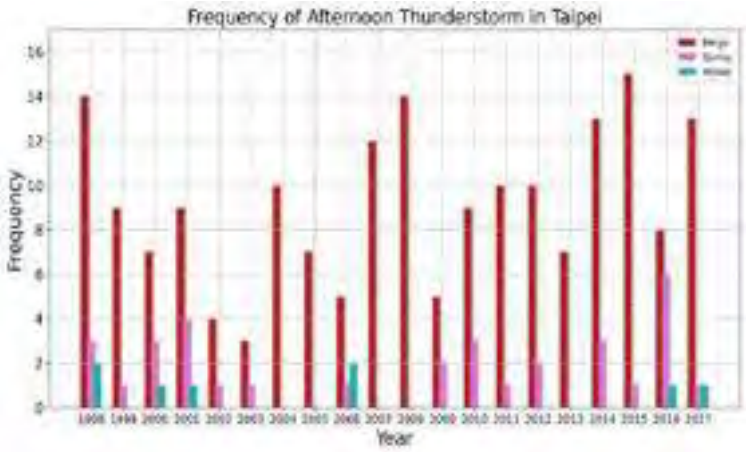

Figure 6. Yearly and seasonal distribution of thunderstorm in Taipei

The utilization of Empirical Orthogonal Function (EOF) analysis on the 225 thunderstorm occurrences in the Taipei basin allowed for the identification of main spatial variances. The variance explained by the first EOF (Figure 7(a)) was 42.36% (Table 2), suggesting that 42.36% of the observed thunderstorm events exhibited spatial fluctuations similar to the first EOF. Notably, thunderstorms were found to be concentrated in urban regions according to the first EOF, while the second EOF indicated 24.84% variance centered in rural-coastal areas (Figure 7(b)).

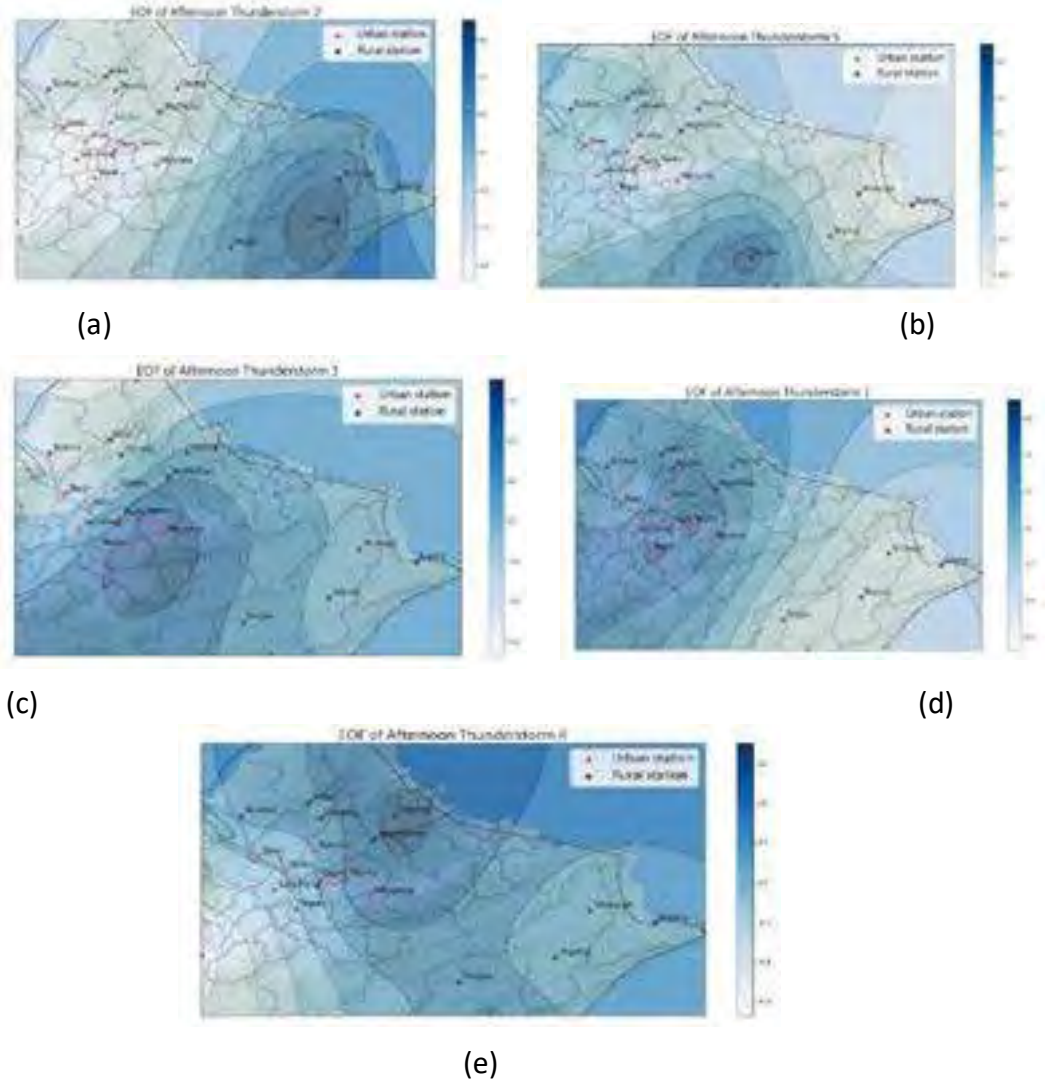

Figure 7. (a) to (e) is the result of spatial variations of thunderstorm events using EOF analysis starting from the first to fifth variations, respectively.

Table 2. Variance explained for each spatial variation

Pattern (EOF)	Variance explained (%)
1	42.36
2	24.84
3	8.03
4	4.65
5	4.38

A more focused study was carried out by performing EOF analysis on two separate fiveyear thunderstorm periods: (1) thunderstorm events from 1998 to 2002, and (2) thunderstorm events from 2013 to 2017. It was observed that the geographical variances from each time series were dissimilar. In the past, thunderstorms tended to be localized in metropolitan areas (Figure 8(b)), but in recent years, short-duration rainstorms spread to adjacent suburbs (Figure 8(c)). This suggests a shift in thunderstorm spatial patterns, with an increase in thunderstorm days and frequencies (Figure 6). Previous research has indicated an increase in rainfall in Taipei since 1897, especially after 1980 [32], and thunderstorm event days have also grown during the last two decades. As a result, both downtown areas and rural regions are now at a higher risk of flash flooding.

Analyzing the HHT trend data in Figure 9(a), it appears that the concentration of thunderstorms in the urban region has remained consistent or even decreased over the last 20 years. Although most thunderstorms still occur in urban areas, the concentration has not significantly increased, as indicated by the EOF results. However, this does not mean that the concern about thunderstorms should be disregarded, as the possibility of more frequent afternoon thunderstorms in the future could extend beyond metropolitan areas. It is essential to be prepared for unexpected thunderstorms and their potential impacts.

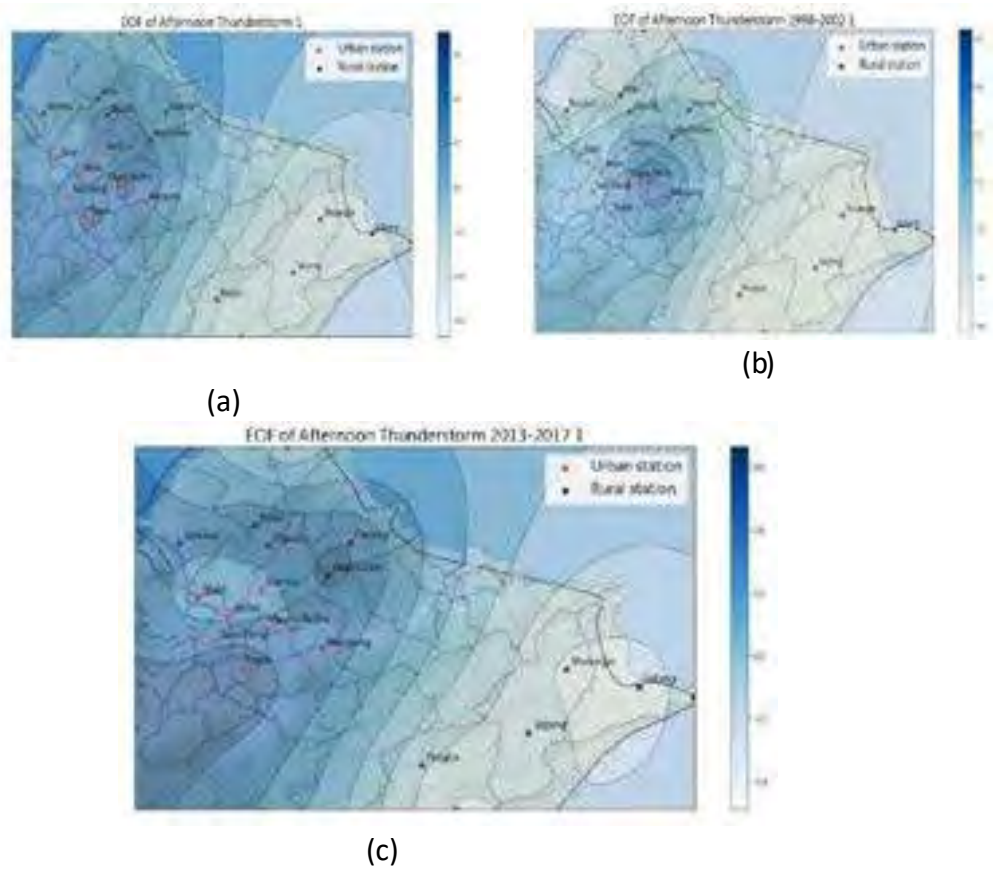

Figure 8. Result of spatial variations of thunderstorms in two different time series, (a) First EOF of afternoon thunderstorm from 1998 - 2017, (b) First EOF of afternoon thunderstorm from 1998 – 2002, and (c) First EOF of afternoon thunderstorm from 2013 – 2017

The impact of UHI towards thunderstorms

The HHT analysis of urban heat island (UHI) and afternoon thunderstorms indicates that consistent patterns of UHI may lead to a reduction in the frequency of thunderstorms. This can be attributed to the fact that steady UHI patterns imply minimal fluctuations in temperature differences between urban and rural areas, resulting in fewer natural cooling mechanisms. Consequently, this reduced cooling potential could lead to a decrease in afternoon thunderstorm activity.

The UHI effect occurs due to the absorption and re-emission of solar radiation by urban infrastructure like buildings and roads, causing elevated temperatures in urban areas. The HHT analysis of UHI reveals that in certain weather stations (Figure 5), the UHI effect remains relatively stable over time, with little variation in the temperature difference between urban and rural regions. This stability suggests fewer opportunities for natural cooling mechanisms, such as convective clouds, to form and trigger afternoon thunderstorms. On the other hand, the HHT analysis of afternoon thunderstorms (Figure 9a) indicates decreasing patterns in some weather stations. This decrease may be attributed to the lack of natural cooling mechanisms typically associated with thunderstorm activity, as these mechanisms rely on temperature and moisture gradients, which may be less pronounced in areas with a steady UHI effect.

It is also crucial to examine which parts of the Taipei area experienced the most significant changes in thunderstorm behavior over time. As shown in Figure 9(b), the lightest blue indicates a declining trend in thunderstorm occurrence, while the darkest blue signifies the most substantial growth trend. The picture illustrates the concentration of thunderstorms shifting towards the rural and mountainous areas in the basin's east and north. However, it is essential to note that an accumulation of thunderstorms in a short period of time in these regions may elevate the risk of landslides.

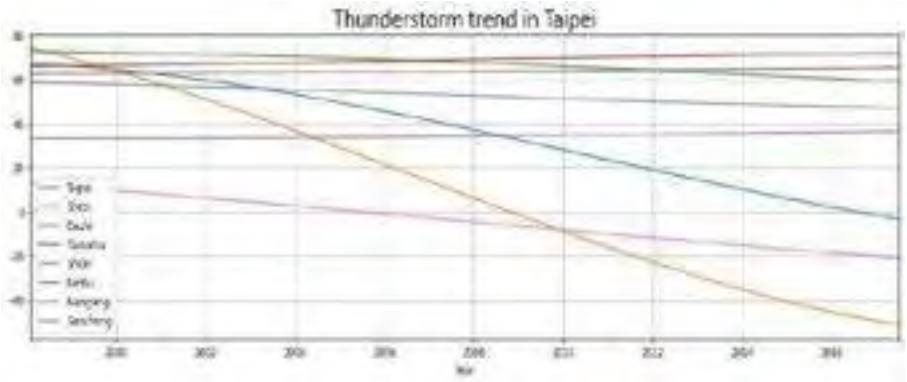

(a)

(b)

Figure 9. (a) HHT trend result of a thunderstorm in urban areas, (b) Mapping of HHT trend result slope of urban areas

It is essential to emphasize that even though the concentration of thunderstorms in the mountain area is increasing, it still represents a small portion of the overall rainfall (Table 3). As shown in Figure 10(b), thunderstorms in the rural region contribute only modestly to the total rainfall. The primary concern that arises from the EOF results of thunderstorms in the mountain area is the potential disruption of the water supply for the Taipei region, given that the main water source for Taipei is located in the Pinglin station area.

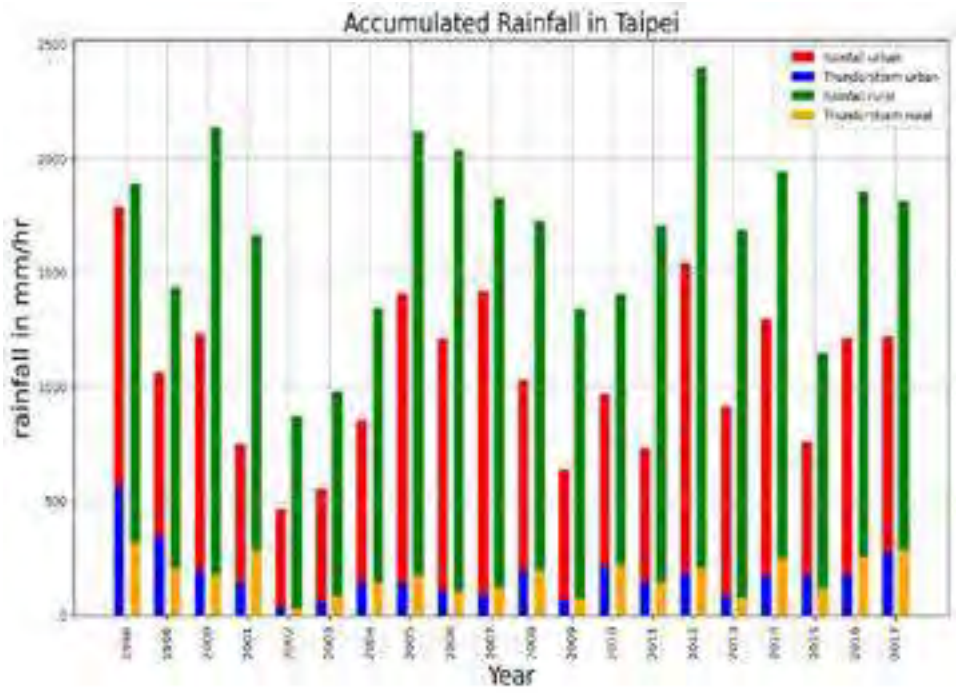

Figure 10. Overall changes of accumulated rainfall and thunderstorm in urban and rural areas.

Table 3. Accumulated rainfall in urban areas (A) and rural areas (B)

Year	Rainfall (A) (mm)	Thunderstorm (A) (mm)	Contribution (A) (%)	Rainfall (B) (mm)	Thunderstorm (B) (mm)	Contribution (B) (%)	Difference (mm)
				1891			240.7
1998	1788	564.2	31.6		323.5	17.1	
1999	1063.4	348.6	32.8	1439.7	207.6	14.4	141
2000	1234.1	199	16.1	2138.2	181	8.5	18
2001	750.7	146.9	19.6	1664.2	291.1	17.5	-144.2
2002	467.8	37.5	8	875.6	31.7	3.6	5.8
2003	554.6	60.5	10.9	980.8	88.4	9	-27.9
2004	854.8	146.5	17.1	1346.9	146.8	10.9	-0.3
2005	1410.7	143.1	10.1	2117.6	176.1	8.3	-33
2006	1215.5	110.6	9.1	2038.1	105.9	5.2	4.7
2007	1420.6	91.1	6.4	1830.2	122.3	6.7	-31.2
2008	1032.6	202.2	19.6	1728.6	201.6	11.7	0.6
2009	638.7	69.8	10.9	1342.5	75.8	5.7	-6
2010	970.5	214.3	22.1	1407.1	228.9	16.3	-14.6
2011	733	151.6	20.7	1706.5	147.8	8.7	3.8
2012	1542.3	188.4	12.2	2399.8	209.5	8.7	-21.1
2013	917.5	86.2	9.4	1691.2	79.8	4.7	6.4
2014	1297	180.7	13.9	1945.8	251	12.9	-70.3
2015	761.1	174.6	22.9	1150.9	116.6	10.1	58
2016	1215.8			1856.2			-78.2

		178.8	14.7		257	13.8
2017	1222.3	279	22.8	181	292.1	16.1

However, upon closer examination of Table 3, it becomes evident that the contribution of thunderstorms to the total rainfall trend in the rural region is at most around 17 percent. This implies that the scenario of thunderstorms significantly impacting water resources is unlikely to occur. In other words, the afternoon rainstorms concentrated in downtown Taipei do not have a substantial impact on water resources (such as reservoirs in the suburbs), but the characteristics of the afternoon rainstorms spreading to metropolitan areas may actually benefit water sources. Nonetheless, it is more probable that such thunderstorms may result in short-term hydrological disasters.

Discussion

Given the rising urban heat island (UHI) effect in Taipei over the last two decades, thunderstorms in the region often initiate in the mountain peaks, spread to the terrain slope, and bring heavy rain to the basin [36]. Thunderstorms in the Taipei region are frequently linked to the interaction between the sea breeze and UHI in the central metropolitan area and the southern mountain area of the basin [14]. The thunderstorm phase begins with sufficient moisture, and the sea-breeze circulation transports unstable flow to the basin. By 1400 LST, the interaction of the sea breeze with UHI in the Taipei region and the orography of the southern section of the basin can trigger thunderstorm convection and rainfall over the mountain slopes [37]. This mechanism indicates that the increased frequency of thunderstorms over the past 20 years could be attributed to the intensification of UHI in the Taipei area, leading to the possibility of even more frequent thunderstorms in the future.

The urbanization of Taipei, which has accelerated since 1967, and the subsequent urban warming since 1985, have prompted concerns about local weather and climate change [32]. As urban surface temperatures rise over time, the severity of UHI becomes unavoidable. The sudden downpours and accompanying thunderstorms can cause havoc in the urban area. Thunderstorms not only impact the comfort of living in a city but also influence urban environmental sustainability. In metropolitan areas, it is crucial to swiftly direct rainwater to drainage systems during heavy rainfall to prevent road hazards. However, with the intensity and brevity of these rainfall events, excess precipitation can overwhelm drainage systems. Due to the predominance of impermeable surfaces like asphalt or concrete in urban areas, rainwater cannot be absorbed, leading to more frequent occurrences of urban flash floods.

Conclusion

Over the past two decades, the urban heat island (UHI) effect in Taipei has shown a significant increase, which has led to a higher risk of thunderstorms. The number of thunderstorms in Taipei has risen by 25%, and while they are becoming more frequent in metropolitan areas, their intensity is relatively lower. This poses a threat to the drainage system and urban areas, making them more vulnerable to flash floods. Notably, the Shuangxi station area in the eastern mountains has experienced the highest increase in thunderstorm concentration. Thunderstorms now account for 32% of overall rainfall patterns in metropolitan areas, underscoring the importance of acknowledging and addressing the potential risks associated with thunderstorms.

As UHI severity continues to escalate in Taipei, so does the likelihood of unexpected thunderstorms. The results of EOF analysis show that 42.36% of thunderstorm occurrences are concentrated in urban areas, while 24.84% are observed in rural-coastal areas. The analysis also reveals a trend of thunderstorms becoming more localized in urban regions, with short-duration rainstorms spreading to suburban areas in recent years. However, it is crucial to note that although the accumulated concentration of thunderstorms is relatively stable and decreasing, this does not rule out the possibility of severe thunderstorms occurring. The combination of frequent, lowintensity thunderstorms alongside occasional severe ones may potentially overwhelm the drainage system.

In light of these findings, it is paramount for Taipei to prepare and mitigate the potential risks posed by the escalating UHI and thunderstorms. This includes improving the drainage system and ensuring that urban areas are equipped to handle flash floods effectively. Additionally,

closely monitoring areas with high thunderstorm concentration is crucial for timely response and risk management. Implementing measures to reduce UHI intensity, such as increasing green spaces and utilizing green roofs, should also be seriously considered. With proper planning, preparation, and proactive measures, Taipei can effectively mitigate the potential risks associated with UHI and thunderstorms, providing its residents with a sense of safety and security.

Acknowledgements

This study was supported by the National Science and Technology Council (Ministry of Science and Technology), Taiwan (MOST 108-2625-M-008-002, MOST 108-2119-M-008-003, MOST 111-2119-M-008-004, MOST 110-2634-F-008-008, and MOST 111-2119-M-008-006), Young Scholar Fellowship Program (MOST 108-2636-E-008-004, MOST 109-2636-E-008-008, 110- 2636-E-008-006, and 111-2636-E-008-014), and Shackleton Program Grant (MOST 108-2638-E008-001-MY2). We are also thankful for the Python programing language and related data analysis modules that provided powerful tools for that data analysis.

References

P. D. United Nations, Department of Economic and Social Affairs, “World Urbanization Prospects. The 2018 Revision. Methodology,” Webpage, p. 22, 2018.

D. Argüeso, J. P. Evans, L. Fita, and K. J. Bormann, “Temperature response to future urbanization and climate change,” Climate Dynamics, vol. 42, no. 7–8, pp. 2183–2199, 2014, doi: 10.1007/s00382-013-1789-6.

K. M. Chen, C. H. Leu, and T. M. Wang, “Measurement and Determinants of Multidimensional Poverty: Evidence from Taiwan,” Social Indicators Research, vol. 145, no. 2, pp. 459–478, 2019, doi: 10.1007/s11205-019-02118-8.

C. Y. Lin, C. Y. Hsu, D. Gunnell, Y. Y. Chen, and S. Sen Chang, “Spatial patterning, correlates, and inequality in suicide across 432 neighborhoods in Taipei City, Taiwan,” Social Science and Medicine, vol. 222, pp. 20–34, 2019, doi: 10.1016/j.socscimed.2018.12.011.

A. Patt, “Beyond the tragedy of the commons: Reframing effective climate change governance,” Energy Research and Social Science, vol. 34, no. May, pp. 1–3, 2017, doi: 10.1016/j.erss.2017.05.023.

W. Nordhaus, “Climate change: The ultimate challenge for economics,” American Economic Review, vol. 109, no. 6, pp. 1991–2014, 2019, doi: 10.1257/aer.109.6.1991.

P. A. Mirzaei and F. Haghighat, “Approaches to study Urban Heat Island - Abilities and limitations,” Building and Environment, vol. 45, no. 10, pp. 2192–2201, 2010, doi:

10.1016/j.buildenv.2010.04.001.

S. Arifwidodo and O. Chandrasiri, Urban Heat Island and Household Energy Consumption in Bangkok, Thailand, vol. 79. Elsevier B.V., 2015. doi: 10.1016/j.egypro.2015.11.461.

T. Tokairin, A. Sofyan, and T. Kitada, “Numerical Study on Temperature Variation in the Jakarta Area Due To Urbanization,” The Seventh International on Conference of Urban Climate, vol. 5, no. July, pp. 3–6, 2009.

IPCC, Climate Change 2001: The Scientific Basis. Contribution of Working Group I to the Third Assessment Report of the Intergovernmental Panel on Climate Change. 2000. doi: 10.1016/S1058-2746(02)86826-4.

C. D. Holmes et al., “Thunderstorms increase mercury wet deposition,” Environmental Science and Technology, vol. 50, no. 17, pp. 9343–9350, 2016, doi: 10.1021/acs.est.6b02586. [12] J. A. I. Paski, D. S. Permana, N. Alfuadi, M. F. Handoyo, M. H. Nurrahmat, and E. E. S. Makmur, “A Multiscale analysis of the extreme rainfall triggering flood and landslide events over bengkulu on 27th April 2019,” AIP Conference Proceedings, vol. 2320, no. March, 2021, doi: 10.1063/5.0037508.

R. Brázdil et al., “Fatalities associated with the weather in the Czech Republic, 2000–2019,” Natural Hazards and Earth System Sciences, no. 2016, pp. 1–47, 2021, doi: 10.5194/nhess2021-14.

T. C. Chen, S. Y. Wang, and M. C. Yen, “Enhancement of afternoon thunderstorm activity by urbanization in a valley: Taipei,” Journal of Applied Meteorology and Climatology, vol. 46, no. 9, pp. 1324–1340, 2007, doi: 10.1175/JAM2526.1.

P. Grady Dixon and T. L. Mote, “Patterns and causes of Atlanta’s urban heat island-initiated precipitation,” Journal of Applied Meteorology, vol. 42, no. 9, pp. 1273–1284, 2003, doi:

10.1175/1520-0450(2003)042<1273:PACOAU>2.0.CO;2.

K. P. Naccarato, O. Pinto, and I. R. C. A. Pinto, "Evidence of thermal and aerosol effects on the cloud-to-ground lightning density and polarity over large urban areas of Southeastern Brazil," Geophysical Research Letters, vol. 30, no. 13, pp. 1–4, 2003, doi:

10.1029/2003GL017496.

T. L. Mote, M. C. Lacke, and J. M. Shepherd, "Radar signatures of the urban effect on precipitation distribution: A case study for Atlanta, Georgia," Geophysical Research Letters, vol. 34, no. 20, pp. 2–5, 2007, doi: 10.1029/2007GL031903.

J. M. Shepherd, "A review of current investigations of urban-induced rainfall and recommendations for the future," Earth Interactions, vol. 9, no. 12, 2005, doi:

10.1175/EI156.1.

J. J. Baik, Y. H. Kim, and H. Y. Chun, "Dry and moist convection forced by an urban heat island," Journal of Applied Meteorology, vol. 40, no. 8, pp. 1462–1475, 2001, doi:

10.1175/1520-0450(2001)040<1462:DAMCFB>2.0.CO;2.

R. Bornstein and Q. Lin, "Urban heat islands and summertime convective thunderstorms in Atlanta: Three case studies," Atmospheric Environment, vol. 34, no. 3, pp. 507–516, 2000, doi: 10.1016/S1352-2310(99)00374-X.

C. M. Rozoff, W. R. Cotton, and J. O. Adegoke, "Simulation of St. Louis, Missouri, land use impacts on thunderstorms," Journal of Applied Meteorology, vol. 42, no. 6, pp. 716–738, 2003, doi: 10.1175/1520-0450(2003)042<0716:SOSLML>2.0.CO;2.

S. A. Changnon, "the La Porte weather anomaly—fact or fiction?," Bulletin of the American Meteorological Society, vol. 49, no. 1, pp. 4–11, 1968, doi: 10.1175/1520-0477-49.1.4.

F. A. Huff and S. A. Changnon Jr., "Climatological Assessment of Urban Effects on Precipitation at St. Louis," Journal of Applied Meteorology and Climatology, vol. 11, no. 5, pp. 823–841, 1972.

H. E. Landsberg, "Man-Made Climatic Changes," Science, vol. 170, no. 3964, pp. 1265– 1274, 1970.

W. Y. Shih, S. Ahmad, Y. C. Chen, T. P. Lin, and L. Mabon, "Spatial relationship between land development pattern and intra-urban thermal variations in Taipei," Sustainable Cities and Society, vol. 62, no. May 2019, p. 102415, 2020, doi: 10.1016/j.scs.2020.102415.

C. R. Chang, M. H. Li, and S. D. Chang, "A preliminary study on the local cool-island intensity of Taipei city parks," Landscape and Urban Planning, vol. 80, no. 4, pp. 386–395, 2007, doi: 10.1016/j.landurbplan.2006.09.005.

K. F. A. Lo and S. B. Koralegedara, "Effects of climate change on urban rainwater harvesting in colombo city, sri lanka," Environments - MDPI, vol. 2, no. 1, pp. 105–124, 2015, doi:

10.3390/environments2010105.

C. S. Chen and J. M. Huang, "A numerical study of precipitation characteristics over Taiwan island during the winter season," Meteorology and Atmospheric Physics, vol. 70, no. 3–4, pp. 167–183, 1999, doi: 10.1007/s007030050032.

C. C. Wang, N. C. Su, J. P. Hou, and D. I. Lee, "Evaluation of the 2.5-km Cloud-Resolving

Storm Simulator in Predicting Local Afternoon Convection during the Summer in Taiwan," Asia-Pacific Journal of Atmospheric Sciences, vol. 54, no. 3, pp. 489–498, 2018, doi: 10.1007/s13143-018-0054-7.

N. E. Huang and Z. Wu, "a Review on Hilbert-Huang Transform : Method and Its Applications," Reviews of Geophysics, vol. 46, no. 2007, pp. 1–23, 2008, doi:

10.1029/2007RG000228.1.INTRODUCTION.

D. A. Addo, F. T. Oduro, and R. K. Ansah, "Empirical orthogonal function (EOF) analysis of precipitation over Ghana," International Journal of Statistics: Advances in Theory and Applications Vol., vol. 1, no. September, pp. 121–141, 2017.

Y. Bai, J.-Y. Juang, and A. Kondoh, "Urban Warming and Urban Heat Islands in Taipei, Taiwan," Groundwater and Subsurface Environments: Human Impacts in Asian Coastal Cities, no. January 2011, pp. 231–246, 2011, doi: 10.1007/978-4-431-53904-9.

M. Hsu et al., "Flood Damage Assessment in Taipei City , Taiwan," 9th International Conference on Urban Drainage Modelling, no. January, p. 9, 2012.

C. Sen Chen and Y. L. Chen, "The rainfall characteristics of Taiwan," Monthly Weather

Review, vol. 131, no. 7, pp. 1323–1341, 2003, doi: 10.1175/15200493(2003)131<1323:TRCOT>2.0.CO;2.

J. E. Miao and M. J. Yang, A modeling study of the severe afternoon thunderstorm event at taipei on 14 june 2015: The roles of Sea Breeze, microphysics, and terrain, vol. 98, no. 1.

2020. doi: 10.2151/jmsj.2020-008.

B. J.-D. Jou, "Mountain-Originated Mesoscale Precipitation System in Northern Taiwan: A Case Study 21 June 1991," Terrestrial, Atmospheric and Oceanic Sciences, vol. 5, no. 2, p. 169, 1994, doi: 10.3319/tao.1994.5.2.169(tamex).

T. C. Chen, M. C. Yen, J. D. Tsay, C. C. Liao, and E. S. Takle, "Impact of afternoon thunderstorms on the land-sea breeze in the Taipei basin during summer: An experiment," Journal of Applied Meteorology and Climatology, vol. 53, no. 7, pp. 1714–1738, 2014, doi:
10.1175/JAMC-D-13-098.1.

ICID Products & Services
Directory

ICID•CIID

Are you a consultant/ manufacturer/ dealer/ professional institution dealing in irrigation and drainage products/services.

Don't miss this opportunity to list your products/ services FREE of cost!

Information dissemination plays a critical role in the field of irrigation, drainage and flood management. For sharing the available knowledge across a wide spectrum of users, ICID has recently launched a new web service on ICID website <http://www.icid.org> as "Irrigation & Drainage - Products & Services" **<https://icid-ciid.org/services/product_services_search/40>** to help various stakeholders in locating required services, products and business information through a few clicks.

This online directory provides a platform to enlist all the services and products being provided by consultants, manufacturing companies, dealers, and other professional institutions dealing in irrigation and drainage sector. Any service provider can submit their information online **<https://icid-ciid.org/services/add_services>** for inclusion in this directory.

At present, the information is listed/ collected in the following categories and sub-categories:

A. Consultancy Services (1. Individuals/ Experts/ Freelancer; 2. Organizations);

B. Companies / Manufacturers/ Dealers (1. Company/ Implementing Agency; 2. Dealer/ Distributor / Contractor; 3. Manufacturer; 4. Publisher; 5. Software developers/ vendors);

C. Institutions (1. Academic Institutions; 2. Farmer's Associations; 3. Funding Agencies; 4. Govt./ Non-Governmental Organizations (NGO)/ Not for Profit Organizations; 5. Research Institutions; 6. Training Institutions); and

D. Others

Take out your time and join the new online service to enhance your visibility to the irrigation, drainage and flood management community.

For more information, please contact:

The Secretary General, **International Commission on Irrigation and Drainage (ICID)**
48 Nyaya Marg, Chanakyapuri, New Delhi 110021, India. E-mail: icid@icid.org, Website: http://www.icid.org / icidat / icidonline

25È INTERNATIONAL DES IRRIGATIONS ET DU DRAINAGE

1-8 NOVEMBRE 2023, VISHAKHAPATNAM (VIZAG), INDE

Question 64: What alternative water resources could be tapped for irrigated agriculture?

Quelles ressources alternatives en eau pourraient être exploitées pour l'agriculture irriguée?

Question 65: Which on-farm techniques can increase water productivity?

Quelles techniques agricoles peuvent augmenter la productivité de l'eau?

TRANSACTIONS / ACTES

Hosted by:

Indian National Committee on Irrigation and Drainage (INCID)
C/o Remote Sensing Directorate,
Central Water Commission, Department of Water Resources (RD and GR),
Ministry of Jal Shakti, Govt. of India
425(N), Sewa Bhawan, R.K. Puram,
New Delhi 110066, India

Email: incid-cwc@gov.in
Website: http://www.incid.cwc.gov.in/

USB flash drive included in this book contains full length papers.
Of no commercial value.

ICID Central Office:
48 Nyaya Marg, Chanakyapuri, New Delhi 110 021, India
Tel : +91 11 2611 6837, +91 11 2611 5679
E-mail : icid@icid.org, Website : https://icid.org

/icidat **/icidorg** **/icidonline**
/in/icidonline